MCEER
EARTHQUAKE ENGINEERING TO EXTREME EVENTS

ISSN 1520-295X

# Dynamics of Cable Structures: Modeling and Applications

by
Nicholas D. Oliveto and Mettupalayam V. Sivaselvan

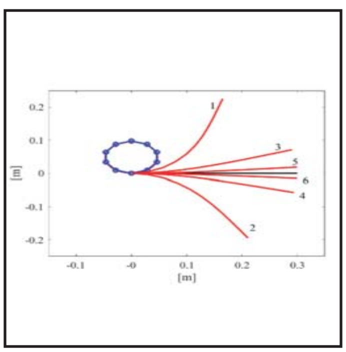



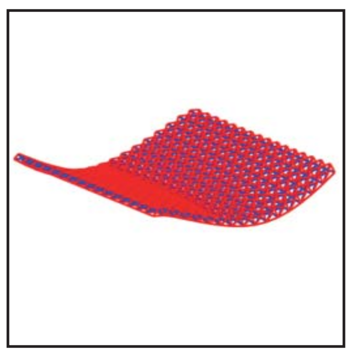

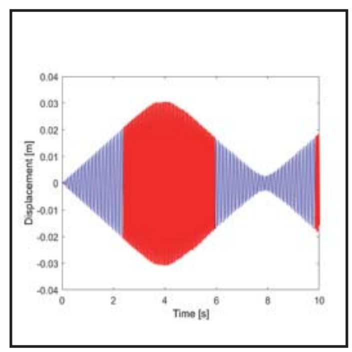


Technical Report MCEER-17-0006

December 1, 2017

This research was conducted at the University at Buffalo, State University of New York,
and was supported primarily by MCEER.

# Dynamics of Cable Structures: Modeling and Applications

by

Nicholas D. Oliveto[1] and Mettupalayam V. Sivaselvan[2]

Publication Date: December 1, 2017
Submittal Date: July 6, 2017

Technical Report MCEER-17-0006

1 Research Scientist, Department of Civil, Structural and Environmental Engineering, University at Buffalo, State University of New York
2 Associate Professor, Department of Civil, Structural and Environmental Engineering, University at Buffalo, State University of New York

MCEER
University at Buffalo, State University of New York
212 Ketter Hall, Buffalo, NY 14260
E-mail: *mceer@buffalo.edu*; Website: *http://mceer.buffalo.edu*

# Preface

MCEER is a national center of excellence dedicated to the discovery and development of new knowledge, tools and technologies that equip communities to become more disaster resilient in the face of earthquakes and other extreme events. MCEER accomplishes this through a system of multidisciplinary, multi-hazard research, in tandem with complimentary education and outreach initiatives.

Headquartered at the University at Buffalo, The State University of New York, MCEER was originally established by the National Science Foundation in 1986, as the first National Center for Earthquake Engineering Research (NCEER). In 1998, it became known as the Multidisciplinary Center for Earthquake Engineering Research (MCEER), from which the current name, MCEER, evolved.

Comprising a consortium of researchers and industry partners from numerous disciplines and institutions throughout the United States, MCEER's mission has expanded from its original focus on earthquake engineering to one which addresses the technical and socio-economic impacts of a variety of hazards, both natural and man-made, on critical infrastructure, facilities, and society.

The Center derives support from several Federal agencies, including the National Science Foundation, Federal Highway Administration, Department of Energy, Nuclear Regulatory Commission, and the State of New York, foreign governments and private industry.

*The use of cables may be seen in different engineering applications such as suspension and cable-stayed bridges, tensegrity systems, power transmission lines and moorings in ocean engineering. During extreme excitations, cables can undergo large displacements and be subjected to complex three-dimensional motion. Besides tension, cables can be subjected to shear, bending and torsion. In electrical substations, cable configurations can be seen that cannot be explained by simple tension. In the first part of this report, a 3-D finite deformation beam formulation is presented and applied to the analysis of the complex nonlinear dynamic behavior of flexible bus conductors used in electrical substations. Comparison of the finite element analyses with experiments clearly shows that stiffness and damping in these conductors are dependent on the amplitude of motion. The second part of the work is focused on tensegrity structures, a particular type of prestressed cable structure. An approach is presented for the dynamic analysis of these structures based on casting the computation in each time increment as a complementarity problem.*

# ABSTRACT

The objective of the present work is to re-examine and appropriately modify the geometrically exact beam theory, originally developed by Simo, and develop a nonlinear finite-element formulation to describe the static and dynamic behavior of flexible electrical equipment cables. The work is motivated by the need to better understand and predict the highly nonlinear response of flexible electrical conductors to earthquake excitations. Dynamic interaction between flexible cables and interconnected substation equipment is in fact believed to explain some of the severe damage sustained by such equipment in recent earthquakes.

In the first part of this report, the nonlinear equations of motion of a beam undergoing large displacements and rotations are derived from the 3D theory of continuum mechanics by use of the virtual power equation. A linear viscoelastic constitutive equation and an additional mass proportional damping mechanism are used to account for energy dissipation. The weak form of the equations of motion is linearized and discretized, in time and space, leading to the definition of a tangent operator and a system of equations solvable by means of an iterative scheme of the Newton type. Particular attention is focused on issues related to how large rotations are handled and how the configuration update process is performed. Numerical examples are presented, and energy balance calculations demonstrate the accuracy of the computed solutions. The beam model developed is then applied to describe the static and dynamic behavior of an electrical conductor tested at the Structural Engineering and Earthquake Simulation Laboratory (SEESL) at the University at Buffalo. Preliminary results of the simulation of free and forced vibration tests are presented.

In the second part of the report, an approach is presented for the dynamic analysis of tensegrity structures, a subclass of pin-jointed structures in which the cables can be considered as tension-only members. Such analyses are characterized by cables in the structure switching between taut and slack states. The approach is based on casting the computation in each time increment as a complementarity problem. Numerical examples are presented to illustrate the approach. Despite the non-smooth nature of cables switching between taut and slack states, the computed solutions exhibit remarkable long-term energy balance. Furthermore, by exploiting some features of the tensegrity model, significant computational efficiency can be gained in the solution of the complementarity problem in each time increment.

# ACKNOWLEDGEMENTS

The authors gratefully acknowledge financial support from the National Science Foundation through the grant CMMI-0847053. The authors also acknowledge Dr. Leon Kempner and Bonneville Power Authority (BPA) who sponsored the experimental study (with Professors A. Reinhorn and A. Filiatrault as PIs), which provided the data for the current study and part of the financial support for the first author.

# TABLE OF CONTENTS

**SECTION 1 INTRODUCTION**..........1

**SECTION 2 3D FINITE DEFORMATION BEAM MODEL**..........3

2.1 Introduction..........3
2.2 Virtual power equation..........4
2.2.1 Equilibrium equation..........4
2.2.2 Preliminary result..........5
2.2.3 Virtual power equation..........5
2.3 Beam model kinematics..........6
2.3.1 Reference and current configurations..........6
2.3.2 Derivatives of the rotation tensor..........8
2.3.3 Derivatives of the moving frame..........8
2.3.4 Deformation gradient tensor..........9
2.4 Beam virtual power equation..........9
2.4.1 External power..........10
2.4.2 Internal power..........10
2.4.3 Virtual power equation..........11
2.5 Equations of motion..........12
2.5.1 Strain and strain rate measures..........13
2.6 Constitutive equations..........14
2.7 Weak form of the equations of motion..........15
2.8 Time integration algorithm..........16
2.8.1 Configuration update..........17
2.8.2 Velocities and accelerations updates..........19
2.8.3 Remarks on configuration update..........19
2.9 Linearization of the weak form..........20
2.9.1 Tangent material stiffness operator..........21
2.9.2 Tangent damping operator..........23
2.9.3 Tangent geometric stiffness operator..........28
2.9.4 Tangent inertia operator..........29
2.10 Space discretization of the linearized weak form..........31

# TABLE OF CONTENTS (CONT'D)


2.11 Remarks on numerical implementation....33

2.11.1 Quaternion representation of rotations....33

2.11.2 Interpolation of rotation vectors....34

2.11.3 Update of curvature vectors....35

2.12 Numerical examples....36

2.12.1 Free vibration of rolled over cantilever....36

2.12.1.1 Static analysis....36

2.12.1.2 Dynamic analyses....37

2.12.2 Forced and free vibration of cable with clamped ends....40

2.12.2.1 Cable form finding....40

2.12.2.2 Harmonic ground motion inputs....42

2.12.3 Remarks on the choice of time step in numerical simulations....44

2.12.4 Energy calculations....45

2.12.5 Concluding remarks....47

**SECTION 3 NON-LINEAR DYNAMICS OF ELECTRICAL EQUIPMENT CABLES..49**

3.1 Introduction....49

3.1.1 Literature review....50

3.1.1.1 Experimental studies....50

3.1.1.2 Numerical studies....51

3.1.2 Objective and organization of the present work....52

3.2 Summary of governing equations....53

3.2.1 Kinematics....53

3.2.2 Equilibrium equations....54

3.2.3 Strain and strain rate measures....55

3.2.4 Constitutive equations....56

3.3 Mass proportional damping....57

3.4 Numerical simulation of dynamic cable tests....59

3.4.1 Modeling cable properties....59

3.4.2 Cable form finding....61

3.4.3 Modes and frequencies....62

# TABLE OF CONTENTS (CONT'D)


3.4.4 Free vibration tests ....................63
3.4.5 Forced vibration tests ....................66
3.5 Concluding remarks ....................71

**SECTION 4 DYNAMIC ANALYSIS OF TENSEGRITY STRUCTURES USING A COMPLEMENTARITY FRAMEWORK ....................73**
4.1 Introduction ....................73
4.2 Modeling for dynamic analysis ....................74
4.2.1 Implications of linearized kinematics ....................76
4.3 Time discretization ....................77
4.4 Mixed Complementarity problem (MCP) ....................79
4.4.1 Relationship to existing literature ....................79
4.5 Numerical examples ....................81
4.5.1 Example 1 ....................81
4.5.2 Example 2 ....................86
4.5.2.1 Free vibration analysis ....................88
4.5.2.2 Forced vibration analysis with harmonic input ....................92
4.6 Concluding remarks ....................97

**SECTION 5 CONCLUSION ....................99**
5.1 Summary ....................99
5.2 Contributions ....................99
5.3 Future work ....................100

**REFERENCES ....................101**

**APPENDIX A ....................107**
A.1 External Power ....................107
A.2 Internal power ....................112

**APPENDIX B ....................117**

# LIST OF ILLUSTRATIONS


Figure 2-1 Fixed and moving coordinate systems, reference and current configurations ............. 7

Figure 2-2 Geometric interpretation of the incremental iterative update procedure .................... 20

Figure 2-3 Incremental deformation of cantilever beam into a full circle .................................. 37

Figure 2-4 Displacement of free end of cantilever beam in free vibration: (a) vertical position; (b) horizontal position ........................................................................................................ 38

Figure 2-5 Dynamic unwinding of rolled over cantilever beam ................................................. 38

Figure 2-6 Cantilever beam in free vibration: (a) energy balance; (b) energy decay .................. 39

Figure 2-7 (a) Rolled over cantilever in ABAQUS; (b) free vibration response – ABAQUS versus proposed formulation ........................................................................................................ 40

Figure 2-8 (a) Static deformed shapes of cable with clamped ends; (b) magnification of cable under its own weight and subjected to step 1 .......................................................................... 41

Figure 2-9 (a) Imposed out-of-plane support motion; (b) imposed in-plane support motion....... 43

Figure 2-10 Numerical response of reference point to out-of-plane resonant excitation: (a) out-of-plane displacement; (b) in-plane horizontal displacement; (c) vertical displacement; (d) deformed shapes of cable at onset of free vibration and end of analysis .................................................... 44

Figure 2-11 Cable in out-of-plane forced vibration: (a) energy components; (b) energy balance 45

Figure 2-12 Numerical response of reference point to in-plane horizontal resonant excitation: (a) out-of-plane displacement; (b) in-plane horizontal displacement; (c) vertical displacement; (d) deformed shapes of cable at onset of free vibration and end of analysis .................................... 46

Figure 2-13 Cable in in-plane forced vibration: (a) energy components; (b) energy balance ...... 47

Figure 2-14 Cable in out-of-plane forced vibration: (a) energy error for different values of the time step h; (b) detail of energy error for h=0.005 s and h=0.001 s .................................................. 48

Figure 2-15 Cable in in-plane forced vibration: (a) energy error for different values of the time step h; (b) detail of energy error for h=0.001 s and h=0.0001 s ................................................. 48

Figure 3-1 Fixed and moving coordinate systems, reference and current configuration............. 54

Figure 3-2 Configuration of cable tested (Chandran, 2012) ....................................................... 59

Figure 3-3 Schematics of Jefferson conductor............................................................................ 61

Figure 3-4 Static deformed shape of cable with clamped ends .................................................. 62

Figure 3-5 Mode shapes of linearized cable model .................................................................... 63

Figure 3-6 Pull-release tests: (a) Deformed shape of cable prior to release (green), final shape of cable (red); (b) free vibration response of point 2 ...................................................................... 64

Figure 3-7 Free vibration acceleration response of control points shown in Figure 6(a) ............ 65
Figure 3-8 Cable in free vibration: (a) energu components; (b) energy balance; (c) energy error as defined in Eq. (3-32) ........................................................................................ 66
Figure 3-9 Free vibration acceleration of control point 2 shown in Figure 3-6(a): (a) using $I$ equal to the lower bound of $I_{\min}$; (b) using $I$=(1+$N$)$I_{\min}$ and the upper boundof $I_{\min}$ ............................ 67
Figure 3-10 Imposed support displacement and acceleration .................................................... 68
Figure 3-11 Displacement history of control points shown in Figure 3-6(a). Constant $\eta$=$\mu$=0.012 s (left hand side plots); $\eta$=$\mu$=0.012 s for stationary response and $\eta$=$\mu$=0.016 s for free vibration response (right hand side plots). ......................................................................................... 69
Figure 3-12 Acceleration history of control points shown in Figure 3-6(a). Constant $\eta$=$\mu$=0.012 s (left hand side plots); $\eta$=$\mu$=0.012 s for stationary response and $\eta$=$\mu$=0.016 s for free vibration response (right hand side plots). ......................................................................................... 70
Figure 3-13 Zoom-in of acceleration response - non-harmonic nature possibly due to higher modes or non-linearity.................................................................................................................. 71
Figure 3-14 Cable in forced vibration: (a) energy components; (b) energy balance; (c) energy error as defined in Eq. (3-32)......................................................................................................... 72
Figure 4-1 Conceptual model of a cable in a tensegrity structure ............................................. 75
Figure 4-2 Example 1: Single module in the tensegrity structure (a) Isometric view (b) Plan view (cables are shown as thin (red) lines and bars as thick (blue) lines)........................................... 81
Figure 4-3. Example 1: Undeformed configuration (a) Isometric view (b) Plan view (cables are shown in thin red and bars in thick blue. ......................................................................... 83
Figure 4-4 Example 1: Deformed configuration for α = 1 with slack cables shown in thick (red) lines (a) Isometric view (b) Plan view ........................................................................... 84
Figure 4-5 Example 1: (a) Cable tensions, and (b) Fractions of slack cables, for different values of the load factor α (these computational results are identical to the respective results in(Nineb et al., 2007)))........................................................................................................................... 85
Figure 4-6 Example 1- Computational time (In this example, there are 2397 free DOF and 3072 cables, so that the size of the MCP in equation (4-11) is 5469) ................................................. 86
Figure 4-7 Example 2: Undeformed configuration (a) Isometric view (b) Plan view (cables are shown in thin red and bars in thick blue)........................................................................ 87

## LIST OF ILLUSTRATIONS (CONT'D)

Figure 4-8 Example 2: (a) Isometric view of undeformed shape (b) Front view of undeformed shape (c) Isometric view of first mode (frequency, $f_1$ = 12.7185 Hz) (d) Front view of first mode ........ 89
Figure 4-9 Example 2: Free vibration response starting from a deformed configuration ........ 90
Figure 4-10 Example 2: Deformed configuration with 24 slack cables shown as thick (red) lines (a) Isometric view (b) Plan view ........ 91
Figure 4-11 Example 2: Free vibration response starting from a deformed configuration with 24 slack cables computed using time step 0.001 s. (a) Displacement of the center ........ 92
Figure 4-12 Example 2: Free vibration response starting from a deformed configuration with 24 slack cables computed using time step 0.01s (a) Displacement of the center node (b) Energy balance ........ 93
Figure 4-13 Example 2: Convergence of displacement of the center node with decreasing time step size for free vibration starting from a deformed configuration with 12 slack cables ........ 93
Figure 4-14 Example 2: Forced vibration with input acceleration amplitude 0.01g, computed using time step 0.001s (a) Displacement of center node (b) Energy balance (c) Energy error as defined in equation (4-16) ........ 94
Figure 4-15 Example 2: Forced vibration with input acceleration amplitude 0.05 g, computed using time step 0.001 s. (a) Displacement of the center node with the phase where some cables could be slack is shown in red. (b) Number of slack cables. (c) Energy balance. (d) Energy error as defined in Eq. (4-16) ........ 95
Figure 4-16 Example 2: Forced vibration with input acceleration amplitude 0.1 g, computed using time step 0.001 s. (a) Displacement of the center node with the phase where ........ 96

# LIST OF TABLES

Table 2-1 Time integration algorithm ........ 17
Table 2-2 Update procedure ........ 18
Table 2-3 Statically rolled over cantilever – convergence rate of Newton's method ........ 37
Table 2-4 Dynamic unwinding of cantilever – convergence of Newton's method ........ 39
Table 2-5 Cable form finding – loading sequence ........ 41
Table 2-6 Cable form finding – convergence of Newton's method ........ 41
Table 2-7 Out-of-plane excitation: convergence of Newton's method ........ 45
Table 2-8 In-plane excitation: convergence rate of Newton's method ........ 47
Table 3-1 Strain measures ........ 55
Table 3-2 Strain rate measures ........ 55
Table 3-3 Values of *I* considered ........ 61
Table 3-4 Frequencies and periods of cable ........ 64
Table 4-1 Example 1- Summary of module parameters ........ 82
Table 4-2 Example 1: Options for the PATH solver to imitate Lemke's method ........ 86
Table 4-3 Example 2: Summary of module parameters ........ 88
Table 4-4 Example 2: Free vibration analysis cases ........ 89

# SECTION 1
# INTRODUCTION

The use of cables may be seen in different engineering applications such as suspension and cable-stayed bridges, wide-span roof structures, power transmission lines and moorings in ocean engineering. Cables are particularly appealing for long-span structures because they have high strength-to-weight ratio, they are easily engineered and they possess very high axial stiffness. However, during extreme excitations cables can undergo large displacements and rotations, and be subjected to complex three-dimensional motion. Furthermore, besides tension, cables can be subjected to shear, bending and torsion. It is common in electrical substations to observe cable configurations that cannot be explained by a state of stress of simple tension. Well-developed theories exist for the static response of cables, as well as for the linear free-vibration response of taut cables. However, no analytical results may be obtained, accounting for the geometric nonlinearity due to finite displacements and rotations. For these reasons, researchers involved in the dynamic analysis of cables have recently turned to finite element implementations of geometrically exact beam theories.

The present report is composed of two parts. The first part is motivated by the need to better understand and predict the highly nonlinear response of flexible electrical conductors to earthquake excitations. In fact, dynamic interaction between flexible cables and interconnected substation equipment is believed to explain some of the severe damage observed in recent earthquakes. Due to the complexity of this interaction, there are deficiencies in how this effect is accounted for in current seismic design and qualification standards. The seismic qualification procedures in the IEEE 693-2005 Standard are limited to individual equipment, with recognition that additional forces due to conductor dynamics have to be accounted for separately. Guidelines for magnitudes of such forces at cable terminations are included in the IEEE 1527-2006 Standard. However, these are based on experimental measures on specific conductor configurations that do not exhaust all the possible configurations in the field. Although inspired by and applied to the study of electrical conductors (Oliveto and Sivaselvan, 2014; 2015), the models developed in this study can be naturally extended to the analysis of a broader class of cable applications such as suspension bridges and ocean mooring systems (Petrone et al., 2015). Furthermore, similar models have recently been considered for applications in the fields of robotics and biomedical engineering.

In some applications, cables can be considered as being in one of two limiting states - taut or slack. An example where such a modeling approach can be used is tensegrity structures - a subclass of pin-jointed structures composed of cables or strings, which can only resist tension forces, and bars or struts that are mainly meant to work in compression (Oliveto and Sivaselvan, 2011). In the second part of the report, an approach is presented for the dynamic analysis of tensegrity structures. These are generally used for wide-span roofs, domes, stadiums, and most recently for robots. The dynamic vibrations of this kind of structure are characterized by cables in the structure switching between taut and slack states. The novelty of the proposed approach is based on casting the computation in each time increment as a complementarity problem.

The report is organized as follows. In Section 2, the 3D finite deformation beam model developed by Simo is re-examined and appropriately modified to derive a finite element formulation for the static and dynamic analysis of flexible cables. Numerical examples are carried out and energy balance calculations are performed to assess the accuracy of the computed solutions. In Section 3, the beam model described in Section 2 is applied to describe the static and dynamic behavior of an electrical conductor tested at the Structural Engineering and Earthquake Simulation Laboratory at the University at Buffalo. Preliminary results of the simulation of free and forced vibration tests are presented. Section 4 deals with the dynamic analysis of tensegrity structures using a complementarity framework. Numerical applications are presented to illustrate the approach and to assess the long-term energy balance of the computed solutions. Concluding remarks are made in Section 5. The major contributions of the report are clearly stated and the topics of ongoing work discussed.

# SECTION 2
# 3D FINITE DEFORMATION BEAM MODEL

## 2.1 Introduction

In the past two or three decades, extensive research has been done on the formulation and implementation of geometrically nonlinear beam models. Pioneering work in the field is due to Simo (1985), who generalized to the fully three-dimensional (3D) dynamic case, a finite deformation beam formulation originally developed by Reissner (1972) for the plane static problem. In his model, Simo presented a simple and clear representation of the beam's deformation in terms of position of the cross-sectional centroid and rotation of the cross section. The formulation was regarded by Simo as a convenient parameterization of an extension to the classical Kirchhoff-Love model (Love, 1944), subsequently developed by Antman (1974) to include extension and shearing. Simo (1986), and Simo and Vu-Quoc (1988), then developed a finite-element formulation of the model for statics and dynamics, which was later extended to incorporate shear and torsional warping deformation (Simo, 1991).

Following Simo's work, numerous studies have been conducted concerning the development of efficient finite-element models based on different ways of representing and interpolating rotations. Significant work along these lines was done by Ibrahimbegovic et al. (1995), and Ibrahimbegovic and Mikdad (1988), who presented finite-element implementations and time-stepping schemes for different parameterizations of finite rotations. Furthermore, Crisfield and Jelenic (1999), and Jelenic and Crisfield (1999), proposed a new interpolation scheme for rotations that prevents non-objectivity of the strain measures.

Though generally linear elastic constitutive relations are used, in a work by Mata et al. (2007), the geometrically nonlinear beam model was extended to account for nonlinear constitutive behavior. A clear explanation of how finite-deformation kinematics may be combined with a small-strain constitutive behavior is not trivial. Auricchio et al. (2008) provided an elegant demonstration based on neglecting the quadratic pure strain term of the Green-Lagrange strain tensor and introducing a linear elastic and isotropic relation between the second Piola-Kirchhoff stress tensor and the small-strain Green-Lagrange tensor.

To be attractive for realistic dynamic applications, a numerical model should be able to account for some form of energy dissipation. Recently, Lang et al. (2011) and Linn et al. (2013), following the work of Antman (1996; 2003) on nonlinearly viscoelastic rods, introduced viscous material damping into a quaternionic reformulation of Simo's beam model.

In this section, the 3D finite-deformation beam model developed by Simo is modified appropriately and extended to describe the static and dynamic behavior of flexible beams. Most importantly, building on the work of Lang et al. (2011), linear viscoelastic constitutive equations are introduced in the beam model to account for energy dissipation. Furthermore, a solution to issues concerning the interpolation of total rotation vectors of magnitude greater than $\pi$ is proposed. Finally, an alternative approach for the update of curvatures is suggested, based on total rotation vectors and taking advantage of special features of Lie groups and of the notion of right-trivialized derivative (Ortolan, 2011).

This section is organized as follows. In Subsections 2.2 to 2.5, using the deformation map and kinematics introduced by Simo (1985), the equations of motion, as well as the boundary conditions, of the finite deformation beam model are derived from the virtual power equation for the 3D continuum. In Subsection 2.6, the constitutive equations are described. A new aspect here is the introduction of an extension of the Kelvin-Voigt damping model to the 3D geometrically nonlinear beam, in a physically consistent way, through the constitutive equations. Viscous contributions are added to the elastic stress resultants and moments, proportionally to the strain rates. The weak form of the equations of motion is derived in Subsection 2.7, and in Subsection 2.8 the time integration algorithm is presented. The weak form is linearized in Subsection 2.9 and then discretized in space in Subsection 2.10, leading to the definition of a tangent operator and a system of equations solvable by means of an iterative scheme of the Newton type. Subsection 2.11 deals with details of the numerical implementation and with issues related to how large rotations are handled and how the configuration update process is performed. Plane and three-dimensional examples are presented in Subsection 2.12 to illustrate the performance of the numerical implementations.

## 2.2 Virtual power equation

### 2.2.1 Equilibrium equation

In material coordinates the equilibrium equation for the 3D continuum is given by:

$$div\,\mathbf{P} + \rho_0 \mathbf{B} - \rho_0 \ddot{\mathbf{x}} = \mathbf{0} \tag{2-1}$$

where $\mathbf{P}$ is the first Piola-Kirchhoff stress tensor, $\rho_0\mathbf{B}$ is the body force field and $\rho_0\ddot{\mathbf{x}}$ are the inertia forces. The first Piola-Kirchhoff stress tensor relates forces in the current configuration with areas in the reference configuration and is defined as:

$$\mathbf{P} = \det\mathbf{F}\,\mathbf{T}\cdot\mathbf{F}^{\mathrm{T}} \tag{2-2}$$

where $\mathbf{T}$ is the Cauchy stress tensor and $\mathbf{F}$ is the deformation gradient tensor defined as:

$$\mathbf{F} = \frac{\partial x_i}{\partial X_j}\mathbf{E}_i \otimes \mathbf{E}_j = \frac{\partial \mathbf{x}}{\partial X_i}\otimes \mathbf{E}_i \tag{2-3}$$

### 2.2.2 Preliminary result

The time derivative of the deformation gradient tensor $\mathbf{F}$ is given by:

$$\dot{\mathbf{F}} = \frac{\partial \dot{\mathbf{x}}}{\partial X_i}\otimes \mathbf{E}_i = \frac{\partial \dot{x}_i}{\partial X_j}\mathbf{E}_i \otimes \mathbf{E}_j = \mathbf{\Lambda} \tag{2-4}$$

By noting that the first Piola-Kirchhoff stress tensor is energy conjugate to the deformation gradient tensor $\mathbf{F}$ we can write:

$$\begin{aligned}\mathbf{P}:\dot{\mathbf{F}} = tr\left(\mathbf{P}^{\mathrm{T}}\cdot\dot{\mathbf{F}}\right) = tr\left(\mathbf{P}^{\mathrm{T}}\cdot\mathbf{\Lambda}\right) = P_{ij}^{T}\Lambda_{ji} = P_{ij}^{T}\frac{\partial \dot{x}_j}{\partial X_i} = \frac{\partial}{\partial X_i}\left(P_{ij}^{T}\dot{x}_j\right) - \frac{\partial P_{ij}^{T}}{\partial X_i}\dot{x}_j = \\ \frac{\partial}{\partial X_i}\left(P_{ij}^{T}\dot{x}_j\right) - \frac{\partial P_{ji}}{\partial X_i}\dot{x}_j = div\left(\mathbf{P}^{\mathrm{T}}\cdot\dot{\mathbf{x}}\right) - div\,\mathbf{P}\cdot\dot{\mathbf{x}}\end{aligned} \tag{2-5}$$

We have therefore obtained the following important result:

$$div\,\mathbf{P}\cdot\dot{\mathbf{x}} = div\left(\mathbf{P}^{\mathrm{T}}\cdot\dot{\mathbf{x}}\right) - tr\left(\mathbf{P}^{\mathrm{T}}\cdot\dot{\mathbf{F}}\right) \tag{2-6}$$

### 2.2.3 Virtual power equation

Multiplication of each term of (2-1) by an arbitrary velocity field $\bar{\dot{\mathbf{x}}}$ and integration over the volume of the body in the reference configuration $R_0$ gives:

$$\iiint_{R_0}\left(div\,\mathbf{P} + \rho_0\mathbf{B} - \rho_0\ddot{\mathbf{x}}\right)\cdot\bar{\dot{\mathbf{x}}}\,dV = 0 \tag{2-7}$$

Eq. (2-7) can be rearranged as:

$$\iiint_{R_0} div\,\mathbf{P}\cdot\bar{\dot{\mathbf{x}}}\,dV + \iiint_{R_0}\rho_0\mathbf{B}\cdot\bar{\dot{\mathbf{x}}}\,dV = \iiint_{R_0}\rho_0\ddot{\mathbf{x}}\cdot\bar{\dot{\mathbf{x}}}\,dV \tag{2-8}$$

Using (2-6), the first integral may be written as follows:

$$\iiint_{R_0} div\,\mathbf{P}\cdot\bar{\dot{\mathbf{x}}}\,dV = \iiint_{R_0} div\left(\mathbf{P}^{\mathrm{T}}\cdot\bar{\dot{\mathbf{x}}}\right)dV - \iiint_{R_0} tr\left(\mathbf{P}^{\mathrm{T}}\cdot\bar{\dot{\mathbf{F}}}\right)dV \tag{2-9}$$

By applying the divergence theorem to the first term on the right hand side of (2-9) we get:

$$\iiint_{R_0} div\left(\mathbf{P}^{\mathrm{T}}\cdot\bar{\dot{\mathbf{x}}}\right)dV = \iint_{\partial R_0}\left(\mathbf{P}^{\mathrm{T}}\cdot\bar{\dot{\mathbf{x}}}\right)\cdot\mathbf{N}\;dA = \iint_{\partial R_0}\mathbf{N}\cdot\left(\mathbf{P}^{\mathrm{T}}\cdot\bar{\dot{\mathbf{x}}}\right)dA = \iint_{\partial R_0}\left(\mathbf{P}\cdot\mathbf{N}\right)\cdot\bar{\dot{\mathbf{x}}}\,dA \tag{2-10}$$

where $\mathbf{N}$ is the unit vector of the normal to the boundary $\partial R_0$. We then can finally write:

$$\iint_{\partial R_0}\left(\mathbf{P}\cdot\mathbf{N}\right)\cdot\bar{\dot{\mathbf{x}}}\,dA + \iiint_{R_0}\rho_0\mathbf{B}\cdot\bar{\dot{\mathbf{x}}}\,dV - \iiint_{R_0}\rho_0\ddot{\mathbf{x}}\cdot\bar{\dot{\mathbf{x}}}\,dV = \iiint_{R_0} tr\left(\mathbf{P}^{\mathrm{T}}\cdot\bar{\dot{\mathbf{F}}}\right)dV \tag{2-11}$$

The left hand side of (2-11) represents the power developed by external forces while the right hand side represents the internal power.

## 2.3 Beam model kinematics

### 2.3.1 Reference and current configurations

The body kinematics for the beam model are described by a reference and a current configuration, both defined with respect to a fixed global reference system $\{\mathbf{e}_1,\mathbf{e}_2,\mathbf{e}_3\}$ and a set of material coordinates $\{X_1,X_2,S\}$. The beam in the reference configuration is assumed to have a straight axis and uniform cross-sections. Moreover, we introduce a right-handed orthogonal *reference frame* $\{\mathrm{O},\mathbf{E}_1,\mathbf{E}_2,\mathbf{E}_3\}$, with O on the axis of the beam, $\mathbf{E}_1$ and $\mathbf{E}_2$ parallel to a generic cross-section, and $\mathbf{E}_3$ parallel to the axis. For simplicity, we take the reference frame to be coincident with the global frame so that the reference configuration of the beam is then described by the position vector field $\mathbf{X}$:

$$\mathbf{X} = \mathbf{X}_0\left(S,t\right) + X_\alpha\mathbf{E}_\alpha \tag{2-12}$$

where α is ranging from 1 to 2. As shown in Figure 2-1, $\mathbf{X}_0(S,t) = S\mathbf{E}_3$ represents the position of a point along the axis of the beam, while $X_\alpha\mathbf{E}_\alpha$ represents the position of a point within a cross-section of the beam. To describe the beam in the current configuration, we introduce a right handed orthogonal *moving* or *current frame* $\{\mathrm{o},\mathbf{t}_1,\mathbf{t}_2,\mathbf{t}_3\}$. The moving frame can be seen as a rotated reference frame since it can be obtained through a rigid rotation of the reference frame defined by a proper orthogonal tensor $\mathbf{R}(S,t)$ as:

$$\mathbf{t}_i\left(S,t\right) = \mathbf{R}\left(S,t\right)\cdot\mathbf{E}_i \tag{2-13}$$

where $i$ is ranging from 1 to 3. Based on (2-13), a convenient expression for the rotation tensor $\mathbf{R}$ is:

$$\mathbf{R}(S,t)=\mathbf{t}_i(S,t)\otimes\mathbf{E}_i \tag{2-14}$$

The current configuration of the beam is then described by the current position vector field $\mathbf{x}$:

$$\mathbf{x}=\mathbf{x}_0(S,t)+X_\alpha\mathbf{t}_\alpha(S,t) \tag{2-15}$$

where $\mathbf{x}_0(S,t)$ represents the position of a point along the axis of the beam in the current configuration, whereas $X_\alpha\mathbf{t}_\alpha$ represents the position of a point within a generic cross-section of the beam in the current configuration. Using (2-13), the deformation map may be finally written as:

$$\mathbf{x}=\mathbf{x}_0(S,t)+X_\alpha\mathbf{R}(S,t)\cdot\mathbf{E}_\alpha \tag{2-16}$$

Eq. (2-16) clearly shows how the current configuration is uniquely defined in terms of $\mathbf{x}_0(S,t)$ and $\mathbf{R}(S,t)$.

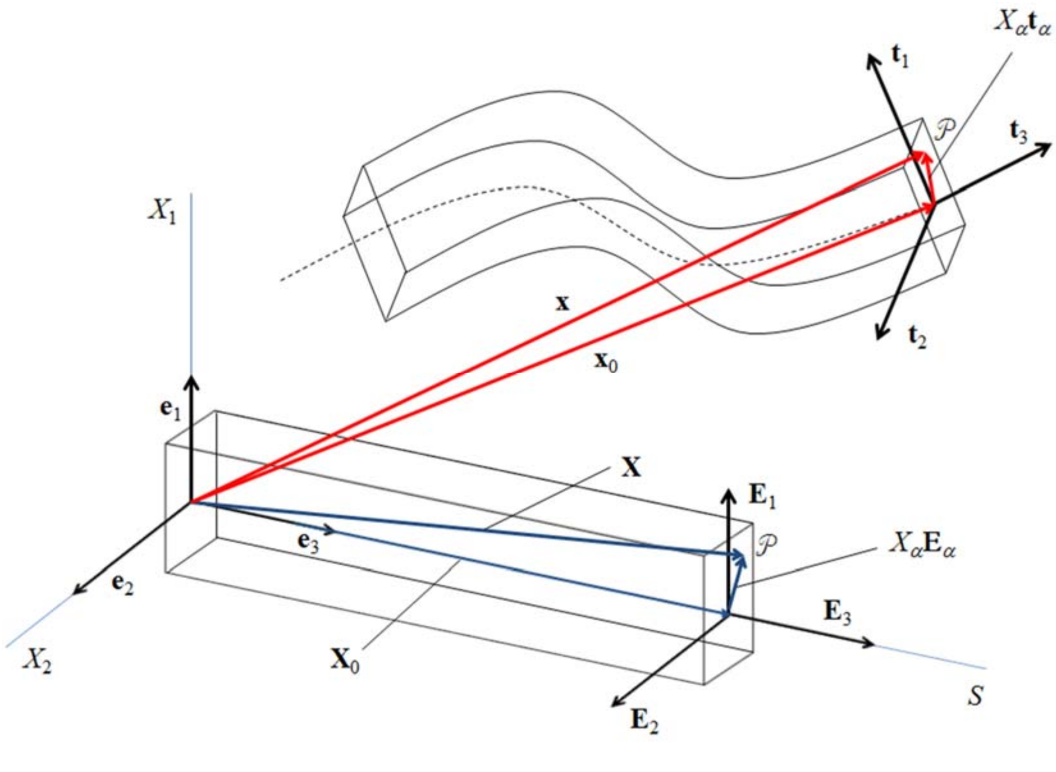


**Figure 2-1 Fixed and moving coordinate systems, reference and current configurations**

### 2.3.2 Derivatives of the rotation tensor

Finite rotations belong to the special orthogonal (Lie) group SO(3). Rotation tensors belonging to this group are characterized by $\mathbf{R}\cdot\mathbf{R}^{\mathrm{T}}=\mathbf{I}$ and det$\mathbf{R}$=1. Based on the first property it is easy to show that the derivatives of the rotation tensor $\mathbf{R}$ with respect to S and t are given by:

$$\frac{\partial}{\partial S}\mathbf{R}(S,t)=\hat{\boldsymbol{\omega}}(S,t)\cdot\mathbf{R}(S,t)=\mathbf{R}(S,t)\cdot\hat{\boldsymbol{\Omega}}(S,t) \tag{2-17}$$

$$\frac{\partial}{\partial t}\mathbf{R}(S,t)=\hat{\mathbf{w}}(S,t)\cdot\mathbf{R}(S,t)=\mathbf{R}(S,t)\cdot\hat{\mathbf{W}}(S,t) \tag{2-18}$$

where $\hat{\boldsymbol{\omega}}$, $\hat{\mathbf{w}}$, $\hat{\boldsymbol{\Omega}}$ and $\hat{\mathbf{W}}$ are skew-symmetric tensors. The first two are defined in the current configuration, while the second two are defined in the reference configuration.

Given that $\mathbf{R}$ represents the rotation of the cross-section, $\hat{\boldsymbol{\omega}}$ and $\hat{\boldsymbol{\Omega}}$ represent the rate of change of the cross-section rotation with respect to S and therefore can be considered measures of bending and torsional strain. We define $\hat{\boldsymbol{\omega}}$ as the *current curvature tensor* and $\hat{\boldsymbol{\Omega}}$ as the *reference curvature tensor*. Moreover $\hat{\mathbf{w}}$ and $\hat{\mathbf{W}}$ represent the rate of change of the cross-section rotation with respect to t and therefore may be interpreted as angular velocities. We define $\hat{\mathbf{w}}$ as the *current angular velocity tensor* and $\hat{\mathbf{W}}$ as the *reference angular velocity tensor*.

The skew symmetric tensors just defined are related by the following expressions:

$$\hat{\boldsymbol{\omega}}=\mathbf{R}\cdot\hat{\boldsymbol{\Omega}}\cdot\mathbf{R}^{\mathrm{T}} \qquad \hat{\boldsymbol{\Omega}}=\mathbf{R}^{\mathrm{T}}\cdot\hat{\boldsymbol{\omega}}\cdot\mathbf{R} \tag{2-19}$$

$$\hat{\mathbf{w}}=\mathbf{R}\cdot\hat{\mathbf{W}}\cdot\mathbf{R}^{\mathrm{T}} \qquad \hat{\mathbf{W}}=\mathbf{R}^{\mathrm{T}}\cdot\hat{\mathbf{w}}\cdot\mathbf{R} \tag{2-20}$$

Moreover, it is easy to show that the components of $\hat{\boldsymbol{\omega}}$ and $\hat{\mathbf{w}}$ in the current frame $\{\mathrm{o},\mathbf{t}_1,\mathbf{t}_2,\mathbf{t}_3\}$ are the same as those of $\hat{\boldsymbol{\Omega}}$ and $\hat{\mathbf{W}}$ in the reference frame $\{\mathrm{O},\mathbf{E}_1,\mathbf{E}_2,\mathbf{E}_3\}$.

### 2.3.3 Derivatives of the moving frame

By means of (2-17) and (2-18) we can now evaluate the derivatives of $\mathbf{t}_i=\mathbf{R}\cdot\mathbf{E}_i$ as:

$$\frac{\partial}{\partial S}\mathbf{t}_i(S,t)=\frac{\partial}{\partial S}\mathbf{R}(S,t)\cdot\mathbf{E}_i=\hat{\boldsymbol{\omega}}(S,t)\cdot\mathbf{R}(S,t)\cdot\mathbf{E}_i=\hat{\boldsymbol{\omega}}(S,t)\cdot\mathbf{t}_i(S,t) \tag{2-21}$$

$$\frac{\partial}{\partial t}\mathbf{t}_i(S,t)=\frac{\partial}{\partial t}\mathbf{R}(S,t)\cdot\mathbf{E}_i=\hat{\mathbf{w}}(S,t)\cdot\mathbf{R}(S,t)\cdot\mathbf{E}_i=\hat{\mathbf{w}}(S,t)\cdot\mathbf{t}_i(S,t) \tag{2-22}$$

By introducing vectors $\boldsymbol{\omega}$ and $\mathbf{w}$, associated respectively to the skew-symmetric tensors $\hat{\boldsymbol{\omega}}$, and $\hat{\mathbf{w}}$, (2-21) and (2-22) may also be written as:

$$\frac{\partial}{\partial S}\mathbf{t}_i(S,t)=\hat{\boldsymbol{\omega}}(S,t)\cdot\mathbf{t}_i(S,t)=\boldsymbol{\omega}(S,t)\times\mathbf{t}_i(S,t) \tag{2-23}$$

$$\frac{\partial}{\partial t}\mathbf{t}_i(S,t)=\hat{\mathbf{w}}(S,t)\cdot\mathbf{t}_i(S,t)=\mathbf{w}(S,t)\times\mathbf{t}_i(S,t) \tag{2-24}$$

We define $\boldsymbol{\omega}$ as the *current curvature vector* and $\mathbf{w}$ the *current angular velocity vector*. We then introduce $\boldsymbol{\Omega}$ and $\mathbf{W}$ as the *reference curvature vector* and the *reference angular velocity* associated respectively to $\hat{\boldsymbol{\Omega}}$ and $\hat{\mathbf{W}}$. These are related to the previously defined current vectors by:

$$\boldsymbol{\omega}=\mathbf{R}\cdot\boldsymbol{\Omega} \qquad \boldsymbol{\Omega}=\mathbf{R}^{\mathbf{T}}\cdot\boldsymbol{\omega} \tag{2-25}$$

$$\mathbf{w}=\mathbf{R}\cdot\mathbf{W} \qquad \mathbf{W}=\mathbf{R}^{\mathbf{T}}\cdot\mathbf{w} \tag{2-26}$$

Again, it is easy to show that the components of $\boldsymbol{\omega}$ and $\mathbf{w}$ in the current frame $\{o,\mathbf{t}_1,\mathbf{t}_2,\mathbf{t}_3\}$ are the same as those of $\boldsymbol{\Omega}$ and $\mathbf{W}$ in the reference frame $\{O,\mathbf{E}_1,\mathbf{E}_2,\mathbf{E}_3\}$.

### 2.3.4 Deformation gradient tensor

Substituting (2-15) into (2-3) the deformation gradient tensor $\mathbf{F}$ may be written as:

$$\mathbf{F}=\mathbf{t}_\alpha\otimes\mathbf{E}_\alpha+\left[\frac{\partial\mathbf{x}_0}{\partial S}+X_\alpha\frac{\partial\mathbf{t}_\alpha}{\partial S}\right]\otimes\mathbf{E}_3 \tag{2-27}$$

Using (2-23) to evaluate the derivative with respect to $S$ of $\mathbf{t}_\alpha$, (2-27) can then be written in the following equivalent form:

$$\mathbf{F}=\mathbf{t}_\alpha\otimes\mathbf{E}_\alpha+\left[\frac{\partial\mathbf{x}_0}{\partial S}+\boldsymbol{\omega}\times X_\alpha\mathbf{t}_\alpha\right]\otimes\mathbf{E}_3 \tag{2-28}$$

## 2.4 Beam virtual power equation

Using the kinematics described above, in this section we particularize the continuum virtual power equation to the case of prismatic beams. The complete derivation for each term of (2-11) is presented in APPENDIX A. As follows we present the final results only.

### 2.4.1 External power

*Boundary terms.* The first term on the left-hand side of (2-11) becomes:

$$\iint_{\partial R_0} (\mathbf{P}\cdot\mathbf{N})\cdot\bar{\dot{\mathbf{x}}}\,dA = -\mathbf{n}(0,t)\cdot\bar{\dot{\mathbf{x}}}_0(0,t) - \mathbf{m}(0,t)\cdot\bar{\mathbf{w}}(0,t) + \mathbf{n}(L,t)\cdot\bar{\dot{\mathbf{x}}}_0(L,t) + \mathbf{m}(L,t)\cdot\bar{\mathbf{w}}(L,t) + \int_0^L\left(\oint_\Gamma (\mathbf{P}\cdot\mathbf{N})\,d\Gamma\right)\cdot\bar{\dot{\mathbf{x}}}_0\,dS + \int_0^L\left(\oint_\Gamma (\mathbf{x}-\mathbf{x}_0)\times(\mathbf{P}\cdot\mathbf{N})\,d\Gamma\right)\cdot\bar{\mathbf{w}}\,dS \tag{2-29}$$

In (2-29) $\mathbf{n}(0,t)$ and $\mathbf{m}(0,t)$ are the resultant force and moment acting on the cross section at $S=0$:

$$\mathbf{n}(0,t) = \iint_{A_0} \mathbf{P}_3\,dA \tag{2-30}$$

$$\mathbf{m}(0,t) = \iint_{A_0} (\mathbf{x}-\mathbf{x}_0)\times\mathbf{P}_3\,dA \tag{2-31}$$

Furthermore $\mathbf{n}(L,t)$ and $\mathbf{m}(L,t)$ are the resultant force and moment acting on the cross section at $S=L$:

$$\mathbf{n}(L,t) = \iint_{A_L} \mathbf{P}_3\,dA \tag{2-32}$$

$$\mathbf{m}(L,t) = \iint_{A_L} (\mathbf{x}-\mathbf{x}_0)\times\mathbf{P}_3\,dA \tag{2-33}$$

Finally $\Gamma$ is the boundary of the cross section in the reference configuration.

*Body forces.* The term of (2-11) related to the body forces becomes:

$$\iiint_{R_0} \rho_0\mathbf{B}\cdot\bar{\dot{\mathbf{x}}}\,dV = \int_0^L\left(\iint_A \rho_0\mathbf{B}\,dA\right)\cdot\bar{\dot{\mathbf{x}}}_0\,dS + \int_0^L\left(\iint_A (\mathbf{x}-\mathbf{x}_0)\times\rho_0\mathbf{B}\,dA\right)\cdot\bar{\mathbf{w}}\,dS \tag{2-34}$$

*Inertia forces.* The term on the left hand side of (2-11) related to the inertia forces becomes:

$$\iiint_{R_0} \rho_0\ddot{\mathbf{x}}\cdot\bar{\dot{\mathbf{x}}}dV = \int_0^L A_\rho\ddot{\mathbf{x}}_0\cdot\bar{\dot{\mathbf{x}}}_0 dS + \int_0^L\left[\mathbf{I}_\rho\cdot\dot{\mathbf{w}} + \mathbf{w}\times(\mathbf{I}_\rho\cdot\mathbf{w})\right]\cdot\bar{\mathbf{w}}\,dS \tag{2-35}$$

where $A_\rho = \iint_A \rho_0 dA$ is the mass per unit length of the beam, and $\mathbf{I}_\rho$ is the *current inertia tensor* defined as:

$$\mathbf{I}_\rho = \iint_{A_0} \rho_0\left[(\mathbf{x}-\mathbf{x}_0)\cdot(\mathbf{x}-\mathbf{x}_0)\mathbf{I} - (\mathbf{x}-\mathbf{x}_0)\otimes(\mathbf{x}-\mathbf{x}_0)\right]dA \tag{2-36}$$

### 2.4.2 Internal power

The right-hand side of (2-11) becomes

$$\iiint_{R_0} tr\left(\mathbf{P}^{\mathrm{T}} \cdot \dot{\mathbf{F}}\right) dV = \int_0^L \left[ \mathbf{n} \cdot \left( \frac{\partial^2 \mathbf{x}_0}{\partial S \partial t} - \overline{\mathbf{w}} \times \frac{\partial \mathbf{x}_0}{\partial S} \right) + \mathbf{m} \cdot \left( \bar{\dot{\boldsymbol{\omega}}} - \overline{\mathbf{w}} \times \boldsymbol{\omega} \right) \right] dS \qquad (2\text{-}37)$$

where

$$\mathbf{n} = \iint_A \mathbf{P}_3 \, dA \qquad (2\text{-}38)$$

$$\mathbf{m} = \iint_A \left( \mathbf{x} - \mathbf{x}_0 \right) \times \mathbf{P}_3 \, dA \qquad (2\text{-}39)$$

### 2.4.3 Virtual power equation

By collecting the results from the previous sections and substituting them into (2-11), the virtual power equation for the beam model may be written as:

$$\begin{aligned}
&-\mathbf{n}(0,t) \cdot \bar{\dot{\mathbf{x}}}_0(0,t) - \mathbf{m}(0,t) \cdot \overline{\mathbf{w}}(0,t) + \mathbf{n}(L,t) \cdot \bar{\dot{\mathbf{x}}}_0(L,t) + \mathbf{m}(L,t) \cdot \overline{\mathbf{w}}(L,t) + \\
&\int_0^L \left( \oint_\Gamma (\mathbf{P} \cdot \mathbf{N}) \, d\Gamma \right) \cdot \bar{\dot{\mathbf{x}}}_0 \, dS + \int_0^L \left( \oint_\Gamma (\mathbf{x} - \mathbf{x}_0) \times (\mathbf{P} \cdot \mathbf{N}) \, d\Gamma \right) \cdot \overline{\mathbf{w}} \, dS + \\
&\int_0^L \left( \iint_A \rho_0 \mathbf{B} \, dA \right) \cdot \bar{\dot{\mathbf{x}}}_0 \, dS + \int_0^L \left( \iint_{A_0} (\mathbf{x} - \mathbf{x}_0) \times \rho_0 \mathbf{B} dA \right) \cdot \overline{\mathbf{w}} \, dS + \\
&-\int_0^L A_\rho \ddot{\mathbf{x}}_0 \cdot \bar{\dot{\mathbf{x}}}_0 \, dS - \int_0^L \left[ \mathbf{I}_\rho \cdot \dot{\mathbf{w}} + \mathbf{w} \times \left( \mathbf{I}_\rho \cdot \mathbf{w} \right) \right] \cdot \overline{\mathbf{w}} \, dS = \\
&\int_0^L \left[ \mathbf{n} \cdot \left( \frac{\partial^2 \mathbf{x}_0}{\partial S \partial t} - \overline{\mathbf{w}} \times \frac{\partial \mathbf{x}_0}{\partial S} \right) + \mathbf{m} \cdot \left( \bar{\dot{\boldsymbol{\omega}}} - \overline{\mathbf{w}} \times \boldsymbol{\omega} \right) \right] dS
\end{aligned} \qquad (2\text{-}40)$$

We can write (2-40) more concisely as:

$$\begin{aligned}
&\mathbf{n}_0 \cdot \bar{\dot{\mathbf{x}}}_0(0,t) + \mathbf{m}_0 \cdot \overline{\mathbf{w}}(0,t) + \mathbf{n}_L \cdot \bar{\dot{\mathbf{x}}}_0(L,t) + \mathbf{m}_L \cdot \overline{\mathbf{w}}(L,t) + \\
&\int_0^L \tilde{\mathbf{n}}(S,t) \cdot \bar{\dot{\mathbf{x}}}_0 dS + \int_0^L \tilde{\mathbf{m}}(S,t) \cdot \overline{\mathbf{w}} dS - \int_0^L A_\rho \ddot{\mathbf{x}}_0 \cdot \bar{\dot{\mathbf{x}}}_0 \, dS + \\
&-\int_0^L \left[ \mathbf{I}_\rho \cdot \dot{\mathbf{w}} + \mathbf{w} \times \left( \mathbf{I}_\rho \cdot \mathbf{w} \right) \right] \cdot \overline{\mathbf{w}} \, dS = \\
&\int_0^L \left[ \mathbf{n} \cdot \left( \frac{\partial \mathbf{x}_0}{\partial S \partial t} - \overline{\mathbf{w}} \times \frac{\partial \mathbf{x}_0}{\partial S} \right) + \mathbf{m} \cdot \left( \bar{\dot{\boldsymbol{\omega}}} - \overline{\mathbf{w}} \times \boldsymbol{\omega} \right) \right] dS
\end{aligned} \qquad (2\text{-}41)$$

where $\mathbf{n}_0$, $\mathbf{n}_L$, $\mathbf{m}_0$, and $\mathbf{m}_L$ are concentrated forces and moments applied at the ends of the beam, $\tilde{\mathbf{n}}$ and $\tilde{\mathbf{m}}$ are the externally applied forces and moments per unit length. These are defined as:

$$\mathbf{n}_0 = -\mathbf{n}(0,t) \qquad \mathbf{m}_0 = -\mathbf{m}(0,t) \qquad (2\text{-}42)$$

$$\mathbf{n}_L = \mathbf{n}(L,t) \qquad \mathbf{m}_L = \mathbf{m}(L,t) \tag{2-43}$$

$$\tilde{\mathbf{n}}(S,t) = \iint_A \rho_0 \mathbf{B}\, dA + \oint_\Gamma \mathbf{P}\cdot\mathbf{N}\ d\Gamma \tag{2-44}$$

$$\tilde{\mathbf{m}}(S,t) = \iint_{A_0} (\mathbf{x}-\mathbf{x}_0)\times\rho_0\mathbf{B}\, dA + \oint_\Gamma (\mathbf{x}-\mathbf{x}_0)\times\mathbf{P}\cdot\mathbf{N}\ d\Gamma \tag{2-45}$$

## 2.5 Equations of motion

The equations of motion are obtained by integrating by parts the internal power term:

$$\iiint_{R_0} tr\left(\mathbf{P}^{\mathrm{T}}\cdot\dot{\bar{\mathbf{F}}}\right)dV = \int_0^L \left[\mathbf{n}\cdot\left(\frac{\partial^2 \mathbf{x}_0}{\partial S\partial t} - \bar{\mathbf{w}}\times\frac{\partial \mathbf{x}_0}{\partial S}\right) + \mathbf{m}\cdot\left(\dot{\bar{\boldsymbol{\omega}}} - \bar{\mathbf{w}}\times\boldsymbol{\omega}\right)\right]dS \tag{2-46}$$

It is proved in APPENDIX B that $\dot{\boldsymbol{\omega}} - \mathbf{w}\times\boldsymbol{\omega} = \mathbf{w}'$. Eq. (2-46) may then be written as:

$$\iiint_{R_0} tr\left(\mathbf{P}^{\mathrm{T}}\cdot\dot{\bar{\mathbf{F}}}\right)dV = \int_0^L \left[\mathbf{n}\cdot\left(\frac{\partial^2 \mathbf{x}_0}{\partial S\partial t} - \bar{\mathbf{w}}\times\frac{\partial \mathbf{x}_0}{\partial S}\right) + \mathbf{m}\cdot\bar{\mathbf{w}}'\right]dS \tag{2-47}$$

Integration by parts with respect to S then leads to:

$$\begin{aligned}\int_0^L \mathbf{n}\cdot\left(\frac{\partial \bar{\dot{\mathbf{x}}}_0}{\partial S} - \bar{\mathbf{w}}\times\frac{\partial \mathbf{x}_0}{\partial S}\right)dS + \int_0^L \mathbf{m}\cdot\frac{\partial \bar{\mathbf{w}}}{\partial S}dS = \left[\mathbf{n}\cdot\bar{\dot{\mathbf{x}}}_0\right]_0^L + \left[\mathbf{m}\cdot\bar{\mathbf{w}}\right]_0^L + \\ -\int_0^L \left(\frac{\partial \mathbf{n}}{\partial S}\cdot\bar{\dot{\mathbf{x}}}_0 + \mathbf{n}\cdot\bar{\mathbf{w}}\times\frac{\partial \mathbf{x}_0}{\partial S}\right)dS - \int_0^L \frac{\partial \mathbf{m}}{\partial S}\cdot\bar{\mathbf{w}}\, dS\end{aligned} \tag{2-48}$$

Using the permutation rule of the mixed product of three vectors, (2-48) may be written as:

$$\begin{aligned}\int_0^L \mathbf{n}\cdot\left(\frac{\partial \bar{\dot{\mathbf{x}}}_0}{\partial S} - \bar{\mathbf{w}}\times\frac{\partial \mathbf{x}_0}{\partial S}\right)dS + \int_0^L \mathbf{m}\cdot\frac{\partial \mathbf{w}}{\partial S}dS = \left[\mathbf{n}\cdot\bar{\dot{\mathbf{x}}}_0\right]_0^L + \left[\mathbf{m}\cdot\bar{\mathbf{w}}\right]_0^L + \\ -\int_0^L \left(\frac{\partial \mathbf{n}}{\partial S}\cdot\bar{\dot{\mathbf{x}}}_0 + \frac{\partial \mathbf{x}_0}{\partial S}\times\mathbf{n}\cdot\bar{\mathbf{w}}\right)dS - \int_0^L \frac{\partial \mathbf{m}}{\partial S}\cdot\bar{\mathbf{w}}\, dS\end{aligned} \tag{2-49}$$

We may now write the virtual power equation (2-41) as follows:

$$\begin{aligned}\int_0^L \left\{\left[\frac{\partial \mathbf{n}}{\partial S} + \tilde{\mathbf{n}} - A_\rho\ddot{\mathbf{x}}_0\right]\cdot\bar{\dot{\mathbf{x}}}_0 + \left[\frac{\partial \mathbf{m}}{\partial S} + \frac{\partial \mathbf{x}_0}{\partial S}\times\mathbf{n} + \tilde{\mathbf{m}} - \mathbf{I}_\rho\cdot\dot{\mathbf{w}} - \mathbf{w}\times\left(\mathbf{I}_\rho\cdot\mathbf{w}\right)\right]\cdot\bar{\mathbf{w}}\right\}dS + \\ \left[\mathbf{n}_0(t) + \mathbf{n}(0,t)\right]\cdot\bar{\dot{\mathbf{x}}}_0(0,t) + \left[\mathbf{m}_0(t) + \mathbf{m}(0,t)\right]\cdot\bar{\mathbf{w}}(0,t) + \\ \left[\mathbf{n}_L(t) - \mathbf{n}(L,t)\right]\cdot\bar{\dot{\mathbf{x}}}_0(L,t) + \left[\mathbf{m}_L(t) - \mathbf{m}(L,t)\right]\cdot\bar{\mathbf{w}}(L,t) = 0\end{aligned} \tag{2-50}$$

Since (2-50) holds for any velocity field $\left(\bar{\dot{\mathbf{x}}}_0, \bar{\mathbf{w}}\right)$, the following equilibrium equations and boundary conditions are obtained:

$$\frac{\partial \mathbf{n}}{\partial S} + \tilde{\mathbf{n}} = A_\rho \ddot{\mathbf{x}}_0 \tag{2-51}$$

$$\frac{\partial \mathbf{m}}{\partial S} + \frac{\partial \mathbf{x}_0}{\partial S} \times \mathbf{n} + \tilde{\mathbf{m}} = \mathbf{I}_\rho \cdot \dot{\mathbf{w}} + \mathbf{w} \times \left( \mathbf{I}_\rho \cdot \mathbf{w} \right) \tag{2-52}$$

$$\mathbf{n}_0 \left( t \right) + \mathbf{n}\left( 0, t \right) = \mathbf{0} \tag{2-53}$$

$$\mathbf{m}_0 \left( t \right) + \mathbf{m}\left( 0, t \right) = \mathbf{0} \tag{2-54}$$

$$\mathbf{n}_L \left( t \right) - \mathbf{n}\left( L, t \right) = \mathbf{0} \tag{2-55}$$

$$\mathbf{m}_L \left( t \right) - \mathbf{m}\left( L, t \right) = \mathbf{0} \tag{2-56}$$

### 2.5.1 Strain and strain rate measures

We may rewrite the internal power (2-37) as:

$$\iiint_{R_0} tr\left( \mathbf{P}^{\mathrm{T}} \cdot \dot{\mathbf{F}} \right) dV = \int_0^L \left( \mathbf{n} \cdot \overset{\triangledown}{\boldsymbol{\gamma}} + \mathbf{m} \cdot \overset{\triangledown}{\boldsymbol{\omega}} \right) dS \tag{2-57}$$

where $\overset{\triangledown}{\boldsymbol{\gamma}}$ and $\overset{\triangledown}{\boldsymbol{\omega}}$ represent the following objective rates:

$$\overset{\triangledown}{\boldsymbol{\gamma}} = \frac{\partial^2 \mathbf{x}_0}{\partial S \partial t} - \mathbf{w} \times \frac{\partial \mathbf{x}_0}{\partial S} = \frac{\partial}{\partial t}\left( \frac{\partial \mathbf{x}_0}{\partial S} - \mathbf{t}_3 \right) - \mathbf{w} \times \left( \frac{\partial \mathbf{x}_0}{\partial S} - \mathbf{t}_3 \right) = \dot{\boldsymbol{\gamma}} - \mathbf{w} \times \boldsymbol{\gamma} \tag{2-58}$$

$$\overset{\triangledown}{\boldsymbol{\omega}} = \dot{\boldsymbol{\omega}} - \mathbf{w} \times \boldsymbol{\omega} \tag{2-59}$$

and $\boldsymbol{\gamma}$ is the *current shear-axial strain vector* given by:

$$\boldsymbol{\gamma}\left( S, t \right) = \frac{\partial \mathbf{x}_0}{\partial S}\left( S, t \right) - \mathbf{t}_3 \left( S, t \right) \tag{2-60}$$

The internal power may be recast in terms of the reference configuration fields $\mathbf{N} = \mathbf{R}^{\mathrm{T}} \cdot \mathbf{n}$ and $\mathbf{M} = \mathbf{R}^{\mathrm{T}} \cdot \mathbf{m}$ as:

$$\begin{aligned} \iiint_{R_0} tr\left( \mathbf{P}^{\mathrm{T}} \cdot \dot{\mathbf{F}} \right) dV &= \int_0^L \left( \mathbf{n} \cdot \overset{\triangledown}{\boldsymbol{\gamma}} + \mathbf{m} \cdot \overset{\triangledown}{\boldsymbol{\omega}} \right) dS = \int_0^L \left( \mathbf{R} \cdot \mathbf{N} \cdot \overset{\triangledown}{\boldsymbol{\gamma}} + \mathbf{R} \cdot \mathbf{M} \cdot \overset{\triangledown}{\boldsymbol{\omega}} \right) dS = \\ &\int_0^L \left( \mathbf{N} \cdot \mathbf{R}^{\mathrm{T}} \cdot \overset{\triangledown}{\boldsymbol{\gamma}} + \mathbf{M} \cdot \mathbf{R}^{\mathrm{T}} \cdot \overset{\triangledown}{\boldsymbol{\omega}} \right) dS = \int_0^L \left[ \mathbf{N} \cdot \dot{\boldsymbol{\Gamma}} + \mathbf{M} \cdot \dot{\boldsymbol{\Omega}} \right] dS \end{aligned} \tag{2-61}$$

where $\dot{\boldsymbol{\Gamma}} = \mathbf{R}^{\mathrm{T}} \cdot \overset{\triangledown}{\boldsymbol{\gamma}}$ and $\dot{\boldsymbol{\Omega}} = \mathbf{R}^{\mathrm{T}} \cdot \overset{\triangledown}{\boldsymbol{\omega}}$ are the reference strain rate measures of $\boldsymbol{\Gamma}$ and $\boldsymbol{\Omega}$, which are defined as:

$$\mathbf{\Gamma} = \mathbf{R}^{\mathrm{T}} \cdot \boldsymbol{\gamma} = \mathbf{R}^{\mathrm{T}} \cdot \frac{\partial \mathbf{x}_0}{\partial S} - \mathbf{E}_3 \tag{2-62}$$

$$\mathbf{\Omega} = \mathbf{R}^{\mathrm{T}} \cdot \boldsymbol{\omega} \tag{2-63}$$

The above expressions for $\dot{\mathbf{\Gamma}}$ and $\dot{\mathbf{\Omega}}$ can be obtained from (2-62) and (2-63) as follows. Taking the time derivative of $\mathbf{\Gamma}$ yields:

$$\dot{\mathbf{\Gamma}} = \left(\dot{\mathbf{R}}\right)^{\mathrm{T}} \cdot \frac{\partial \mathbf{x}_0}{\partial S} + \mathbf{R}^{\mathrm{T}} \cdot \frac{\partial^2 \mathbf{x}_0}{\partial S \partial t} \tag{2-64}$$

Substituting Eq. (2-18) into Eq. (2-64) gives:

$$\begin{aligned} \dot{\mathbf{\Gamma}} &= \left(\hat{\mathbf{w}} \cdot \mathbf{R}\right)^{\mathrm{T}} \cdot \frac{\partial \mathbf{x}_0}{\partial S} + \mathbf{R}^{\mathrm{T}} \cdot \frac{\partial^2 \mathbf{x}_0}{\partial S \partial t} = \mathbf{R}^{\mathrm{T}} \cdot \hat{\mathbf{w}}^{\mathrm{T}} \cdot \frac{\partial \mathbf{x}_0}{\partial S} + \mathbf{R}^{\mathrm{T}} \cdot \frac{\partial^2 \mathbf{x}_0}{\partial S \partial t} = \\ & -\mathbf{R}^{\mathrm{T}} \cdot \hat{\mathbf{w}} \cdot \frac{\partial \mathbf{x}_0}{\partial S} + \mathbf{R}^{\mathrm{T}} \cdot \frac{\partial^2 \mathbf{x}_0}{\partial S \partial t} = \mathbf{R}^{\mathrm{T}} \cdot \left( \frac{\partial^2 \mathbf{x}_0}{\partial S \partial t} - \mathbf{w} \times \frac{\partial \mathbf{x}_0}{\partial S} \right) = \mathbf{R}^{\mathrm{T}} \cdot \overset{\nabla}{\boldsymbol{\gamma}} \end{aligned} \tag{2-65}$$

Taking the time derivative of $\mathbf{\Omega}$ yields:

$$\begin{aligned} \dot{\mathbf{\Omega}} &= \left(\dot{\mathbf{R}}\right)^{\mathrm{T}} \cdot \boldsymbol{\omega} + \mathbf{R}^{\mathrm{T}} \cdot \dot{\boldsymbol{\omega}} = \left(\hat{\mathbf{w}} \cdot \mathbf{R}\right)^{\mathrm{T}} \cdot \boldsymbol{\omega} + \mathbf{R}^{\mathrm{T}} \cdot \dot{\boldsymbol{\omega}} = \mathbf{R}^{\mathrm{T}} \cdot \hat{\mathbf{w}}^{\mathrm{T}} \cdot \boldsymbol{\omega} + \mathbf{R}^{\mathrm{T}} \cdot \dot{\boldsymbol{\omega}} = \\ & -\mathbf{R}^{\mathrm{T}} \cdot \hat{\mathbf{w}} \cdot \boldsymbol{\omega} + \mathbf{R}^{\mathrm{T}} \cdot \dot{\boldsymbol{\omega}} = \mathbf{R}^{\mathrm{T}} \cdot \left(\dot{\boldsymbol{\omega}} - \mathbf{w} \times \boldsymbol{\omega}\right) = \mathbf{R}^{\mathrm{T}} \cdot \overset{\nabla}{\boldsymbol{\omega}} \end{aligned} \tag{2-66}$$

## 2.6 Constitutive equations

As generally done in the literature, we assume large deformations but locally small strains so that the elastic forces and moments in the reference configuration, namely $\mathbf{N}^{\mathrm{e}}$ and $\mathbf{M}^{\mathrm{e}}$, are linearly proportional to the corresponding strains $\mathbf{\Gamma}$, and curvatures $\mathbf{\Omega}$, through a constant and diagonal elasticity tensor $\mathbf{C}$ defined as:

$$\mathbf{C} = \mathrm{diag}\left[\mathbf{C}^{\mathrm{N}}, \mathbf{C}^{\mathrm{M}}\right] \tag{2-67}$$

where

$$\mathbf{C}^{\mathrm{N}} = \mathrm{diag}\left[GA_1, GA_2, EA\right] \qquad \mathbf{C}^{\mathrm{M}} = \left[EI_1, EI_2, GJ_t\right] \tag{2-68}$$

In (2-68), E is the Young's modulus, G is the shear modulus, A is the area of the rigid cross-section, $A_1$ and $A_2$ are effective cross-section areas for shearing, $I_1$ and $I_2$ are the second moments of area of the cross-section, and $J_t$ is the torsion constant. It may be worth noticing that (2-67) and (2-68) assume that the reference frame and the moving frame are principal axes of the cross-section. Furthermore, slightly more general expressions could be used to account for axial and torsional coupling.

Building on the work of Antman (1996; 2003) on nonlinearly viscoelastic rods, Lang et al. (2011) recently introduced viscous material damping into a quaternionic reformulation of Simo's beam model. Here we use the same Kelvin-Voigt damping model to account for energy dissipation, but introduce it directly into the formulation developed by Simo. The internal dissipative forces and moments in the reference configuration, namely $\mathbf{N}^{\mathrm{d}}$ and $\mathbf{M}^{\mathrm{d}}$, are taken as linearly proportional to the corresponding strain rate $\dot{\mathbf{\Gamma}}$ and curvature rate $\dot{\mathbf{\Omega}}$ through a constant tensor $\mathbf{C}_{\mathrm{d}}$ defined as:

$$\mathbf{C}_{\mathrm{d}} = \mathrm{diag}\left[\mathbf{C}_{\mathrm{d}}^{\mathrm{N}}, \mathbf{C}_{\mathrm{d}}^{\mathrm{M}}\right] \tag{2-69}$$

where

$$\mathbf{C}_{\mathrm{d}}^{\mathrm{N}} = \mathrm{diag}\left[\mu GA_1, \mu GA_2, \eta EA\right] \qquad \mathbf{C}_{\mathrm{d}}^{\mathrm{M}} = \left[\eta EI_1, \eta EI_2, \mu GJ_t\right] \tag{2-70}$$

where $\eta$ and $\mu$ are retardation time constants transforming the elastic moduli $E$ and $G$ into viscous constants, akin to stiffness proportional damping coefficients.

Thus, the constitutive equations, relating the total internal forces to their corresponding strains and strain rates, and the total internal moments to their corresponding curvatures and curvature rates, are given by:

$$\mathbf{N} = \mathbf{N}^{\mathrm{e}} + \mathbf{N}^{\mathrm{d}} = \mathbf{C}^{\mathrm{N}} \cdot \mathbf{\Gamma} + \mathbf{C}_{\mathrm{d}}^{\mathrm{N}} \cdot \dot{\mathbf{\Gamma}} \tag{2-71}$$

$$\mathbf{M} = \mathbf{M}^{\mathrm{e}} + \mathbf{M}^{\mathrm{d}} = \mathbf{C}^{\mathrm{M}} \cdot \mathbf{\Omega} + \mathbf{C}_{\mathrm{d}}^{\mathrm{M}} \cdot \dot{\mathbf{\Omega}} \tag{2-72}$$

Subsequently, the constitutive equations (2-71) and (2-72) are introduced in the weak form of the equations of motion to set the stage for the derivation of a tangent damping operator.

## 2.7 Weak form of the equations of motion

Following Simo (1986) and Simo and Vu-Quoc (1988), the weak form of the equations of motion is obtained by multiplying the equilibrium equations (2-51) and (2-52) by an admissible variation $\boldsymbol{\eta} = \left(\boldsymbol{\eta}_u, \boldsymbol{\eta}_\theta\right)$:

$$\begin{aligned} G\left(\boldsymbol{\varphi}, \boldsymbol{\eta}\right) = &\int_0^L \left[\left(\frac{\partial \mathbf{n}}{\partial S} + \tilde{\mathbf{n}}\right) \cdot \boldsymbol{\eta}_u + \left(\frac{\partial \mathbf{m}}{\partial S} + \frac{\partial \mathbf{x}_0}{\partial S} \times \mathbf{n} + \tilde{\mathbf{m}}\right) \cdot \boldsymbol{\eta}_\theta\right] dS + \\ &-\int_0^L \left\{A_\rho \ddot{\mathbf{x}}_0 \cdot \boldsymbol{\eta}_u + \left[\mathbf{I}_\rho \cdot \dot{\mathbf{w}} + \mathbf{w} \times \left(\mathbf{I}_\rho \cdot \mathbf{w}\right)\right] \cdot \boldsymbol{\eta}_\theta\right\} dS = 0 \end{aligned} \tag{2-73}$$

If $\boldsymbol{\varphi}(S,t)=\left[\mathbf{x}_0(S,t),\mathbf{R}(S,t)\right]$ represents an arbitrary configuration, $\boldsymbol{\eta}_u$ can be interpreted as a superposed infinitesimal displacement on the line of centroids $\mathbf{x}_0$, and $\boldsymbol{\eta}_\theta$ as a superposed infinitesimal rotation onto the moving frame defined by **R**.

Integration by parts of the first integral of (2-73) leads to the following weak form of the equilibrium equations:

$$
\begin{aligned}
G(\boldsymbol{\varphi},\boldsymbol{\eta}) = & \int_0^L \left[ \mathbf{n}\cdot\left(\frac{\partial \boldsymbol{\eta}_u}{\partial S} - \boldsymbol{\eta}_\theta \times \frac{\partial \mathbf{x}_0}{\partial S}\right) + \mathbf{m}\cdot\frac{\partial \boldsymbol{\eta}_\theta}{\partial S}\right] dS - \int_0^L \left(\tilde{\mathbf{n}}\cdot\boldsymbol{\eta}_u + \tilde{\mathbf{m}}\cdot\boldsymbol{\eta}_\theta\right) dS + \\
& \int_0^L \left\{ A_\rho \ddot{\mathbf{x}}_0\cdot\boldsymbol{\eta}_u + \left[\mathbf{I}_\rho\cdot\dot{\mathbf{w}} + \mathbf{w}\times\left(\mathbf{I}_\rho\cdot\mathbf{w}\right)\right]\cdot\boldsymbol{\eta}_\theta \right\} dS = 0
\end{aligned}
\tag{2-74}
$$

Introducing quantities defined in the reference frame, (2-74) may be recast as:

$$
\begin{aligned}
G(\boldsymbol{\varphi},\boldsymbol{\eta}) = & \int_0^L \left[ \left(\frac{\partial \boldsymbol{\eta}_u}{\partial S} - \boldsymbol{\eta}_\theta \times \frac{\partial \mathbf{x}_0}{\partial S}\right)\cdot\mathbf{R}\cdot\mathbf{N} + \frac{\partial \boldsymbol{\eta}_\theta}{\partial S}\cdot\mathbf{R}\cdot\mathbf{M}\right] dS - \int_0^L \left(\tilde{\mathbf{n}}\cdot\boldsymbol{\eta}_u + \tilde{\mathbf{m}}\cdot\boldsymbol{\eta}_\theta\right) dS + \\
& \int_0^L \left\{ A_\rho \ddot{\mathbf{x}}_0\cdot\boldsymbol{\eta}_u + \mathbf{R}\cdot\left[\mathbf{J}_\rho\cdot\dot{\mathbf{W}} + \mathbf{W}\times\left(\mathbf{J}_\rho\cdot\mathbf{W}\right)\right]\cdot\boldsymbol{\eta}_\theta \right\} dS = 0
\end{aligned}
\tag{2-75}
$$

where $\mathbf{J}_\rho = \mathbf{R}^\mathbf{T}\cdot\mathbf{I}_\rho\cdot\mathbf{R}$ is the time-independent *reference inertia tensor* and $\mathbf{W}=\mathbf{R}^\mathbf{T}\cdot\mathbf{w}$ is the *reference angular velocity vector*.

Linearization and discretization are needed to solve the weak form, Eq. (2-75), by Newton's method. We point out that, because of the nonlinear nature of finite rotations, linearization and spatial discretization generally do not commute. However, following Simo and Vu-Quoc (1986;1988), we choose to first linearize and then discretize. Before doing so, in the next subsections we describe the time integration and configuration update schemes used in the numerical implementation and needed in the linearization process.

## 2.8 Time integration algorithm

Given the configuration $\boldsymbol{\varphi}_n\left(\mathbf{x}_{0,n},\mathbf{R}_n\right)$ at time $t_n$, the problem of finding the configuration $\boldsymbol{\varphi}_{n+1}\left(\mathbf{x}_{0,n+1},\mathbf{R}_{n+1}\right)$ at time $t_{n+1} = t_n + h$ is dealt with by an extension to large rotations of Newmark's time integration algorithm. This is summarized in Table 2-1 (Simo and Vu-Quoc 1988), where the notation $\mathbf{v}_0 = \dot{\mathbf{x}}_0$, $\mathbf{a}_0 = \dot{\mathbf{v}}_0 = \ddot{\mathbf{x}}_0$, and $\mathbf{A} = \dot{\mathbf{W}}$ is used.

**Table 2-1 Time integration algorithm**

| Translation | Rotation |
|---|---|
| $\mathbf{x}_{0,n+1}=\mathbf{x}_{0,n}+\mathbf{u}_n$ | $\mathbf{R}_{n+1}=\mathbf{R}_n\cdot\exp(\hat{\mathbf{\Theta}}_n)=\exp(\hat{\mathbf{\theta}}_n)\cdot\mathbf{R}_n$ |
| $\mathbf{u}_n=h\mathbf{v}_{0,n}+h^2[(0.5-\beta)\mathbf{a}_{0,n}+\beta\mathbf{a}_{0,n+1}]$ | $\mathbf{\Theta}_n=h\mathbf{W}_n+h^2[(0.5-\beta)\mathbf{A}_n+\beta\mathbf{A}_{n+1}]$ |
| $\mathbf{v}_{0,n+1}=\mathbf{v}_{0,n}+h[(1-\gamma)\mathbf{a}_{0,n}+\gamma\mathbf{a}_{0,n+1}]$ | $\mathbf{W}_{n+1}=\mathbf{W}_n+h[(1-\gamma)\mathbf{A}_n+\gamma\mathbf{A}_{n+1}]$ |

In Table 2-1, $\hat{\mathbf{\Theta}}_n$ is a *reference* skew symmetric tensor related to the *current* skew symmetric tensor $\hat{\mathbf{\theta}}_n$ by:

$$\hat{\mathbf{\theta}}_n = \mathbf{R}\cdot\hat{\mathbf{\Theta}}_n\cdot\mathbf{R}^{\mathrm{T}} \qquad \hat{\mathbf{\Theta}}_n = \mathbf{R}^{\mathrm{T}}\cdot\hat{\mathbf{\theta}}_n\cdot\mathbf{R} \tag{2-76}$$

Moreover, the associated axial vectors $\mathbf{\Theta}_n$ and $\mathbf{\theta}_n$ are related by:

$$\mathbf{\theta}_n = \mathbf{R}\cdot\mathbf{\Theta}_n \qquad \mathbf{\Theta}_n = \mathbf{R}^{\mathrm{T}}\cdot\mathbf{\theta}_n \tag{2-77}$$

### 2.8.1 Configuration update

Owing to the nonlinear nature of the implicit time integration scheme, the weak form of the equations of motion $G(\mathbf{\varphi}_{n+1},\mathbf{\eta})=0$ is a nonlinear variational equation, and its solution is achieved by an iterative procedure of the Newton type. The Newton iteration counter is denoted by the superscript i and it is assumed that $\mathbf{\varphi}_{n+1}^{(i)}\left(\mathbf{x}_{0,n+1}^{(i)},\mathbf{R}_{n+1}^{(i)}\right)$ is known. By solving the linearized weak form about $\mathbf{\varphi}_{n+1}^{(i)}$, one obtains the incremental displacement and rotation fields $\mathbf{\Delta\varphi}_{n+1}^{(i)}\left(\mathbf{\delta}u_{n+1}^{(i)},\mathbf{\delta\theta}_{n+1}^{(i)}\right)$ . Given $\mathbf{\Delta\varphi}_{n+1}^{(i)}$, our goal is to update $\mathbf{\varphi}_{n+1}^{(i)}$ to $\mathbf{\varphi}_{n+1}^{(i+1)}$ in a way that is consistent with the time integration algorithm given in Table 2.1. The update procedure is summarized in Table 2-2 (see Simo and Vu-Quoc (1988)), and a geometric interpretation is presented in Figure 2-2. The update of the linear displacements, velocities and accelerations is performed in standard fashion. The update of the incremental rotation is however more involved.

To obtain the expressions presented in Table 2-2 we first write:

$$\mathbf{R}_{n+1}^{(i)} = \exp\left[\hat{\boldsymbol{\theta}}_n^{(i)}\right]\cdot\mathbf{R}_n \qquad \mathbf{R}_{n+1}^{(i+1)} = \exp\left[\hat{\boldsymbol{\theta}}_n^{(i+1)}\right]\cdot\mathbf{R}_n \tag{2-78}$$

**Table 2-2 Update procedure**

| **Translation** | **Rotation** |
|---|---|
| $\mathbf{x}_{0,n+1}^{(i+1)} = \mathbf{x}_{0,n+1}^{(i)} + \boldsymbol{\delta}\mathbf{u}_{n+1}^{(i)}$ | $\mathbf{R}_{n+1}^{(i+1)} = \exp\left(\boldsymbol{\delta\theta}_{n+1}^{(i)}\right)\cdot\mathbf{R}_{n+1}^{(i)}$ |
| $\mathbf{v}_{0,n+1}^{(i+1)} = \mathbf{v}_{0,n+1}^{(i)} + \dfrac{\gamma}{\beta h}\boldsymbol{\delta}\mathbf{u}_{n+1}^{(i)}$ | $\exp\left[\hat{\boldsymbol{\theta}}_n^{(i+1)}\right] = \exp\left[\boldsymbol{\delta}\hat{\boldsymbol{\theta}}_{n+1}^{(i)}\right]\cdot\exp\left[\hat{\boldsymbol{\theta}}_n^{(i)}\right]$ |
| $\mathbf{a}_{0,n+1}^{(i+1)} = \mathbf{a}_{0,n+1}^{(i)} + \dfrac{1}{\beta h^2}\boldsymbol{\delta}\mathbf{u}_{n+1}^{(i)}$ | $\mathbf{W}_{n+1}^{(i+1)} = \mathbf{W}_{n+1}^{(i)} + \dfrac{\gamma}{\beta h}\left[\boldsymbol{\Theta}_n^{(i+1)} - \boldsymbol{\Theta}_n^{(i)}\right]$ |
| | $\mathbf{A}_{n+1}^{(i+1)} = \mathbf{A}_{n+1}^{(i)} + \dfrac{1}{\beta h^2}\left[\boldsymbol{\Theta}_n^{(i+1)} - \boldsymbol{\Theta}_n^{(i)}\right]$ |

Next, we write:

$$\mathbf{R}_{n+1}^{(i+1)} = \exp\left[\boldsymbol{\delta}\hat{\boldsymbol{\theta}}_{n+1}^{(i)}\right]\cdot\mathbf{R}_{n+1}^{(i)} \tag{2-79}$$

Equating the right-hand side of the second of (2-78) to the right-hand side of (2-79) gives:

$$\exp\left[\hat{\boldsymbol{\theta}}_n^{(i+1)}\right]\cdot\mathbf{R}_n = \exp\left[\boldsymbol{\delta}\hat{\boldsymbol{\theta}}_{n+1}^{(i)}\right]\cdot\mathbf{R}_{n+1}^{(i)} \tag{2-80}$$

Now substituting the first of (2-78) into the right-hand side of (2-80) leads to:

$$\exp\left[\hat{\boldsymbol{\theta}}_n^{(i+1)}\right]\cdot\mathbf{R}_n = \exp\left[\boldsymbol{\delta}\hat{\boldsymbol{\theta}}_{n+1}^{(i)}\right]\cdot\exp\left[\hat{\boldsymbol{\theta}}_n^{(i)}\right]\cdot\mathbf{R}_n \tag{2-81}$$

From (2-81) we finally obtain:

$$\exp\left[\hat{\boldsymbol{\theta}}_n^{(i+1)}\right] = \exp\left[\boldsymbol{\delta}\hat{\boldsymbol{\theta}}_{n+1}^{(i)}\right]\cdot\exp\left[\hat{\boldsymbol{\theta}}_n^{(i)}\right] \tag{2-82}$$

Equations (2-79) and (2-82) are the expressions included in Table 2-2. Following Simo and Vu-Quoc (1988), we picked $\mathbf{R}_{n+1}$ as unknown and, as shown in Table 2-2, this choice requires the extraction of the rotation vector, $\boldsymbol{\theta}_n$, from the exponential map. Notably, this would not be needed if the rotational velocity, $\mathbf{W}_{n+1}$, rather than $\mathbf{R}_{n+1}$, were selected as unknown. Whereas with the former choice Newton's method is applied to the Lie group SO(3), the latter choice leads to the Lie algebra method (Owren and Welfert, 2000).

### 2.8.2 Velocities and accelerations updates

The update of velocities and accelerations in the Newton iteration process is obtained by exploiting the time integration formulas contained in Table 2-1. For time step $t_{n+1}$, at iterations $i$ and $i$+1, we have:

$$\boldsymbol{\Theta}_n^{(i+1)} = h\mathbf{W}_n + h^2\left[\left(\frac{1}{2}-\beta\right)\mathbf{A}_n + \beta\mathbf{A}_{n+1}^{(i+1)}\right] \tag{2-83}$$

$$\boldsymbol{\Theta}_n^{(i)} = h\mathbf{W}_n + h^2\left[\left(\frac{1}{2}-\beta\right)\mathbf{A}_n + \beta\mathbf{A}_{n+1}^{(i)}\right] \tag{2-84}$$

Subtracting (2-84) from (2-83) gives:

$$\mathbf{A}_{n+1}^{(i+1)} = \mathbf{A}_{n+1}^{(i)} + \frac{1}{\beta h^2}\left[\boldsymbol{\Theta}_{n+1}^{(i+1)} - \boldsymbol{\Theta}_{n+1}^{(i)}\right] \tag{2-85}$$

Similarly, for the angular velocity at time step $t_{n+1}$, and iterations $i$ and $i$+1, we have:

$$\mathbf{W}_{n+1}^{(i+1)} = \mathbf{W}_n + h\left[(1-\gamma)\mathbf{A}_n + \gamma\mathbf{A}_{n+1}^{(i+1)}\right] \tag{2-86}$$

$$\mathbf{W}_{n+1}^{(i)} = \mathbf{W}_n + h\left[(1-\gamma)\mathbf{A}_n + \gamma\mathbf{A}_{n+1}^{(i)}\right] \tag{2-87}$$

Subtracting (2-87) from (2-86), and using (2-85), we get:

$$\mathbf{W}_{n+1}^{(i+1)} = \mathbf{W}_{n+1}^{(i)} + \frac{\gamma}{\beta h}\left[\boldsymbol{\Theta}_{n+1}^{(i+1)} - \boldsymbol{\Theta}_{n+1}^{(i)}\right] \tag{2-88}$$

Equations (2-88) and (2-85) are the expressions included in Table 2-2. The update formulae for linear velocities and accelerations are obtained in the same fashion.

### 2.8.3 Remarks on configuration update

The update procedure in Table 2-2 is applied for $i \geq 1$. For $i = 0$, we set $\mathbf{x}_{0,n+1}^{(0)} = \mathbf{x}_n$, and $\mathbf{R}_{n+1}^{(0)} = \mathbf{R}_n$, as the initial guess in the Newton process. We then compute $\mathbf{v}_{0,n+1}^{(0)}$, $\mathbf{a}_{0,n+1}^{(0)}$, $\mathbf{W}_{n+1}^{(0)}$ and $\mathbf{A}_{n+1}^{(0)}$ from the time integration scheme formulae given in Table 2-1 as follows:

$$\mathbf{v}_{0,n+1}^{(0)} = \left(1-\frac{\gamma}{\beta}\right)\mathbf{v}_{0.n} + h\left(1-\frac{\gamma}{2\beta}\right)\mathbf{a}_{0,n} \qquad \mathbf{W}_{n+1}^{(0)} = \left(1-\frac{\gamma}{\beta}\right)\mathbf{W}_n + h\left(1-\frac{\gamma}{2\beta}\right)\mathbf{A}_n \tag{2-89}$$

$$\mathbf{a}_{0,n+1}^{(0)} = -\frac{1}{\beta h}\mathbf{v}_{0.n} - \frac{1}{\beta}\left(\frac{1}{2}-\beta\right)\mathbf{a}_{0,n} \qquad \mathbf{A}_{n+1}^{(0)} = -\frac{1}{\beta h}\mathbf{W}_n - \frac{1}{\beta}\left(\frac{1}{2}-\beta\right)\mathbf{A}_n \tag{2-90}$$

Other starting procedures, such as $\left(\mathbf{v}_{0,n+1}^{(0)}, \mathbf{a}_{0,n+1}^{(0)}\right) = \left(\mathbf{v}_{0,n}, \mathbf{a}_{0,n}\right)$ and $\left(\mathbf{W}_{n+1}^{(0)}, \mathbf{A}_{n+1}^{(0)}\right) = \left(\mathbf{W}_{0,n}, \mathbf{A}_{0,n}\right)$, often result in spurious behavior.

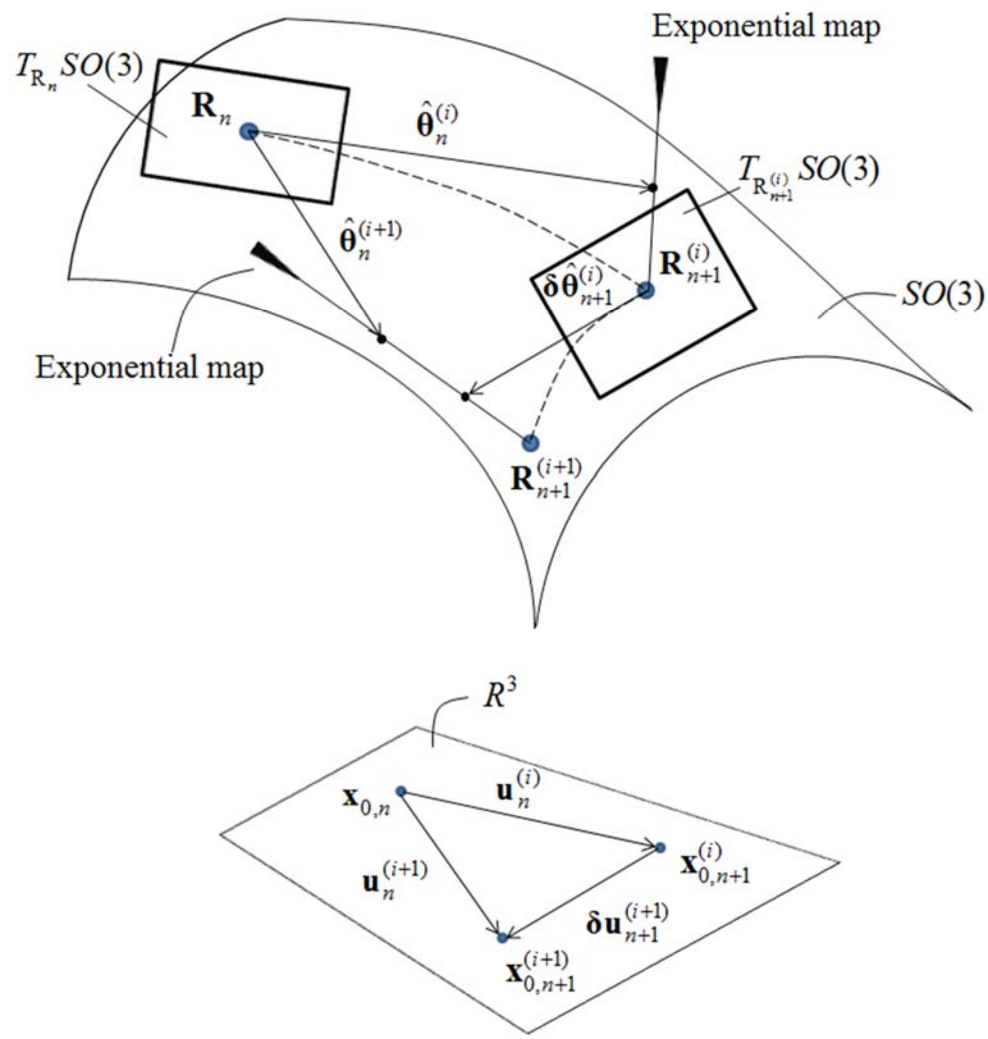


**Figure 2-2 Geometric interpretation of the incremental iterative update procedure**

## 2.9 Linearization of the weak form

Writing the weak form of the equations of motion, given by (2-75), at configuration $\left(\boldsymbol{\varphi}_{n+1}^{(i)}, \boldsymbol{\eta}\right)$, and using the notation $\mathbf{a}_0 = \ddot{\mathbf{x}}_0$ and $\mathbf{A} = \dot{\mathbf{W}}$, we get:

$$
\begin{aligned}
G\left(\boldsymbol{\varphi}_{n+1}^{(i)},\boldsymbol{\eta}\right) &= \int_0^L \left[\left(\frac{\partial \boldsymbol{\eta}_u}{\partial S} - \boldsymbol{\eta}_\theta \times \frac{\partial \mathbf{x}_{0,n+1}^{(i)}}{\partial S}\right)\cdot \mathbf{R}_{n+1}^{(i)} \cdot \mathbf{N}_{n+1}^{(i)} + \frac{\partial \boldsymbol{\eta}_\theta}{\partial S}\cdot \mathbf{R}_{n+1}^{(i)} \cdot \mathbf{M}_{n+1}^{(i)}\right] dS + \\
&- \int_0^L \left(\tilde{\mathbf{n}}\cdot\boldsymbol{\eta}_u + \tilde{\mathbf{m}}\cdot\boldsymbol{\eta}_\theta\right) dS + \int_0^L \left\{A_\rho \mathbf{a}_{0,n+1}^{(i)}\cdot\boldsymbol{\eta}_u + \mathbf{R}_{n+1}^{(i)}\cdot\left[\mathbf{J}_\rho \cdot \mathbf{A}_{n+1}^{(i)} + \mathbf{W}_{n+1}^{(i)} \times \left(\mathbf{J}_\rho \cdot \mathbf{W}_{n+1}^{(i)}\right)\right]\cdot \boldsymbol{\eta}_\theta\right\} dS = 0
\end{aligned}
\tag{2-91}
$$

The linear part of (2-91) is then given by:

$$
L\left[G\left(\boldsymbol{\varphi}_{n+1}^{(i)},\boldsymbol{\eta}\right)\right] = G\left(\boldsymbol{\varphi}_{n+1}^{(i)},\boldsymbol{\eta}\right) + \delta G\left(\boldsymbol{\varphi}_{n+1}^{(i)},\boldsymbol{\eta}\right) \tag{2-92}
$$

where $G\left(\boldsymbol{\varphi}_{n+1}^{(i)},\boldsymbol{\eta}\right)$ represents the unbalanced force at configuration $\left(\boldsymbol{\varphi}_{n+1}^{(i)},\boldsymbol{\eta}\right)$, while the term $\delta G\left(\boldsymbol{\varphi}_{n+1}^{(i)},\boldsymbol{\eta}\right)$, linear in the incremental displacement field $\boldsymbol{\Delta\varphi}_{n+1}^{(i)}\left(\boldsymbol{\delta u}_{n+1}^{(i)},\boldsymbol{\delta\theta}_{n+1}^{(i)}\right)$, leads to the definition of a tangent operator as follows:

$$
\delta G\left(\boldsymbol{\varphi}_{n+1}^{(i)},\boldsymbol{\eta}\right) = \delta G_M\left(\boldsymbol{\varphi}_{n+1}^{(i)},\boldsymbol{\eta}\right) + \delta G_G\left(\boldsymbol{\varphi}_{n+1}^{(i)},\boldsymbol{\eta}\right) + \delta G_D\left(\boldsymbol{\varphi}_{n+1}^{(i)},\boldsymbol{\eta}\right) + \delta G_I\left(\boldsymbol{\varphi}_{n+1}^{(i)},\boldsymbol{\eta}\right) \tag{2-93}
$$

Each term on the right hand side of (2-93) represents a different part of the tangent operator, namely the material and geometric stiffness parts, the damping part and the inertia part. In the following, we will evaluate each term separately. To alleviate the notation, we drop the subscript $n$+1 denoting that a quantity is evaluated at time $t_{n+1}$, and the superscript $i$ denoting the Newton iteration counter.

### 2.9.1 Tangent material stiffness operator

We recall that the internal forces **N** and **M** have been decomposed into their elastic and dissipative components as:

$$
\mathbf{N} = \mathbf{N}^{\mathrm{e}} + \mathbf{N}^{\mathrm{d}} \tag{2-94}
$$

$$
\mathbf{M} = \mathbf{M}^{\mathrm{e}} + \mathbf{M}^{\mathrm{d}} \tag{2-95}
$$

Therefore, substitution of (2-94) and (2-95) into (2-91) gives:

$$
\begin{aligned}
G(\boldsymbol{\varphi},\boldsymbol{\eta}) &= \int_0^L \left[\left(\frac{\partial \boldsymbol{\eta}_u}{\partial S} - \boldsymbol{\eta}_\theta \times \frac{\partial \mathbf{x}_0}{\partial S}\right)\cdot \mathbf{R}\cdot\left(\mathbf{N}^{\mathrm{e}} + \mathbf{N}^{\mathrm{d}}\right) + \frac{\partial \boldsymbol{\eta}_\theta}{\partial S}\cdot \mathbf{R}\cdot\left(\mathbf{M}^{\mathrm{e}} + \mathbf{M}^{\mathrm{d}}\right)\right] dS + \\
&- \int_0^L \left(\tilde{\mathbf{n}}\cdot\boldsymbol{\eta}_u + \tilde{\mathbf{m}}\cdot\boldsymbol{\eta}_\theta\right) dS + \int_0^L \left\{A_\rho \mathbf{a}_0\cdot\boldsymbol{\eta}_u + \mathbf{R}\cdot\left[\mathbf{J}_\rho\cdot\mathbf{A} + \mathbf{W}\times\left(\mathbf{J}_\rho\cdot\mathbf{W}\right)\right]\cdot\boldsymbol{\eta}_\theta\right\} dS = 0
\end{aligned}
\tag{2-96}
$$

Differentiation of the internal elastic forces $\mathbf{N}^{\mathrm{e}}$ and $\mathbf{M}^{\mathrm{e}}$ leads to:

$$
\delta G_M(\boldsymbol{\varphi},\boldsymbol{\eta}) = \int_0^L \left[\left(\frac{\partial \boldsymbol{\eta}_u}{\partial S} - \boldsymbol{\eta}_\theta \times \frac{\partial \mathbf{x}_0}{\partial S}\right)\cdot \mathbf{R}\cdot \delta\mathbf{N}^{\mathrm{e}} + \frac{\partial \boldsymbol{\eta}_\theta}{\partial S}\cdot \mathbf{R}\cdot\delta\mathbf{M}^{\mathrm{e}}\right] dS \tag{2-97}
$$

We now make use of the constitutive equations to write:

$$\delta \mathbf{N}^{\mathrm{e}} = \mathbf{C}^{\mathrm{N}} \cdot \delta \boldsymbol{\Gamma} \tag{2-98}$$

$$\delta \mathbf{M}^{\mathrm{e}} = \mathbf{C}^{\mathrm{M}} \cdot \delta \boldsymbol{\Omega} \tag{2-99}$$

Substituting (2-98) and (2-99) into (2-97), then yields:

$$\delta G_M\left(\boldsymbol{\varphi}, \boldsymbol{\eta}\right) = \int_0^L \left[ \left( \frac{\partial \boldsymbol{\eta}_u}{\partial S} - \boldsymbol{\eta}_\theta \times \frac{\partial \mathbf{x}_0}{\partial S} \right) \cdot \mathbf{R} \cdot \mathbf{C}^{\mathrm{N}} \cdot \delta \boldsymbol{\Gamma} + \frac{\partial \boldsymbol{\eta}_\theta}{\partial S} \cdot \mathbf{R} \cdot \mathbf{C}^{\mathrm{M}} \cdot \delta \boldsymbol{\Omega} \right] dS \tag{2-100}$$

The reference shear-axial strain vector $\boldsymbol{\Gamma}$ is given by:

$$\boldsymbol{\Gamma} = \mathbf{R}^{\mathrm{T}} \cdot \frac{\partial \mathbf{x}_0}{\partial S} - \mathbf{E}_3 \tag{2-101}$$

By differentiating (2-101), we get:

$$\delta \boldsymbol{\Gamma} = \left(\delta \mathbf{R}\right)^{\mathrm{T}} \cdot \frac{\partial \mathbf{x}_0}{\partial S} \cdot + \delta \frac{\partial \mathbf{x}_0}{\partial S} \cdot \mathbf{R} \tag{2-102}$$

As shown by Simo and Vu-Quoc (1988), we have:

$$\delta \mathbf{R} = \boldsymbol{\delta} \hat{\boldsymbol{\theta}} \cdot \mathbf{R} \tag{2-103}$$

and

$$\delta \frac{\partial \mathbf{x}_0}{\partial S} = \frac{\partial}{\partial S} \delta \mathbf{x}_0 = \frac{\partial}{\partial S} \boldsymbol{\delta} \mathbf{u} \tag{2-104}$$

Substituting (2-103) and (2-104) into (2-102), then gives:

$$\begin{aligned} \delta \boldsymbol{\Gamma} = \mathbf{R}^{\mathrm{T}} \cdot \boldsymbol{\delta} \hat{\boldsymbol{\theta}}^{\mathrm{T}} \cdot \frac{\partial \mathbf{x}_0}{\partial S} + \frac{\partial}{\partial S} \boldsymbol{\delta} \mathbf{u} \cdot \mathbf{R} = \mathbf{R}^{\mathrm{T}} \cdot \left( \frac{\partial}{\partial S} \boldsymbol{\delta} \mathbf{u} - \boldsymbol{\delta} \hat{\boldsymbol{\theta}} \cdot \frac{\partial \mathbf{x}_0}{\partial S} \right) = \\ \mathbf{R}^{\mathrm{T}} \cdot \left( \frac{\partial}{\partial S} \boldsymbol{\delta} \mathbf{u} - \boldsymbol{\delta \theta} \times \frac{\partial \mathbf{x}_0}{\partial S} \right) = \mathbf{R}^{\mathrm{T}} \cdot \left( \frac{\partial}{\partial S} \boldsymbol{\delta} \mathbf{u} + \frac{\partial \mathbf{x}_0}{\partial S} \times \boldsymbol{\delta \theta} \right) \end{aligned} \tag{2-105}$$

The derivative of the curvature vector, $\boldsymbol{\Omega}$, is carried out in a different way than by Simo and Vu-quoc (1986). The curvature tensor $\hat{\boldsymbol{\Omega}}$ is given by:

$$\hat{\boldsymbol{\Omega}} = \mathbf{R}^{\mathrm{T}} \cdot \mathbf{R}' \tag{2-106}$$

By differentiating (2-106), we get:

$$\delta \hat{\boldsymbol{\Omega}} = \left(\delta \mathbf{R}\right)^{\mathrm{T}} \cdot \mathbf{R}' + \mathbf{R}^{\mathrm{T}} \cdot \left(\delta \mathbf{R}\right)' \tag{2-107}$$

Substituting (2-103) into (2-107) then leads to:

$$\begin{aligned} \delta \hat{\boldsymbol{\Omega}} = \mathbf{R}^{\mathrm{T}} \cdot \boldsymbol{\delta} \hat{\boldsymbol{\theta}}^{\mathrm{T}} \cdot \mathbf{R}' + \mathbf{R}^{\mathrm{T}} \cdot \left( \boldsymbol{\delta} \hat{\boldsymbol{\theta}} \cdot \mathbf{R} \right)' = \\ -\mathbf{R}^{\mathbf{T}} \cdot \boldsymbol{\delta} \hat{\boldsymbol{\theta}} \cdot \mathbf{R}' + \mathbf{R}^{\mathrm{T}} \cdot \boldsymbol{\delta} \hat{\boldsymbol{\theta}}' \cdot \mathbf{R} + \mathbf{R}^{\mathrm{T}} \cdot \boldsymbol{\delta} \hat{\boldsymbol{\theta}} \cdot \mathbf{R}' = \mathbf{R}^{\mathrm{T}} \cdot \boldsymbol{\delta} \hat{\boldsymbol{\theta}}' \cdot \mathbf{R} = \boldsymbol{\delta} \hat{\boldsymbol{\Theta}}' \end{aligned} \tag{2-108}$$

Thus, the derivative of the curvature vector, $\mathbf{\Omega}$, can be written as:

$$\delta\mathbf{\Omega} = \boldsymbol{\delta\Theta}' = \mathbf{R}^{\mathrm{T}} \cdot \boldsymbol{\delta\theta}' \tag{2-109}$$

With (2-105) and (2-109) in hand, we can now write (2-100) as:

$$\begin{aligned} \delta G_M\left(\boldsymbol{\varphi},\boldsymbol{\eta}\right) = & \int_0^L \left[\frac{\partial \boldsymbol{\eta}_u}{\partial S} + \frac{\partial \mathbf{x}_0}{\partial S} \times \boldsymbol{\eta}_\theta\right] \cdot \mathbf{R} \cdot \mathbf{C}^{\mathrm{N}} \cdot \mathbf{R}^{\mathrm{T}} \cdot \left(\frac{\partial}{\partial S}\boldsymbol{\delta}\mathbf{u} + \frac{\partial \mathbf{x}_0}{\partial S} \times \boldsymbol{\delta\theta}\right) dS + \\ & \int_0^L \frac{\partial \boldsymbol{\eta}_\theta}{\partial S} \cdot \mathbf{R} \cdot \mathbf{C}^{\mathrm{M}} \cdot \mathbf{R}^{\mathrm{T}} \cdot \frac{\partial}{\partial S} \boldsymbol{\delta\theta}\, dS \end{aligned} \tag{2-110}$$

We then introduce the current elasticity tensors, $\mathbf{c}^{\mathrm{N}} = \mathbf{R}\cdot\mathbf{C}^{\mathrm{N}}\cdot\mathbf{R}^{\mathrm{T}}$ and $\mathbf{c}^{\mathrm{M}} = \mathbf{R}\cdot\mathbf{C}^{\mathrm{M}}\cdot\mathbf{R}^{\mathrm{T}}$, so that (2-110) becomes:

$$\begin{aligned} \delta G_M\left(\boldsymbol{\varphi},\boldsymbol{\eta}\right) = & \int_0^L \left[\frac{\partial \boldsymbol{\eta}_u}{\partial S} + \frac{\partial \mathbf{x}_0}{\partial S} \times \boldsymbol{\eta}_\theta\right] \cdot \mathbf{c}^{\mathrm{N}} \cdot \left(\frac{\partial}{\partial S}\boldsymbol{\delta}\mathbf{u} + \frac{\partial \mathbf{x}_0}{\partial S} \times \boldsymbol{\delta\theta}\right) dS + \\ & \int_0^L \frac{\partial \boldsymbol{\eta}_\theta}{\partial S} \cdot \mathbf{c}^{\mathrm{M}} \cdot \frac{\partial}{\partial S} \boldsymbol{\delta\theta}\, dS \end{aligned} \tag{2-111}$$

Moreover, by use of a tensor differential operator $\mathbf{\Xi}$, defined as

$$\mathbf{\Xi}^{\mathrm{T}} = \begin{bmatrix} \dfrac{\partial}{\partial S}\mathbf{I} & \dfrac{\partial \hat{\mathbf{x}}_0}{\partial S} \\ \mathbf{0} & \dfrac{\partial}{\partial S}\mathbf{I} \end{bmatrix} \tag{2-112}$$

it is easy to prove that (2-111) may be finally written as:

$$\delta G_M\left(\boldsymbol{\varphi},\boldsymbol{\eta}\right) = \int_0^L \boldsymbol{\eta} \cdot \mathbf{\Xi} \cdot \mathbf{c} \cdot \mathbf{\Xi}^{\mathrm{T}} \cdot \boldsymbol{\Delta\varphi}\, dS \tag{2-113}$$

where $\mathbf{c} = \mathrm{diag}\left[\mathbf{c}^{\mathrm{N}}, \mathbf{c}^{\mathrm{M}}\right]$.

### 2.9.2 Tangent damping operator

The formulation of Simo (1986), and Simo and Vu-Quoc (1988), does not account for energy dissipation, and the derivations in this subsection are significantly different. Differentiation of the internal dissipative forces $\mathbf{N}^{\mathrm{d}}$ and $\mathbf{M}^{\mathrm{d}}$ in (2-96) leads to:

$$\delta G_D\left(\boldsymbol{\varphi},\boldsymbol{\eta}\right) = \int_0^L \left[\left(\frac{\partial \boldsymbol{\eta}_u}{\partial S} - \boldsymbol{\eta}_\theta \times \frac{\partial \mathbf{x}_0}{\partial S}\right) \cdot \mathbf{R} \cdot \delta\mathbf{N}^{\mathrm{d}} + \frac{\partial \boldsymbol{\eta}_\theta}{\partial S} \cdot \mathbf{R} \cdot \delta\mathbf{M}^{\mathrm{d}}\right] dS \tag{2-114}$$

Again, we make use of the constitutive equations to write:

$$\delta \mathbf{N}^{\mathrm{d}} = \mathbf{C}_{\mathrm{d}}^{\mathrm{N}} \cdot \delta \dot{\boldsymbol{\Gamma}} \tag{2-115}$$

$$\delta \mathbf{M}^{\mathrm{d}} = \mathbf{C}_{\mathrm{d}}^{\mathrm{M}} \cdot \delta \dot{\boldsymbol{\Omega}} \tag{2-116}$$

Substituting (2-115) and (2-116) into (2-114), then yields:

$$\delta G_D(\boldsymbol{\varphi}, \boldsymbol{\eta}) = \int_0^L \left[ \left( \frac{\partial \boldsymbol{\eta}_u}{\partial S} - \boldsymbol{\eta}_\theta \times \frac{\partial \mathbf{x}_0}{\partial S} \right) \cdot \mathbf{R} \cdot \mathbf{C}_{\mathrm{d}}^{\mathrm{N}} \cdot \delta \dot{\boldsymbol{\Gamma}} + \frac{\partial \boldsymbol{\eta}_\theta}{\partial S} \cdot \mathbf{R} \cdot \mathbf{C}_{\mathrm{d}}^{\mathrm{M}} \cdot \delta \dot{\boldsymbol{\Omega}} \right] dS \tag{2-117}$$

The rate of the reference shear-axial strain vector, $\boldsymbol{\Gamma}$, is given by:

$$\begin{aligned} \dot{\boldsymbol{\Gamma}} = \mathbf{R}^{\mathrm{T}} \cdot \overset{\nabla}{\boldsymbol{\gamma}} = \mathbf{R}^{\mathrm{T}} \cdot \left( \frac{\partial^2 \mathbf{x}_0}{\partial S \partial t} - \mathbf{w} \times \frac{\partial \mathbf{x}_0}{\partial S} \right) = \mathbf{R}^{\mathrm{T}} \cdot \left( \frac{\partial \mathbf{v}_0}{\partial S} - \mathbf{w} \times \frac{\partial \mathbf{x}_0}{\partial S} \right) = \\ \mathbf{R}^{\mathrm{T}} \cdot \left[ \frac{\partial \mathbf{v}_0}{\partial S} - (\mathbf{R} \cdot \mathbf{W}) \times \frac{\partial \mathbf{x}_0}{\partial S} \right] \end{aligned} \tag{2-118}$$

By differentiating (2-118), we get:

$$\begin{aligned} \delta \dot{\boldsymbol{\Gamma}} = (\delta \mathbf{R})^{\mathrm{T}} \cdot \left( \frac{\partial \mathbf{v}_0}{\partial S} - \mathbf{w} \times \frac{\partial \mathbf{x}_0}{\partial S} \right) + \\ \mathbf{R}^{\mathrm{T}} \cdot \left[ \delta \frac{\partial \mathbf{v}_0}{\partial S} - \delta (\mathbf{R} \cdot \mathbf{W}) \times \frac{\partial \mathbf{x}_0}{\partial S} - (\mathbf{R} \cdot \mathbf{W}) \times \delta \frac{\partial \mathbf{x}_0}{\partial S} \right] \end{aligned} \tag{2-119}$$

Substituting (2-103) and (2-104) into (2-119), and recalling that

$$\delta \frac{\partial \mathbf{v}_0}{\partial S} = \frac{\partial \delta \mathbf{v}_0}{\partial S} = \frac{\gamma}{\beta h} \frac{\partial}{\partial S} \boldsymbol{\delta} \mathbf{u} \tag{2-120}$$

we may write (2-119) as:

$$\begin{aligned} \delta \dot{\boldsymbol{\Gamma}} = \mathbf{R}^{\mathrm{T}} \cdot \boldsymbol{\delta} \hat{\boldsymbol{\theta}}^{\mathrm{T}} \cdot \left( \frac{\partial \mathbf{v}_0}{\partial S} - \mathbf{w} \times \frac{\partial \mathbf{x}_0}{\partial S} \right) + \\ \mathbf{R}^{\mathrm{T}} \cdot \left[ \frac{\gamma}{\beta h} \frac{\partial}{\partial S} \boldsymbol{\delta} \mathbf{u} - (\delta \mathbf{R} \cdot \mathbf{W}) \times \frac{\partial \mathbf{x}_0}{\partial S} - (\mathbf{R} \cdot \delta \mathbf{W}) \times \frac{\partial \mathbf{x}_0}{\partial S} - (\mathbf{R} \cdot \mathbf{W}) \times \frac{\partial}{\partial S} \boldsymbol{\delta} \mathbf{u} \right] \end{aligned} \tag{2-121}$$

We then recall (Simo and Vu-Quoc, 1988) that

$$\delta \mathbf{W} = \frac{\gamma}{\beta h} \mathbf{R}_n^{\mathrm{T}} \cdot \mathbf{T} \cdot \boldsymbol{\delta} \boldsymbol{\theta} \tag{2-122}$$

where

$$\mathbf{T} = \mathbf{e} \otimes \mathbf{e} + \frac{\|\boldsymbol{\theta}_n\| / 2}{\tan(\|\boldsymbol{\theta}_n\| / 2)} [1 - \mathbf{e} \otimes \mathbf{e}] - \frac{\hat{\boldsymbol{\theta}}_n}{2} \tag{2-123}$$

with $\mathbf{e} = \boldsymbol{\theta}_n / \|\boldsymbol{\theta}_n\|$.

Substituting (2-103) and (2-122) into (2-121) now leads to:

$$\delta\dot{\boldsymbol{\Gamma}} = -\mathbf{R}^{\mathrm{T}} \cdot \boldsymbol{\delta}\hat{\boldsymbol{\theta}} \cdot \left( \frac{\partial \mathbf{v}_0}{\partial S} - \mathbf{w} \times \frac{\partial \mathbf{x}_0}{\partial S} \right) + \mathbf{R}^{\mathrm{T}} \cdot \left[ \frac{\gamma}{\beta h} \frac{\partial}{\partial S} \boldsymbol{\delta}\mathbf{u} - \left( \boldsymbol{\delta}\hat{\boldsymbol{\theta}} \cdot \mathbf{R} \cdot \mathbf{W} \right) \times \frac{\partial \mathbf{x}_0}{\partial S} + \frac{\partial \mathbf{x}_0}{\partial S} \times \left( \mathbf{R} \cdot \frac{\gamma}{\beta h} \mathbf{R}_n^{\mathrm{T}} \cdot \mathbf{T} \cdot \boldsymbol{\delta\theta} \right) - \mathbf{w} \times \frac{\partial}{\partial S} \boldsymbol{\delta}\mathbf{u} \right] \tag{2-124}$$

The first term on the right hand side of (2-124) may be written as:

$$-\mathbf{R}^{\mathrm{T}} \cdot \boldsymbol{\delta}\hat{\boldsymbol{\theta}} \cdot \left( \frac{\partial \mathbf{v}_0}{\partial S} - \mathbf{w} \times \frac{\partial \mathbf{x}_0}{\partial S} \right) = -\mathbf{R}^{\mathrm{T}} \cdot \left[ \boldsymbol{\delta\theta} \times \left( \frac{\partial \mathbf{v}_0}{\partial S} - \mathbf{w} \times \frac{\partial \mathbf{x}_0}{\partial S} \right) \right] = \mathbf{R}^{\mathrm{T}} \cdot \left[ \left( \frac{\partial \mathbf{v}_0}{\partial S} - \mathbf{w} \times \frac{\partial \mathbf{x}_0}{\partial S} \right) \times \boldsymbol{\delta\theta} \right] = \mathbf{R}^{\mathrm{T}} \cdot \left( \frac{\partial \mathbf{v}_0}{\partial S} - \mathbf{w} \times \frac{\partial \mathbf{x}_0}{\partial S} \right)^{\wedge} \cdot \boldsymbol{\delta\theta} \tag{2-125}$$

Moreover, the second term within square brackets may be reduced to:

$$\left( \boldsymbol{\delta}\hat{\boldsymbol{\theta}} \cdot \mathbf{R} \cdot \mathbf{W} \right) \times \frac{\partial \mathbf{x}_0}{\partial S} = \left( \boldsymbol{\delta}\hat{\boldsymbol{\theta}} \cdot \mathbf{w} \right) \times \frac{\partial \mathbf{x}_0}{\partial S} = -\left( \mathbf{w} \cdot \boldsymbol{\delta}\hat{\boldsymbol{\theta}} \right) \times \frac{\partial \mathbf{x}_0}{\partial S} = \frac{\partial \mathbf{x}_0}{\partial S} \times \left( \mathbf{w} \cdot \boldsymbol{\delta}\hat{\boldsymbol{\theta}} \right) = \frac{\partial \hat{\mathbf{x}}_0}{\partial S} \cdot \left( \mathbf{w} \cdot \boldsymbol{\delta}\hat{\boldsymbol{\theta}} \right) = \left( \frac{\partial \hat{\mathbf{x}}_0}{\partial S} \cdot \mathbf{w} \right) \cdot \boldsymbol{\delta}\hat{\boldsymbol{\theta}} = \left( \frac{\partial \hat{\mathbf{x}}_0}{\partial S} \cdot \mathbf{w} \right) \times \boldsymbol{\delta\theta} = \left( \frac{\partial \mathbf{x}_0}{\partial S} \times \mathbf{w} \right)^{\wedge} \cdot \boldsymbol{\delta\theta} \tag{2-126}$$

Using (2-125) and (2-126) into (2-124), we get:

$$\delta\dot{\boldsymbol{\Gamma}} = \mathbf{R}^{\mathrm{T}} \cdot \left( \frac{\partial \mathbf{v}_0}{\partial S} - \mathbf{w} \times \frac{\partial \mathbf{x}_0}{\partial S} \right)^{\wedge} \cdot \boldsymbol{\delta\theta} + \mathbf{R}^{\mathrm{T}} \cdot \left[ \frac{\gamma}{\beta h} \frac{\partial}{\partial S} \boldsymbol{\delta}\mathbf{u} - \left( \frac{\partial \mathbf{x}_0}{\partial S} \times \mathbf{w} \right)^{\wedge} \cdot \boldsymbol{\delta\theta} + \left( \frac{\partial \hat{\mathbf{x}}_0}{\partial S} \cdot \mathbf{R} \cdot \frac{\gamma}{\beta h} \mathbf{R}_n^{\mathrm{T}} \cdot \mathbf{T} \right) \cdot \boldsymbol{\delta\theta} - \hat{\mathbf{w}} \cdot \frac{\partial}{\partial S} \boldsymbol{\delta}\mathbf{u} \right] \tag{2-127}$$

Following some rearrangements, (2-127) may be finally written as:

$$\delta\dot{\boldsymbol{\Gamma}} = \mathbf{R}^{\mathrm{T}} \cdot \left[ \left( \frac{\gamma}{\beta h} \mathbf{I} - \hat{\mathbf{w}} \right) \cdot \frac{\partial}{\partial S} \mathbf{I} \right] \cdot \boldsymbol{\delta}\mathbf{u} + \mathbf{R}^{\mathrm{T}} \cdot \left[ \frac{\gamma}{\beta h} \frac{\partial \hat{\mathbf{x}}_0}{\partial S} \cdot \mathbf{R} \cdot \mathbf{R}_n^{\mathrm{T}} \cdot \mathbf{T} + \frac{\partial \hat{\mathbf{v}}_0}{\partial S} \right] \cdot \boldsymbol{\delta\theta} \tag{2-128}$$

The rate of the reference curvature vector, $\boldsymbol{\Omega}$, is given by:

$$\dot{\boldsymbol{\Omega}} = \mathbf{R}^{\mathrm{T}} \cdot \overset{\nabla}{\boldsymbol{\omega}} = \mathbf{R}^{\mathrm{T}} \cdot \left( \dot{\boldsymbol{\omega}} - \mathbf{w} \times \boldsymbol{\omega} \right) = \mathbf{R}^{\mathrm{T}} \cdot \mathbf{w}' \tag{2-129}$$

By differentiating (2-129), we get:

$$\delta\dot{\boldsymbol{\Omega}} = \left( \delta\mathbf{R} \right)^{\mathrm{T}} \cdot \mathbf{w}' + \mathbf{R}^{\mathrm{T}} \cdot \left( \delta\mathbf{w} \right)' = \left( \delta\mathbf{R} \right)^{\mathrm{T}} \cdot \mathbf{w}' + \mathbf{R}^{\mathrm{T}} \cdot \left( \delta\mathbf{R} \cdot \mathbf{W} + \mathbf{R} \cdot \delta\mathbf{W} \right)' \tag{2-130}$$

Substituting (2-103) and (2-122) into (2-130), we get:

$$\delta\dot{\mathbf{\Omega}} = \mathbf{R}^{\mathrm{T}} \cdot \boldsymbol{\delta}\hat{\boldsymbol{\theta}}^{\mathrm{T}} \cdot \mathbf{w}' + \mathbf{R}^{\mathrm{T}} \cdot \left( \boldsymbol{\delta}\hat{\boldsymbol{\theta}} \cdot \mathbf{R} \cdot \mathbf{W} + \mathbf{R} \cdot \frac{\gamma}{\beta h} \mathbf{R}_n^{\mathrm{T}} \cdot \mathbf{T} \cdot \boldsymbol{\delta\theta} \right)' \tag{2-131}$$

The first term on the right hand side of (2-131) may be written as:

$$\mathbf{R}^{\mathrm{T}} \cdot \boldsymbol{\delta}\hat{\boldsymbol{\theta}}^{\mathrm{T}} \cdot \mathbf{w}' = -\mathbf{R}^{\mathrm{T}} \cdot \boldsymbol{\delta}\hat{\boldsymbol{\theta}} \cdot \mathbf{w}' = -\mathbf{R}^{\mathrm{T}} \cdot \left( \boldsymbol{\delta\theta} \times \mathbf{w}' \right) = \mathbf{R}^{\mathrm{T}} \cdot \left( \mathbf{w}' \times \boldsymbol{\delta\theta} \right) \tag{2-132}$$

Moreover, the second term may be reduced to:

$$\mathbf{R}^{\mathrm{T}} \cdot \left( \boldsymbol{\delta}\hat{\boldsymbol{\theta}} \cdot \mathbf{R} \cdot \mathbf{W} + \mathbf{R} \cdot \frac{\gamma}{\beta h} \mathbf{R}_n^{\mathrm{T}} \cdot \mathbf{T} \cdot \boldsymbol{\delta\theta} \right)' = \mathbf{R}^{\mathrm{T}} \cdot \left( \boldsymbol{\delta}\hat{\boldsymbol{\theta}} \cdot \mathbf{w} \right)' + \frac{\gamma}{\beta h} \mathbf{R}^{\mathrm{T}} \cdot \left( \mathbf{R} \cdot \mathbf{R}_n^{\mathrm{T}} \cdot \mathbf{T} \cdot \boldsymbol{\delta\theta} \right)' \tag{2-133}$$

The first term of (2-133) may be decomposed as:

$$\mathbf{R}^{\mathrm{T}} \cdot \left( \boldsymbol{\delta}\hat{\boldsymbol{\theta}} \cdot \mathbf{w} \right)' = \mathbf{R}^{\mathrm{T}} \cdot \left( \boldsymbol{\delta\theta} \times \mathbf{w} \right)' = -\mathbf{R}^{\mathrm{T}} \cdot \left( \mathbf{w} \times \boldsymbol{\delta\theta} \right)' = -\mathbf{R}^{\mathrm{T}} \cdot \left( \mathbf{w}' \times \boldsymbol{\delta\theta} + \mathbf{w} \times \boldsymbol{\delta\theta}' \right) \tag{2-134}$$

Furthermore, the second term can be written as:

$$\begin{aligned} &\frac{\gamma}{\beta h} \mathbf{R}^{\mathrm{T}} \cdot \left( \mathbf{R} \cdot \mathbf{R}_n^{\mathrm{T}} \cdot \mathbf{T} \cdot \boldsymbol{\delta\theta} \right)' = \\ &\frac{\gamma}{\beta h} \mathbf{R}^{\mathrm{T}} \cdot \left( \mathbf{R}' \cdot \mathbf{R}_n^{\mathrm{T}} \cdot \mathbf{T} \cdot \boldsymbol{\delta\theta} + \mathbf{R} \cdot \mathbf{R}_n'^{\mathrm{T}} \cdot \mathbf{T} \cdot \boldsymbol{\delta\theta} + \mathbf{R} \cdot \mathbf{R}_n^{\mathrm{T}} \cdot \mathbf{T}' \cdot \boldsymbol{\delta\theta} + \mathbf{R} \cdot \mathbf{R}_n^{\mathrm{T}} \cdot \mathbf{T} \cdot \boldsymbol{\delta\theta}' \right) \end{aligned} \tag{2-135}$$

Recalling that

$$\mathbf{R}' = \mathbf{R} \cdot \hat{\mathbf{\Omega}} \tag{2-136}$$

we may write (2-135) as:

$$\begin{aligned} &\frac{\gamma}{\beta h} \mathbf{R}^{\mathrm{T}} \cdot \left( \mathbf{R} \cdot \mathbf{R}_n^{\mathrm{T}} \cdot \mathbf{T} \cdot \boldsymbol{\delta\theta} \right)' = \\ &\frac{\gamma}{\beta h} \mathbf{R}^{\mathrm{T}} \cdot \left[ \mathbf{R} \cdot \hat{\mathbf{\Omega}} \cdot \mathbf{R}_n^{\mathrm{T}} \cdot \mathbf{T} \cdot \boldsymbol{\delta\theta} + \mathbf{R} \cdot \left( \mathbf{R}_n \cdot \hat{\mathbf{\Omega}}_n \right)^{\mathrm{T}} \cdot \mathbf{T} \cdot \boldsymbol{\delta\theta} + \mathbf{R} \cdot \mathbf{R}_n^{\mathrm{T}} \cdot \mathbf{T}' \cdot \boldsymbol{\delta\theta} + \mathbf{R} \cdot \mathbf{R}_n^{\mathrm{T}} \cdot \mathbf{T} \cdot \boldsymbol{\delta\theta}' \right] = \\ &\frac{\gamma}{\beta h} \mathbf{R}^{\mathrm{T}} \cdot \left[ \mathbf{R} \cdot \hat{\mathbf{\Omega}} \cdot \mathbf{R}_n^{\mathrm{T}} \cdot \mathbf{T} \cdot \boldsymbol{\delta\theta} - \mathbf{R} \cdot \hat{\mathbf{\Omega}}_n \cdot \mathbf{R}_n^{\mathrm{T}} \cdot \mathbf{T} \cdot \boldsymbol{\delta\theta} + \mathbf{R} \cdot \mathbf{R}_n^{\mathrm{T}} \cdot \mathbf{T}' \cdot \boldsymbol{\delta\theta} + \mathbf{R} \cdot \mathbf{R}_n^{\mathrm{T}} \cdot \mathbf{T} \cdot \boldsymbol{\delta\theta}' \right] \end{aligned} \tag{2-137}$$

Using (2-132), (2-134) and (2-137) into (2-131), we get:

$$\begin{aligned} \delta\dot{\mathbf{\Omega}} = &-\mathbf{R}^{\mathrm{T}} \cdot \hat{\mathbf{w}} \cdot \boldsymbol{\delta\theta}' + \frac{\gamma}{\beta h} \hat{\mathbf{\Omega}} \cdot \mathbf{R}_n^{\mathrm{T}} \cdot \mathbf{T} \cdot \boldsymbol{\delta\theta} - \frac{\gamma}{\beta h} \hat{\mathbf{\Omega}}_n \cdot \mathbf{R}_n^{\mathrm{T}} \cdot \mathbf{T} \cdot \boldsymbol{\delta\theta} + \\ &\frac{\gamma}{\beta h} \mathbf{R}_n^{\mathrm{T}} \cdot \mathbf{T}' \cdot \boldsymbol{\delta\theta} + \frac{\gamma}{\beta h} \mathbf{R}_n^{\mathrm{T}} \cdot \mathbf{T} \cdot \boldsymbol{\delta\theta}' \end{aligned} \tag{2-138}$$

Following some rearrangements, (2-138) may be finally written as:

$$\delta\dot{\mathbf{\Omega}} = \left[\frac{\gamma}{\beta h}\left(\hat{\mathbf{\Omega}} - \hat{\mathbf{\Omega}}_n\right)\cdot \mathbf{R}_n^{\mathrm{T}} \cdot \mathbf{T} + \frac{\gamma}{\beta h}\mathbf{R}_n^{\mathrm{T}} \cdot \mathbf{T}' + \left(\frac{\gamma}{\beta h}\mathbf{R}_n^{\mathrm{T}} \cdot \mathbf{T} - \mathbf{R}^{\mathrm{T}} \cdot \hat{\mathbf{w}}\right)\cdot \frac{\partial}{\partial S}\mathbf{I}\right]\cdot \boldsymbol{\delta\theta} \tag{2-139}$$

With (2-128) and (2-139) in hand, we can now write (2-117) as:

$$\begin{aligned}\delta G_D(\boldsymbol{\varphi},\boldsymbol{\eta}) = \int_0^L \left[\frac{\partial \boldsymbol{\eta}_u}{\partial S} + \frac{\partial \mathbf{x}_0}{\partial S} \times \boldsymbol{\eta}_\theta\right]\cdot \mathbf{R}\cdot \mathbf{C}_{\mathrm{d}}^{\mathrm{N}} \cdot \mathbf{R}^{\mathrm{T}} \cdot \left\{\left[\left(\frac{\gamma}{\beta h}\mathbf{I} - \hat{\mathbf{w}}\right)\cdot \frac{\partial}{\partial S}\mathbf{I}\right]\cdot \boldsymbol{\delta}\mathbf{u} + \right.\\ \left.\left[\frac{\gamma}{\beta h}\frac{\partial \hat{\mathbf{x}}_0}{\partial S}\cdot \mathbf{R}\cdot \mathbf{R}_n^{\mathrm{T}} \cdot \mathbf{T} + \frac{\partial \hat{\mathbf{v}}_0}{\partial S}\right]\cdot \boldsymbol{\delta\theta}\right\} dS + \int_0^L \frac{\partial \boldsymbol{\eta}_\theta}{\partial S}\cdot \mathbf{R}\cdot \mathbf{C}_{\mathrm{d}}^{\mathrm{M}} \cdot \mathbf{R}^{\mathrm{T}} \cdot \mathbf{R}\cdot \left[\frac{\gamma}{\beta h}\left(\hat{\mathbf{\Omega}} - \hat{\mathbf{\Omega}}_n\right)\cdot \mathbf{R}_n^{\mathrm{T}} \cdot \mathbf{T} + \right.\\ \left.\frac{\gamma}{\beta h}\mathbf{R}_n^{\mathrm{T}} \cdot \mathbf{T}' + \left(\frac{\gamma}{\beta h}\mathbf{R}_n^{\mathrm{T}} \cdot \mathbf{T} - \mathbf{R}^{\mathrm{T}} \cdot \hat{\mathbf{w}}\right)\cdot \frac{\partial}{\partial S}\mathbf{I}\right]\cdot \boldsymbol{\delta\theta}\, dS\end{aligned} \tag{2-140}$$

We then introduce the current dissipation tensors, $\mathbf{c}_{\mathrm{d}}^{\mathrm{N}} = \mathbf{R}\cdot \mathbf{C}_{\mathrm{d}}^{\mathrm{N}} \cdot \mathbf{R}^{\mathrm{T}}$ and $\mathbf{c}_{\mathrm{d}}^{\mathrm{M}} = \mathbf{R}\cdot \mathbf{C}_{\mathrm{d}}^{\mathrm{M}} \cdot \mathbf{R}^{\mathrm{T}}$, so that (2-140) becomes:

$$\begin{aligned}\delta G_D(\boldsymbol{\varphi},\boldsymbol{\eta}) = \int_0^L \left[\frac{\partial \boldsymbol{\eta}_u}{\partial S} + \frac{\partial \mathbf{x}_0}{\partial S} \times \boldsymbol{\eta}_\theta\right]\cdot \mathbf{c}_{\mathrm{d}}^{\mathrm{N}} \cdot \left\{\left[\left(\frac{\gamma}{\beta h}\mathbf{I} - \hat{\mathbf{w}}\right)\cdot \frac{\partial}{\partial S}\mathbf{I}\right]\cdot \boldsymbol{\delta}\mathbf{u} + \right.\\ \left.\left[\frac{\gamma}{\beta h}\frac{\partial \hat{\mathbf{x}}_0}{\partial S}\cdot \mathbf{R}\cdot \mathbf{R}_n^{\mathrm{T}} \cdot \mathbf{T} + \frac{\partial \hat{\mathbf{v}}_0}{\partial S}\right]\cdot \boldsymbol{\delta\theta}\right\} dS + \int_0^L \frac{\partial \boldsymbol{\eta}_\theta}{\partial S}\cdot \mathbf{c}_{\mathrm{d}}^{\mathrm{M}} \cdot \mathbf{R}\cdot \left[\frac{\gamma}{\beta h}\left(\hat{\mathbf{\Omega}} - \hat{\mathbf{\Omega}}_n\right)\cdot \mathbf{R}_n^{\mathrm{T}} \cdot \mathbf{T} + \right.\\ \left.\frac{\gamma}{\beta h}\mathbf{R}_n^{\mathrm{T}} \cdot \mathbf{T}' + \left(\frac{\gamma}{\beta h}\mathbf{R}_n^{\mathrm{T}} \cdot \mathbf{T} - \mathbf{R}^{\mathrm{T}} \cdot \hat{\mathbf{w}}\right)\cdot \frac{\partial}{\partial S}\mathbf{I}\right]\cdot \boldsymbol{\delta\theta}\, dS\end{aligned} \tag{2-141}$$

Moreover, by use of the tensor $\mathbf{\Xi}_{\mathrm{d}}$, defined as

$$\mathbf{\Xi}_{\mathrm{d}}^{\mathrm{T}} = \begin{bmatrix} \left[\left(\frac{\gamma}{\beta h}\mathbf{I} - \hat{\mathbf{w}}\right)\cdot \frac{\partial}{\partial S}\mathbf{I}\right] & \frac{\gamma}{\beta h}\frac{\partial \hat{\mathbf{x}}_0}{\partial S}\cdot \mathbf{R}\cdot \mathbf{R}_n^{\mathrm{T}} \cdot \mathbf{T} + \frac{\partial \hat{\mathbf{v}}_0}{\partial S} \\ \mathbf{0} & \mathbf{R}\cdot \left[\frac{\gamma}{\beta h}\left(\hat{\mathbf{\Omega}} - \hat{\mathbf{\Omega}}_n\right)\cdot \mathbf{R}_n^{\mathrm{T}} \cdot \mathbf{T} + \frac{\gamma}{\beta h}\mathbf{R}_n^{\mathrm{T}} \cdot \mathbf{T}' + \left(\frac{\gamma}{\beta h}\mathbf{R}_n^{\mathrm{T}} \cdot \mathbf{T} - \mathbf{R}^{\mathrm{T}} \cdot \hat{\mathbf{w}}\right)\cdot \frac{\partial}{\partial S}\mathbf{I}\right] \end{bmatrix} \tag{2-142}$$

it is easy to prove that (2-141) may be finally written as:

$$\delta G_D(\boldsymbol{\varphi},\boldsymbol{\eta}) = \int_0^L \boldsymbol{\eta}\cdot \mathbf{\Xi}\cdot \mathbf{c}_{\mathrm{d}} \cdot \mathbf{\Xi}_{\mathrm{d}}^{\mathrm{T}} \cdot \boldsymbol{\Delta\varphi}\, dS \tag{2-143}$$

where $\mathbf{c}_{\mathrm{d}} = \mathrm{diag}\left[\mathbf{c}_{\mathrm{d}}^{\mathrm{N}}, \mathbf{c}_{\mathrm{d}}^{\mathrm{M}}\right]$.

In order to evaluate $\mathbf{\Xi}_{\mathrm{d}}^{\mathrm{T}}$, we need to carry out the derivative of $\mathbf{T}$. This is given by:

$$\mathbf{T}' = \left[1 - \frac{\|\boldsymbol{\theta}_n\|/2}{\tan\left(\|\boldsymbol{\theta}_n\|/2\right)}\right]\left[\mathbf{e}'\otimes\mathbf{e} + \mathbf{e}\otimes\mathbf{e}'\right] + D\left[\frac{\|\boldsymbol{\theta}_n\|/2}{\tan\left(\|\boldsymbol{\theta}_n\|/2\right)}\right]\left[\mathbf{I} - \mathbf{e}\otimes\mathbf{e}\right] - \frac{1}{2}\hat{\boldsymbol{\theta}}_n' \tag{2-144}$$

where

$$D\frac{\|\boldsymbol{\theta}_n\|/2}{\tan\left(\|\boldsymbol{\theta}_n\|/2\right)}=\frac{1}{2}\frac{\boldsymbol{\theta}'_n\cdot\boldsymbol{\theta}_n}{\|\boldsymbol{\theta}_n\|}\left[\frac{1}{\tan\left(\|\boldsymbol{\theta}_n\|/2\right)}-\frac{\|\boldsymbol{\theta}_n\|/2}{\sin^2\left(\|\boldsymbol{\theta}_n\|/2\right)}\right] \tag{2-145}$$

### 2.9.3 Tangent geometric stiffness operator

Differentiation, in (2-96), of the terms that multiply the internal forces **N** and **M** leads to:

$$\delta G_G\left(\boldsymbol{\varphi},\boldsymbol{\eta}\right)=\int_0^L\left\{\delta\left[\left(\frac{\partial\boldsymbol{\eta}_u}{\partial S}-\boldsymbol{\eta}_\theta\times\frac{\partial\mathbf{x}_0}{\partial S}\right)\cdot\mathbf{R}\right]\cdot\mathbf{N}+\delta\left(\frac{\partial\boldsymbol{\eta}_\theta}{\partial S}\cdot\mathbf{R}\right)\cdot\mathbf{M}\right\}dS \tag{2-146}$$

By differentiating the first term, we get:

$$\begin{aligned}\delta\left[\left(\frac{\partial\boldsymbol{\eta}_u}{\partial S}-\boldsymbol{\eta}_\theta\times\frac{\partial\mathbf{x}_0}{\partial S}\right)\cdot\mathbf{R}\right]&=\delta\left(\frac{\partial\boldsymbol{\eta}_u}{\partial S}-\boldsymbol{\eta}_\theta\times\frac{\partial\mathbf{x}_0}{\partial S}\right)\cdot\mathbf{R}+\left(\frac{\partial\boldsymbol{\eta}_u}{\partial S}-\boldsymbol{\eta}_\theta\times\frac{\partial\mathbf{x}_0}{\partial S}\right)\cdot\delta\mathbf{R}=\\ -\left(\boldsymbol{\eta}_\theta\times\delta\frac{\partial\mathbf{x}_0}{\partial S}\right)\cdot\mathbf{R}&+\left(\frac{\partial\boldsymbol{\eta}_u}{\partial S}-\boldsymbol{\eta}_\theta\times\frac{\partial\mathbf{x}_0}{\partial S}\right)\cdot\delta\mathbf{R}\end{aligned} \tag{2-147}$$

Substituting (2-103) and (2-104) into (2-147), we obtain:

$$\begin{aligned}\delta\left[\left(\frac{\partial\boldsymbol{\eta}_u}{\partial S}-\boldsymbol{\eta}_\theta\times\frac{\partial\mathbf{x}_0}{\partial S}\right)\cdot\mathbf{R}\right]&=-\left(\boldsymbol{\eta}_\theta\times\frac{\partial}{\partial S}\boldsymbol{\delta}\mathbf{u}\right)\cdot\mathbf{R}+\left(\frac{\partial\boldsymbol{\eta}_u}{\partial S}-\boldsymbol{\eta}_\theta\times\frac{\partial\mathbf{x}_0}{\partial S}\right)\cdot\boldsymbol{\delta}\hat{\boldsymbol{\theta}}\cdot\mathbf{R}=\\ \left[-\left(\boldsymbol{\eta}_\theta\times\frac{\partial}{\partial S}\boldsymbol{\delta}\mathbf{u}\right)+\left(\frac{\partial\boldsymbol{\eta}_u}{\partial S}-\boldsymbol{\eta}_\theta\times\frac{\partial\mathbf{x}_0}{\partial S}\right)\times\boldsymbol{\delta\theta}\right]&\cdot\mathbf{R}\end{aligned} \tag{2-148}$$

By differentiating the second term in (2-146), we get:

$$\delta\left(\frac{\partial\boldsymbol{\eta}_\theta}{\partial S}\cdot\mathbf{R}\right)=\frac{\partial\boldsymbol{\eta}_\theta}{\partial S}\cdot\delta\mathbf{R}=\frac{\partial\boldsymbol{\eta}_\theta}{\partial S}\cdot\boldsymbol{\delta}\hat{\boldsymbol{\theta}}\cdot\mathbf{R}=\left(\frac{\partial\boldsymbol{\eta}_\theta}{\partial S}\times\boldsymbol{\delta\theta}\right)\cdot\mathbf{R} \tag{2-149}$$

With (2-147) and (2-149) in hand, we can now write (2-146) as:

$$\delta G_G\left(\boldsymbol{\varphi},\boldsymbol{\eta}\right)=\int_0^L\left\{\left[-\left(\boldsymbol{\eta}_\theta\times\frac{\partial}{\partial S}\boldsymbol{\delta}\mathbf{u}\right)+\left(\frac{\partial\boldsymbol{\eta}_u}{\partial S}-\boldsymbol{\eta}_\theta\times\frac{\partial\mathbf{x}_0}{\partial S}\right)\times\boldsymbol{\delta\theta}\right]\cdot\mathbf{n}+\left(\frac{\partial\boldsymbol{\eta}_\theta}{\partial S}\times\boldsymbol{\delta\theta}\right)\cdot\mathbf{m}\right\}dS \tag{2-150}$$

It is convenient to rearrange each term in (2-150) as follows. We write the first term as:

$$-\boldsymbol{\eta}_\theta\times\frac{\partial}{\partial S}\boldsymbol{\delta}\mathbf{u}\cdot\mathbf{n}=-\mathbf{n}\times\boldsymbol{\eta}_\theta\cdot\frac{\partial}{\partial S}\boldsymbol{\delta}\mathbf{u}=\boldsymbol{\eta}_\theta\times\mathbf{n}\cdot\frac{\partial}{\partial S}\boldsymbol{\delta}\mathbf{u}=\boldsymbol{\eta}_\theta\cdot\hat{\mathbf{n}}\cdot\frac{\partial}{\partial S}\boldsymbol{\delta}\mathbf{u}=\boldsymbol{\eta}_\theta\cdot\mathbf{n}\times\frac{\partial}{\partial S}\boldsymbol{\delta}\mathbf{u} \tag{2-151}$$

In the same fashion, the second term may be written as:

$$\frac{\partial\boldsymbol{\eta}_u}{\partial S}\times\boldsymbol{\delta\theta}\cdot\mathbf{n}=\mathbf{n}\times\frac{\partial\boldsymbol{\eta}_u}{\partial S}\cdot\boldsymbol{\delta\theta}=-\frac{\partial\boldsymbol{\eta}_u}{\partial S}\times\mathbf{n}\cdot\boldsymbol{\delta\theta}=-\frac{\partial\boldsymbol{\eta}_u}{\partial S}\cdot\hat{\mathbf{n}}\cdot\boldsymbol{\delta\theta}=-\frac{\partial\boldsymbol{\eta}_u}{\partial S}\cdot\mathbf{n}\times\boldsymbol{\delta\theta} \tag{2-152}$$

Moreover, the third term can be expressed as:

$$
\begin{aligned}
&-\left[\left(\boldsymbol{\eta}_\theta \times \frac{\partial \mathbf{x}_0}{\partial S}\right)\times \boldsymbol{\delta\theta}\right]\cdot \mathbf{n} = -\left[\left(\boldsymbol{\delta\theta}\cdot\boldsymbol{\eta}_\theta\right)\frac{\partial \mathbf{x}_0}{\partial S} - \left(\boldsymbol{\delta\theta}\cdot\frac{\partial \mathbf{x}_0}{\partial S}\right)\boldsymbol{\eta}_\theta\right]\cdot\mathbf{n} = \\
&\left[-\frac{\partial \mathbf{x}_0}{\partial S}\left(\boldsymbol{\eta}_\theta\cdot\boldsymbol{\delta\theta}\right)+\boldsymbol{\eta}_\theta\left(\frac{\partial \mathbf{x}_0}{\partial S}\cdot\boldsymbol{\delta\theta}\right)\right]\cdot\mathbf{n} = \mathbf{n}\cdot\left[\left(-\frac{\partial \mathbf{x}_0}{\partial S}\otimes\boldsymbol{\eta}_\theta+\boldsymbol{\eta}_\theta\otimes\frac{\partial \mathbf{x}_0}{\partial S}\right)\cdot\boldsymbol{\delta\theta}\right] = \\
&\left[\mathbf{n}\cdot\left(\boldsymbol{\eta}_\theta\otimes\frac{\partial \mathbf{x}_0}{\partial S}-\frac{\partial \mathbf{x}_0}{\partial S}\otimes\boldsymbol{\eta}_\theta\right)\right]\cdot\boldsymbol{\delta\theta} = \left[\left(\mathbf{n}\cdot\boldsymbol{\eta}_\theta\right)\frac{\partial \mathbf{x}_0}{\partial S}-\left(\mathbf{n}\cdot\frac{\partial \mathbf{x}_0}{\partial S}\right)\boldsymbol{\eta}_\theta\right]\cdot\boldsymbol{\delta\theta} = \\
&\left[\left(\boldsymbol{\eta}_\theta\cdot\mathbf{n}\right)\frac{\partial \mathbf{x}_0}{\partial S}-\left(\mathbf{n}\cdot\frac{\partial \mathbf{x}_0}{\partial S}\right)\boldsymbol{\eta}_\theta\right]\cdot\boldsymbol{\delta\theta} = \boldsymbol{\eta}_\theta\cdot\left[\mathbf{n}\otimes\frac{\partial \mathbf{x}_0}{\partial S}-\left(\mathbf{n}\cdot\frac{\partial \mathbf{x}_0}{\partial S}\right)\mathbf{I}\right]\cdot\boldsymbol{\delta\theta}
\end{aligned}
\tag{2-153}
$$

Finally, we write the fourth term as:

$$
\frac{\partial \boldsymbol{\eta}_\theta}{\partial S}\times\boldsymbol{\delta\theta}\cdot\mathbf{m} = \mathbf{m}\times\frac{\partial \boldsymbol{\eta}_\theta}{\partial S}\cdot\boldsymbol{\delta\theta} = -\frac{\partial \boldsymbol{\eta}_\theta}{\partial S}\times\mathbf{m}\cdot\boldsymbol{\delta\theta} = -\frac{\partial \boldsymbol{\eta}_\theta}{\partial S}\cdot\hat{\mathbf{m}}\cdot\boldsymbol{\delta\theta} = -\frac{\partial \boldsymbol{\eta}_\theta}{\partial S}\cdot\mathbf{m}\times\boldsymbol{\delta\theta} \tag{2-154}
$$

With these results in hand, (2-150) becomes:

$$
\begin{aligned}
\delta G_G\left(\boldsymbol{\varphi},\boldsymbol{\eta}\right) = \int_0^L \Bigg\{ & \boldsymbol{\eta}_\theta\cdot\mathbf{n}\times\frac{\partial}{\partial S}\boldsymbol{\delta}\mathbf{u} - \frac{\partial}{\partial S}\boldsymbol{\eta}_u\cdot\mathbf{n}\times\boldsymbol{\delta\theta} + \boldsymbol{\eta}_\theta\cdot\left[\mathbf{n}\otimes\frac{\partial \mathbf{x}_0}{\partial S}-\left(\mathbf{n}\cdot\frac{\partial \mathbf{x}_0}{\partial S}\right)\mathbf{I}\right]\cdot\boldsymbol{\delta\theta} + \\
& -\frac{\partial \boldsymbol{\eta}_\theta}{\partial S}\cdot\mathbf{m}\times\boldsymbol{\delta\theta}\Bigg\}dS
\end{aligned}
\tag{2-155}
$$

It can be easily verified that (2-155) may be written as:

$$
\delta G_G\left(\boldsymbol{\varphi},\boldsymbol{\eta}\right) = \int_0^L \boldsymbol{\eta}\cdot\boldsymbol{\Psi}\cdot\mathbf{B}\cdot\boldsymbol{\Psi}^{\mathrm{T}}\cdot\boldsymbol{\Delta\varphi}\, dS \tag{2-156}
$$

where

$$
\boldsymbol{\Psi} = \begin{bmatrix} \frac{\partial}{\partial S}\mathbf{I} & \mathbf{0} & \mathbf{0} \\ \mathbf{0} & \frac{\partial}{\partial S}\mathbf{I} & \mathbf{I} \end{bmatrix} \qquad \mathbf{B} = \begin{bmatrix} \mathbf{0} & \mathbf{0} & -\hat{\mathbf{n}} \\ \mathbf{0} & \mathbf{0} & -\hat{\mathbf{m}} \\ \hat{\mathbf{n}} & \mathbf{0} & \mathbf{n}\otimes\frac{\partial \mathbf{x}_0}{\partial S}-\left(\mathbf{n}\cdot\frac{\partial \mathbf{x}_0}{\partial S}\right)\mathbf{I} \end{bmatrix} \tag{2-157}
$$

### 2.9.4 Tangent inertia operator

We finally differentiate the last integral of (2-96), that is

$$
\delta G_I\left(\boldsymbol{\varphi},\boldsymbol{\eta}\right) = \delta\int_0^L \left\{A_\rho\mathbf{a}_0\cdot\boldsymbol{\eta}_u + \mathbf{R}\cdot\left[\mathbf{J}_\rho\cdot\mathbf{A}+\mathbf{W}\times\left(\mathbf{J}_\rho\cdot\mathbf{W}\right)\right]\cdot\boldsymbol{\eta}_\theta\right\}dS \tag{2-158}
$$

We can decompose (2-158) as follows:

$$\delta G_I(\boldsymbol{\varphi},\boldsymbol{\eta}) = \int_0^L A_\rho \delta \mathbf{a}_0 \cdot \boldsymbol{\eta}_u \, dS + \int_0^L \delta \mathbf{R} \cdot \left[ \mathbf{J}_\rho \cdot \mathbf{A} + \mathbf{W} \times \left( \mathbf{J}_\rho \cdot \mathbf{W} \right) \right] \cdot \boldsymbol{\eta}_\theta \, dS + \int_0^L \mathbf{R} \cdot \delta \left[ \mathbf{J}_\rho \cdot \mathbf{A} + \mathbf{W} \times \left( \mathbf{J}_\rho \cdot \mathbf{W} \right) \right] \cdot \boldsymbol{\eta}_\theta \, dS \tag{2-159}$$

Recalling that

$$\delta \mathbf{a}_0 = \frac{1}{\beta h^2} \boldsymbol{\delta} \mathbf{u} \tag{2-160}$$

the first integral in (2-159) becomes:

$$\int_0^L A_\rho \delta \mathbf{a}_0 \cdot \boldsymbol{\eta}_u \, dS = \int_0^L \frac{1}{\beta h^2} A_\rho \boldsymbol{\delta} \mathbf{u} \cdot \boldsymbol{\eta}_u \, dS = \int_0^L \boldsymbol{\eta}_u \cdot \frac{1}{\beta h^2} A_\rho \boldsymbol{\delta} \mathbf{u} \, dS \tag{2-161}$$

By using (2-103), the second integral in (2-159) may be written as:

$$\begin{aligned} &\int_0^L \delta \mathbf{R} \cdot \left[ \mathbf{J}_\rho \cdot \mathbf{A} + \mathbf{W} \times \left( \mathbf{J}_\rho \cdot \mathbf{W} \right) \right] \cdot \boldsymbol{\eta}_\theta \, dS = \int_0^L \boldsymbol{\delta} \hat{\boldsymbol{\theta}} \cdot \mathbf{R} \cdot \left[ \mathbf{J}_\rho \cdot \mathbf{A} + \mathbf{W} \times \left( \mathbf{J}_\rho \cdot \mathbf{W} \right) \right] \cdot \boldsymbol{\eta}_\theta \, dS = \\ &-\int_0^L \mathbf{R} \cdot \left[ \mathbf{J}_\rho \cdot \mathbf{A} + \mathbf{W} \times \left( \mathbf{J}_\rho \cdot \mathbf{W} \right) \right] \cdot \boldsymbol{\delta} \hat{\boldsymbol{\theta}} \cdot \boldsymbol{\eta}_\theta \, dS = \\ &-\int_0^L \mathbf{R} \cdot \left[ \mathbf{J}_\rho \cdot \mathbf{A} + \mathbf{W} \times \left( \mathbf{J}_\rho \cdot \mathbf{W} \right) \right]^\wedge \cdot \boldsymbol{\delta} \boldsymbol{\theta} \cdot \boldsymbol{\eta}_\theta \, dS = \\ &-\int_0^L \boldsymbol{\eta}_\theta \cdot \mathbf{R} \cdot \left[ \mathbf{J}_\rho \cdot \mathbf{A} + \mathbf{W} \times \left( \mathbf{J}_\rho \cdot \mathbf{W} \right) \right]^\wedge \cdot \boldsymbol{\delta} \boldsymbol{\theta} \, dS \end{aligned} \tag{2-162}$$

The third integral in (2-159) can be decomposed as:

$$\int_0^L \mathbf{R} \cdot \delta \left[ \mathbf{J}_\rho \cdot \mathbf{A} + \mathbf{W} \times \left( \mathbf{J}_\rho \cdot \mathbf{W} \right) \right] \cdot \boldsymbol{\eta}_\theta \, dS = \int_0^L \mathbf{R} \cdot \left[ \mathbf{J}_\rho \cdot \delta \mathbf{A} + \delta \mathbf{W} \times \left( \mathbf{J}_\rho \cdot \mathbf{W} \right) + \mathbf{W} \times \left( \mathbf{J}_\rho \cdot \delta \mathbf{W} \right) \right] \cdot \boldsymbol{\eta}_\theta dS \tag{2-163}$$

Using (2-122), and recalling (Simo and Vu-Quoc, 1988) that

$$\delta \mathbf{A} = \frac{1}{\beta h^2} \mathbf{R}_n^{\mathrm{T}} \cdot \mathbf{T} \cdot \boldsymbol{\delta} \boldsymbol{\theta} \tag{2-164}$$

we can write (2-163) as:

$$\begin{aligned} &\int_0^L \mathbf{R} \cdot \delta \left[ \mathbf{J}_\rho \cdot \mathbf{A} + \mathbf{W} \times \left( \mathbf{J}_\rho \cdot \mathbf{W} \right) \right] \cdot \boldsymbol{\eta}_\theta \, dS = \int_0^L \mathbf{R} \cdot \Bigg[ \mathbf{J}_\rho \cdot \frac{1}{\beta h^2} \mathbf{R}_n^{\mathrm{T}} \cdot \mathbf{T} \cdot \boldsymbol{\delta} \boldsymbol{\theta} + \\ &\left( \frac{\gamma}{\beta h} \mathbf{R}_n^{\mathrm{T}} \cdot \mathbf{T} \cdot \boldsymbol{\delta} \boldsymbol{\theta} \right) \times \left( \mathbf{J}_\rho \cdot \mathbf{W} \right) + \mathbf{W} \times \left( \mathbf{J}_\rho \cdot \frac{\gamma}{\beta h} \mathbf{R}_n^{\mathrm{T}} \cdot \mathbf{T} \cdot \boldsymbol{\delta} \boldsymbol{\theta} \right) \Bigg] \cdot \boldsymbol{\eta}_\theta \, dS \end{aligned} \tag{2-165}$$

Following some manipulations, (2-165) may be written as:

$$\int_0^L \mathbf{R}\cdot\delta\left[\mathbf{J}_\rho\cdot\mathbf{A}+\mathbf{W}\times\left(\mathbf{J}_\rho\cdot\mathbf{W}\right)\right]\cdot\boldsymbol{\eta}_\theta\,dS=\int_0^L \boldsymbol{\eta}_\theta\cdot\mathbf{R}\cdot\left[\frac{1}{\beta h^2}\mathbf{J}_\rho-\frac{\gamma}{\beta h}\left(\mathbf{J}_\rho\cdot\mathbf{W}\right)^\wedge+\frac{\gamma}{\beta h}\hat{\mathbf{W}}\cdot\mathbf{J}_\rho\right]\cdot\mathbf{R}_n^{\mathrm{T}}\cdot\mathbf{T}\cdot\boldsymbol{\delta\theta}\,dS \tag{2-166}$$

Substituting (2-161), (2-162) and (2-166) into (2-159), we finally get:

$$\delta G_I\left(\boldsymbol{\varphi},\boldsymbol{\eta}\right)=\int_0^L \boldsymbol{\eta}_u\cdot\frac{1}{\beta h^2}A_\rho\boldsymbol{\delta}\mathbf{u}\,dS+\int_0^L \boldsymbol{\eta}_\theta\cdot\left\{-\mathbf{R}\cdot\left[\mathbf{J}_\rho\cdot\mathbf{A}+\mathbf{W}\times\left(\mathbf{J}_\rho\cdot\mathbf{W}\right)\right]^\wedge+\mathbf{R}\cdot\left[\frac{1}{\beta h^2}\mathbf{J}_\rho-\frac{\gamma}{\beta h}\left(\mathbf{J}_\rho\cdot\mathbf{W}\right)^\wedge+\frac{\gamma}{\beta h}\hat{\mathbf{W}}\cdot\mathbf{J}_\rho\right]\cdot\mathbf{R}_n^{\mathrm{T}}\cdot\mathbf{T}\right\}\cdot\boldsymbol{\delta\theta}\,dS \tag{2-167}$$

## 2.10 Space discretization of the linearized weak form

Regarding the finite-element discretization in space of the linearized weak form, as in Simo and Vu-Quoc (1986), the incremental displacement and rotation fields are interpolated on an element basis as:

$$\boldsymbol{\delta}\mathbf{u}\left(S\right)=\sum_{i=1}^{N}N_i\left(S\right)\boldsymbol{\delta}\mathbf{u}_i \qquad \boldsymbol{\delta\theta}\left(S\right)=\sum_{i=1}^{N}N_i\left(S\right)\boldsymbol{\delta\theta}_i \tag{2-168}$$

where $N$ is the number of nodes of the element, $N_i(S)$ is the element shape function associated with node $i$, and $\boldsymbol{\delta}\mathbf{u}_i$ and $\boldsymbol{\delta\theta}_i$ are the incremental displacement and rotation fields at node $i$.

As in the standard Galerkin method, the admissible variation $\boldsymbol{\eta}$ is approximated using the same interpolation functions as in (2-168). Moreover, the following interpolation scheme is used for the rotation tensor $\mathbf{R}$:

$$\mathbf{R}\left(S\right)=\exp\left[\hat{\boldsymbol{\chi}}\left(S\right)\right] \qquad \boldsymbol{\chi}\left(S\right)=\sum_{i=1}^{N}N_i\left(S\right)\boldsymbol{\chi}_i \tag{2-169}$$

where $\hat{\boldsymbol{\chi}}$ is the skew-symmetric tensor associated with the total rotation vector $\boldsymbol{\chi}$.

Substituting these interpolations into the linearized weak form leads to the following discrete approximation of the linearized weak form:

$$\sum_{i,j=1}^{N}\boldsymbol{\eta}_i\cdot\left[\mathbf{P}_i\left(\boldsymbol{\varphi}\right)+\mathbf{K}_{ij}\left(\mathbf{R}_n,\hat{\boldsymbol{\Omega}}_n,\boldsymbol{\varphi}\right)\cdot\boldsymbol{\Delta\varphi}_j\right]=0 \qquad \forall\,\boldsymbol{\eta}_i \tag{2-170}$$

where the discrete tangent operator $\mathbf{K}_{ij}$ is given by the sum of the material stiffness operator $\mathbf{S}_{ij}$, the damping operator $\mathbf{D}_{ij}$, the geometric stiffness operator $\mathbf{G}_{ij}$, and the inertia operator $\bar{\mathbf{M}}_{ij}$, that is

$$\mathbf{K}_{ij}=\mathbf{S}_{ij}+\mathbf{D}_{ij}+\mathbf{G}_{ij}+\bar{\mathbf{M}}_{ij} \tag{2-171}$$

$\mathbf{P}_i$ is the residual or out-of-balance force, and $\Delta\boldsymbol{\varphi}_j$ the incremental displacement and rotation vector. From (2-113) and (2-112), the discrete material stiffness operator may be written as:

$$\mathbf{S}_{ij}=\int_{I_e}\boldsymbol{\Xi}_i\cdot\mathbf{c}\cdot\boldsymbol{\Xi}_j^{\mathrm{T}}\,dS \tag{2-172}$$

where

$$\boldsymbol{\Xi}_i=\begin{bmatrix} N_i'\mathbf{I} & \mathbf{0} \\ -N_i\left[\dfrac{\partial\mathbf{x}_0}{\partial S}\times\right] & N_i'\mathbf{I}\end{bmatrix} \tag{2-173}$$

From (2-143) and (2-142), we write the discrete damping operator as:

$$\mathbf{D}_{ij}=\int_{I_e}\boldsymbol{\Xi}_i\cdot\mathbf{c}_{\mathrm{d}}\cdot\boldsymbol{\Xi}_{\mathrm{d}j}^{\mathrm{T}}\,dS \tag{2-174}$$

where

$$\boldsymbol{\Xi}_{\mathrm{d}j}^{\mathrm{T}}=\begin{bmatrix}\left[\left(\dfrac{\gamma}{\beta h}\mathbf{I}-\hat{\mathbf{w}}\right)\cdot N_j'\mathbf{I}\right] & \left[\dfrac{\gamma}{\beta h}\dfrac{\partial\hat{\mathbf{x}}_0}{\partial S}\cdot\mathbf{R}\cdot\mathbf{R}_n^{\mathrm{T}}\cdot\mathbf{T}+\dfrac{\partial\hat{\mathbf{v}}_0}{\partial S}\right]N_j \\ \mathbf{0} & \mathbf{R}\cdot\left[N_j\dfrac{\gamma}{\beta h}\left(\hat{\boldsymbol{\Omega}}-\hat{\boldsymbol{\Omega}}_n\right)\cdot\mathbf{R}_n^{\mathrm{T}}\cdot\mathbf{T}+N_j\dfrac{\gamma}{\beta h}\mathbf{R}_n^{\mathrm{T}}\cdot\mathbf{T}'+\left(\dfrac{\gamma}{\beta h}\mathbf{R}_n^{\mathrm{T}}\cdot\mathbf{T}-\mathbf{R}^{\mathrm{T}}\cdot\hat{\mathbf{w}}\right)\cdot N_j'\mathbf{I}\right]\end{bmatrix} \tag{2-175}$$

From (2-156) and (2-157), we get the following expression for the geometric stiffness operator:

$$\mathbf{G}_{ij}=\int_{I_e}\boldsymbol{\Psi}_i\cdot\mathbf{B}\cdot\boldsymbol{\Psi}_j^{\mathrm{T}}\,dS \tag{2-176}$$

where

$$\boldsymbol{\Psi}_i=\begin{bmatrix} N_i'\mathbf{I} & \mathbf{0} & \mathbf{0} \\ \mathbf{0} & N_i'\mathbf{I} & N_i\,\mathbf{I}\end{bmatrix} \tag{2-177}$$

From (2-167), the expression for the discrete tangent inertia operator is:

$$\bar{\mathbf{M}}_{ij}=\int_{I_e}\begin{bmatrix}\mathbf{m}_{ij}^{11} & \mathbf{0} \\ \mathbf{0} & \mathbf{m}_{ij}^{22}\end{bmatrix}dS \tag{2-178}$$

where

$$\mathbf{m}_{ij}^{11}=\frac{1}{\beta h^2}A_\rho\int_{I_e}N_iN_j\,dS\,\mathbf{I} \tag{2-179}$$

$$\begin{aligned}\mathbf{m}_{ij}^{22}=\int_{I_e}\Big\{&-\mathbf{R}\cdot\left[\mathbf{J}_\rho\cdot\mathbf{A}+\mathbf{W}\times\left(\mathbf{J}_\rho\cdot\mathbf{W}\right)\right]^\wedge+ \\ &\mathbf{R}\cdot\left[\frac{1}{\beta h^2}\mathbf{J}_\rho-\frac{\gamma}{\beta h}\left(\mathbf{J}_\rho\cdot\mathbf{W}\right)^\wedge+\frac{\gamma}{\beta h}\hat{\mathbf{W}}\cdot\mathbf{J}_\rho\right]\cdot\mathbf{R}_n^{\mathrm{T}}\cdot\mathbf{T}\Big\}N_iN_j\,dS\end{aligned} \tag{2-180}$$

Finally, from (2-74), the discrete residual force vector takes the form:

$$\mathbf{P}_i = \int_{I_e} \left\{ \boldsymbol{\Xi}_i \cdot \begin{bmatrix} \mathbf{n} \\ \mathbf{m} \end{bmatrix} - N_i \mathbf{I} \cdot \begin{bmatrix} \tilde{\mathbf{n}} \\ \tilde{\mathbf{m}} \end{bmatrix} + N_i \mathbf{I} \cdot \begin{bmatrix} A_\rho \mathbf{a}_0 \\ \mathbf{R} \cdot \left[ \mathbf{J}_\rho \cdot \mathbf{A} + \mathbf{W} \times \left( \mathbf{J}_\rho \cdot \mathbf{W} \right) \right] \end{bmatrix} \right\} dS \tag{2-181}$$

## 2.11 Remarks on numerical implementation

In this section, some details are presented on the numerical implementation of the formulation presented above. First, we are concerned with the evaluation of the exponential of a skew-symmetric matrix needed in the update of rotations given in Table 2-2. A simple expression for the exponential of a skew-symmetric tensor $\hat{\boldsymbol{\chi}}$ is given by Rodrigues' formula:

$$\exp\left(\hat{\boldsymbol{\chi}}\right) = \mathbf{I} + \frac{\sin\|\boldsymbol{\chi}\|}{\|\boldsymbol{\chi}\|}\hat{\boldsymbol{\chi}} + \frac{1-\cos\|\boldsymbol{\chi}\|}{\|\boldsymbol{\chi}\|^2}\hat{\boldsymbol{\chi}}^2 \tag{2-182}$$

However, as proposed by Simo and Vu-Quoc (1986), we choose to use a quaternion representation of rotations that relies on the singularity-free quaternion extraction procedure due to Spurrier (1978).

Details on the quaternion parametrization of rotations are presented in Section 2.11.1. In Section 2.11.2, we discuss and propose a solution to some issues that arise in the interpolation of total rotation vectors. Finally, in Section 2.11.3, we propose an approach for the update of the curvature vectors that has not been presented in the literature.

### 2.11.1 Quaternion representation of rotations

Quaternions are a generalization of complex numbers, and are a convenient way to represent rotations. A quaternion $\tilde{\mathbf{q}}$ consists of a scalar component $q_0$ and a vector component $\mathbf{q}$, and is written $\tilde{\mathbf{q}} = q_0 + \mathbf{q}$.

One of the advantages of representing rotations by quaternions is that when numerical errors cause a rotation matrix to deviate from being orthogonal, it is difficult to restore orthogonality. On the other hand, a quaternion simply needs to be normalized to unit length to ensure that it is a rotation. The unit quaternion corresponding to a rotation $\boldsymbol{\chi}$ is given by:

$$\tilde{\mathbf{q}} = q_0 + \mathbf{q} = \cos\frac{\|\boldsymbol{\chi}\|}{2} + \frac{\boldsymbol{\chi}}{\|\boldsymbol{\chi}\|}\sin\frac{\|\boldsymbol{\chi}\|}{2} \tag{2-183}$$

*Computation of a rotation matrix R from a given rotation vector* $\boldsymbol{\chi}$. After computing the 4 quaternion parameters $(q_0, q_1, q_2, q_3)$ using (2-183), the associated rotation matrix is given by:

$$R = 2\begin{bmatrix} q_0^2 + q_1^2 - 1/2 & q_1 q_2 - q_3 q_0 & q_1 q_3 + q_2 q_0 \\ q_2 q_1 + q_3 q_0 & q_0^2 + q_2^2 - 1/2 & q_2 q_3 - q_1 q_0 \\ q_3 q_1 - q_2 q_0 & q_3 q_2 + q_1 q_0 & q_0^2 + q_3^2 - 1/2 \end{bmatrix} \tag{2-184}$$

*Extraction of a rotation vector* $\boldsymbol{\chi}$ *from a rotation matrix R.* Several algorithms exist for the extraction of a unit quaternion from an orthogonal matrix. After extracting the 4 quaternion parameters $(q_0, q_1, q_2, q_3)$ using Spurrier's algorithm (Spurrier, 1978), the associated rotation vector is obtained as:

$$\|\boldsymbol{\chi}\| = 2\sin^{-1}\|\mathbf{q}\| \tag{2-185}$$

$$\boldsymbol{\chi} = \|\boldsymbol{\chi}\|\frac{\mathbf{q}}{\|\mathbf{q}\|} \tag{2-186}$$

### 2.11.2 Interpolation of rotation vectors

The discrete tangent operator, $\mathbf{K}_{ij}$, and the out-of-balance force, $\mathbf{P}_i$, described previously are evaluated using Gauss integration. This involves the evaluation of the rotation tensor, $\mathbf{R}$, and the curvature vector, $\boldsymbol{\omega}$, at the Gauss points, requiring careful interpolation of the nodal rotation vectors, $\boldsymbol{\chi}_i$. These are extracted from $\exp(\boldsymbol{\chi}_i)$ using Spurrier's algorithm (Spurrier, 1978), which is reported to be the most efficient for the extraction of a quaternion from an orthogonal tensor. Spurrier's algorithm computes a positive quaternion some times and its negative other times. The two, however, are completely interchangeable, as they correspond to the same rotation tensor. One represents a rotation of π or less and the other represents a rotation of opposite sense, about the same axis, of 2π minus the same angle. We choose to uniquely extract rotation vectors, $\boldsymbol{\chi}_i$, of magnitude between -π and π, by selecting the sign of the associated quaternion $\tilde{\mathbf{q}} = q_0 + \mathbf{q}$ that makes its scalar component, $q_0$, positive.

Issues can occur, however, when the nodal rotation vectors, $\boldsymbol{\chi}_i$, are interpolated by means of (2-169) to evaluate the rotation vectors at the Gauss points. These are not evaluated correctly when the magnitude of the real rotations is larger than π. In this work's implementations we tackle the problem as follows. For a 2-noded element, let $\boldsymbol{\chi}_i$ and $\boldsymbol{\chi}_j$ be the extracted rotation vectors at nodes

$i$ and $j$. In interpolating, one takes $\boldsymbol{\chi}_i$ as it is, whereas three rotation vectors are considered at node $j$. These are $\boldsymbol{\chi}_j$, $\boldsymbol{\chi}_j+2\pi\mathbf{n}$ and $\boldsymbol{\chi}_j-2\pi\mathbf{n}$, with $\mathbf{n}=\mathbf{q}/\|\mathbf{q}\|$ being the unit vector along the rotation axis. Of the three, the one that has the minimum Euclidean distance from $\boldsymbol{\chi}_i$ is taken.

### 2.11.3 Update of curvature vectors

In this subsection we derive an expression for the update of the curvature vectors that depends only on the total rotation vectors at the current iteration. This is in contrast with what generally has been done in the literature, where the curvature vectors are updated using incremental rotation vectors and the curvature vectors at the previous iteration or time step (Simo and Vu-Quoc, 1988; Ibrahimbegovic and Mikdad, 1998; Jelenic and Crisfield, 1998). This was done to avoid path dependence in the constitutive equation, because the exponentiation and interpolation do not commute.

As introduced previously, the curvature tensor in the *current* configuration is given by:

$$\hat{\boldsymbol{\omega}}=\frac{\partial}{\partial S}\mathbf{R}\cdot\mathbf{R}^{\mathrm{T}} \tag{2-187}$$

To carry out the calculation, one needs to evaluate the derivative with respect to $S$ of the rotation tensor $\mathbf{R}=\exp(\hat{\boldsymbol{\chi}})$. A simple expression for the exponential of a skew-symmetric tensor is given by Rodrigues' formula (2-182). A similar expression was used by Simo and Vu-Quoc (1986) to derive a closed-form solution for the derivative of the exponential of a skew-symmetric tensor. However, we follow a different approach that takes advantage of the notion of right-trivialized derivative of the exponential map defined as:

$$\mathrm{d}\exp_{\chi}=\frac{\sin\|\boldsymbol{\chi}\|}{\|\boldsymbol{\chi}\|}\mathbf{I}+\frac{1-\cos\|\boldsymbol{\chi}\|}{\|\boldsymbol{\chi}\|^{2}}\hat{\boldsymbol{\chi}}+\frac{\|\boldsymbol{\chi}\|-\sin\|\boldsymbol{\chi}\|}{\|\boldsymbol{\chi}\|^{3}}\boldsymbol{\chi}\otimes\boldsymbol{\chi} \tag{2-188}$$

It can be shown (Ortolan, 2011) that

$$\left(\mathrm{d}\exp_{\chi}\cdot\delta\boldsymbol{\chi}\right)^{\wedge}=\left(\mathrm{D}\exp\left(\hat{\boldsymbol{\chi}}\right)\cdot\delta\boldsymbol{\chi}\right)\cdot\exp\left(\hat{\boldsymbol{\chi}}\right)^{\mathrm{T}} \tag{2-189}$$

Using (2-189), the current curvature tensor given by (2-187) may be evaluated as:

$$\hat{\boldsymbol{\omega}}=\left[\mathrm{D}\exp\left(\hat{\boldsymbol{\chi}}\right)\cdot\boldsymbol{\chi}'\right]\cdot\exp\left(\hat{\boldsymbol{\chi}}\right)^{\mathrm{T}}=\left(\mathrm{d}\exp_{\chi}\cdot\boldsymbol{\chi}'\right)^{\wedge} \tag{2-190}$$

While $\mathrm{D}\exp(\hat{\boldsymbol{\chi}})$ is a third-order tensor, which is hard to evaluate, $\mathrm{d}\exp_{\chi}$ is a second-order tensor for which the simple closed form is given by (2-188). Based on (2-190), the curvature vector in the *current* configuration is simply

$$\boldsymbol{\omega} = \mathrm{d}\exp_{\chi} \cdot \boldsymbol{\chi}' \tag{2-191}$$

## 2.12 Numerical examples

In this section we consider a series of numerical simulations that illustrate the performance of the formulation described above. Each example consists of both a static and a dynamic phase. The first example is a plane problem involving rotations of magnitude greater than π, while the following examples concern the 3D static and dynamic analysis of a conductor commonly used in electrical substations. Convergence rates and energy balance calculations are presented for each example to show the performance of the computations. Finally, the results are compared to those obtained with the commercial software ABAQUS.

### 2.12.1 Free vibration of rolled over cantilever

The first application consists of statically deforming a cantilever beam into a circle and then releasing it. The properties of the beam, taken from Linn et al. (2012), are as follows: length $L$=0.3 m, cross-section area $A$=0.01x0.01 m$^2$, Young's modulus $E$=10$^6$ Pa, Poisson's ratio $\nu$=0.3, and mass density $\rho$=10$^3$ kg/m$^3$. The finite element mesh consists of 10 2-noded (linear) elements. The internal force vector, the dissipative force vector, the material and geometric stiffness matrices, and the damping matrix are computed using reduced Gaussian integration (1-point), while 2-point Gaussian integration is used for the inertial force vector and the inertia matrix. The parameters used in the time integration scheme are $\beta$=0.25 and $\gamma$=0.5.

#### 2.12.1.1 Static analysis

The beam is rolled over by applying a concentrated moment $M$ at its free end. Since the exact deformed shape is a circle of radius $r$=$EI$/$M$, a moment $M$=2π$EI$/$L$ will force the beam to deform into a full circle. The moment $M$ is applied in 10 load steps. The final static configuration of the beam is shown in Figure 2-3, along with the exact solution and the deformed shapes at each load increment. The rate of convergence of Newton's method is given for each load step in Table 2-3. The residual decrease in the last few iterations suggests a quadratic rate of convergence.

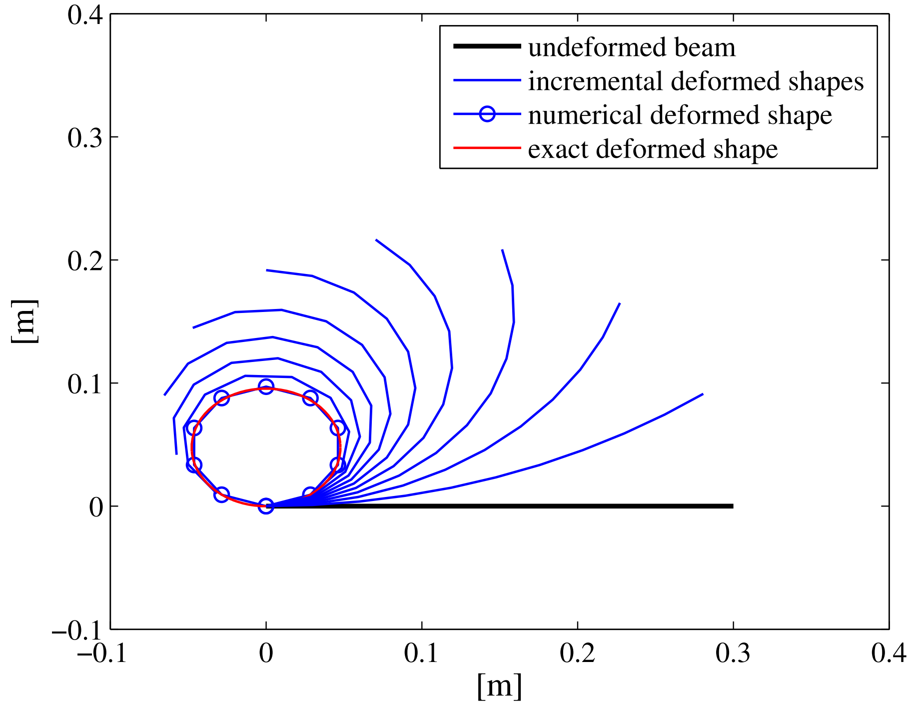


**Figure 2-3 Incremental deformation of cantilever beam into a full circle**

**Table 2-3 Statically rolled over cantilever – convergence rate of Newton's method**

| iteration | Load increment | | | | | | | | | |
|---|---|---|---|---|---|---|---|---|---|---|
| | 1 | 2 | 3 | 4 | 5 | 6 | 7 | 8 | 9 | 10 |
| 1 | 1.74E-03 | 1.74E-03 | 1.74E-03 | 1.74E-03 | 1.74E-03 | 1.74E-03 | 1.74E-03 | 1.74E-03 | 1.74E-03 | 1.74E-03 |
| 2 | 1.76E+01 | 1.77E+01 | 1.80E+01 | 1.83E+01 | 1.88E+01 | 1.94E+01 | 2.00E+01 | 2.07E+01 | 2.15E+01 | 2.23E+01 |
| 3 | 6.43E-01 | 6.46E-01 | 6.51E-01 | 6.57E-01 | 6.67E-01 | 6.74E-01 | 6.84E-01 | 6.95E-01 | 7.08E-01 | 7.21E-01 |
| 4 | 4.74E-02 | 4.91E-02 | 5.22E-02 | 5.63E-02 | 6.11E-02 | 6.66E-02 | 7.25E-02 | 7.88E-02 | 8.53E-02 | 9.20E-02 |
| 5 | 3.88E-02 | 3.91E-02 | 3.97E-02 | 4.05E-02 | 4.14E-02 | 4.24E-02 | 4.36E-02 | 4.49E-02 | 4.64E-02 | 4.80E-02 |
| 6 | 2.43E-02 | 2.48E-02 | 2.55E-02 | 2.66E-02 | 2.79E-02 | 2.94E-02 | 3.10E-02 | 3.28E-02 | 3.47E-02 | 3.67E-02 |
| 7 | 6.55E-03 | 6.63E-03 | 6.77E-03 | 6.95E-03 | 7.18E-03 | 7.46E-03 | 7.76E-03 | 8.09E-03 | 8.46E-03 | 8.84E-03 |
| 8 | 2.89E-03 | 2.94E-03 | 3.01E-03 | 3.11E-03 | 3.23E-03 | 3.37E-03 | 3.53E-03 | 3.69E-03 | 3.88E-03 | 4.07E-03 |
| 9 | 8.39E-05 | 8.51E-05 | 8.70E-05 | 8.97E-05 | 9.30E-05 | 9.69E-05 | 1.01E-04 | 1.06E-04 | 1.11E-04 | 1.16E-04 |
| 10 | 6.29E-07 | 6.39E-07 | 6.54E-07 | 6.74E-07 | 7.03E-07 | 7.29E-07 | 7.62E-07 | 7.99E-07 | 8.37E-07 | 8.71E-07 |
| 11 | 3.89E-12 | 3.86E-12 | 3.95E-12 | 4.17E-12 | 1.37E-10 | 4.43E-12 | 4.63E-12 | 4.86E-12 | 5.09E-12 | 9.78E-11 |

#### 2.12.1.2 Dynamic analyses

The free vibration analyses are performed with three different values of the retardation constants $\mu=\eta$, namely 0.02, 0.04 and 0.08 s. The time step used is $h$=0.001 s. The vertical and horizontal positions of the free end of the beam are plotted in Fig. 2-4 for each value of the retardation constants considered. Fig. 2-5 shows snapshots of the beam at times identified by circles and numbers in Fig. 2-4. The rate of convergence of Newton's method is shown for those same times in Table 2-4.

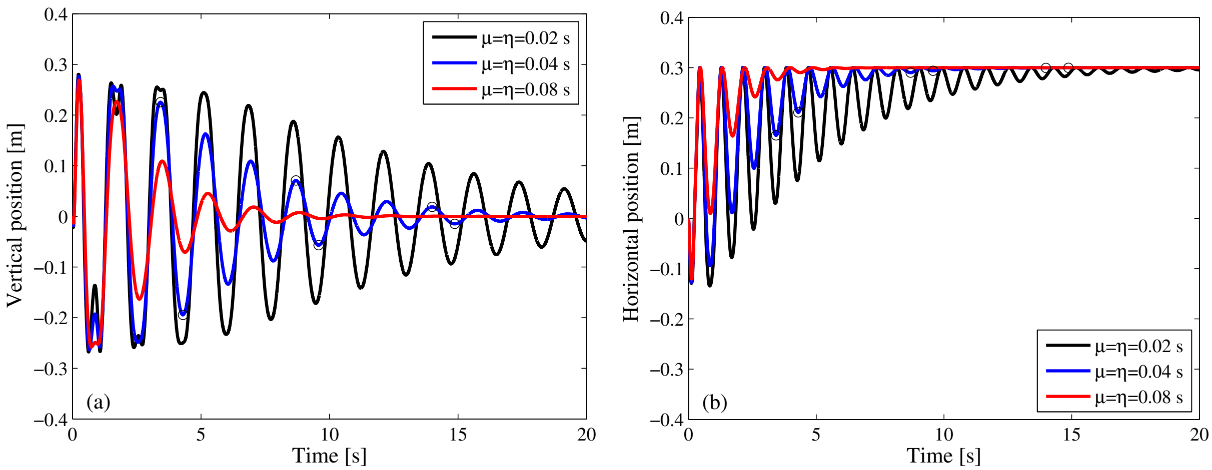


**Figure 2-4 Displacement of free end of cantilever beam in free vibration: (a) vertical position; (b) horizontal position**

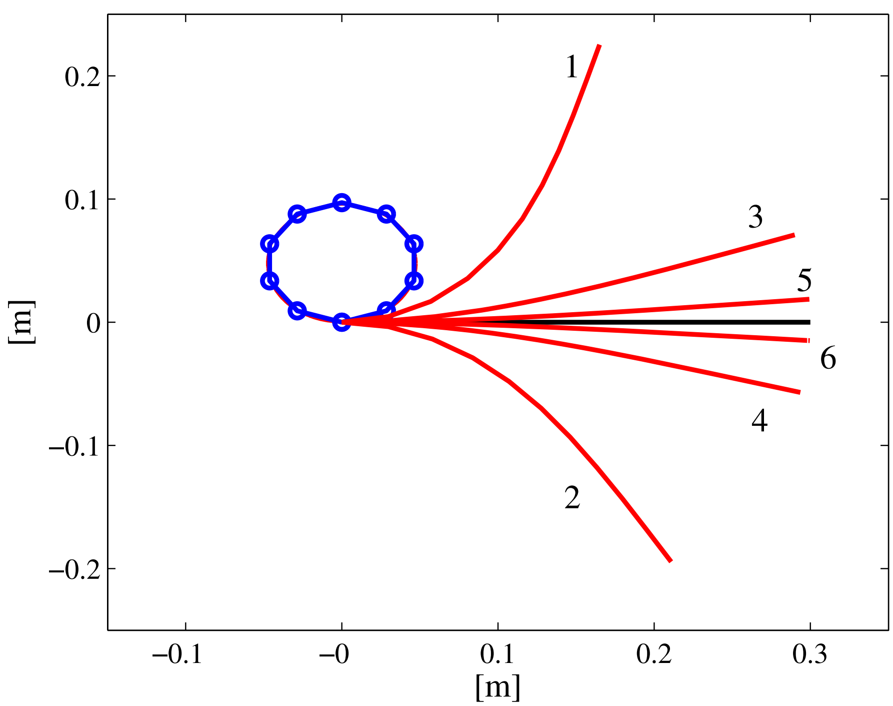


**Figure 2-5 Dynamic unwinding of rolled over cantilever beam**

**Table 2-4 Dynamic unwinding of cantilever – convergence of Newton's method**

| iteration | Time increment | | | | | |
|---|---|---|---|---|---|---|
| | 1 ($t$=3.427 s) | 2 ($t$=4.300 s) | 3 ($t$=8.695 s) | 4 ($t$=9.577 s) | 5 ($t$=13.989 s) | 6 ($t$=14.872 s) |
| 1 | 2.03E-01 | 8.75E-02 | 6.02E-03 | 4.40E-03 | 4.16E-03 | 2.39E-03 |
| 2 | 2.75E-04 | 4.10E-05 | 1.53E-07 | 6.21E-08 | 1.78E-08 | 6.19E-09 |
| 3 | 3.27E-09 | 3.09E-10 | 3.30E-13 | | | |

The reliability of computations is assessed by performing energy calculations and making sure that the energy balance is achieved. In free vibration the sum of strain energy, kinetic energy and dissipated energy should be constant and equal to the initial strain energy prior to release. Figure 2-6(a) shows the energy balance for the case $\mu$=$\eta$=0.02 s. Similar plots are obtained for the other values of the retardation constants. The decay of the total energy, sum of strain and kinetic energy, is shown in Figure 2-6(b) for each value of the retardation constants considered.

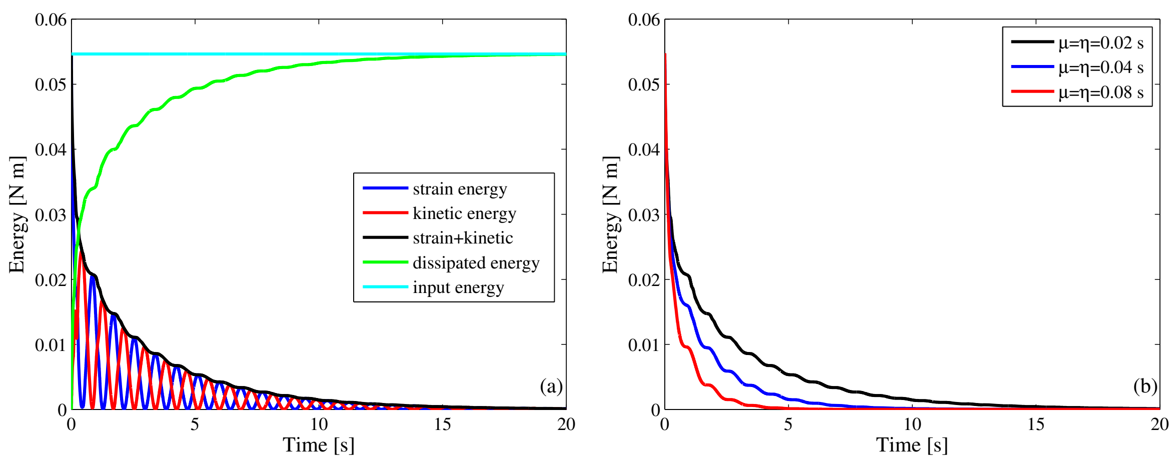


**Figure 2-6 Cantilever beam in free vibration: (a) energy balance; (b) energy decay**

In the following, the results of the proposed formulation are verified with those obtained using ABAQUS. The cantilever beam was modeled in ABAQUS using 30 CPS4I elements (4-node continuum incompatible modes linear elements), and stiffness proportional damping is introduced through the Rayleigh damping factor $\beta^R$. ABAQUS uses the Hilber-Hughes-Taylor implicit time integration method. In order to obtain the Newmark's scheme used in our formulation ($\beta$=0.25, $\gamma$=0.5), we set the parameter $\alpha$ to zero. The time step used is the same as that used for our formulation, namely $h$=0.001 s. The results for the case $\mu$=$\eta$=0.04 s are shown in Figure 2-7 where they are compared to those obtained with our formulation.

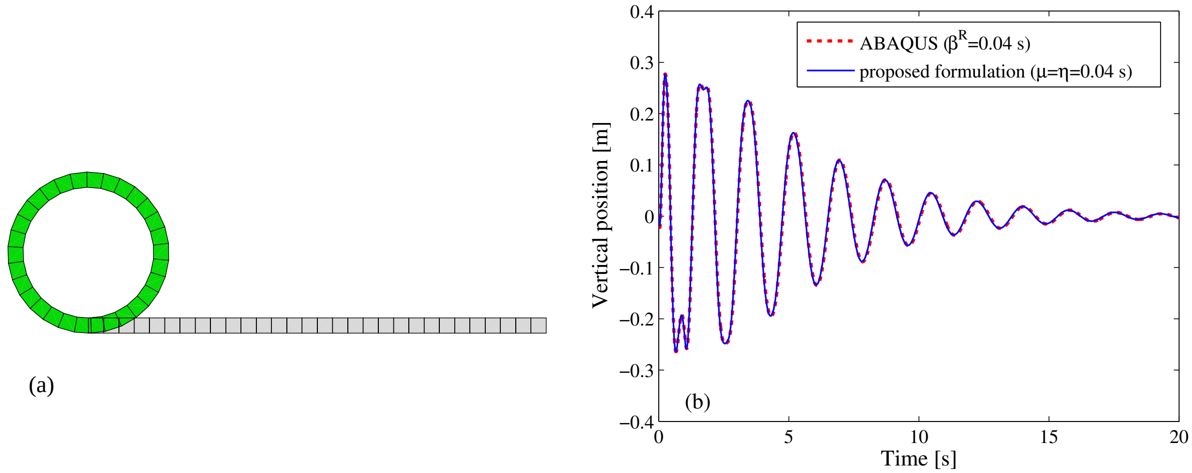


**Figure 2-7 (a) Rolled over cantilever in ABAQUS; (b) free vibration response – ABAQUS versus proposed formulation**

### 2.12.2 Forced and free vibration of cable with clamped ends

In the following examples, an electrical conductor cable in a vertical drop configuration commonly seen in electrical substations is subjected to resonant harmonic excitation of its supports. This kind of excitation is contemplated in the IEEE 1527 Standard (Recommended Practice for the Design of Flexible Buswork Located in Seismically Active Areas), and recent testing of conductor cables with vertical drops has been reported by Chandran (2012).

The material and geometric properties of the cable are: Young's modulus $E$=69000 MPa ($10^7$ psi), Poisson's ratio $\upsilon$=0.3, length $L$=3683 mm (145 in), cross section area $A$=1335 mm$^2$ (2.07 in$^2$), cross-section second moments of area $I_1=I_2$=2830 mm$^4$ (0.0068 in$^4$) and cross-section torsion constant $J_t=I_1+I_2$. The weight per unit length of the cable is 0.033 N/mm (0.188 lbs/in). The finite element mesh consists of 80 2-noded (linear) elements. As in the previous example, reduced Gaussian integration (1-point) is used to compute the internal force vector, the dissipative force vector, the material and geometric stiffness matrices, and the damping matrix, while 2-point Gaussian integration is used for the inertial force vector and the inertia matrix.

#### 2.12.2.1 Cable form finding

The initial configuration of the cable is obtained by imposing end displacements and rotations to an initially straight and unstrained cable. The problem of deforming the cable into its initial configuration is not a trivial one. A particular load path has to be followed in order to obtain the expected final configuration. The cable is first subjected to its own weight and then, in arc-length control, statically displaced in the steps described in Table 2-5. An additional step in displacement control is carried out after step 4 to obtain the exact boundary conditions. The deformed shapes of the cable after each step are plotted in Fig. 2-8. The rate of convergence of Newton's method for some selected arc-length increments is given in Table 2-6.

**Table 2-5 Cable form finding – loading sequence**

| step | Boundary condition | Increments |
|---|---|---|
| 1 | 0.2 $\pi/2$ rotation at left end | 7 |
| 2 | -856 mm (34.5 in) horizontal displacement at right end | 40 |
| 3 | 0.8 $\pi/2$ rotation at left end | 9 |
| 4 | 1323 mm (52.1 in) vertical displacement at right end | 14 |

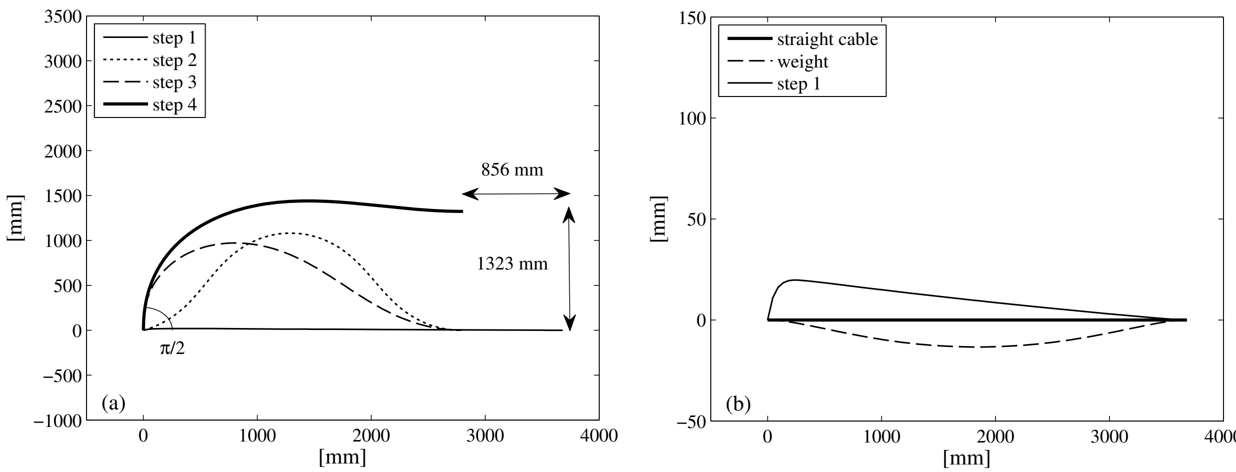


**Figure 2-8 (a) Static deformed shapes of cable with clamped ends; (b) magnification of cable under its own weight and subjected to step 1**

**Table 2-6 Cable form finding – convergence of Newton's method**

| iteration | Step | | | |
|---|---|---|---|---|
| | 1 ($\lambda$=0.63) | 2 ($\lambda$=0.54) | 3 ($\lambda$=0.22) | 4 ($\lambda$=0.71) |
| 1 | 1.37E+04 | 3.06E+03 | 6.55E+04 | 1.09E+04 |
| 2 | 3.34E+03 | 1.70E+00 | 1.27E+04 | 1.26E+02 |
| 3 | 2.29E+02 | 1.42E-01 | 1.68E+04 | 5.85E+01 |
| 4 | 1.09E-01 | 9.08E-07 | 4.29E+02 | 1.11E+00 |
| 5 | 9.17E-07 | | 1.39E+01 | 7.20E-03 |
| 6 | | | 2.92E-04 | 5.54E-07 |
| 7 | | | 7.32E-07 | |

#### 2.12.2.2 Harmonic ground motion inputs

Starting from the configuration obtained in the previous section, the cable is then subjected to in-plane and out-of-plane horizontal harmonic excitations at its supports of the form:

$$u(t)=U\left\{\exp(-\zeta\omega_n t)\left[\cos\omega_D t+\frac{\zeta}{\sqrt{1-\zeta^2}}\sin\omega_D t\right]-\cos\omega_n t\right\} \tag{2-192}$$

Eq. (2-192) represents the response of a damped single degree of freedom system (SDOF) of frequency $\omega_n$ and damping ratio $\zeta$ to a sinusoidal force of frequency $\omega=\omega_n$ (Chopra 2007). In Eq. (2-192), $U$ is the steady state amplitude of the response, and $\omega_D=\omega_n\sqrt{1-\zeta^2}$ is the damped natural frequency of the SDOF. At a specified time $\bar{t}$, the motion at the supports is gradually stopped, in a time $\tau_s$, according to the following polynomial rule:

$$u(\bar{t}+\tau)=C_5\left(1-\frac{\tau}{\tau_s}\right)^5+C_4\left(1-\frac{\tau}{\tau_s}\right)^4+C_3\left(1-\frac{\tau}{\tau_s}\right)^3 \tag{2-193}$$

The three constants $C_5$, $C_4$ and $C_3$ are obtained by imposing the continuity conditions of displacement, velocity and acceleration at time $\tau=0$.

In the present applications, displacement amplitudes of 50.8 mm (2 in) are considered, and the exciting frequencies are taken equal to the linearized fundamental natural frequencies of the cable in the initial deformed configuration. These were estimated by linear eigenvalue analysis using the tangent stiffness matrix at the given initial configuration and an appropriate consistent mass matrix. The computed frequencies are 1.5 Hz for the out-of-plane motion and 4.1 Hz for the in-plane motion.

*Out-of-plane excitation*: The time step used for the out-of-plane simulation is $h$=0.001 s. Substituting the frequency of the out-of-plane motion into Eq. (2-192), and using $\zeta$=0.1, we get the support excitation shown in Figure 2-9(a). At time $\bar{t}$ =10 s, according to Eq. (2-193), the support excitation is gradually stopped in a time $\tau_s$=200$h$, and thereafter the cable undergoes a phase of free vibration. The retardation constants used in the analyses are $\mu=\eta$=0.01 s.

The components of the response of a reference point along the cable ($S$=1793 mm), to the out-of-plane excitation, are shown in Figure 2-10, along with the deformed shape of the cable at the onset of free vibration, and the deformed shape at the end of the analysis. The reference point is marked in Figure 2-10(d). Again, the reliability of computations is assessed in terms of energy balance. In forced vibration the input energy has to be equal at all times to the sum of strain, kinetic and dissipated energy. Each energy component is plotted in Figure 2-11(a), and the energy balance is shown in Figure 2-11(b). The rate of convergence of Newton's method, for the time increments identified by circles in Figure 2-10(a), is given in Table 2-7.

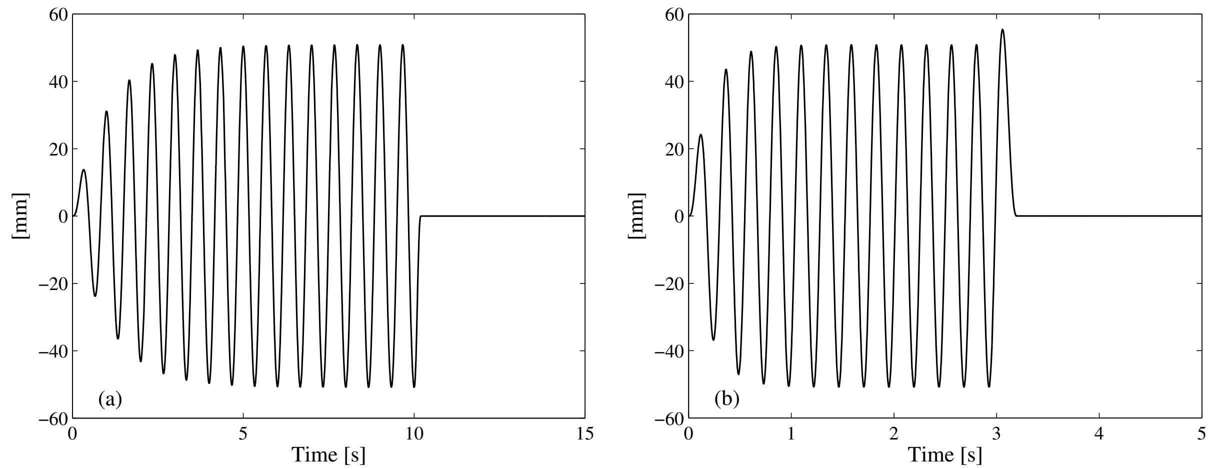


**Figure 2-9 (a) Imposed out-of-plane support motion; (b) imposed in-plane support motion**

As shown in Figure 2-10, the results of the simulation are verified against those obtained with ABAQUS. The cable was modeled in ABAQUS using 80 B31 elements (2-node linear beam element in space), and stiffness proportional damping was included through the Rayleigh damping factor $\beta^R$=0.01 s. Results from the proposed formulation compare favorably with ABAQUS results obtained by setting α to zero and using time step $h$=0.001 s.

*In-plane horizontal excitation*: The time step used is in this case is again $h$=0.001 s. Substituting the frequency of the in-plane motion into Eq. (2-192), and using $\zeta$=0.2, we get the support excitation shown in Figure 2-9(b). At time $\bar{t}$ =3 s, the support excitation is gradually stopped, in a time $\tau_s$=200$h$, and thereafter the cable undergoes a phase of free vibration. Again, we use $\mu$=$\eta$=0.01 s as retardation constants.

The components of the response of a reference point along the cable ($S$=1793 mm), to the in-plane horizontal excitation, are shown in Figure 2-12, along with the deformed shape of the cable at the onset of free vibration, and the deformed shape at the end of the analysis. The reference point is marked in Fig. 2-12(d). Each energy component is plotted in Figure 13(a), and the energy balance is shown in Figure 13(b). The rate of convergence of Newton's method, for the time increments identified by circles in Figure 2-12(b), is given in Table 2-8.

As shown in Fig. 2-12, the results of the simulation are verified favorably with those obtained with ABAQUS.

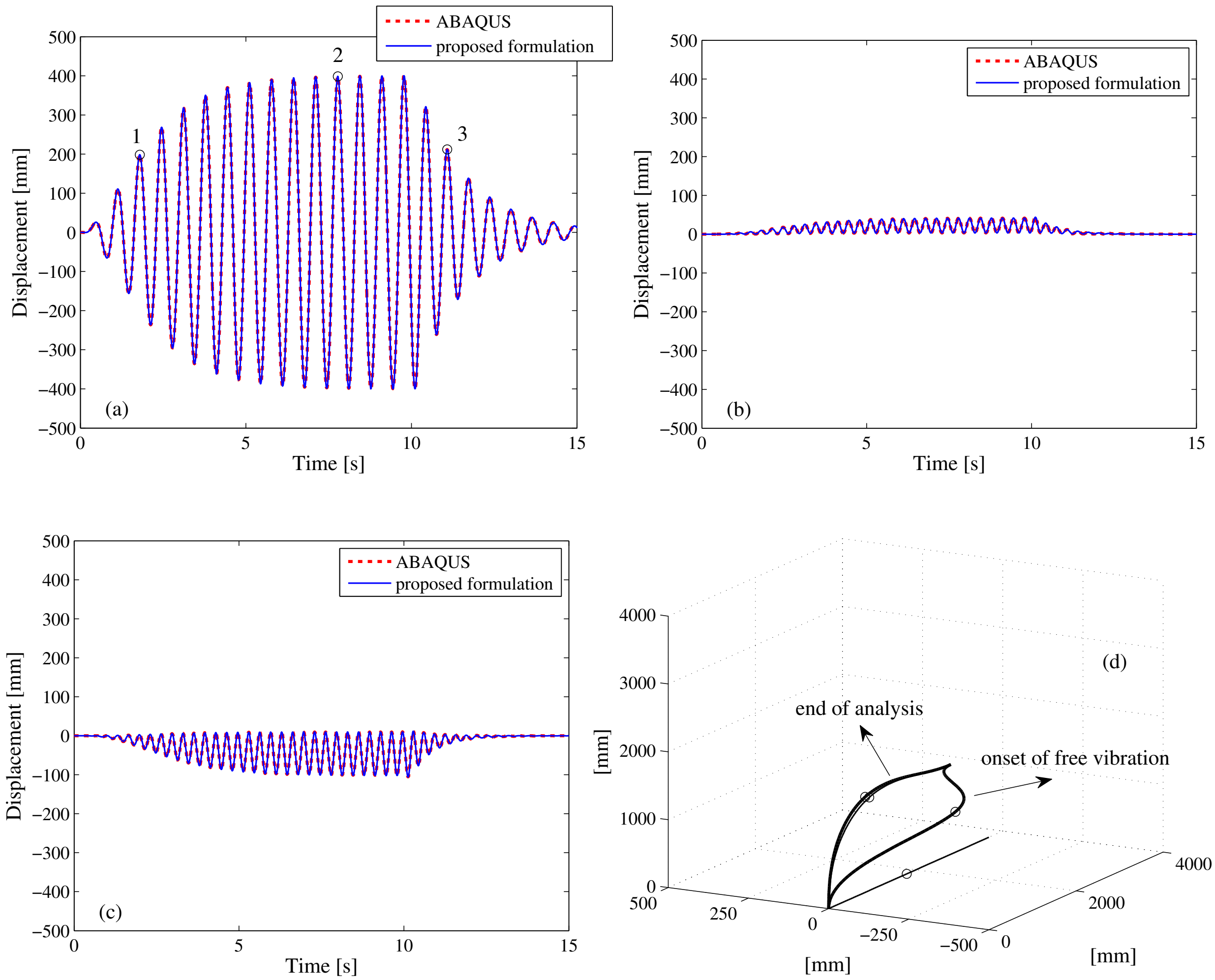


**Figure 2-10 Numerical response of reference point to out-of-plane resonant excitation: (a) out-of-plane displacement; (b) in-plane horizontal displacement; (c) vertical displacement; (d) deformed shapes of cable at onset of free vibration and end of analysis**

### 2.12.3 Remarks on the choice of time step in numerical simulations

In the numerical examples presented above a time step $h$=0.001 s was used. Although the numerical algorithm still converges when larger time steps are used, the energy balance is not always guaranteed. To illustrate this concept, Figures 2-14 and 2-15 show the energy error obtained by running the cable example with different time steps. We note that significantly larger errors can be obtained in the simulation of the in-plane excitation of the cable, requiring that smaller time steps be used in such case. An explanation is given by the fact that, when excited in-plane, the axial stiffness of the cable can dominate its response and generate high frequency effects that can lead to errors and instability problems (Hong et al. 2001).

**Table 2-7 Out-of-plane excitation: convergence of Newton's method**

| iteration | Time increment | | |
|---|---|---|---|
| | 1 ($t$=1.793 s) | 2 ($t$=7.776 s) | 3 ($t$=11.079 s) |
| 1 | 2.23E+06 | 2.50E+06 | 4.65E+01 |
| 2 | 5.14E+02 | 1.23E+03 | 6.99E+01 |
| 3 | 3.77E+01 | 1.90E+02 | 9.97E-03 |
| 4 | 4.82E-03 | 6.05E-02 | 8.34E-06 |
| 5 | 9.01E-07 | 1.82E-05 | 1.21E-07 |
| 6 | | 5.97E-07 | |

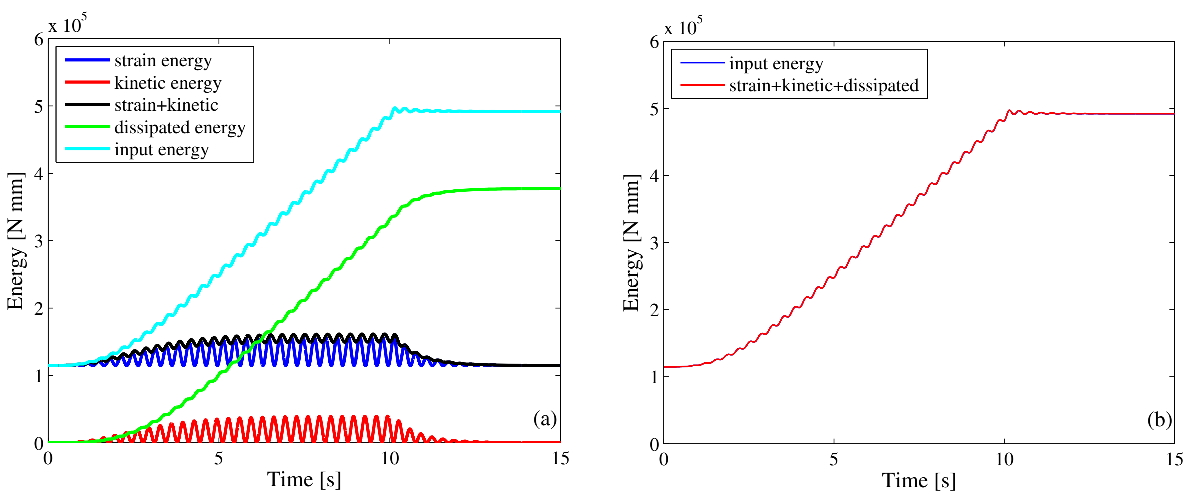


**Figure 2-11 Cable in out-of-plane forced vibration: (a) energy components; (b) energy balance**

### 2.12.4 Energy calculations

The energy components are evaluated through the following expressions:

Strain energy: $$E_S\left(t\right)=\frac{1}{2}\int_L\left[\mathbf{\Gamma}\left(S,t\right)\cdot\mathbf{C}^{\mathrm{N}}\cdot\mathbf{\Gamma}\left(S,t\right)+\mathbf{\Omega}\left(S,t\right)\cdot\mathbf{C}^{\mathrm{M}}\cdot\mathbf{\Omega}\left(S,t\right)\right]dS$$

Kinetic energy: $E_K(t) = \frac{1}{2}\int_L \left[ A_\rho \mathbf{v}_0(S,t)\cdot\mathbf{v}_0(S,t) + \mathbf{W}(S,t)\cdot\mathbf{J}_\rho\cdot\mathbf{W}(S,t)\right] dS$

Dissipated energy: $E_D(t) = \int_0^t \int_L \left[ \dot{\boldsymbol{\Gamma}}(S,\tau)\cdot\mathbf{C}_\mathrm{d}^\mathrm{N}\cdot\dot{\boldsymbol{\Gamma}}(S,\tau) + \dot{\boldsymbol{\Omega}}(S,\tau)\cdot\mathbf{C}_\mathrm{d}^\mathrm{M}\cdot\dot{\boldsymbol{\Omega}}(S,\tau)\right] dS\, d\tau$

Input energy: $E_I(t) = \int_0^t \mathbf{R}_i^s(\tau)\cdot\mathbf{v}_i^s(\tau)\, d\tau + \int_0^t \int_L \overline{w}(S,\tau)\, v_1(S,\tau)\, dS d\tau$

where $\mathbf{R}_i^s$ and $\mathbf{v}_i^s$ are the reactions and the velocity at the supports, $\overline{w}$ is the weight per unit length and $v_1$ is the vertical component of velocity.

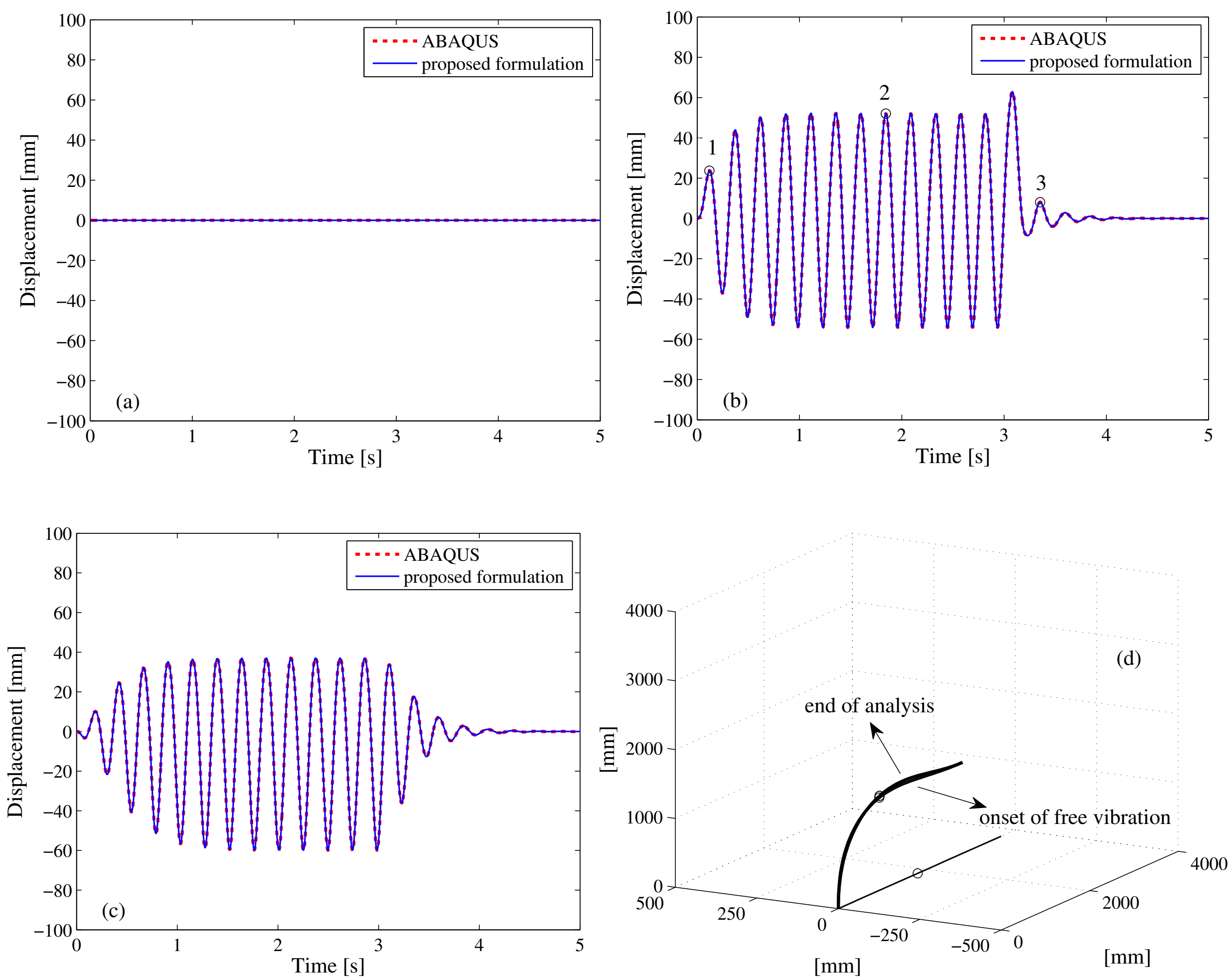


**Figure 2-12 Numerical response of reference point to in-plane horizontal resonant excitation: (a) out-of-plane displacement; (b) in-plane horizontal displacement; (c) vertical displacement; (d) deformed shapes of cable at onset of free vibration and end of analysis**

**Table 2-8 In-plane excitation: convergence rate of Newton's method**

| iteration | Time increment | | |
|---|---|---|---|
| | 1 ($t$=0.120 s) | 2 ($t$=1.844 s) | 3 ($t$=3.353 s) |
| 1 | 7.93E+04 | 4.87E+06 | 6.48E+00 |
| 2 | 5.17E+01 | 4.82E+03 | 2.60E-01 |
| 3 | 1.74E-02 | 3.65E+02 | 6.82E-06 |
| 4 | 4.39E-06 | 2.45E+00 | 7.18E-07 |
| 5 | 6.62E-07 | 2.13E-03 | |
| 6 | | 1.08E-06 | |
| 7 | | 6.33E-07 | |

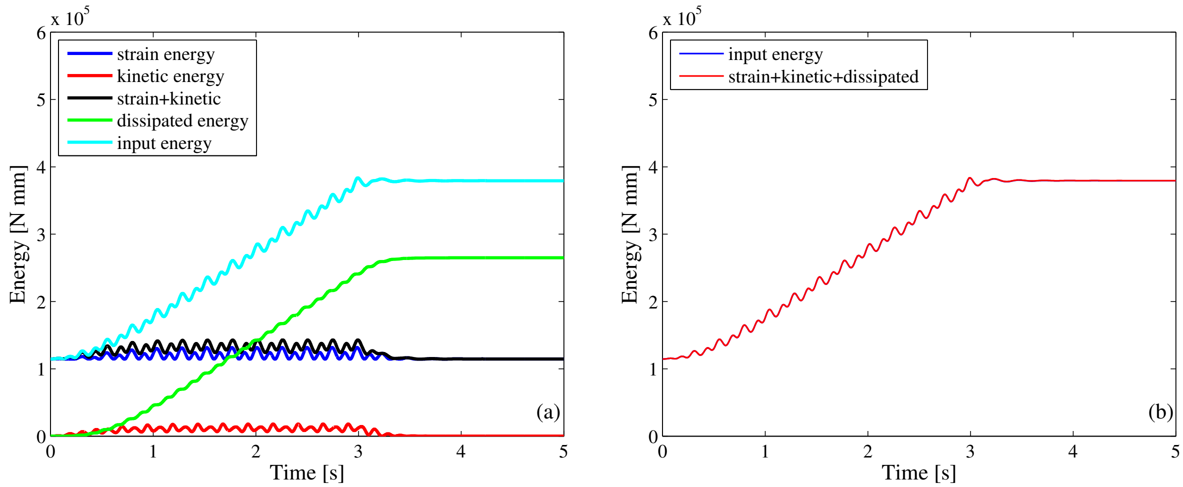


**Figure 2-13 Cable in in-plane forced vibration: (a) energy components; (b) energy balance**

### 2.12.5 Concluding remarks

By appropriately modifying and extending the 3D finite deformation beam model proposed by Simo, a finite element formulation has been developed for the static and dynamic analysis of flexible beams. An extension of the Kelvin-Voigt damping model has been introduced through the constitutive equations to model energy dissipation in a way that is physically consistent with the large displacements and large rotations beam model. A solution to issues concerning interpolation of total rotation vectors of magnitude greater than $\pi$ has been proposed and illustrated through an example. Furthermore, an alternative approach for the update of curvatures has been described, based on total rotation vectors, and taking advantage of special features of Lie groups and of the notion of right trivialized derivative. Both 2D and 3D numerical examples have been considered and energy balance plots, as well as convergence rates of Newton's method, demonstrate the accuracy of the computed solutions. The introduction of additional damping models, within the current framework, is subject of current computational work.

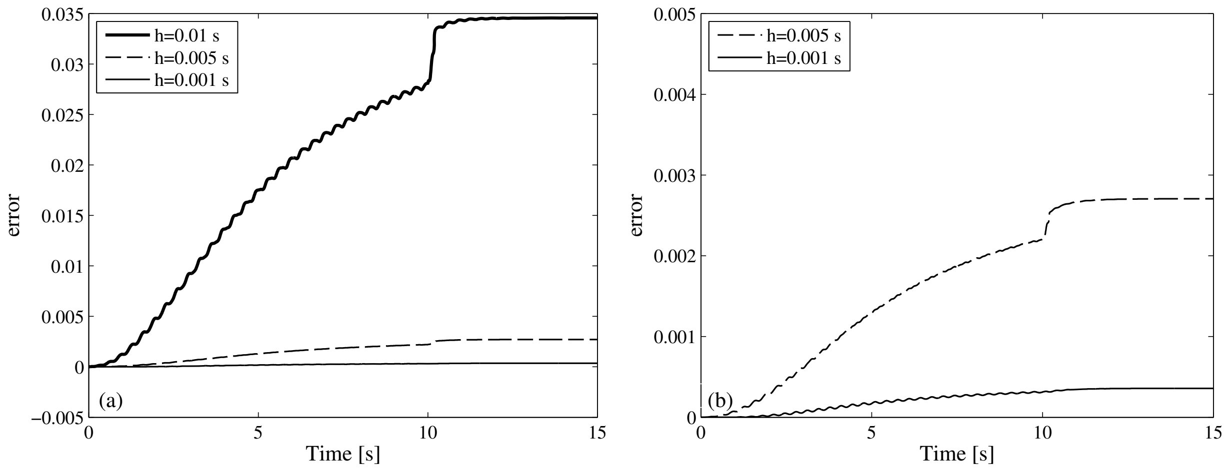


**Figure 2-14 Cable in out-of-plane forced vibration: (a) energy error for different values of the time step h; (b) detail of energy error for h=0.005 s and h=0.001 s**

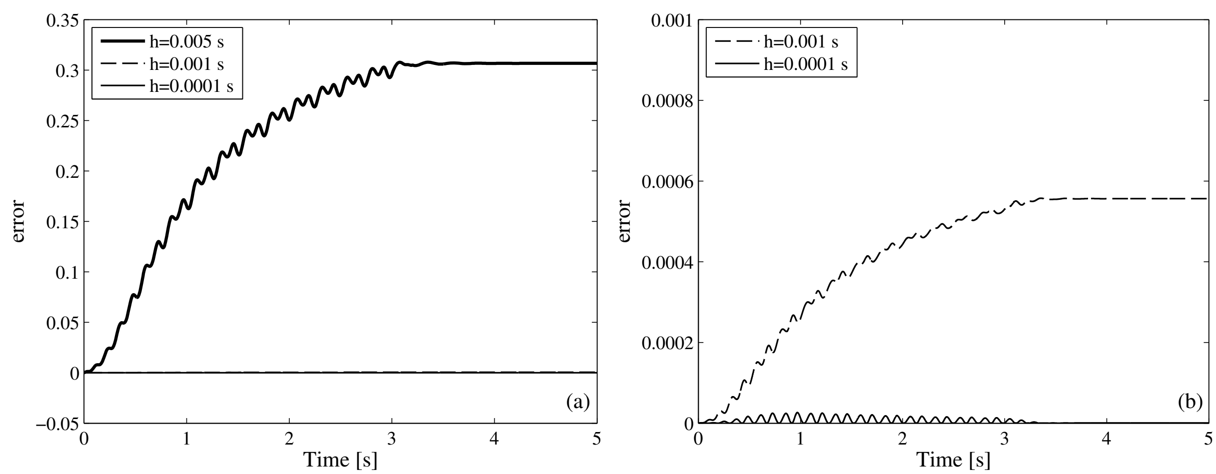


**Figure 2-15 Cable in in-plane forced vibration: (a) energy error for different values of the time step h; (b) detail of energy error for h=0.001 s and h=0.0001 s**

# SECTION 3
# NON-LINEAR DYNAMICS OF ELECTRICAL EQUIPMENT CABLES

## 3.1 Introduction

Cables are widely used in the power industry as essential components of the electrical transmission network. They are usually designed to mainly meet electrical standards rather than structural performance requirements, but during earthquakes and other severe environmental hazards, they are often subjected to large deformations and internal forces that can result in failure of the equipment to which they are connected (Okada et al., 1986; EPRI, 1998; Pierre, 1991; Richter, 1998).

Although it is common practice to provide the cables with sufficient slack to accommodate the expected relative displacement between interconnected equipment during earthquakes, this is not always enough to avoid transfer of destructive forces at the connections. Dynamic interaction between flexible cables and interconnected substation equipment is believed to explain some of the damage observed in previous earthquakes (Okada et al., 1986; EPRI, 1998; Pierre, 1991; Richter, 1998).

Qualification procedures (IEEE, 2005) have been proposed by utilities, manufacturers, and researchers with the objective of minimizing dynamic interaction effects. However, these are only qualitative, because of the variety and complex behavior of the equipment used in substations. Therefore, it is standard practice to seismically qualify equipment in a 'stand-alone' condition (i.e., no interaction with connected equipment). Recently, Dastous and Der Kiureghian (2010) authored a report, where guidelines were presented for design of flexible and rigid bus connections between substation equipment subjected to earthquakes.

A few research projects have been carried out to study the behavior of flexible conductors (Okada et al., 1986; Dastous and Pierre, 1996; Filiatrault and Stearns, 2004; Filiatrault and Stearns, 2005; Ghalibafian et al., 2005; Chandran, 2012; Hong et al., 2001; Hong et al., 2005; Dastous, 2005). However, because of their construction, the dynamic properties and energy dissipation capacity of stranded electrical cables are not easy to determine and model. Further experiments and numerical models are needed to better understand and predict their highly nonlinear response to earthquake excitations.

### 3.1.1 Literature review

Below is a synthesis of experimental and numerical studies over the past few decades to understand and analyze dynamic behavior of substation equipment interconnected using flexible conductors.

#### 3.1.1.1 Experimental studies

Several experimental studies have been carried out to investigate dynamic interaction between flexible conductors and interconnected equipment under earthquake excitation. Dastous and Pierre (1996) performed a series of sine-sweep tests at realistic amplitudes and selected frequencies, as a way of studying the behavior of interconnecting flexible conductors and determining frequencies that are likely to be excited by an earthquake. It was observed that due to nonlinear behavior of cables, these frequencies are dependent on the configuration of the cable and on the amplitude of the excitation. Furthermore, it was suggested that cables be designed so that natural frequencies at which they are likely to be excited be different than those of the equipment to which they are connected.

Filiatrault and Stearns (2004) conducted shake table tests on five different pairs of substation equipment interconnected by three different flexible conductors with different levels of slack. They observed two different types of dynamic response to the seismic tests. While a first type of behavior involves low dynamic interaction between the interconnected equipment due to low intensities of ground motion and large slack of the conductors, on the other hand, the second type of response involves high dynamic interaction due to high intensity ground motions and small slacks. Furthermore, the presence of the conductor was seen to increase the damping ratio of the interconnected equipment.

Filiatrault and Stearns (2005) also conducted quasi-static bending tests on two flexible conductors used to interconnect electrical substation equipment. The results of the tests indicated that for most combinations of axial tension and lateral displacement, the flexural stiffness of the conductors is very small and tends toward the minimum possible value corresponding to the situation where the wires slide freely against each other and are unable to transfer shear forces.

Ghalibafian et al. (2005) carried out quasi-static cyclic tests and a series of shake table tests on largescale equivalent models of substation equipment connected by a class of high-voltage flexible conductors. These tests showed that the presence of the flexible cable can decrease or amplify the response of the interconnected equipment and confirmed how these can experience higher demands than they would in the stand-alone state.

Extensive experimental tests on flexible conductors provided by the Bonneville Power Authority have recently been conducted at the Structural Engineering and Earthquake Simulation laboratory at the University at Buffalo, in the form of pullback tests, harmonic tests, and earthquake excitations (Chandran, 2012). The results of these tests point out the need for the development of numerical models to better understand the nonlinear dynamics and energy dissipation capacity of electrical cables. Numerical simulation of some of the tests performed is considered in subsection 3.4.

#### 3.1.1.2 Numerical studies

During extreme excitations, cables can undergo large displacements and rotations, and be subjected to 3D states of stress. Besides tension, cables can be subjected to shear, bending, and torsion. Moreover, it is common in electrical substations to observe cable configurations that cannot be explained by a state of simple tension.

Well-developed theories exist for the static response of cables, as well as for the linear free vibration response of taut cables (Irvine, 1981). However, no analytical results may be obtained, accounting for the geometric nonlinearity because of finite displacements and rotations of the cable. For these reasons, researchers involved in the dynamic analysis of electrical cables have recently turned to finite element implementations of geometrically nonlinear beam theories. Building on the original formulation proposed by Simo and Vu-Quoc (1986;1988), several of these implementations have been developed, based on different ways of parameterizing and interpolating rotations. A formulation proposed by Ibrahimbegovic and Mikdad (1998), and implemented in the finite-element program FEAP (Taylor, 2001), was used by Hong et al. (2001) in the study of the seismic interaction of cable-connected equipment items. In this study, a constant bending stiffness was used to model the cables. However, electrical conductors are typically made of layers of helically wrapped aluminum wires, and because of this construction, their bending stiffness varies with tension, curvature, and deformation history. A model that accounts for interlayer friction and slipping of wires during bending was developed by Papailiou (1995;1997) and implemented in a static finite-element program based on the secant stiffness method.

Later, based on the physical assumptions of the work by Papailiou, Hong et al. (2005) and Dastous (2005) independently extended the geometrically nonlinear beam model implemented in FEAP to account for the material nonlinearity arising from the variable bending stiffness of stranded cables. In (Dastous, 2005), the numerical model of the cable is calibrated using experiments on cables subjected to sinusoidal excitation of their ends. External sources of equivalent viscous damping, associated with the rotational DOFs of the discretized cable, were introduced in the model and calibrated to fit the experimental results.

Recently, Benassi and Reinhorn (2009) investigated the current capabilities of two finite-element programs, ABAQUS (Dassault Systemes Simulia Corp., 2013) and FEAP, in modeling the dynamic behavior of electrical equipment conductors. An important result they found was that correct evaluation of the initial configuration and state of stress of the cable is essential to reliably predict its dynamic behavior.

Another aspect concerning stranded cables and the way they are constructed is the interaction between axial force and torsion. A treatment of the subject and additional references can be found in the text by Costello (1997), where various theories of wire rope are described. To our knowledge, the coupling effects between axial force and torsion have not yet been considered in a finite element implementation of the geometrically nonlinear beam theory and may be subject of future work.

### 3.1.2 Objective and organization of the present work

The objective of the present work is to develop and implement a finite-element formulation of the geometrically nonlinear beam theory to model the behavior of flexible electrical equipment cables. Although the work is inspired by and applied to the study of electrical conductors commonly used in the power industry, the models developed herein can be naturally extended to the analysis of a broader class of cable applications, such as suspension bridges and ocean mooring systems. Furthermore, similar models have recently been considered for applications in the fields of robotics (Boyer et al., 2011) and biomedical engineering (Vernerey and Moran, 2010).

The cable model presented herein does not account for the material nonlinearity associated with the dependence of bending stiffness on curvature and tension. However, its novelty lies in how energy dissipation is accounted for. To our knowledge, the only way energy dissipation has been modeled in the literature is by adding external sources of viscous damping to the DOFs of the discretized cable (Dastous, 2005). In the present model, energy dissipation is accounted for in a physically consistent way by introducing linear viscoelastic constitutive equations and an additional mass proportional damping mechanism. Although fundamentally the ideas are simple, as shown in Section 2, their implementation in the 3D finite deformation beam model is involved.

The chapter is organized as follows. In subsection 3.2, the governing equations of the 3D finite deformation beam model are briefly described. In subsection 3.2.4, an extension of the Kelvin-Voigt damping model to the 3D geometrically non-linear beam is introduced in a physically consistent way through the constitutive equations, while in subsection 3.3, the equilibrium equations are modified to account for mass proportional damping. In the following subsection 3.4, the model is applied to describe the static and dynamic behavior of an electrical conductor tested at the Structural Engineering and Earthquake Simulation laboratory at the University at Buffalo. Preliminary results of the simulation of free and forced vibration tests are presented.

## 3.2 Summary of governing equations

In this subsection, a summary of the governing equations of the geometrically nonlinear beam model is presented, including kinematics, equilibrium and constitutive equations. We recall that the model considered is basically the one originally developed by Simo and Vu-Quoc (1986;1988), with the addition of a consistent way of modeling energy dissipation. For complete details of the implementation, we refer the reader to Section 2.

### 3.2.1 Kinematics

Following Simo (1985), the motion of the cable through time is uniquely defined by the position of the line of centroids $\mathbf{x}_0(S,t)$ and a rotation tensor $\mathbf{R}(S,t)$, specifying the orientation of a moving (current) frame $\mathbf{t}_i(S,t)$ attached to the cross section, relative to its initial (reference) position $\mathbf{E}_i$. The reference and current configurations of the cable, and their corresponding coordinate systems, both defined with respect to a fixed global reference system $\mathbf{e}_i$, are shown in Figure 3-1. We note that, because of shearing, cross sections remain plane but not necessarily perpendicular to the line of centroids in the current configuration.

$\mathbf{R}(S,t)$ represents a rigid rotation of the cross-section such that

$$\mathbf{t}_i(S,t) = \mathbf{R}(S,t) \cdot \mathbf{E}_i \tag{3-1}$$

The derivatives of $\mathbf{R}(S,t)$ with respect to $S$ and $t$ represent the rates of change of $\mathbf{t}_i(S,t)$ along the line of centroids and in time and are defined by

$$\frac{\partial \mathbf{R}(S,t)}{\partial S} = \hat{\boldsymbol{\omega}}(S,t) \cdot \mathbf{R}(S,t) = \mathbf{R}(S,t) \cdot \hat{\boldsymbol{\Omega}} \tag{3-2}$$

$$\frac{\partial \mathbf{R}(S,t)}{\partial t} = \hat{\mathbf{w}}(S,t) \cdot \mathbf{R}(S,t) = \mathbf{R}(S,t) \cdot \hat{\mathbf{W}} \tag{3-3}$$

where $\hat{\boldsymbol{\omega}}$ and $\hat{\mathbf{w}}$ are skew-symmetric tensors defining the current curvature and rotational velocity, while $\hat{\boldsymbol{\Omega}}$ and $\hat{\mathbf{W}}$ are the corresponding tensors taking value in the reference configuration. The hat notation is used herein to identify skew-symmetric tensors. The axial vectors associated with these tensors will be identified by the same symbol but without the hat.

### 3.2.2 Equilibrium equations

The equations of motion are given by

$$\frac{\partial \mathbf{n}}{\partial S} + \tilde{\mathbf{n}} = A_\rho \ddot{\mathbf{x}}_0 \tag{3-4}$$

$$\frac{\partial \mathbf{m}}{\partial S} + \frac{\partial \mathbf{x}_0}{\partial S} \times \mathbf{n} + \tilde{\mathbf{m}} = \mathbf{I}_\rho \cdot \dot{\mathbf{w}} + \mathbf{w} \times \left(\mathbf{I}_\rho \cdot \mathbf{w}\right) \tag{3-5}$$

In (3-4) and (3-5), $\mathbf{n}$ and $\mathbf{m}$ are force and moment resultants in the current configuration, while $\tilde{\mathbf{n}}$ and $\tilde{\mathbf{m}}$ are distributed applied forces and moments per unit undeformed length of the cable. Moreover, $A\rho$ and $\mathbf{I}\rho$ are the mass and current mass moment of inertia per unit undeformed length of the cable, and $\mathbf{w}$ is the current rotational velocity vector.

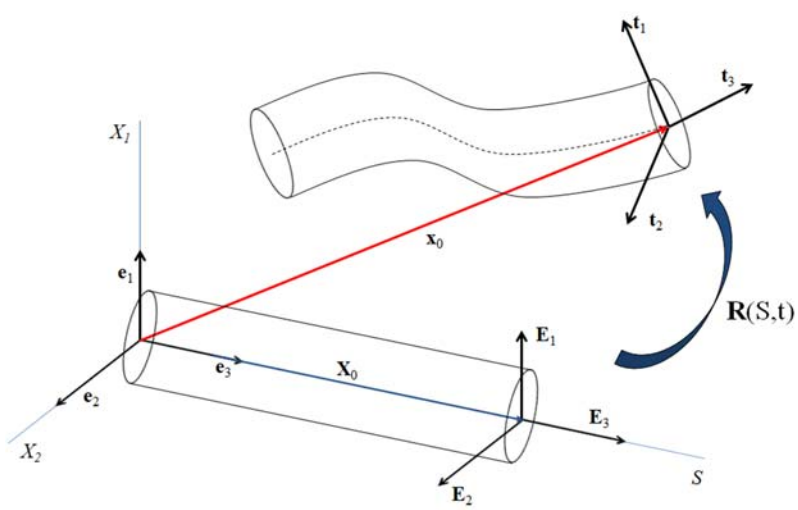


**Figure 3-1 Fixed and moving coordinate systems, reference and current configuration**

### 3.2.3 Strain and strain rate measures

Expressions of the current and reference strain measures are summarized in Table 3-1. Although the equations of motion (4) and (5) are expressed in terms of internal forces in the current configuration, it is convenient to write the constitutive equations in terms of strains in the reference configuration. The strain rate measures, conjugate to the internal force and moment resultants, are derived naturally from the internal power equation:

$$\iiint_{R_0} tr\left(\mathbf{P}^{\mathrm{T}} \cdot \dot{\mathbf{F}}\right) dV = \int_0^L \left( \mathbf{n} \cdot \overset{\triangledown}{\boldsymbol{\gamma}} + \mathbf{m} \cdot \overset{\triangledown}{\boldsymbol{\omega}} \right) dS = \int_0^L \left[ \mathbf{N} \cdot \dot{\boldsymbol{\Gamma}} + \mathbf{M} \cdot \dot{\boldsymbol{\Omega}} \right] dS \tag{3-6}$$

where $\mathbf{P}$ is the first Piola–Kirchhoff stress tensor, $\mathbf{F}$ is the deformation gradient tensor, $\mathbf{N}=\mathbf{R}^{\mathrm{T}}\cdot\mathbf{n}$ and $\mathbf{M}=\mathbf{R}^{\mathrm{T}}\cdot\mathbf{m}$ are the reference force and moment resultants. The strain rate measures are summarized in Table 3-2

**Table 3-1 Strain measures**

| Strain | Current | Reference |
|---|---|---|
| Axial and shear | $\boldsymbol{\gamma}(S,t)= \frac{\partial \mathbf{x}_0}{\partial S}(S,t)-\mathbf{t}_3(S,t)$ | $\boldsymbol{\Gamma}=\mathbf{R}^{\mathrm{T}}\cdot\boldsymbol{\gamma}$ |
| Bending and torsion | $\boldsymbol{\omega}(S,t)$ | $\boldsymbol{\Omega}=\mathbf{R}^{\mathrm{T}}\cdot\boldsymbol{\omega}$ |

**Table 3-2 Strain rate measures**

| Strain rate | Current | Reference |
|---|---|---|
| Axial and shear | $\overset{\triangledown}{\boldsymbol{\gamma}} = \dot{\boldsymbol{\gamma}} - \mathbf{w}\times\boldsymbol{\gamma}$ | $\dot{\boldsymbol{\Gamma}} = \mathbf{R}^{\mathrm{T}}\cdot \overset{\triangledown}{\boldsymbol{\gamma}}$ |
| Bending and torsion | $\overset{\triangledown}{\boldsymbol{\omega}} = \dot{\boldsymbol{\omega}} - \mathbf{w}\times\boldsymbol{\omega}$ | $\dot{\boldsymbol{\Omega}} = \mathbf{R}^{\mathrm{T}}\cdot \overset{\triangledown}{\boldsymbol{\omega}}$ |

We note that in the current configuration, the strain rate measures $\overset{\triangledown}{\boldsymbol{\gamma}}$ and $\overset{\triangledown}{\boldsymbol{\omega}}$, conjugate to the internal forces $\mathbf{n}$ and $\mathbf{m}$, are not simply the time derivatives $\dot{\boldsymbol{\gamma}}$ and $\dot{\boldsymbol{\omega}}$ of the corresponding strain measures $\boldsymbol{\gamma}$ and $\boldsymbol{\omega}$. As explained by Simo (1985), $\overset{\triangledown}{\boldsymbol{\gamma}}$ and $\overset{\triangledown}{\boldsymbol{\omega}}$ denote corotated rates; that is, the rates measured by an observer attached to the moving (current) frame. We note the similarity to the Coriolis term when considering the acceleration of a particle in a rotating frame.

### 3.2.4 Constitutive equations

Large deformations, but locally small strains are assumed, so that the elastic forces and moments in the reference configuration, namely $\mathbf{N}^e$ and $\mathbf{M}^e$, are linearly proportional to the corresponding strains, $\mathbf{\Gamma}$, and curvatures, $\mathbf{\Omega}$, through a constant and diagonal elasticity tensor, $\mathbf{C}$, defined as:

$$\mathbf{C} = \mathrm{diag}\left[\mathbf{C}^{\mathrm{N}}, \mathbf{C}^{\mathrm{M}}\right] \tag{3-7}$$

where

$$\mathbf{C}^{\mathrm{N}} = \mathrm{diag}\left[GA_1, GA_2, EA\right] \qquad \mathbf{C}^{\mathrm{M}} = \left[EI_1, EI_2, GJ_t\right] \tag{3-8}$$

In (3-8) $E$ is the Young's modulus, $G$ is the shear modulus, $A$ is the area of the rigid cross-section, $A_1$ and $A_2$ are effective cross-section areas for shearing, $I_1$ and $I_2$ are the area moments of inertia of the cross-section, and $J_t$ is the torsion constant. In writing (3-7) and (3-8), we assume that the reference frame and the moving frame are principal axes of the cross-section.

As explained in Section 2, energy dissipation is modeled by a Kelvin-Voigt damping model. The internal dissipative forces and moments in the reference configuration, namely $\mathbf{N}^d$ and $\mathbf{M}^d$, are assumed to be linearly proportional to the corresponding strain rate, $\dot{\mathbf{\Gamma}}$, and curvature rate, $\dot{\mathbf{\Omega}}$, through a constant tensor, $\mathbf{C}_d$, defined as:

$$\mathbf{C}_{\mathrm{d}} = \mathrm{diag}\left[\mathbf{C}_{\mathrm{d}}^{\mathrm{N}}, \mathbf{C}_{\mathrm{d}}^{\mathrm{M}}\right] \tag{3-9}$$

where

$$\mathbf{C}^{\mathrm{N}} = \mathrm{diag}\left[\mu GA_1, \mu GA_2, \eta EA\right] \qquad \mathbf{C}^{\mathrm{M}} = \left[\eta EI_1, \eta EI_2, \mu GJ_t\right] \tag{3-10}$$

In (3-10), $\eta$ and $\mu$ are retardation time constants transforming the elastic moduli $E$ and $G$ into viscous constants, akin to stiffness proportional damping coefficients.

The constitutive equations, relating the total internal forces to their corresponding strains and strain rates, and the total internal moments to their corresponding curvatures and curvature rates, are therefore given by

$$\mathbf{N} = \mathbf{N}^{\mathrm{e}} + \mathbf{N}^{\mathrm{d}} = \mathbf{C}^{\mathrm{N}} \cdot \mathbf{\Gamma} + \mathbf{C}_{\mathrm{d}}^{\mathrm{N}} \cdot \dot{\mathbf{\Gamma}} \tag{3-11}$$

$$\mathbf{M} = \mathbf{M}^{\mathrm{e}} + \mathbf{M}^{\mathrm{d}} = \mathbf{C}^{\mathrm{M}} \cdot \mathbf{\Omega} + \mathbf{C}_{\mathrm{d}}^{\mathrm{M}} \cdot \dot{\mathbf{\Omega}} \tag{3-12}$$

### 3.3 Mass proportional damping

The constitutive equations described above allow for the introduction of a Kelvin-Voigt type of damping in the model. To potentially model mass proportional damping, we define the following dissipation potential:

$$P_D = \frac{1}{2}\left[\lambda_t A_\rho \dot{\mathbf{x}}_0 \cdot \dot{\mathbf{x}}_0 + \lambda_r \mathbf{w} \cdot \mathbf{I}_\rho \cdot \mathbf{w}\right] \tag{3-13}$$

Taking the derivative of $P_D$, with respect to $\dot{\mathbf{x}}_0$ and **w,** we get dissipation forces that we add to the right hand side of each of the equations of motion, (3-4) and (3-5), as follows:

$$\frac{\partial \mathbf{n}}{\partial S} + \tilde{\mathbf{n}} = A_\rho \ddot{\mathbf{x}}_0 + \lambda_t A_\rho \dot{\mathbf{x}}_0 \tag{3-14}$$

$$\frac{\partial \mathbf{m}}{\partial S} + \frac{\partial \mathbf{x}_0}{\partial S} \times \mathbf{n} + \tilde{\mathbf{m}} = \mathbf{I}_\rho \cdot \dot{\mathbf{w}} + \mathbf{w} \times \left(\mathbf{I}_\rho \cdot \mathbf{w}\right) + \lambda_r \mathbf{I}_\rho \cdot \mathbf{w} \tag{3-15}$$

Proceeding in the same fashion as in Section 2, we derive the following weak form of the equations of motion:

$$\begin{aligned} G(\boldsymbol{\varphi}, \boldsymbol{\eta}) = &\int_0^L \left[\left(\frac{\partial \boldsymbol{\eta}_u}{\partial S} - \boldsymbol{\eta}_\theta \times \frac{\partial \mathbf{x}_0}{\partial S}\right) \cdot \mathbf{R} \cdot \mathbf{N} + \frac{\partial \boldsymbol{\eta}_\theta}{\partial S} \cdot \mathbf{R} \cdot \mathbf{M}\right] dS - \int_0^L \left(\tilde{\mathbf{n}} \cdot \boldsymbol{\eta}_u + \tilde{\mathbf{m}} \cdot \boldsymbol{\eta}_\theta\right) dS + \\ &\int_0^L \left\{\left(A_\rho \ddot{\mathbf{x}}_0 + \lambda_t A_\rho \dot{\mathbf{x}}_0\right) \cdot \boldsymbol{\eta}_u + \mathbf{R} \cdot \left[\mathbf{J}_\rho \cdot \dot{\mathbf{W}} + \lambda_r \mathbf{J}_\rho \cdot \mathbf{W} + \mathbf{W} \times \left(\mathbf{J}_\rho \cdot \mathbf{W}\right)\right] \cdot \boldsymbol{\eta}_\theta\right\} dS = 0 \end{aligned} \tag{3-16}$$

Due to the presence of the newly added terms, linearization of the new weak form (3-16) leads to the definition of an additional mass proportional damping operator:

$$\delta G_{MPD}(\boldsymbol{\varphi}, \boldsymbol{\eta}) = \int_0^L \boldsymbol{\eta}_u \cdot \delta\left(\lambda_t A_\rho \mathbf{v}_0\right) dS + \int_0^L \boldsymbol{\eta}_\theta \cdot \delta\left(\mathbf{R} \cdot \lambda_r \mathbf{J}_\rho \cdot \mathbf{W}\right) dS \tag{3-17}$$

where we have used the notation $\mathbf{v}_0 = \dot{\mathbf{x}}_0$. Recalling from Section 2 that

$$\delta \mathbf{v}_0 = \frac{\gamma}{\beta h} \boldsymbol{\delta} \mathbf{u} \tag{3-18}$$

the first integral of (3-17) becomes:

$$\int_0^L \boldsymbol{\eta}_u \cdot \delta\left(\lambda_r A_\rho \mathbf{v}_0\right) dS = \int_0^L \boldsymbol{\eta}_u \cdot \lambda_t A_\rho \frac{\gamma}{\beta h} \boldsymbol{\delta} \mathbf{u}\, dS \tag{3-19}$$

The second integral in (3-17) may be decomposed as:

$$\int_0^L \boldsymbol{\eta}_\theta \cdot \delta\left(\mathbf{R}\cdot\lambda_r \mathbf{J}_\rho \cdot \mathbf{W}\right) dS = \int_0^L \boldsymbol{\eta}_\theta \cdot \delta\mathbf{R}\cdot\left(\lambda_r \mathbf{J}_\rho \cdot \mathbf{W}\right) dS + \int_0^L \boldsymbol{\eta}_\theta \cdot \mathbf{R}\cdot\left(\lambda_r \mathbf{J}_\rho \cdot \delta\mathbf{W}\right) dS \tag{3-20}$$

We now recall that

$$\delta\mathbf{R} = \boldsymbol{\delta}\hat{\boldsymbol{\theta}} \cdot \mathbf{R} \tag{3-21}$$

The first integral in (3-20) can then be written as:

$$\begin{aligned}&\int_0^L \boldsymbol{\eta}_\theta \cdot \delta\mathbf{R}\cdot\left(\lambda_r \mathbf{J}_\rho \cdot \mathbf{W}\right) dS = \int_0^L \boldsymbol{\eta}_\theta \cdot \left[\boldsymbol{\delta}\hat{\boldsymbol{\theta}}\cdot\mathbf{R}\cdot\left(\lambda_r \mathbf{J}_\rho \cdot \mathbf{W}\right)\right] dS = -\int_0^L \boldsymbol{\eta}_\theta \cdot \mathbf{R}\cdot\left[\lambda_r \mathbf{J}_\rho \cdot \mathbf{W}\right]\cdot\boldsymbol{\delta}\hat{\boldsymbol{\theta}}\, dS = \\ &-\int_0^L \boldsymbol{\eta}_\theta \cdot \mathbf{R}\cdot\left[\lambda_r \mathbf{J}_\rho \cdot \mathbf{W}\right]^\wedge\cdot\boldsymbol{\delta\theta}\, dS\end{aligned} \tag{3-22}$$

Moreover, recalling that

$$\delta\mathbf{W} = \frac{\gamma}{\beta h}\mathbf{R}_n^{\mathrm{T}}\cdot\mathbf{T}\cdot\boldsymbol{\delta\theta} \tag{3-23}$$

the second integral in (3-20) becomes:

$$\int_0^L \boldsymbol{\eta}_\theta \cdot \mathbf{R}\cdot\left(\lambda_r \mathbf{J}_\rho \cdot \delta\mathbf{W}\right) dS = \int_0^L \boldsymbol{\eta}_\theta \cdot \left[\mathbf{R}\cdot\lambda_r \mathbf{J}_\rho \cdot \frac{\gamma}{\beta h}\mathbf{R}_n^{\mathrm{T}}\cdot\mathbf{T}\right]\cdot\boldsymbol{\delta\theta}\, dS \tag{3-24}$$

With (3-19), (3-22) and (3-24) in hand, we can finally write (3-17) as:

$$\delta G_5\left(\boldsymbol{\varphi},\boldsymbol{\eta}\right) = \int_0^L \boldsymbol{\eta}_u \cdot \lambda_t A_\rho \frac{\gamma}{\beta h}\boldsymbol{\delta}\mathbf{u}\, dS + \int_0^L \boldsymbol{\eta}_\theta \cdot \left[\mathbf{R}\cdot\lambda_r \mathbf{J}_\rho \cdot \frac{\gamma}{\beta h}\mathbf{R}_n^{\mathrm{T}}\cdot\mathbf{T} - \left(\mathbf{R}\cdot\lambda_r \mathbf{J}_\rho \cdot \mathbf{W}\right)^\wedge\right]\cdot\boldsymbol{\delta\theta}\, dS \tag{3-25}$$

Introducing the space discretization scheme described in Section 2, we get the following discretized version of the tangent mass proportional damping operator:

$$\bar{\mathbf{D}}_{ij} = \int_{I_e} \begin{bmatrix} \mathbf{d}_{ij}^{11} & \mathbf{0} \\ \mathbf{0} & \mathbf{d}_{ij}^{22} \end{bmatrix} dS \tag{3-26}$$

where

$$\mathbf{d}_{ij}^{11} = \frac{\gamma}{\beta h}\lambda_t A_\rho \int_{I_e} N_i N_j \, dS\, \mathbf{I} \tag{3-27}$$

$$\mathbf{d}_{ij}^{22} = \int_{I_e} \mathbf{R}\cdot\left[\lambda_r \mathbf{J}_\rho \cdot \frac{\gamma}{\beta h}\mathbf{R}_n^{\mathrm{T}}\cdot\mathbf{T} - \left(\lambda_r \mathbf{J}_\rho \cdot \mathbf{W}\right)^\wedge\right] N_i N_j \, dS \tag{3-28}$$

Furthermore, the following vector is to be added to the discrete residual force vector:

$$\mathbf{P}_i^{\mathrm{d}} = \int_{I_e} N_i \mathbf{I}\cdot\begin{bmatrix} \lambda_t A_\rho \mathbf{v}_0 \\ \mathbf{R}\cdot\left(\lambda_r \mathbf{J}_\rho \cdot \mathbf{W}\right)\end{bmatrix} dS \tag{3-29}$$

## 3.4 Numerical simulation of dynamic cable tests

In this subsection, the 3D geometrically nonlinear beam model is applied to describe the behavior of an electrical conductor tested by Filiatrault, Reinhorn and Chandran (Chandran, 2012) at the University at Buffalo. The conductor tested was a Jefferson/TW AAC conductor made of 46 helically wrapped aluminum wires in four layers. As shown in Figure 3-2, the cable was connected to a shake table at one end and to a reaction frame at the other. The cable was instrumented with accelerometers and Krypton LEDs (Krypton Electronic Engineering, 2003), and subjected to a series of dynamic excitations in the form of pull-release tests, sine tests, and earthquake simulations. Details on the instrumentation and the dynamic tests can be found in (Chandran, 2012). In the following, we present some preliminary results from the simulation of the out-of-plane pull-release and sine tests. To our knowledge, 3D numerical simulations of electrical cables have not been presented in the literature.

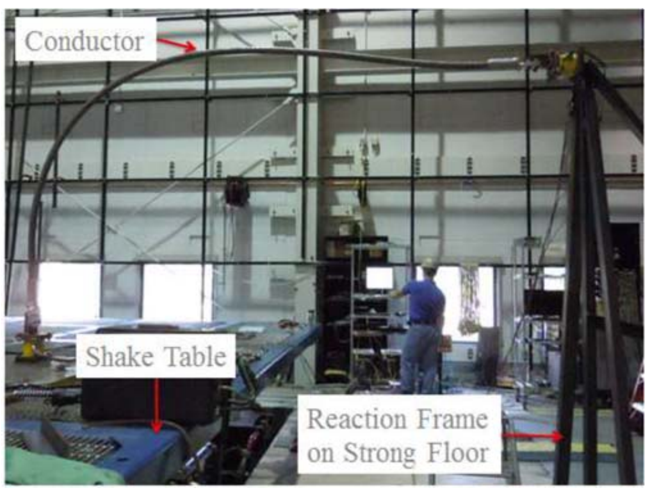


**Figure 3-2 Configuration of cable tested (Chandran, 2012)**

### 3.4.1 Modeling cable properties

The material properties of the aluminum cable used in the analyses are Young's modulus $E$=10×106psi and Poisson's ratio $v$=0.33. These were not directly measured but are based on typical values for aluminum (Costello, 1997). As shown in Figure 3-3, the total length of the cable is $L$=164in. The two swage fittings are modeled with stiffer elements than the rest of the conductor, accounting for not perfectly fixed end conditions. The weight per unit length is 0.212lbs/in. Bounds for the cross-sectional properties of the cable are estimated as described in (Filiatrault and Stearns, 2004; Hong et al., 2001). By neglecting the lay angle that the wires make with the axis of the cable, the cross-sectional area of the conductor is evaluated as

$$A = \sum_{i=1}^{n} \frac{\pi d_i^4}{4} \tag{3-30}$$

where $n$ is the number of wires and $d_i$ is the diameter of the $i$th wire. As shown in Figure 3-3, the wires of the Jefferson/TW AAC conductor are trapezoidal, therefore circular wires of equivalent area have been considered to evaluate the diameter $d_i$. The value of the cross-sectional area of the cable, estimated using (3-30), is $A$=2.01in$^2$.

The area moment of inertia of the cross section can assume considerably different values depending on whether the wires remain connected, or can more or less slide with respect to one another during bending. The minimum value is obtained assuming that there is no friction whatsoever between wires and that these can slide freely against each other. On the other hand, the maximum value is obtained assuming that the wires do not slip but remain attached because of significant friction. These two extreme values are given by

$$I_{\min} = \sum_{i=1}^{n} \frac{\pi d_i^4}{64} \qquad I_{\max} = \sum_{i=1}^{n} \frac{\pi d_i^4}{64} \left( 1 + 16 \frac{y_i^2}{d_i^2} \right) \tag{3-31}$$

where $y_i$ is the distance of the $i$th wire from the neutral axis and $d_c$ is the diameter of the conductor. Moreover, the IEEE (1999) guidelines recommend the approximation $I$=(1+$N$) $I_{\min}$, where $N$ denotes the number of layers of strand. When applied to trapezoidal wires, Eq. (17) yields different values of $I_{\min}$ for different values of the fill factor $\alpha$, defined as the ratio of the total area of trapezoidal wires to the full area of the conductor. The fill factor $\alpha$ is needed to compute the diameter $d_i$ of the equivalent circular wire to be used in (3-31). With fill factors $0.9 \leq \alpha \leq 1$, $I_{\min}$ for the tested Jefferson/TW AAC conductor takes values between 0.0057 and 0.0070 in$^4$. Using $\alpha$=1, (3-31) yields $I_{\max}$=0.3217 in$^4$. Slightly lower values for $I_{\min}$ and $I_{\max}$ are obtained if (3-31)is multiplied by cosβ [19, 20], where β is the lay angle of the wires.

In the dynamic simulations that follow, two different values of $I$ are used to fit the experimental results, namely $I$=0.0077 in$^4$ for the pull-release tests, and $I$=0.0067 in$^4$ for the sine tests. It should be noted that these values approach $I_{\min}$, a trend that was observed by Filiatrault and Stearns (2005). For the free vibration tests, we will also show results of numerical simulations using the lower bound for $I_{\min}$ and the $I$ recommended by the IEEE guidelines. The latter, obtained using the upper bound for $I_{min}$, is $I$=0.0350 in$^4$. The swage fittings are modeled using $I$=0.015 in$^4$. Such value was selected based on measurements of the displacements at the cross sections where the conductor enters the swage fittings. The values of the area moment of inertia used in the numerical analyses are presented in Table 3-3, along with the estimated maximum and minimum values, and the value recommended by the IEEE guidelines.

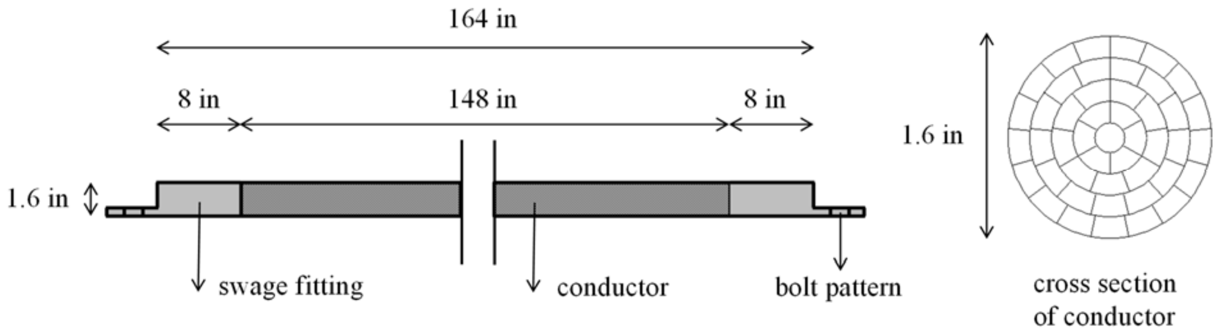


**Figure 3-3 Schematics of Jefferson conductor**

**Table 3-3 Values of *I* considered**

| Second moment of area | Value [in$^4$] |
|---|---|
| $I_{min}$ (expected range) | 0.0057 to 0.0070 |
| $I_{max}$ | 0.3217 |
| $I=(1+N)I_{min}$ (upper bound $I_{min}$) | 0.0350 |
| $I$ used for free vibration tests | 0.0077 |
| $I$ used for forced vibration tests | 0.0067 |

### 3.4.2 Cable form finding

The first numerical application is concerned with determining the static configuration of the cable, which is the starting configuration for the dynamic tests. This is obtained by imposing end displacements and rotations to an initially straight and unstrained cable to match the ends of the experimental configuration. The right end of the cable is subjected to a horizontal displacement of 47.4 in and a vertical displacement of 59.2 in, whereas a rotation of 1.80 rad is applied to the left end of the cable. The finite-element mesh consists of eighty 2-noded (linear) elements for the conductor and five 2-noded (linear) elements for each swage fitting. This number of elements was chosen to ensure convergence of frequencies for the linearized cable model. The deformed shape of the cable, obtained with the numerical model, is plotted in Figure 3-4 against the initial configuration measured by the Krypton LEDs prior to the dynamic experiments. We note that varying the area moment of inertia within the range of its physically acceptable values influences the reactions at the ends but does not significantly affect the static configuration of the cable. However, correct evaluation of the state of stress of the cable is important for the reliable prediction of the dynamic behavior and fatigue of the cable.

### 3.4.3 Modes and frequencies

Once the static shape of the cable has been found, the natural frequencies of the linearized cable model can be estimated by eigenvalue analysis, using the tangent stiffness matrix at the given configuration and an appropriate consistent mass matrix. The latter is obtained by rotating the consistent mass matrix of the beam from the straight and unstrained configuration to the current deformed one. The first four linearized mode shapes, using $I$=0.0077 in$^4$, are shown in Figure 3-5. The corresponding frequencies and periods of vibration are listed in Table 3-4.

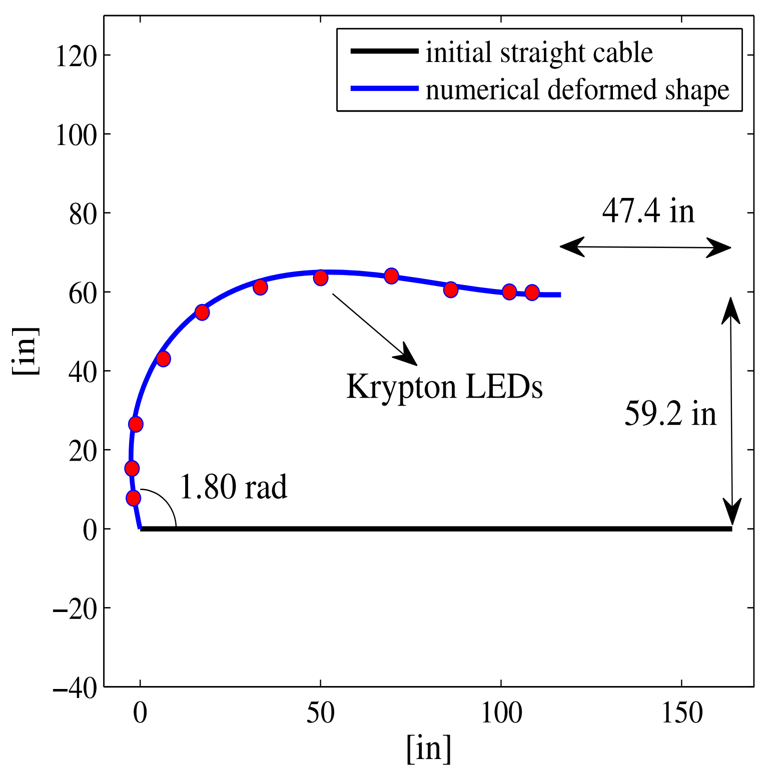


**Figure 3-4 Static deformed shape of cable with clamped ends**

### 3.4.4 Free vibration tests

The pull-release tests performed consist of manually applying, and then instantaneously releasing, an external displacement at the center of the cable. Because we do not have displacement measurements, we numerically apply the displacement that allows a reasonable comparison of the acceleration responses. As a result of applying an out-of-plane displacement of 8 in at its center (point 2), the computed configuration of the cable prior to release is shown in Figure 3-6(a). The displacement response of point 2, during the free vibration phase, is shown in Figure 3-6(b). Kelvin– Voigt damping is considered in the analysis with retardation constants $\eta$=$\mu$=0.016 s. Moreover, a time step $\Delta t$=0.001 s is used. The acceleration histories of the three control points, shown in Figure 3-6(a), are plotted in Figure 3-7 against the responses measured during the experiments.

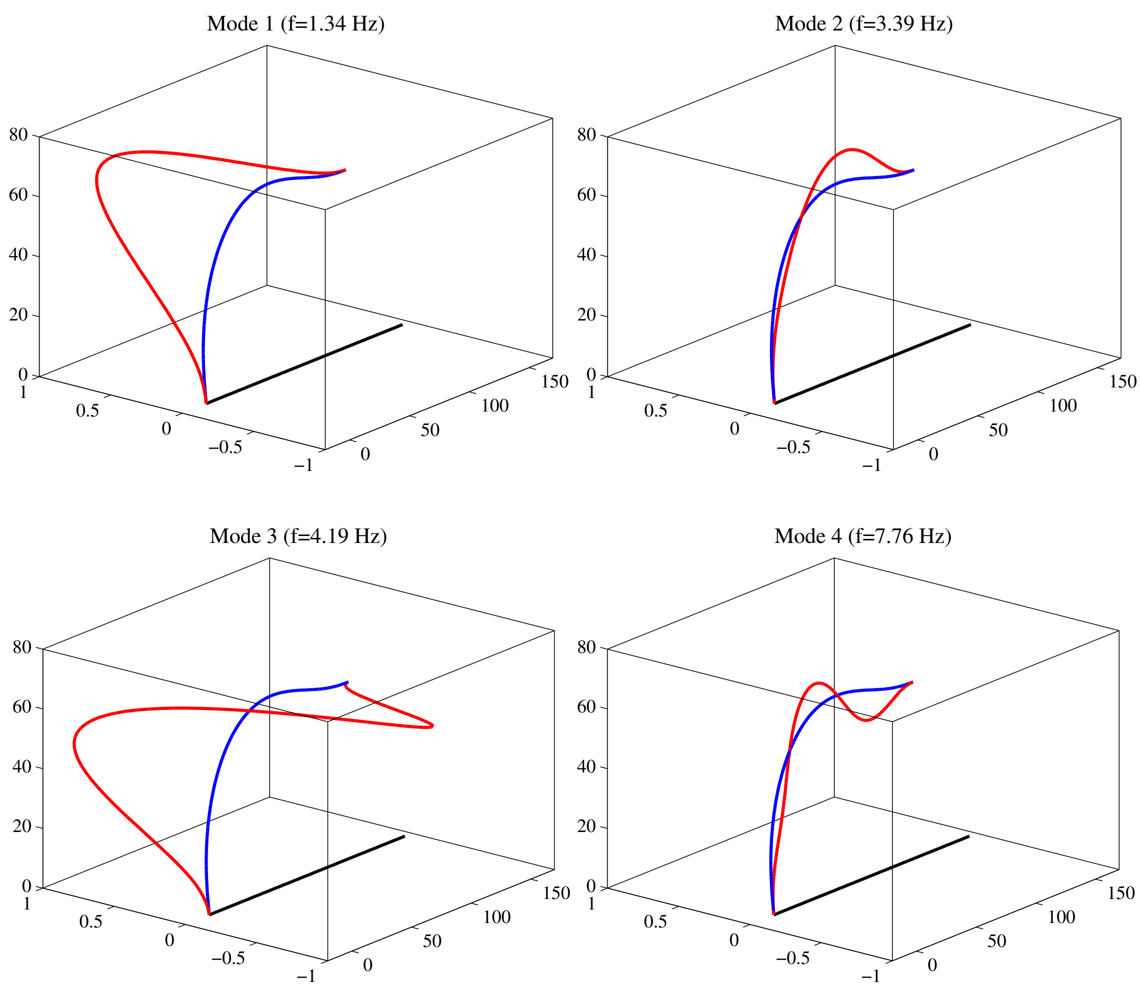


**Figure 3-5 Mode shapes of linearized cable model**

**Table 3-4 Frequencies and periods of cable**

| Mode | Frequency [Hz] | Period [s] |
|---|---|---|
| 1 | 1.34 | 0.75 |
| 2 | 3.39 | 0.29 |
| 3 | 4.19 | 0.24 |
| 4 | 7.76 | 0.13 |

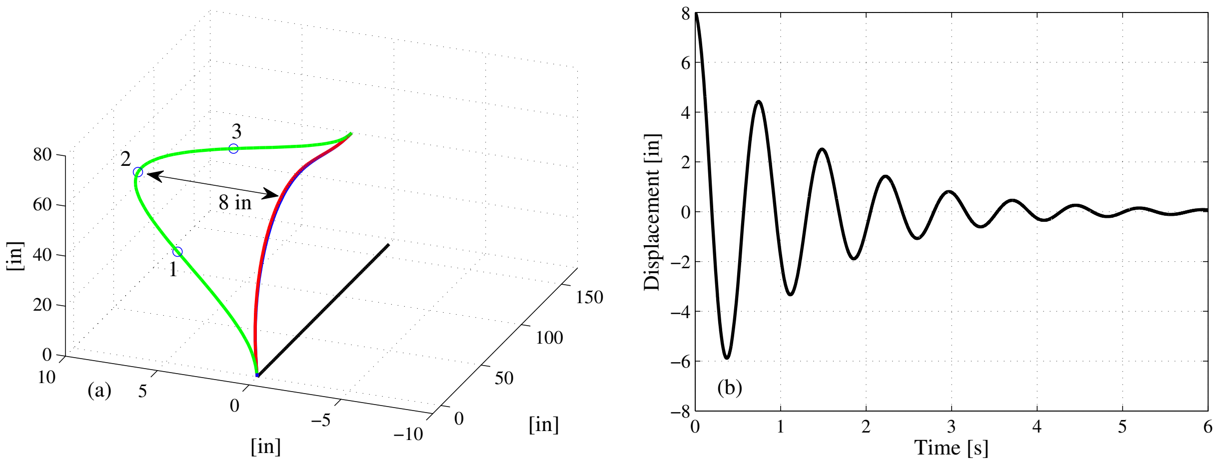


**Figure 3-6 Pull-release tests: (a) Deformed shape of cable prior to release (green), final shape of cable (red); (b) free vibration response of point 2**

The comparisons point out that the period of the experimental response decreases with decreasing amplitudes, revealing the presence of material nonlinear behavior in addition to geometric nonlinearity. A more sophisticated model, capable of accounting for variable bending stiffness, is needed to capture this behavior. The reliability of computations is assessed by performing energy calculations and making sure that the energy balance is achieved. In free vibration, the sum of strain energy, kinetic energy, and dissipated energy should be constant and equal to the initial strain energy prior to release. However, this is true only in the absence of gravity. In the presence of a gravity field, the work developed by weight must also be taken into account in the energy balance. Each energy component is plotted in Figure 3-8(a), and the energy balance is shown in Figure 3-8(b). The latter also represents the energy decay. The energy error defined as

$$\text{energy error} = \frac{\text{input energy} - (\text{strain energy} + \text{kinetic energy} + \text{dissipated energy})}{\text{input energy}} \tag{3-32}$$

is shown in Figure 3-8(c).

The results shown in Figure 3-7 were obtained using $I$=0.0077 in$^4$. In Figure 3-9(a), the results of the simulation using the lower bound for $I_{\min}$ are shown, while Figure 3-9(b) shows the results of the simulation using the value $I=(1+N)I_{\min}$ recommended by the IEEE (1999) guidelines, with the upper bound of $I_{\min}$. In the latter, a smaller out-of-plane displacement is imposed to the cable, namely 2.5 in compared to the previous 8 in, in order to compare the amplitude of the experimental acceleration. Moreover, retardation constants $\eta=\mu$=0.005 s are used. The results presented show how proper estimation of the area moment of inertia $I$ is crucial to obtain a reliable evaluation of the frequency of the cable.

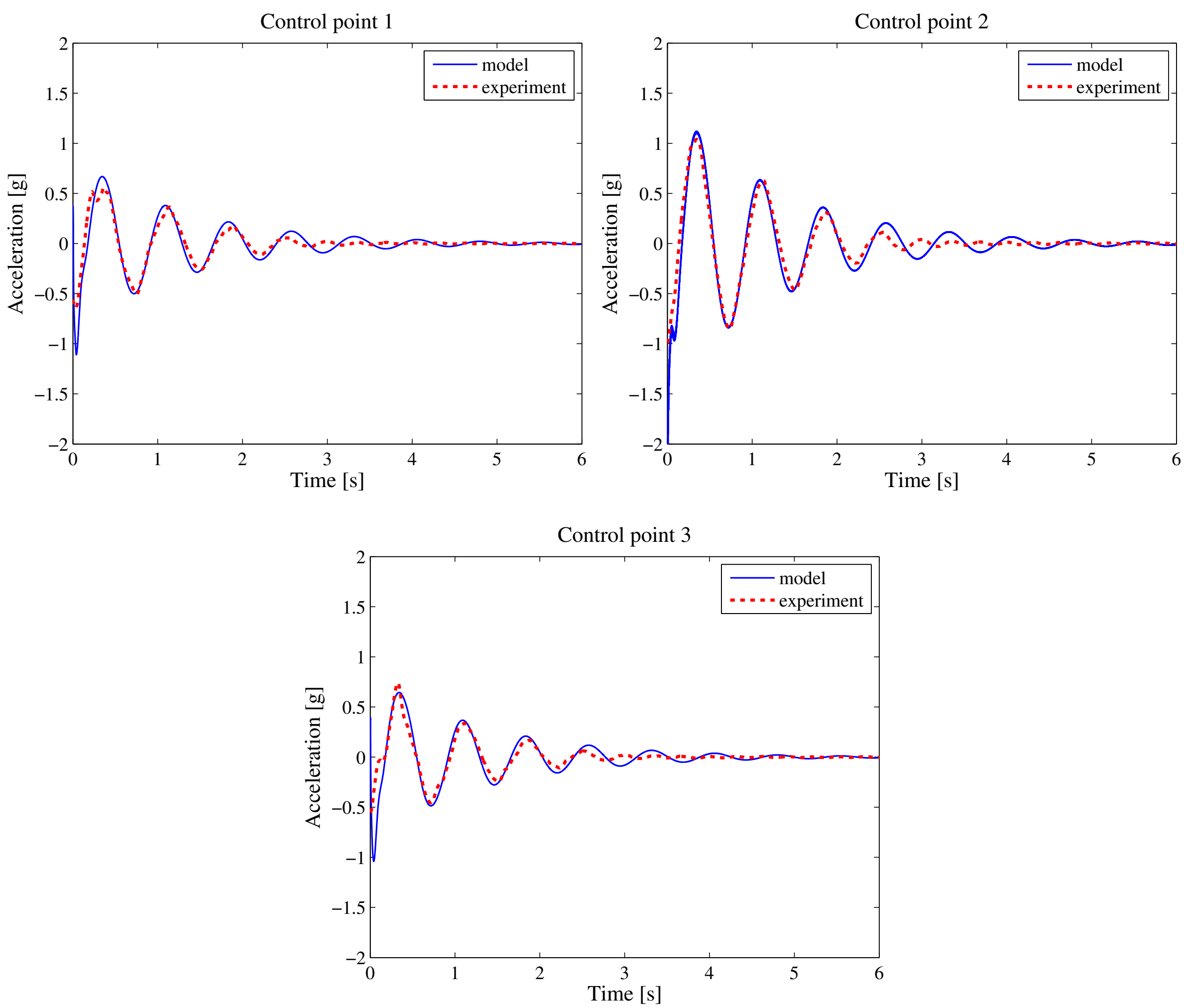


**Figure 3-7 Free vibration acceleration response of control points shown in Figure 6(a)**

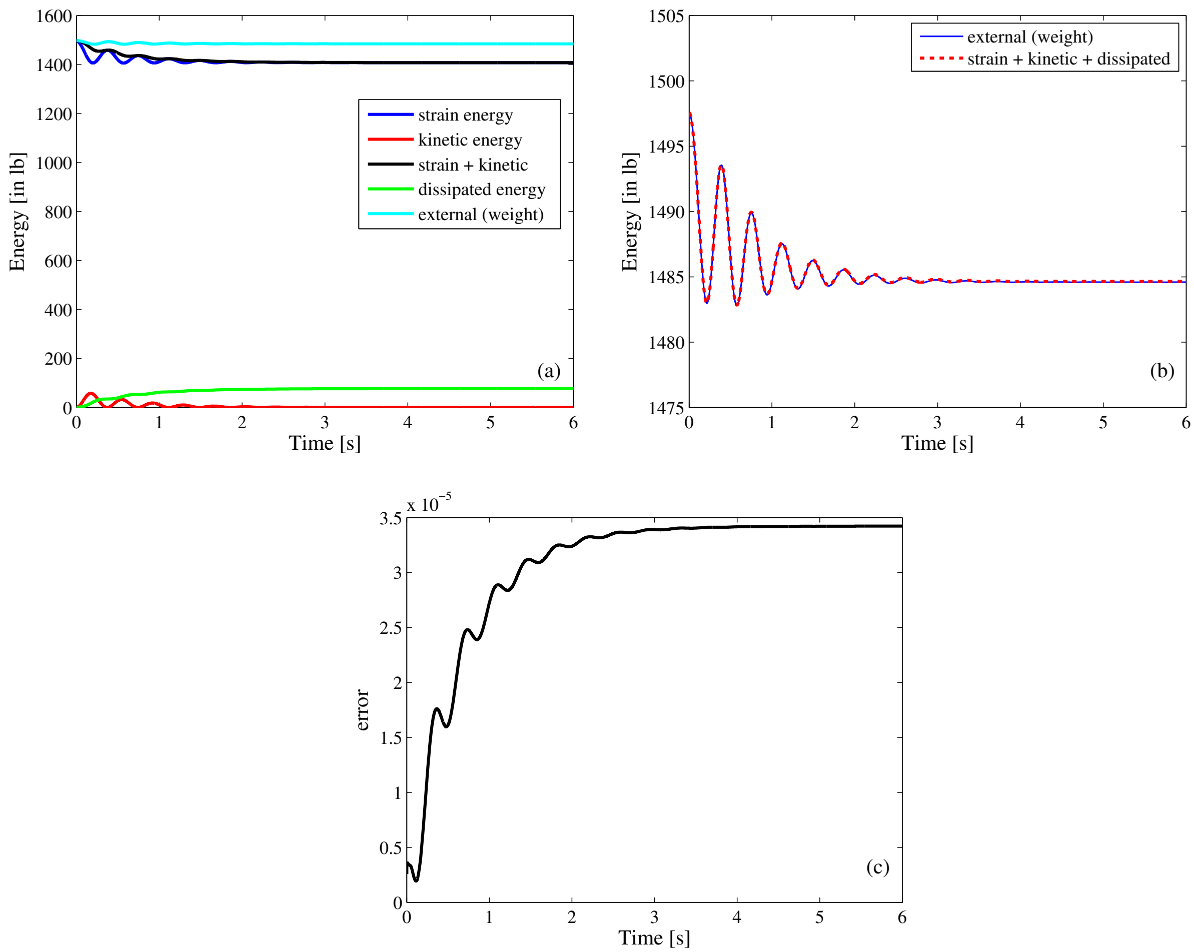


**Figure 3-8 Cable in free vibration: (a) energu components; (b) energy balance; (c) energy error as defined in Eq. (3-32)**

### 3.4.5 Forced vibration tests

These tests consisted of applying a sinusoidal motion of near resonance frequency to one end of the cable by means of the shake table. For the analysis presented here, the input motion was derived from readings of the accelerometer, and the Krypton LED, located at the end of the cable connected to the shake table. Two different acquisition systems were used for the acceleration and the displacement transducers. Because the signals were recorded at different time intervals, it was necessary to synchronize them before they could be used as input for the numerical simulations.

While the entire displacement histories were recorded, the accelerations are available only for a segment of the stationary response, and the subsequent free vibration phase. For this reason, the entire input signals were generated numerically and adjusted to match the available experimental displacement and acceleration signals.

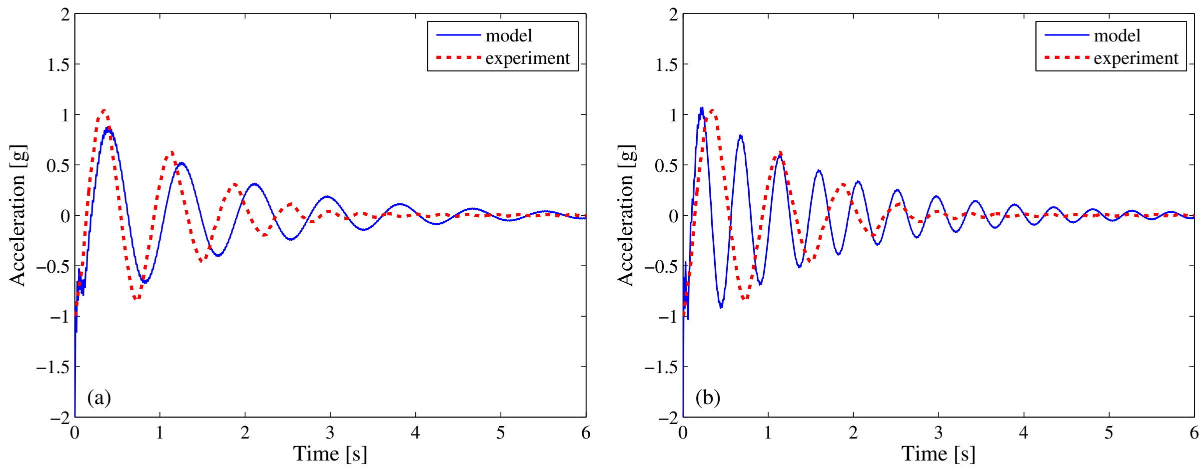


**Figure 3-9 Free vibration acceleration of control point 2 shown in Figure 3-6(a): (a) using $I$ equal to the lower bound of $I_{\min}$; (b) using $I$=(1+$N$)$I_{\min}$ and the upper boundof $I_{\min}$**

The generated input out-of-plane horizontal harmonic excitation is of the form:

$$u(t) = U\left\{\exp(-\zeta\omega_n t)\left[\cos\omega_D t + \frac{\zeta}{\sqrt{1-\zeta^2}}\sin\omega_D t\right] - \cos\omega_n t\right\} \tag{3-33}$$

Equation (3-33) represents the response of a damped SDOF of frequency $\omega_n$, and damping ratio $\zeta$, to a sinusoidal force of frequency $\omega=\omega_n$ (Chopra, 2007). In (3-33), $U$ is the steady state amplitude of the response, and $\omega_D=\omega_n(1-\zeta^2)^{1/2}$ is the damped natural frequency of the SDOF. In the present application, $U$=3 in and the exciting frequency is $f=\omega/2\pi$=1.305 Hz. The parameter $\zeta$ is set equal to 0.1. The numerically generated input displacement and input acceleration are plotted in Figure 3-10, where they are compared to the experimental records. The out-of-plane displacement histories of the control points shown in Figure 3-6(a) are shown in Figure 3-11, where they are compared to those measured during the experiments. A time step $\Delta t$=0.001 s is used in the analysis.

The plots on the left-hand side of Figure 3-11 were obtained using constant Kelvin–Voigt damping with retardation constants $\eta=\mu$=0.012 s. While the stationary part of the computed response matches reasonably well the experimental response, the numerical free vibration response appears to be less damped. By increasing the value of the retardation constants in the free vibration phase to $\eta=\mu$=0.016 s, the plots on the right-hand side of Figure 3-11 are obtained. The experimental results show clearly that damping increases with decreasing displacement amplitude, as may be expected of damping associated with Coulomb friction (Chopra, 2007).

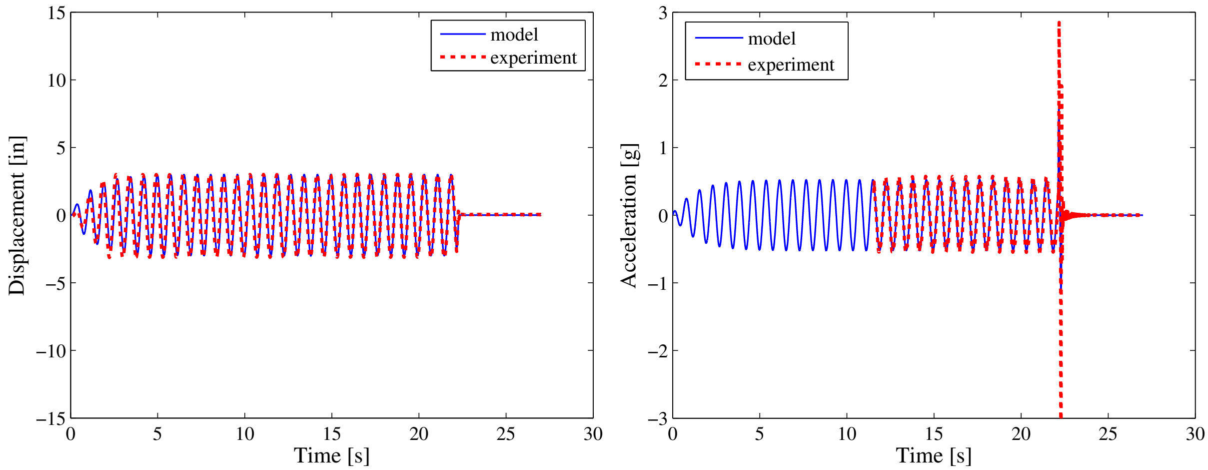


**Figure 3-10 Imposed support displacement and acceleration**

The out-of-plane acceleration histories of the control points shown in Figure 3-6(a) are shown in Figure 3-12, where again they are compared to those measured during the experiments. The plots on the left-hand side of Figure 3-12 were obtained using constant Kelvin–Voigt damping with retardation constants $\eta=\mu=0.012$ s, while those on the right-hand side are obtained by increasing the retardation constants for the free vibration phase to $\eta=\mu=0.016$ s. In this case, the numerical response appears to underestimate the recorded accelerations. Furthermore, the zoom-in shown in Figure 3-13 reveals the nonharmonic nature of the acceleration response, both measured and computed, possibly due to the influence of higher modes and nonlinearity effects. Thus, the influence of damping variation likely plays an even bigger role in the acceleration response.

Again, the reliability of computations is assessed in terms of energy balance. In forced vibration the input energy has to be equal at all times to the sum of strain, kinetic and dissipated energy. Each energy component is plotted in Figure 3-14(a), and the energy balance is shown in Figure 3-14(b). The energy error is plotted in Figure 3-14(c). While energy balance alone does not guarantee accuracy of the solutions, together with other checks such as rate of convergence of Newton's method, it provides confidence in the accuracy of the computations.

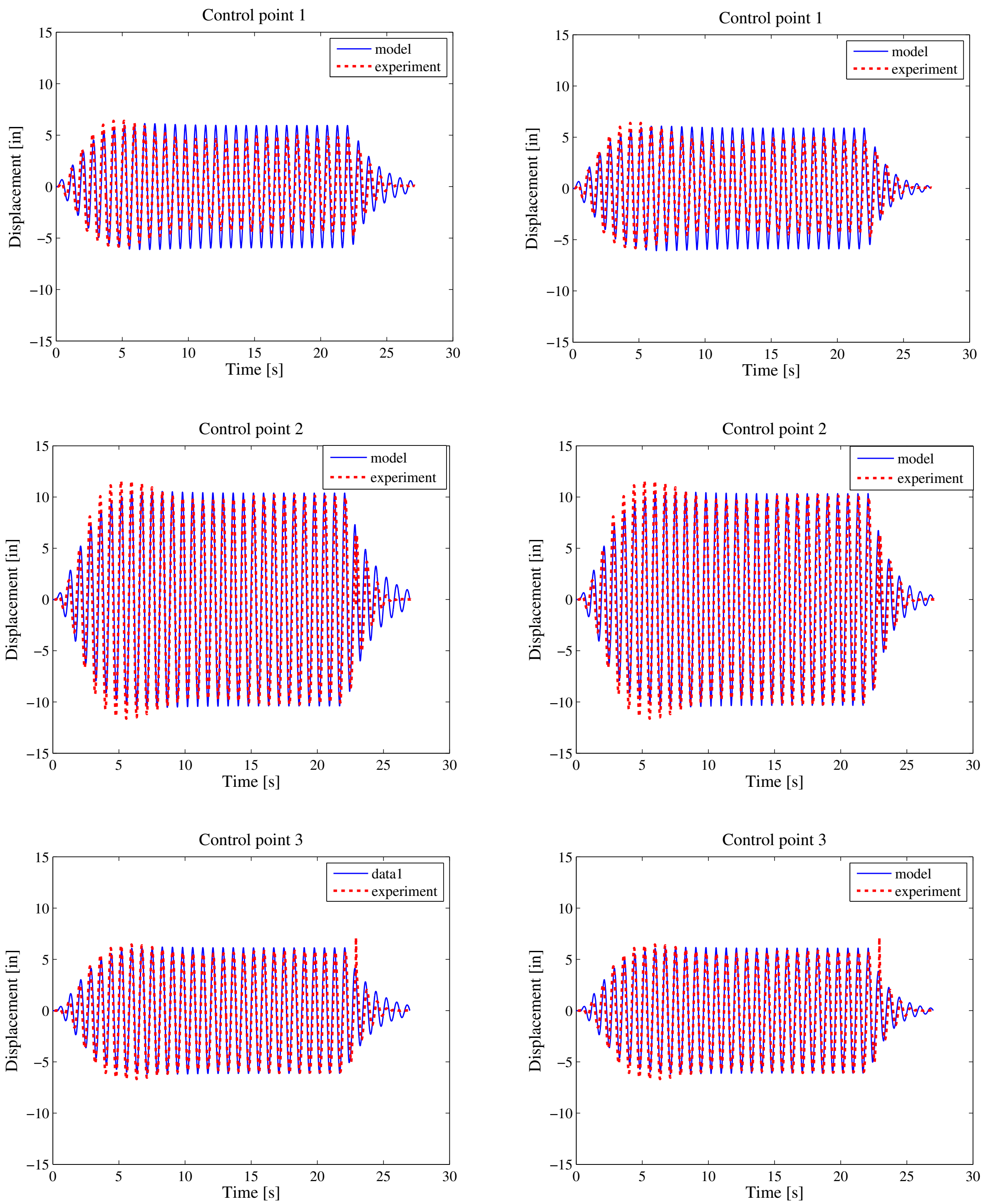


**Figure 3-11 Displacement history of control points shown in Figure 3-6(a). Constant $\eta$=$\mu$=0.012 s (left hand side plots); $\eta$=$\mu$=0.012 s for stationary response and $\eta$=$\mu$=0.016 s for free vibration response (right hand side plots).**

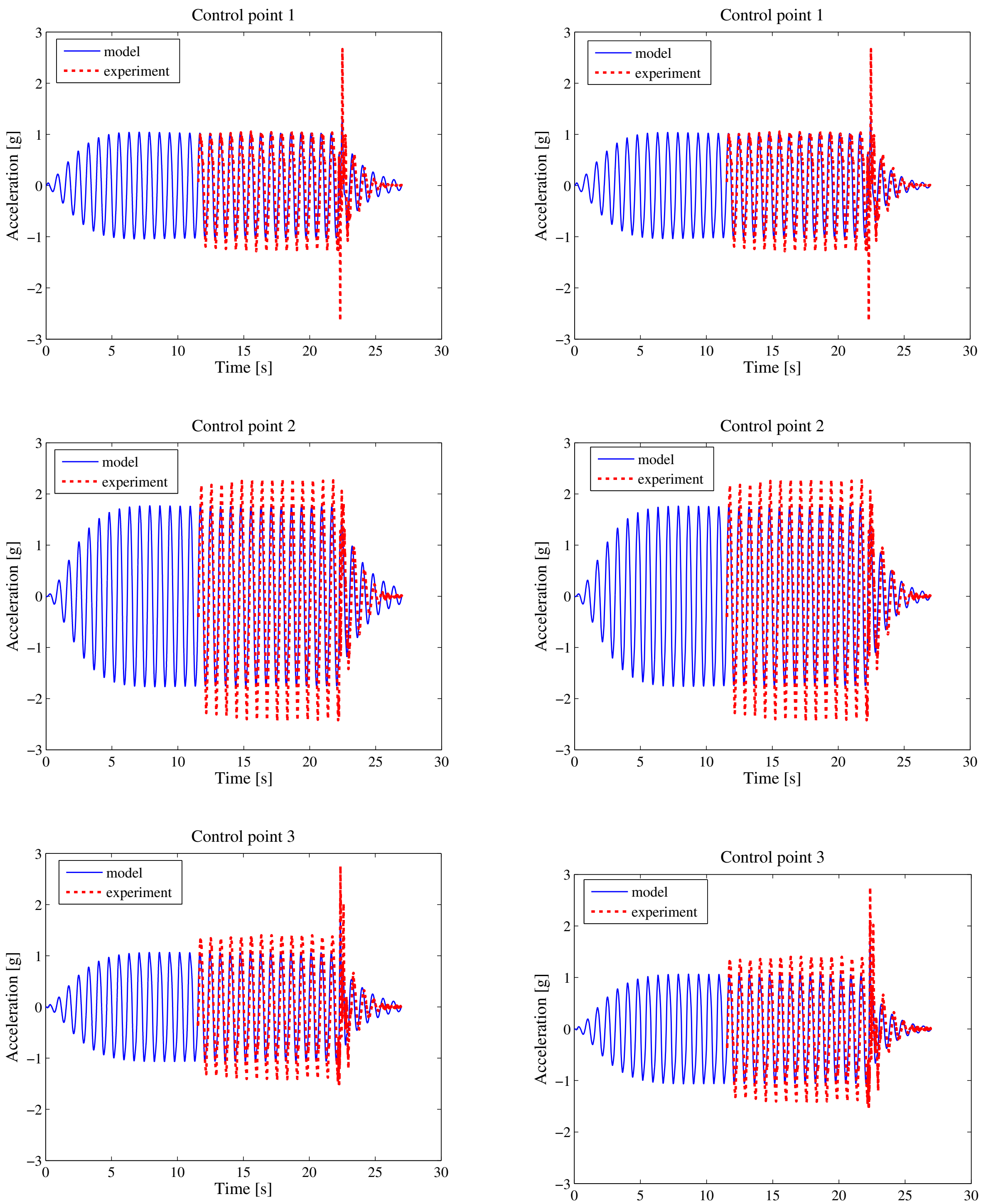


**Figure 3-12 Acceleration history of control points shown in Figure 3-6(a). Constant $\eta=\mu=0.012$ s (left hand side plots); $\eta=\mu=0.012$ s for stationary response and $\eta=\mu=0.016$ s for free vibration response (right hand side plots).**

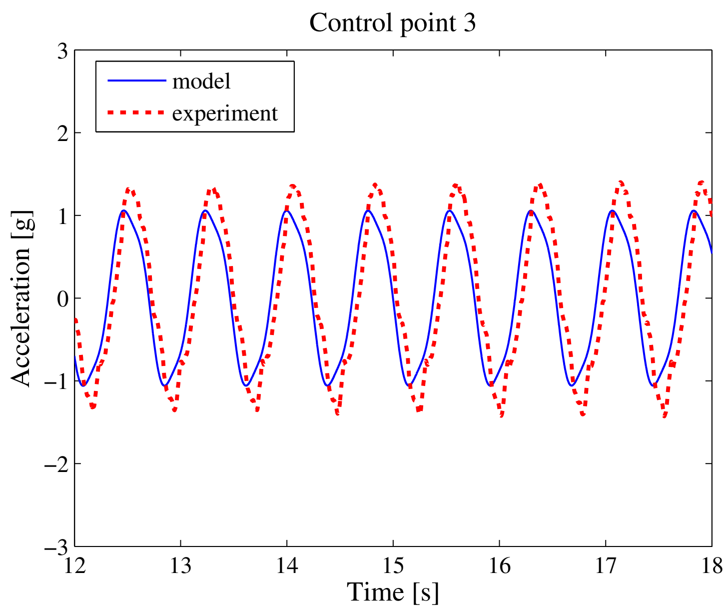


**Figure 3-13 Zoom-in of acceleration response - non-harmonic nature possibly due to higher modes or non-linearity.**

### 3.5 Concluding remarks

The 3D finite deformation beam model originally developed by Simo has been appropriately modified to derive a finite-element formulation for the static and dynamic analysis of flexible electrical cables. A linear viscoelastic constitutive equation and an additional mass proportional damping mechanism have been introduced to account for energy dissipation in a different and physically consistent way. Details of the numerical implementation of such damping model, in the context of large deformation beam theory, are discussed in Section 2.

Preliminary results of the simulation of free and forced vibration tests on an actual electrical conductor have been presented and energy balance calculations demonstrate the reliability of the numerical computations. However, the experiments reveal an amplitude dependence of both stiffness and damping, clearly pointing out the presence of material nonlinearity in the cable. Whereas some bounds are available for stiffness, no guidelines are available for damping. The damping constants used in this study were calibrated to match the experiments and not derived from the geometry or material properties of the cable. Even the stiffness bounds are rather wide to be used readily in practical applications.

The development of numerical models, within the current framework, that can properly account for the amplitude dependence of bending stiffness and energy dissipation capacity is subject of current computational and experimental work.

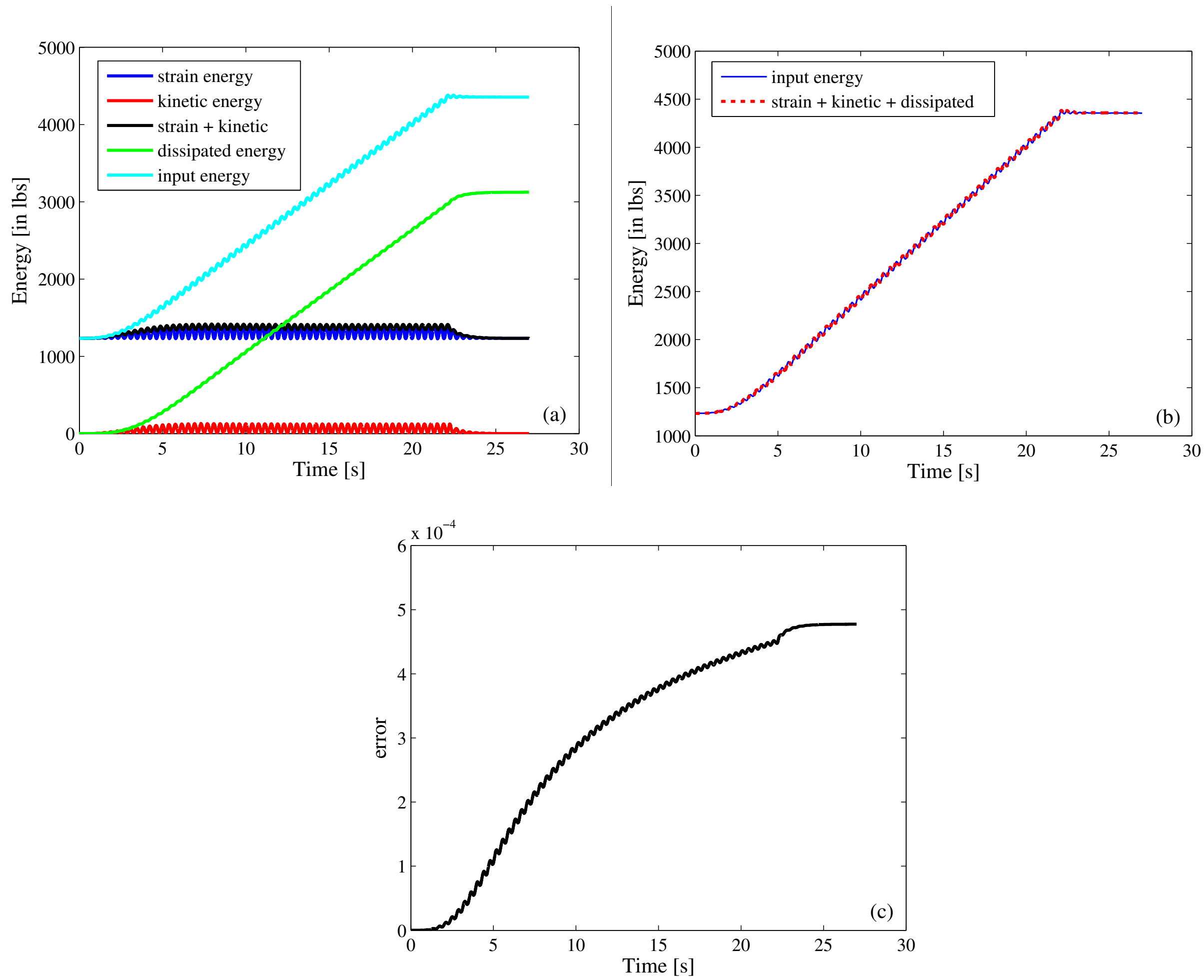


**Figure 3-14 Cable in forced vibration: (a) energy components; (b) energy balance; (c) energy error as defined in Eq. (3-32)**

# SECTION 4
# DYNAMIC ANALYSIS OF TENSEGRITY STRUCTURES USING A COMPLEMENTARITY FRAMEWORK

## 4.1 Introduction

The previous sections where concerned with modeling cables as beams, and therefore as elements subjected to bending, shear and torsion in addition to tension. In this chapter, we switch our attention to tensegrity structures, a particular type of cable structure for which the cables are tension only members and their slack behavior is not generally modeled in analysis, i.e. their buckling and post-buckling force capacity is neglected. Tensegrity structures are a subclass of pin-jointed structures composed of cables or strings, which can only resist tension forces, and bars or struts that are mainly meant to work in compression. To minimize weight, it is desirable in engineering applications to limit the number of stocky bars as compared to the number of the relatively light cables. Stability under external loading is then achieved by pretension of those cables that would otherwise become slack. One of the main requirements for a structure to be categorized as a tensegrity structure is that its initial pre-stressed configuration must be in stable equilibrium in absence of external forces. The evaluation of such configurations, known as form-finding, has been and is currently object of extensive research (Tibert and Pellegrino, 2003). A large body of literature is devoted to the topic, including recent applications using dynamic relaxation methods (Zhang et al., 2006) and evolutionary strategies (Rieffel et al., 2009). Besides the original interest in the field of civil engineering applications, which started developing with work by Calladine (1978), and Pellegrino and Calladine (1986), recent years have seen a multidisciplinary interest in tensegrity structures research (Sultan, 2009), with these emerging as the structural systems of the future. Control, folding and deploying capabilities have inspired aerospace engineering applications concerning for instance space telescopes, flight simulators and antennas (Sultan et al., 1999; Sultan et al., 2000; Tibert and Pellegrino, 2002). Several applications are appearing in the field of biomedical engineering (Ingber, 1998; Yaozhi et al., 2008; Stamenovic et al., 2006), where cell, tissue and organ architecture seem to adhere to models similar to those describing the behavior of tensegrity structures. Some applications have appeared also in the field of robotics where the characteristics of tensegrity structures make them appealing candidates for the design of movable robots as well as for manipulators (Aldrich et al., 2003; Shibata et al., 2009;

Juan et al., 2009). One interesting and promising aspect of tensegrity structures, which to our knowledge has not yet been developed much in the literature, is their potential ability to control the response to seismic excitations. A detailed discussion of tensegrity structures including historical background, analysis, design and control can be found in (Skelton and de Oliveira, 2009). We also refer the reader to the survey articles (Juan and Tur, 2008; Tur and Juan, 2009) on static and dynamic analysis of tensegrity structures.

The objective of this paper is to present an approach for the dynamic analysis of tensegrity structures in the small displacement regime. The novelty of the approach lies in casting the computations that occur in each time increment of the dynamic analysis as a "complementarity" problem. This formulation is made possible by the following fact. For any cable, the force in the cable and the slack are both non-negative, and when the force is positive, the slack is zero, and viceversa. The remarkable feature of the resulting approach is that despite the nonsmooth nature of cables switching between taut and slack states, the computed solutions show excellent long-term energy balance. Nineb et al. (2007) have used a complementarity framework in the context of a domain decomposition approach for non-smooth problems, specifically tensegrity structures. We discuss the relation of the formulation presented here to that of Nineb et al. (2007) at the end of Subsection 4.4.1. The approach presented here builds on previous work on the application of complementarity formulations to elasto-plastic problems (for example: Sivaselvan, 2010; Maier, 1970).

The organization of the section is as follows. In Subsection 4.2, the modeling of tensegrity structures adopted here is discussed, resulting in a differential-algebraic system with complementarity conditions. This system is discretized in time in Subsection 4.3, leading to a complementarity problem in Subsection 4.4. Numerical examples are then presented in Subsection 4.5, highlighting the long-term energy balance in the solutions, and the computational efficiency gained by using some features of the model in solving the complementarity problem.

### 4.2 Modeling for dynamic analysis

We think of a tensegrity structure as a truss with two types of members: "bars" that are capable of acting in both tension and compression (although they are predominantly in compression), and "cables" that act in tension only (they develop slack otherwise). Each cable can be represented conceptually as shown in Figure 4-1. Compatibility of deformations in this model of a cable implies

$$aF(t) - \pi(t) - \Delta(t) = 0 \tag{4-1}$$

where as shown in Figure 4-1, $a$ is the elastic compliance of the cable in tension, $F(t)$ is the force in the cable at time $t$, $\Delta(t)$ is the deformation, and $\pi(t)$ is the slack in the cable. The force in the cable and the slack are nonnegative. Furthermore, when the force in the cable is positive the slack is zero, and vice-versa. This is expressed concisely by the "complementarity" conditions

$$F(t) \ge 0, \pi(t) \ge 0, F(t)\pi(t) = 0 \tag{4-2}$$

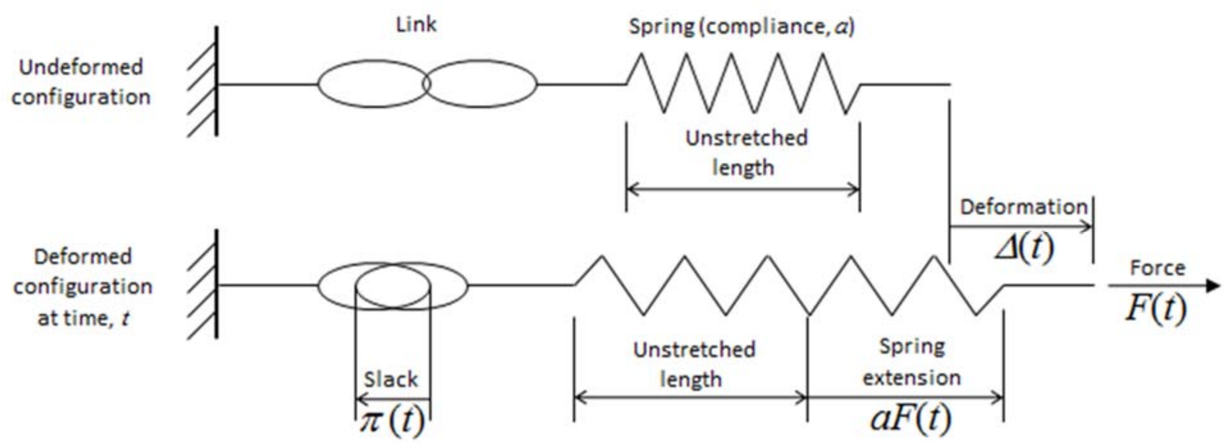


**Figure 4-1 Conceptual model of a cable in a tensegrity structure**

In the following, we consider only linearized kinematics (small displacements). Then the equation of motion of the structure, together with collecting equations (4-1) and (4-2) for all the cables in the structure, results in

$$\begin{gathered}\mathbf{Mu}(t) + \mathbf{Cu}(t) + \mathbf{K}_b^{\text{global}}\mathbf{u}(t) + \mathbf{B}_c{}^T\mathbf{f}^c(t) = \mathbf{p}(t) - \mathbf{B}_b{}^T\mathbf{f}_0^b \\ \mathbf{A}_c\mathbf{f}^c(t) - \boldsymbol{\pi}(t) - \mathbf{B}_c\mathbf{u}(t) - \Delta_0^c = 0 \\ \mathbf{f}^c(t) \ge 0,\ \boldsymbol{\pi}(t) \ge 0,\ \mathbf{f}^c(t)^T\boldsymbol{\pi}(t) = 0\end{gathered} \tag{4-3}$$

where $\mathbf{M}$ is a lumped mass matrix of the structure, $\mathbf{C}$ is a matrix representing inherent damping in the structure, $\mathbf{K}_b^{\text{global}}$ is the part of the structure stiffness matrix arising from the bars, $\mathbf{u}$ is the vector of displacements at the free degrees of freedom (DOF) of the structure, $\mathbf{p}$ is the vector of external nodal forces, $\mathbf{A}_c$ is the diagonal matrix of elastic compliances in tension of all cables in the structure, $\mathbf{B}_c$ and $\mathbf{B}_b$ are the matrices that relate the node displacements to cable deformations and bar deformations respectively, $\mathbf{f}^c$ and $\boldsymbol{\pi}$ are the vectors of forces and slacks respectively in the cables, $\mathbf{f}_0^b$ is the vector of pre-stress forces in the bars, and $\Delta_0^c$ is the vector of pre-stress deformations in the cables.

Equations (4-3) represent a linear differential-algebraic system with complementarity conditions. Due to the presence of the complementarity conditions, it represents non-smooth dynamics. In this work, we do not consider theoretical questions such as the existence and uniqueness of solutions to this system. The reader is referred to (Acary and Bogliato, 2008) for an exposition of such issues. Here, we take a heuristic approach. We formally discretize equations (4-3) in time, and consider the convergence of the resulting solutions with decreasing time increment.

Before discretizing the system (4-3), we cast it into a more general format as follows:

$$\begin{gathered}\mathbf{Mu}(t)+\mathbf{Cu}(t)+\mathbf{K}_b^{\text{global}}\mathbf{u}(t)+\mathbf{B}_c{}^T\mathbf{f}^c(t)=\mathbf{p}(t)-\mathbf{B}_b{}^T\mathbf{f}_0^b \\ \mathbf{A}_c\mathbf{f}^c(t)+\boldsymbol{\Psi}_{\text{UNI}}^T\boldsymbol{\pi}(t)-\mathbf{B}_c\mathbf{u}(t)-\Delta_0^c=0 \\ \boldsymbol{\Psi}_{\text{UNI}}\mathbf{f}^c(t)\le\mathbf{b}_{\text{UNI}},\ \boldsymbol{\pi}(t)\ge 0,\ \left(\mathbf{b}_{\text{UNI}}-\boldsymbol{\Psi}_{\text{UNI}}\mathbf{f}^c(t)\right)^T\boldsymbol{\pi}(t)=0\end{gathered} \tag{4-4}$$

where the subscript UNI stands for "unilateral constraints". The purpose of this generalization is twofold: (a) to allow for slightly more general behavior than tension-only (for example compression-only, interaction between force components etc.), (b) to align the notation with reference (Sivaselvan, 2010), where similar formulations result when modeling the dynamics of systems with softening plasticity. Equations (4-3) are recovered from equations (4-4) by setting $\boldsymbol{\Psi}_{\text{UNI}}=-\text{Identity}$ and $\mathbf{b}_{\text{UNI}}=0$ . Before considering the time-discretization of this system in subsection 4.3, we point out some consequences of the small-displacement assumption.

### 4.2.1 Implications of linearized kinematics

The use of linearized kinematics (small displacements) has some particular implications for tensegrity structures.

1. Internal mechanisms: If the equilibrium matrix $[\mathbf{B}_b\ \mathbf{B}_c]^T$ is not full rank, then the tensegrity structure has internal mechanisms. This is a common occurrence in tensegrity structures. The concept of internal mechanisms is explained in references (Pellegrino and Calladine, 1986; Pellegrino, 1990) using the four fundamental subspaces of the equilibrium matrix, a basic idea in linear algebra. Such internal mechanisms cannot be stabilized within the context of linearized

kinematics. Calladine and Pellegrino (1991,1992) present conditions under which these mechanisms can be stabilized by first order changes in the equilibrium matrix, which in turn are second order changes in the node displacement-member elongation relationship.

2. Geometric stiffness: Tensegrity structures are by definition prestressed frameworks, and carry non-zero internal forces in the reference configuration. Therefore, the effect of geometric stiffness could be significant even in the reference configuration. Geometric stiffness represents a first order change in the equilibrium matrix (see for example (Guest, 2006)), i.e., a second order change in the node displacement-member elongation kinematics.

It is clear that with linearized kinematics, tensegrity structures with internal mechanisms or significant geometric stiffness effects cannot be analyzed. Therefore, the formulation presented here cannot be applied to such situations as is. However, a formulation very similar to that presented here can be used to describe more general nonlinear kinematics, and therefore apply to the large displacement regime and to situations with internal mechanisms and significant geometric stiffness. In that case, due to the nonlinear relationship between member elongations and node displacements, and to the dependence of the equilibrium matrix on the configuration, a Newton-type algorithm would have to be used in each time increment. The exact strategy described in subsection 4.4 of the manuscript (Eqs. (4-9)–(4-11)) would then apply to each iteration of such a Newton-type algorithm. The approach presented in this paper is therefore relevant in the large displacement regime as well. The large-displacement formulation is a topic of current work.

The numerical examples in this section have been chosen such that the equilibrium matrices are full rank (so that there are no internal mechanisms), and the geometric stiffness is small compared to the material stiffness. It also turns out that internal mechanisms are not formed due to cables slackening during the analysis.

## 4.3 Time discretization

We discretize the system (4-4) formally as follows (see also references (Sivaselvan and Reinhorn, 2006; Sivaselvan et al., 2009; Sivaselvan, 2010)):

$$\mathbf{M}\left(\frac{\mathbf{v}_{n+1}-\mathbf{v}_n}{h}\right)+\mathbf{C}\left(\frac{\mathbf{v}_{n+1}+\mathbf{v}_n}{2}\right)+\mathbf{K}_b^{\text{global}}\left(\mathbf{u}_n+\frac{\mathbf{v}_{n+1}+\mathbf{v}_n}{4}h\right)$$
$$+\mathbf{B}_c^T\left(\frac{\mathbf{f}_{n+1}^c+\mathbf{f}_n^c}{2}\right)=\frac{\mathbf{p}_{n+1}+\mathbf{p}_n}{2}-\mathbf{B}_b^T\mathbf{f}_0^b$$

$$
\begin{aligned}
&\mathbf{A}_c(\mathbf{f}_{n+1}^c-\mathbf{f}_n^c)+\boldsymbol{\Psi}_{\mathrm{UNI}}^T(\boldsymbol{\pi}_{n+1}-\boldsymbol{\pi}_{n+1})-\mathbf{B}_c\frac{\mathbf{v}_{n+1}+\mathbf{v}_n}{2}h=0\\
&\boldsymbol{\Psi}_{\mathrm{UNI}}\mathbf{f}_{n+1}^c\le\mathbf{b}_{\mathrm{UNI}},\ \boldsymbol{\pi}_{n+1}\ge 0,\ \left(\mathbf{b}_{\mathrm{UNI}}-\boldsymbol{\Psi}_{\mathrm{UNI}}\mathbf{f}_{n+1}^c\right)^T\boldsymbol{\pi}_{n+1}=0
\end{aligned}
\tag{4-5}
$$

where $h$ is the time increment, $\mathbf{v}$ is the vector of velocities at the free DOF, and the subscripts $n$ and $n$+1 denote discrete times. When no cables are slack, this discretization reduces to the constant average acceleration version of Newmark's method (see for example (Chopra, 2007)). The second of equations (4-5) can be written in the following predictor-corrector form:

$$
\begin{aligned}
&\text{Predictor:}\qquad \tilde{\mathbf{f}}_n^c=\mathbf{f}_n^c+\mathbf{K}_c\left(\frac{h}{2}\mathbf{B}_c\mathbf{v}_n+\boldsymbol{\Psi}_{\mathrm{UNI}}^T\boldsymbol{\pi}_n\right)\\
&\text{Corrector:}\qquad \mathbf{f}_{n+1}^c=\tilde{\mathbf{f}}_n^c+\mathbf{K}_c\left(\frac{h}{2}\mathbf{B}_c\mathbf{v}_{n+1}-\boldsymbol{\Psi}_{\mathrm{UNI}}^T\boldsymbol{\pi}_{n+1}\right)
\end{aligned}
\tag{4-6}
$$

where $\mathbf{K}_c=\mathbf{A}_c^{-1}$ is the diagonal matrix of elastic stiffnesses in tension of all cables in the structure. Substituting the corrector equation into the first of equations (4-5), and into the inequality $\boldsymbol{\Psi}_{\mathrm{UNI}}\mathbf{f}^c{}_{n+1}\le\mathbf{b}_{\mathrm{UNI}}$ gives

$$
\begin{aligned}
&\bar{\mathbf{M}}\mathbf{v}_{n+1}-\frac{h}{2}\mathbf{B}_c^T\mathbf{K}_c\boldsymbol{\Psi}_{\mathrm{UNI}}^T\boldsymbol{\pi}_{n+1}=\mathbf{b}_1\\
&-\frac{h}{2}\boldsymbol{\Psi}_{\mathrm{UNI}}\mathbf{K}_c\mathbf{B}_c\mathbf{v}_{n+1}+\boldsymbol{\Psi}_{\mathrm{UNI}}\mathbf{K}_c\boldsymbol{\Psi}_{\mathrm{UNI}}^T\boldsymbol{\pi}_{n+1}\ge\mathbf{b}_2
\end{aligned}
\tag{4-7}
$$

where $\bar{\mathbf{M}}=\mathbf{M}+\frac{h}{2}\mathbf{C}+\frac{h^2}{4}\mathbf{K}^{\mathrm{global}}$ with $\mathbf{K}^{\mathrm{global}}=\mathbf{K}_b^{\mathrm{global}}+\mathbf{B}_c^T\mathbf{K}_c\mathbf{B}_c$ the elastic global stiffness matrix including the contributions of the bars and cables, and

$$
\begin{aligned}
\mathbf{b}_1&=\frac{h}{2}\left[(\mathbf{p}_{n+1}+\mathbf{p}_n)-\mathbf{B}_c^T(\tilde{\mathbf{f}}_n^c+\mathbf{f}_n^c)\right]\\
&\quad+\left(\mathbf{M}-\frac{h}{2}\mathbf{C}-\frac{h^2}{4}\mathbf{K}_b^{\mathrm{global}}\right)\mathbf{v}_n-h\left(\mathbf{K}_b^{\mathrm{global}}\mathbf{u}_n+\mathbf{B}_b^T\mathbf{f}_0^b\right)\\
\mathbf{b}_2&=\boldsymbol{\Psi}_{\mathrm{UNI}}\tilde{\mathbf{f}}_n^c-\mathbf{b}_{\mathrm{UNI}}
\end{aligned}
\tag{4-8}
$$

In the next subsection, the system of equations (4-7) and (4-8) is cast in the form of a complementarity problem.

## 4.4 Mixed Complementarity problem (MCP)

The computation of the velocities and slacks at time $n$+1 described by (a) the equation and inequality in (4-7), and (b) the complementarity conditions in (4-5), can be cast into a complementarity problem. First we define the matrix

$$\mathcal{M} = \begin{bmatrix} \bar{\mathbf{M}} & -\frac{h}{2}\mathbf{B}_c^T\mathbf{K}_c\mathbf{\Psi}_{\mathrm{UNI}}^T \\ -\frac{h}{2}\mathbf{\Psi}_{\mathrm{UNI}}\mathbf{K}_c\mathbf{B}_c & \mathbf{\Psi}_{\mathrm{UNI}}\mathbf{K}_c\mathbf{\Psi}_{\mathrm{UNI}}^T \end{bmatrix} \tag{4-9}$$

and the vectors

$$\mathbf{b} = \left(\mathbf{b}_1^T, \mathbf{b}_2^T\right)^T, \quad \mathbf{q} = -\mathbf{b} \tag{4-10}$$

Then the problem of computing the velocities and slacks can be stated as

$$\begin{gathered} \mathcal{M}\begin{pmatrix} \mathbf{v} \\ \boldsymbol{\pi} \end{pmatrix} + \mathbf{q} = \begin{pmatrix} 0 \\ \mathbf{w} \end{pmatrix} \\ \boldsymbol{\pi} \geq 0, \quad \mathbf{w} \geq 0, \quad \boldsymbol{\pi}^T\mathbf{w} = 0 \end{gathered} \tag{4-11}$$

The system (4-11) is a special case of a "Mixed Complementarity Problem" (MCP) (Dirkse and Ferris, 1995; Sivaselvan, 2010). The MCP may be solved using a general purpose solver such as the PATH solver (Dirkse and Ferris, 1995; Munson, 2000). However, computational efficiencies can be gained by customizing some linear algebra calculations to take advantage of the special form of the matrix that arises in structural mechanics problems. In particular, a Complementary Pivot Algorithm (CPA) is presented in (Sivaselvan, 2010) that uses such linear algebra customizations. In one of the numerical examples that follow, the computational efficiency gained from the linear algebra customization is highlighted. By transforming the MCP of equation (4-11) to a standard LCP (see Cottle et al., 1992)), it can be shown that it has a unique solution. Thus the problem in each time increment has a unique solution. Thus the problem in each time increment has a unique solution. The computations in each time increment are summarized in Procedure 1.

### 4.4.1 Relationship to existing literature

The conditions in (4-7) are obtained by solving the second of equations (4-5), namely the deformation compatibility equation, for the cable forces $\mathbf{f}_{n+1}^c$, and substituting it into the first of equations (4-5), namely the momentum conservation equation, and into the complementarity condition (using the predictor-corrector format (4-6)). This results in a *Mixed* Complementarity Problem, mixed since the velocity does not have a $\geq 0$ constraint (Dirkse and Ferris, 1995); in fact, it does not have any bound constraints. If instead the reverse is done, i.e., the momentum conservation equation is solved for the velocities $\mathbf{v}_{n+1}$, and this is substituted into the deformation compatibility equation, a Linear Complementarity Problem (LCP) in standard form is obtained, where all the variables, namely the cable slacks, are constrained to be $\geq 0$. This latter standard LCP is similar to the formulation presented in (Nineb et al., 2007). The matrix that arises in this standard LCP when $\Psi_{\mathrm{UNI}} = -\mathrm{Identity}$ is

$$\mathbf{K}_c - \mathbf{K}_c \mathbf{B}_c \bar{\mathbf{M}}^{-1} \mathbf{B}_c^T \mathbf{K}_c \tag{4-12}$$

the Schur complement of $\mathcal{M}$ in (4-9) with respect to $\bar{\mathbf{M}}$. When the mass and damping matrix are ignored (statics), this is identical to the matrix in (Nineb et al., 2007). Unlike the matrix $\bar{\mathbf{M}}$ which has the same sparse structure as the stiffness matrix, the matrix $\mathbf{B}_c \mathbf{M}^{-1} \mathbf{B}_c^T$ that appears in the standard LCP does not have a sparse structure. The sparse structure can be utilized to devise efficient computations to solve the MCP (4-11) (Sivaselvan, 2010). Nineb et al. (2007) develop a domain decomposition approach for large-scale non-smooth problems. The algorithm used to solve the MCP (4-11) can be used in the "local stage" of such a domain decomposition approach. The MCP (4-11) constitutes the Karush-Kuhn-Tucker (KKT) conditions of a Quadratic Program (QP) in $\mathbf{v}$ and $\boldsymbol{\pi}$. This fact can be used for example to compute the necessary derivatives (tangent operator) in the context of a domain decomposition approach. The standard form LCP described above constitutes the KKT conditions of a QP in $\boldsymbol{\pi}$ alone.

**Procedure 1** COMPUTATIONS IN EACH TIME INCREMENT

1: Compute $\tilde{\mathbf{f}}_n^c$ by the first of equations (4.6) ▷ Predictor computed for each cable
2: Compute $\mathbf{b}_1$ by the first of equations (4.8) ▷ Global vector assembly
3: Compute $\mathbf{b}_2$ by the second of equations (4.8) ▷ Computed for each cable
4: Obtain $\mathbf{v}_{n+1}$ and $\boldsymbol{\pi}_{n+1}$ by solving the complementarity problem (4.11)
5: Compute $\mathbf{f}_{n+1}^c$ by the second of equations (4.6) ▷ Corrector computed for each cable
6: Compute $\mathbf{u}_{n+1} = \mathbf{u}_n + (h/2)(\mathbf{v}_{n+1}+\mathbf{v}_n)$

## 4.5 Numerical examples

In this subsection, some numerical examples are presented to illustrate the proposed approach. In particular, two tensegrity structures are considered, both made of the same kind of elementary modules, but different in size, boundary conditions, method of assembly, pre-stresses, and loading conditions. For the first structure, a series of static analyses are performed, and the results are compared to those presented in the literature (Nineb et al., 2007). Furthermore, the computational efficiency gained by the linear algebra customizations of the Complementary Pivot Algorithm (CPA) of reference (Sivaselvan, 2010) is pointed out. The second structure considered is subjected to a set of dynamic analyses in free vibration and under harmonic loading. Energy balance plots are presented as a means of evaluating the performance of the algorithm and the accuracy of the results.

### 4.5.1 Example 1

As a first step in evaluating the performance and reliability of the approach described in the previous sections, the tensegrity grid considered by Nineb et. al. (2007) is analyzed. This example has been chosen so that numerical results can be verified against those presented in (Nineb et al., 2007). The example is not intended to represent a typical design. This grid was obtained by duplication of single 8-node self stressed modules (Quirant et al., 2003), shown in Figure 4-2. Each module consists of 12 cables and 4 bars. The properties of the elements composing the tensegrity structure are the same as in (Nineb et al., 2007), and are summarized in Table 4-1.

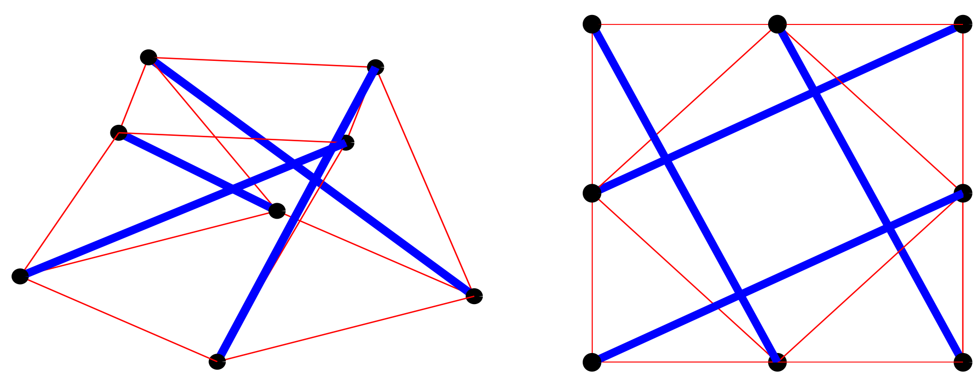

**Figure 4-2 Example 1: Single module in the tensegrity structure (a) Isometric view (b) Plan view (cables are shown as thin (red) lines and bars as thick (blue) lines)**

The elementary modules are placed one next to the other to form a self-stressed tensegrity grid consisting of 833 nodes, 3072 cables and 1024 bars. The assembled structure in its undeformed configuration is shown in Figure 4-3. All the lower nodes on two opposite edges of the grid are clamped, and every node is subjected to a vertical static load $\alpha p$, where $p$ is taken equal to 40 N, and different values of the load factor $\alpha$ are considered in the range from 0 to 1. When $\alpha$=1, the structure assumes the deformed configuration shown in Figure 4-4. Figure 4-5(a) shows the tension force in each of the 3072 cables, sorted in increasing order, for different values of the load factor $\alpha$. Figure 4-5(b) shows how the number of slack cables in the structure increases as $\alpha$ is increased from 0 to 1. When $\alpha$=0, the structure is in its self-stressed configuration, and the forces in the cables are simply equal to the initial pre-stresses. As $\alpha$ increases from 0 to 1, the number of slack cables increases, and for $\alpha$=1, 13.28% of all cables are slack. The graphs in Figures 4-5(a) and 4-5(b), obtained using the PATH solver and the Complementary Pivot Algorithm (CPA), are identical to each other, and appear to be exactly the same as those presented in (Nineb et al., 2007).

**Table 4-1 Example 1- Summary of module parameters**

| Parameter | Value |
|---|---|
| Module height $H$ | 0.5 m |
| Module length $L$ | 1 m |
| Cross section of cables Ac | 0.5 x $10^{-4}$ $m^2$ |
| Young's modulus of cables Ec | $10^{11}$ N/$m^2$ |
| Cross section of bars Ab | 2.8 x $10^{-4}$ $m^2$ |
| Young's modulus of cables Eb | 2 x $10^{11}$ N/$m^2$ |
| Prestress in lower cables | 2000 N |
| Prestress in upper cable | $2000\sqrt{2}$ N |
| Prestress in bracing cables | $2000\ \sqrt{1+4\left(H/L\right)^2}$ N = 2828.4271 N |
| Prestress in bars | $-2000\ \sqrt{5+4\left(H/L\right)^2}$ N = -4898.9795 N |

We next explore the computational efficiency gained by the linear algebra customizations specific to structural mechanics problems utilized in the CPA of (Sivasevan, 2010). This is done by setting the options for the PATH solver as shown in Table 4-2 to emulate the CPA. The PATH solver, however, does not utilize the linear algebra customizations. In Figure 4-6, the computational times of the CPA are plotted against the number of factorization updates. The computational time required by PATH is 6.16 s as indicated by the dashed line in Figure 4-6. The least computational time of 1.44 s is seen to be obtained when the CPA uses 20 factorization updates. The linear algebra customizations thus result in a speedup of about 4.28 for this problem.

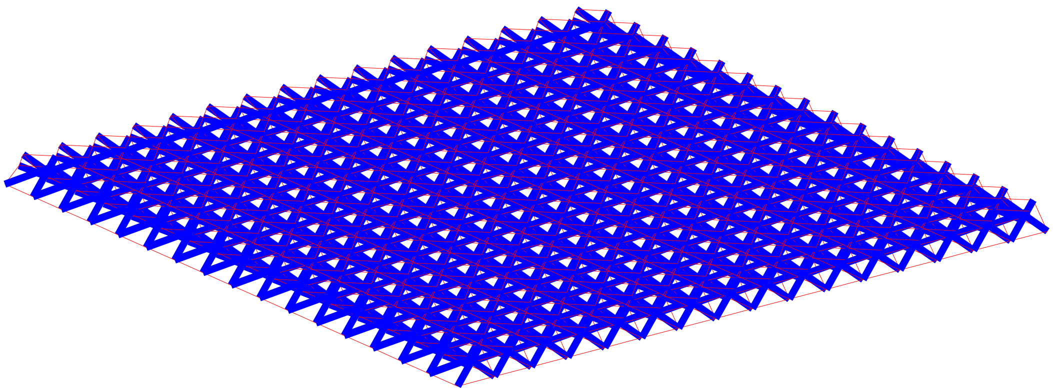

(a)

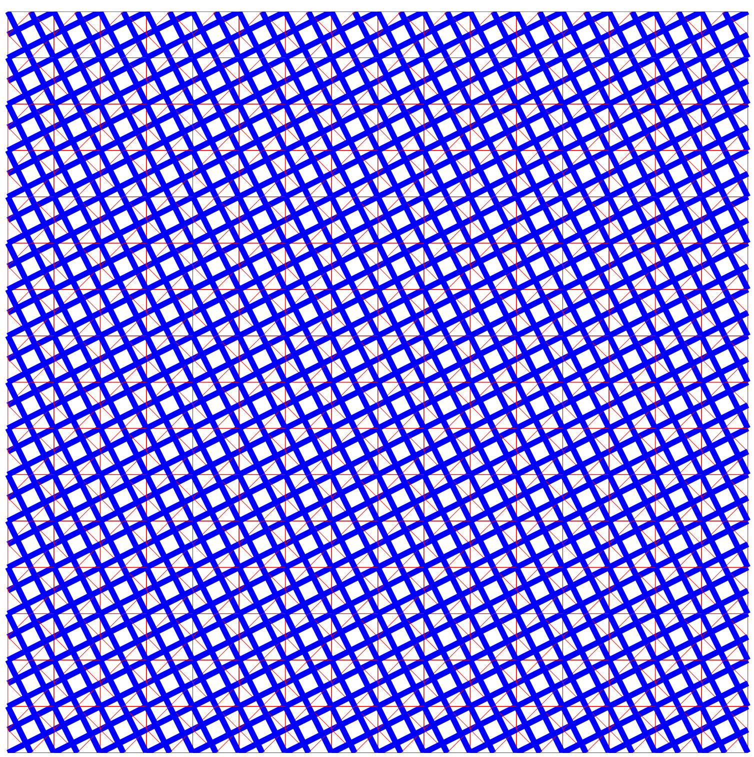

(b)

**Figure 4-3. Example 1: Undeformed configuration (a) Isometric view (b) Plan view (cables are shown in thin red and bars in thick blue.**

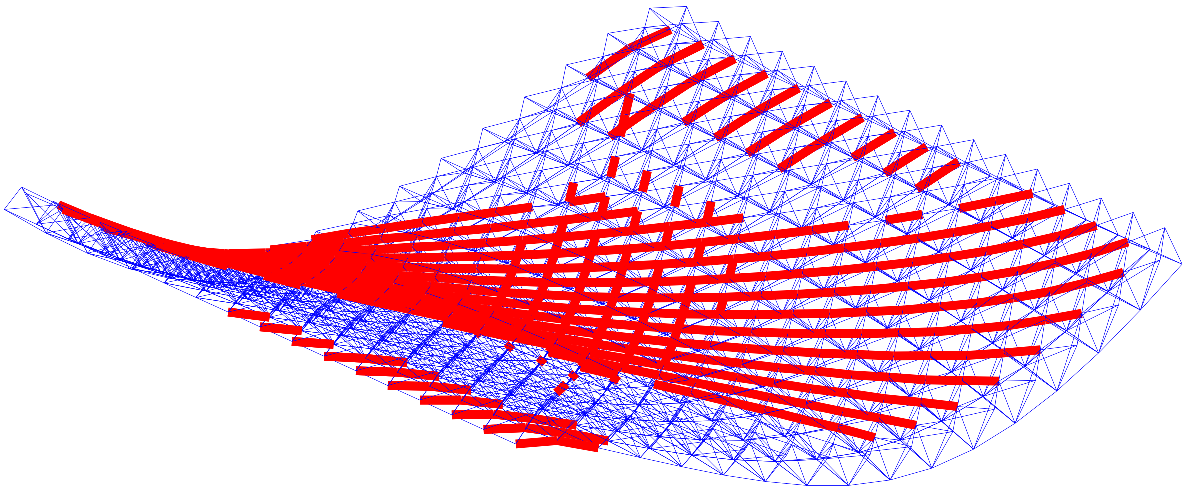

(a)

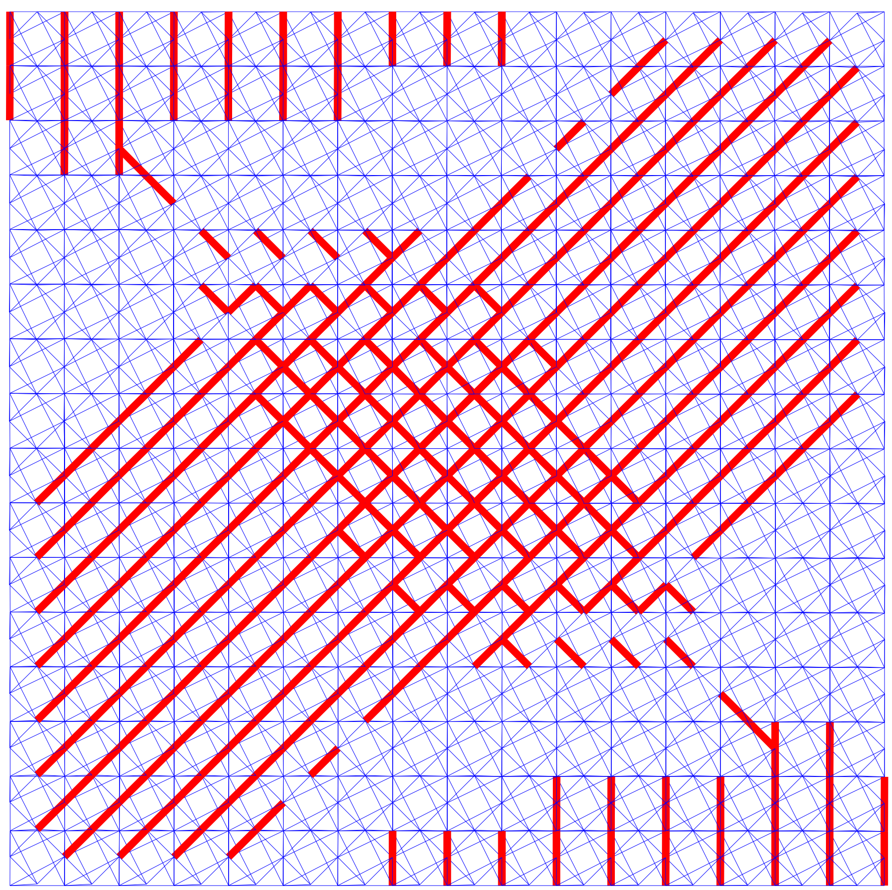

(b)

**Figure 4-4 Example 1: Deformed configuration for α = 1 with slack cables shown in thick (red) lines (a) Isometric view (b) Plan view**

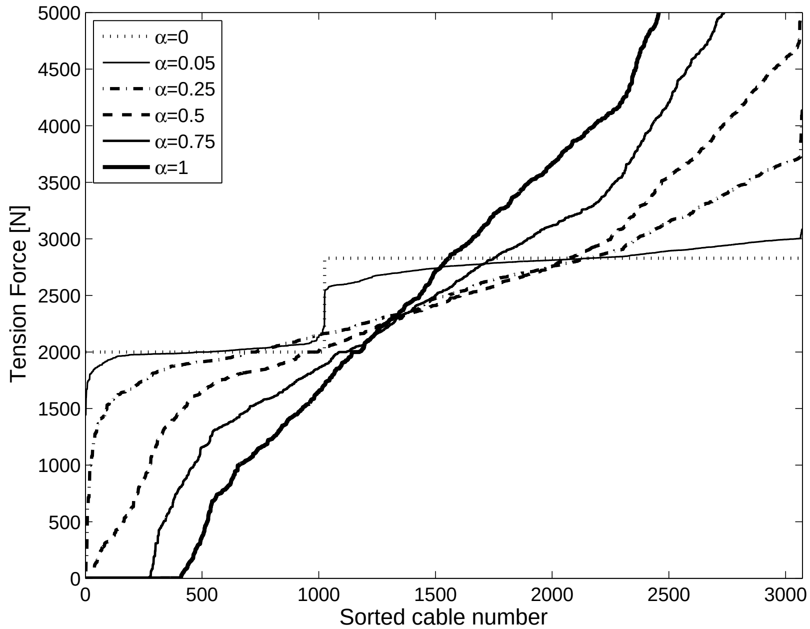


(a)

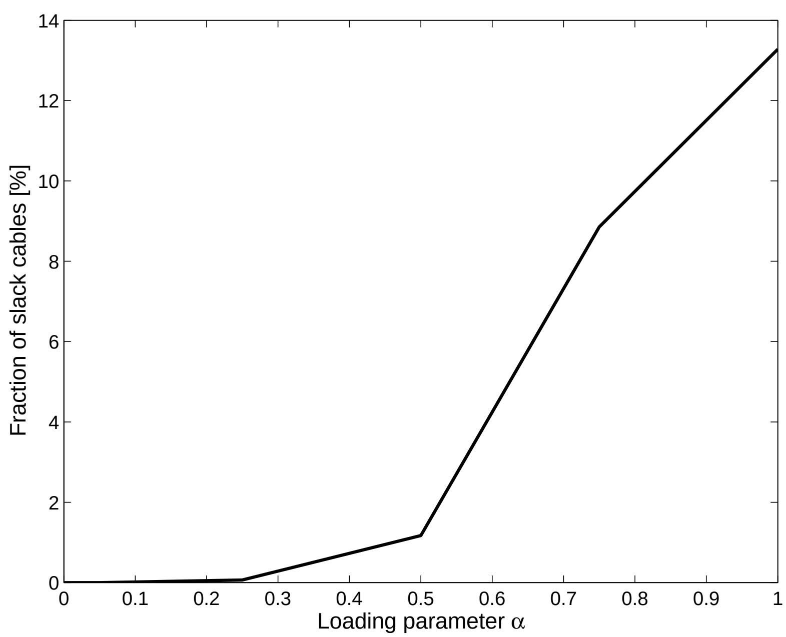


(b)

**Figure 4-5 Example 1: (a) Cable tensions, and (b) Fractions of slack cables, for different values of the load factor α (these computational results are identical to the respective results in(Nineb et al., 2007)))**

**Table 4-2 Example 1: Options for the PATH solver to imitate Lemke's method**

| Option | Value |
|---|---|
| crash_method | none |
| major_iteration_limit | 1 |
| lemke_start | always |
| Output_minor_iteration_frequency | 1 |

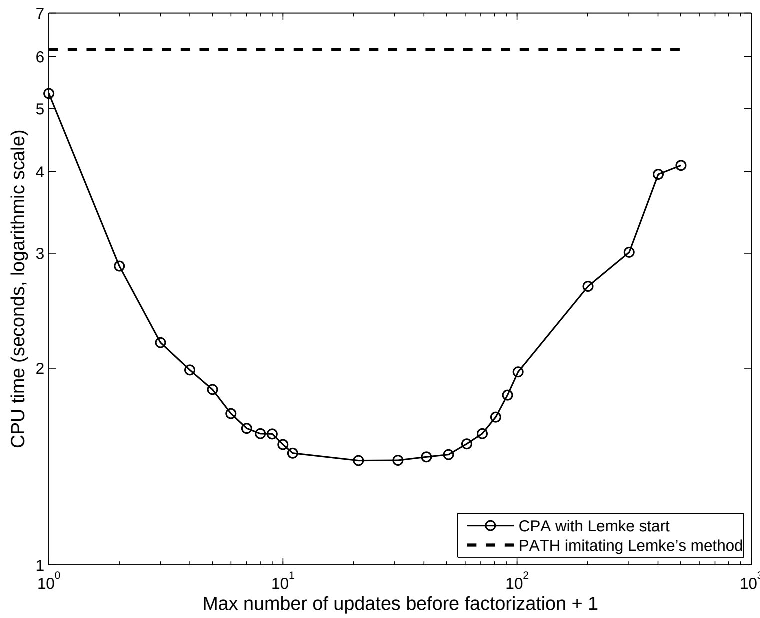


**Figure 4-6 Example 1- Computational time (In this example, there are 2397 free DOF and 3072 cables, so that the size of the MCP in equation (4-11) is 5469)**

### 4.5.2 Example 2

The second example is a 6x6 tensegrity grid designed by Quirant et al. (2003). The elementary modules comprising the grid are of the same kind as the ones in the previous example, but different in size, properties and pre-stresses. Moreover, the modules are assembled in such a way that they share the cables connecting them to the adjacent modules. The grid consists of 133 nodes, 372 cables and 144 bars. As boundary conditions, the four lower corner nodes are clamped while all the other nodes along the four edges are restrained vertically but free to move in the other directions. The properties of the elements composing the tensegrity structure are as presented by Quirant et al. (2003), and are summarized in Table 4-3. The assembled structure in its undeformed configuration is shown in Figure 4-7. The structure is modeled as having no inherent viscous damping.

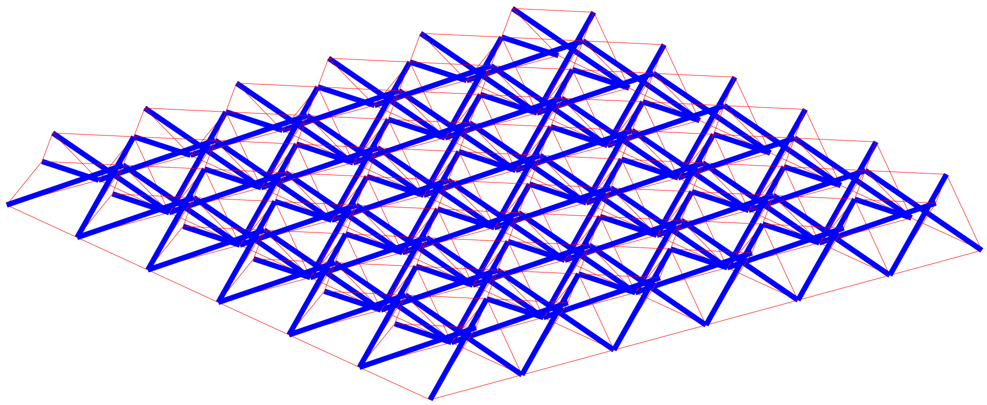

(a)

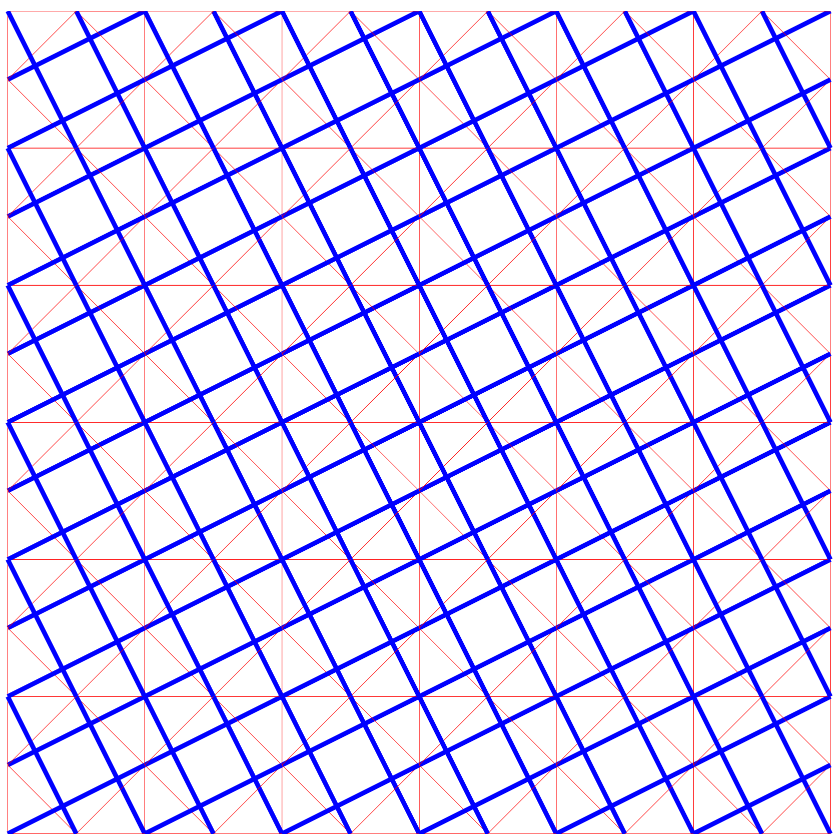

(b)

**Figure 4-7 Example 2: Undeformed configuration (a) Isometric view (b) Plan view (cables are shown in thin red and bars in thick blue)**

First the frequencies and modes of the linearized model are computed. Isometric and front views of the structure in its first mode shape, and in its undeformed configuration are shown in Figure 4-8. The first 6 natural frequencies of the linearized model of the tensegrity grid are $f_1 = 12.7185$ Hz, $f_2 = f_3 = 15.2907$ Hz, $f_4 = 21.2673$ Hz, and $f_5 = f_6 = 28.2729$ Hz.

**Table 4-3 Example 2: Summary of module parameters**

| Parameter | Value |
|---|---|
| Module height *H* | 1.15 m |
| Module length *L* | 1.5 m |
| Cross section of cables Ac | 0.654 x $10^{-4}$ $m^2$ |
| Young's modulus of cables Ec | 1.25 x $10^{11}$ $N/m^2$ |
| Cross section of bars Ab | 4.14 x $10^{-4}$ $m^2$ |
| Young's modulus of cables Eb | 2 x $10^{11}$ $N/m^2$ |
| Prestress in bars | -20000 N |
| Prestress in peripheral lower cables | 7376.5536 N |
| Prestress in internal lower cables | 14753.1072 N |
| Prestress in upper cables | 10432.0221 N |
| Prestress in bracing cables | 13503.5487 N |

#### 4.5.2.1 Free vibration analysis

Free vibration analyses of the tensegrity structure are performed starting from different initial configurations as summarized in Table 4-4.

*Case 1*: First the structure is displaced into the shape of the first mode of the linearized model without slack cables, and then released. The resulting response, as would be expected, is simple harmonic as seen from the displacement of the center node in Figure 4-9.

*Case 2*: Next, the structure is displaced into the configuration shown in Figure 4-10 with 24 slack cables, and then released. The analysis is performed with time increment 0.001s (~1/80 of the first mode period of the linearized model). The computed response is shown in Figure 4-11. Figures 4-11(a) and 4-11(b) show the displacement of the center node. In order to evaluate the accuracy of the proposed approach, the total energy is computed. The system is modeled as undamped, and the slackening and tightening of the cables are not associated with energy dissipation. So the total energy of the system, the sum of the strain and kinetic energies must remain constant, and equal to the strain energy in the deformed configuration from which it is released. This energy balance is shown in Figure 4-11(c).

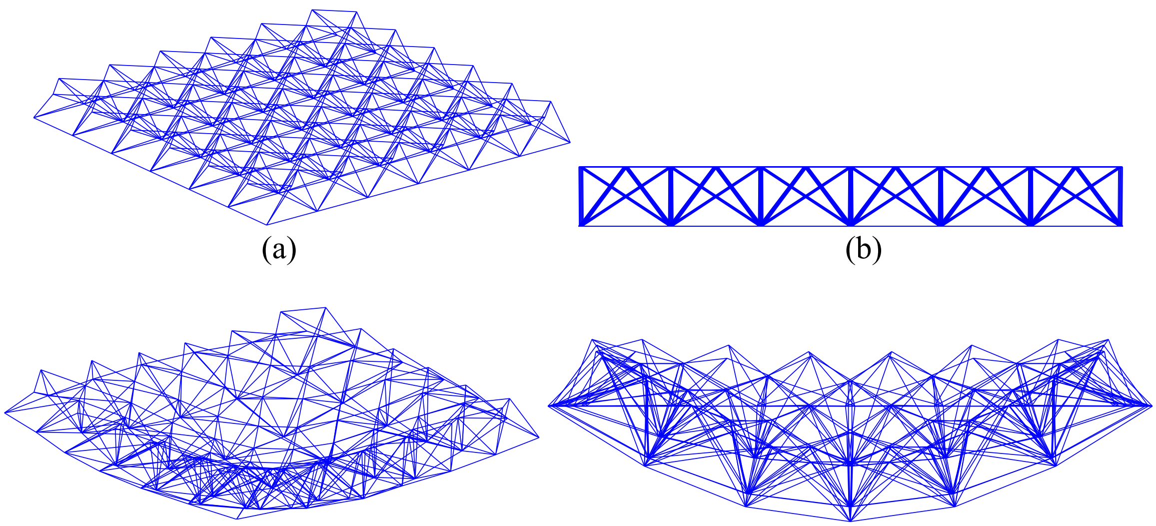

(a) (b)

(c) (d)

**Figure 4-8 Example 2: (a) Isometric view of undeformed shape (b) Front view of undeformed shape (c) Isometric view of first mode (frequency, $f_1$ = 12.7185 Hz) (d) Front view of first mode**

**Table 4-4 Example 2: Free vibration analysis cases**

| Case | Initial configuration | Increment (s) | Result plot |
|---|---|---|---|
| 1 | First mode shape with no slack cables (Figure 4.8) | 0.001 | Figure 4.9 |
| 2 | Displaced configuration with 24 slack cables (Figure 4.10) | 0.001 | Figure 4.11 |
| 3 | Displaced configuration with 24 slack cables (Figure 4.10) | 0.01 | Figure 4.12 |
| 4 | Displaced configuration with 12 slack cables | 0.01, 0.005, 0.001, 0.0005 | Figure 4.13 |

The energy error defined as

$$\text{energy error} = \frac{\text{total energy} - \text{initial strain energy}}{\text{initial strain energy}} \tag{4-13}$$

is shown in Figure 4-11(d). It is remarkable that despite the nonsmooth nature of slackening and tightening of the cables, the relatively large time increment used, and the long duration of the analysis, the largest energy error is only of the order of 0.003. It will be seen later that similarly good long-term energy behavior is obtained in forced vibration analysis as well. This energy balance feature may be attributable to the loose relationship of the time discretization in subsection 4.3 to the notion of Variational Integrators (Fetecau et al., 2003). Further exploration of this relationship is a topic of current work.

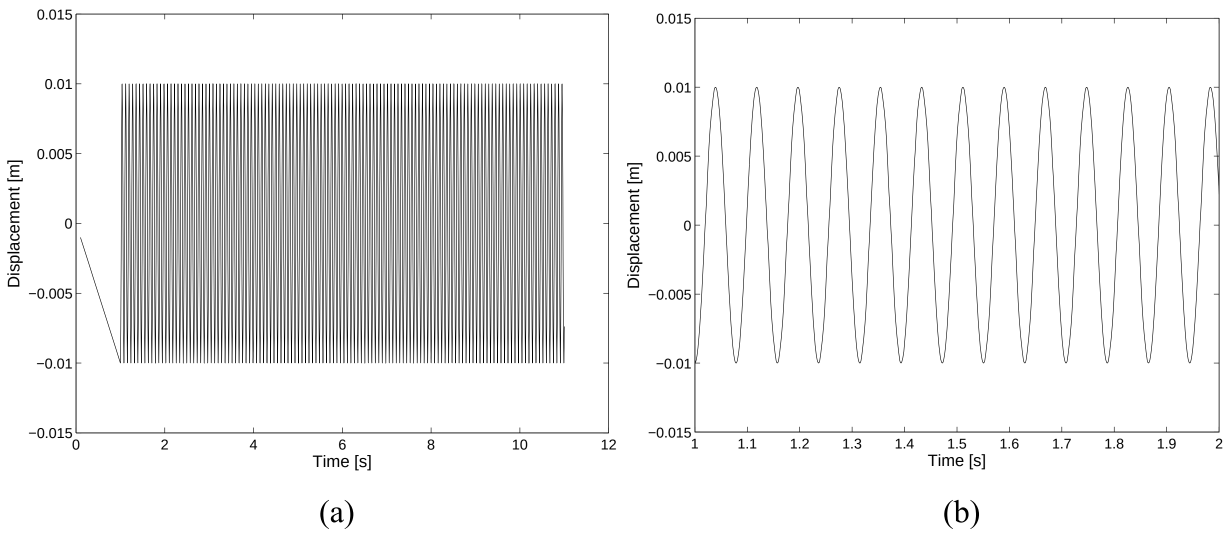


**Figure 4-9 Example 2: Free vibration response starting from a deformed configuration corresponding to the first mode with no slack cables. The dynamic response is computed using time step 0.001s. (a) Displacement of the center node over 10s of oscillation; the initial displacement for the dynamic phase is imposed quasi-statically over the first 1s (b) Zoom-in of the first 1s of oscillation of the center node**

*Case 3*: Although excellent behavior in terms of energy conservation is observed for fairly large time increments, the time increment cannot be arbitrarily large. In this analysis case, the same initial configuration is considered as in Case 2. However, a time increment of 0.01s is used for dynamic analysis. The resulting computation is not stable as seen in Figure 4-12.

*Case 4*: In this analysis case, the goal is to explore convergence of the computed solutions with decreasing time increment. For this, the model is released from an initial configuration with 12 slack cables, and dynamic analysis is performed with four time increments. Figure 4.13 indicates convergence of the center node displacement.

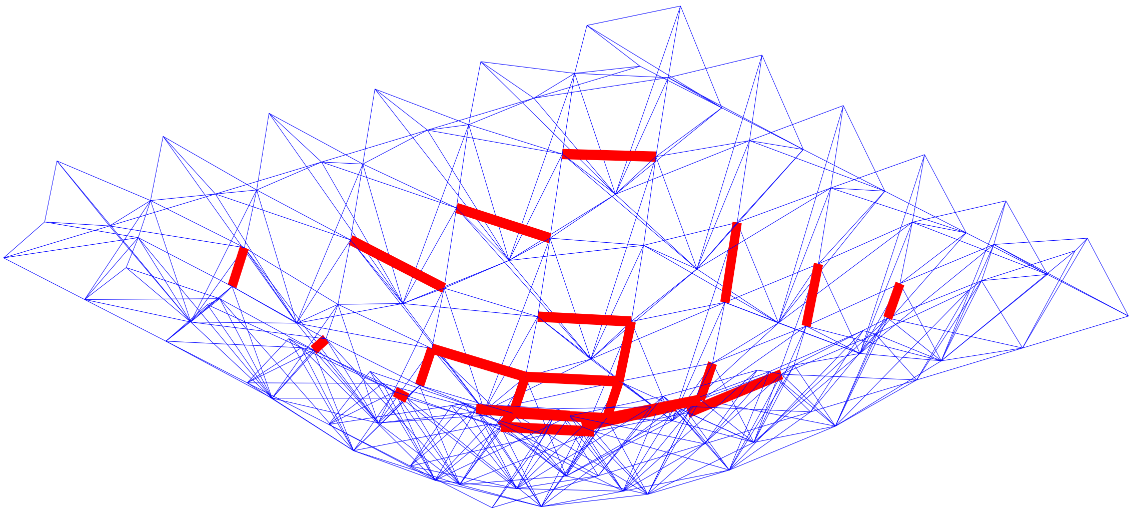

(a)

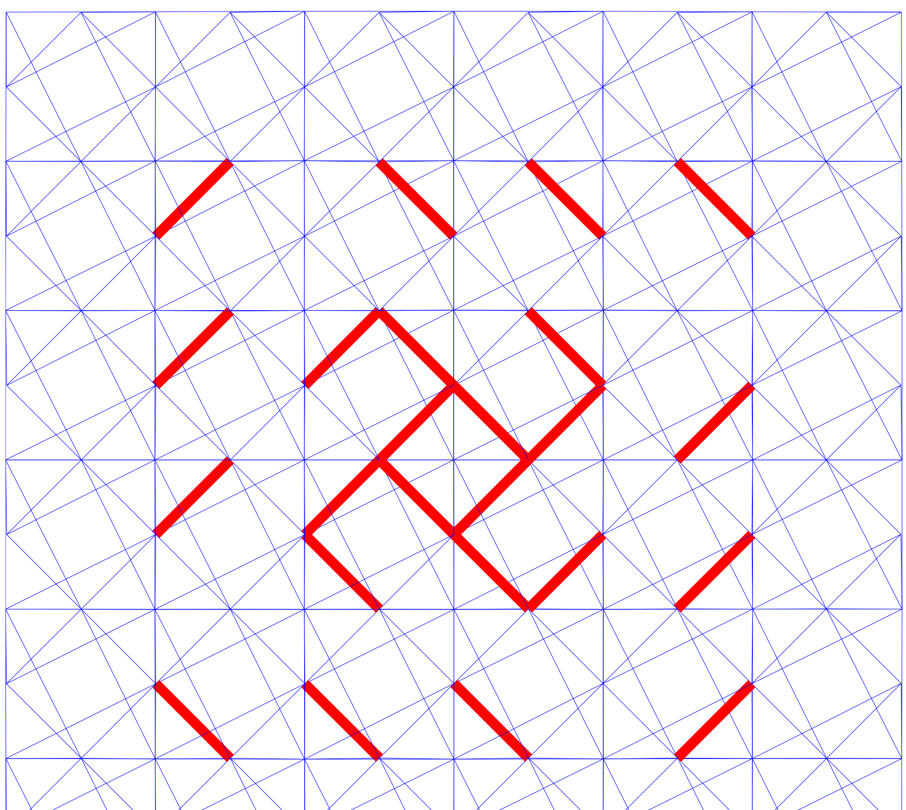

(b)

**Figure 4-10 Example 2: Deformed configuration with 24 slack cables shown as thick (red) lines (a) Isometric view (b) Plan view**

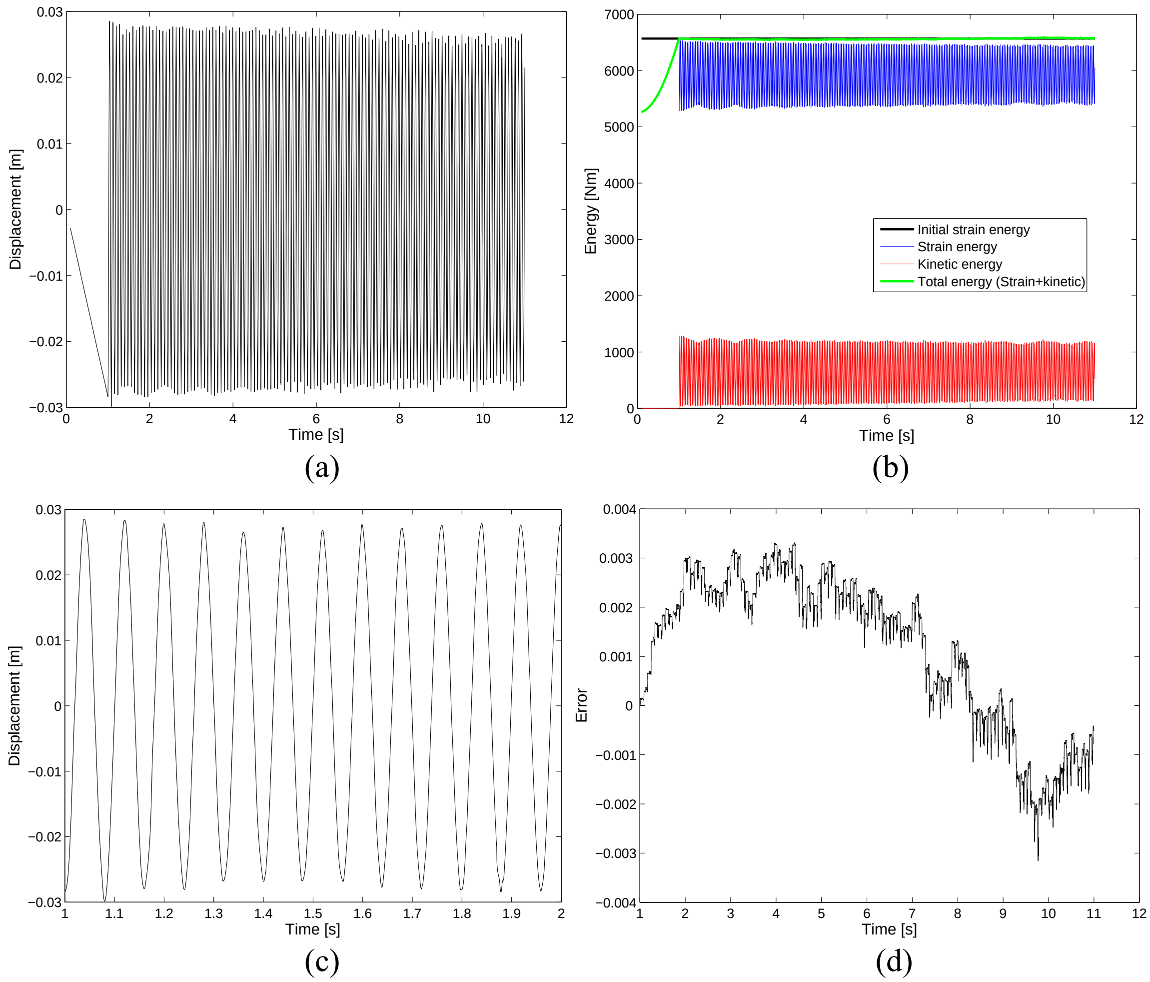


**Figure 4-11 Example 2: Free vibration response starting from a deformed configuration with 24 slack cables computed using time step 0.001 s. (a) Displacement of the center node over 10 s of oscillation; the initial displacement for the dynamic phase is applied quasi-statically over the first 1 s. (b) Zoom-in of the first 1 s of oscillation of the center node. (c) Energy balance. (d) Energy error as defined in Eq. (4-13)**

#### 4.5.2.2 Forced vibration analysis with harmonic input

Another set of analyses is performed with harmonic vertical base motion input. The base input acceleration is of the form

$$\ddot{u}_g(t) = \ddot{u}_{g0} \sin(2\pi f_1 t) \tag{4-14}$$

where $\ddot{u}_{g0}$ is the amplitude of the base acceleration, and $f_1$=12.7185 Hz is the frequency of the first mode of the linearized model. Three analysis cases are considered with increasing amplitudes of the input base acceleration. In each case, the dynamic analysis is performed with time increment 0.001s.

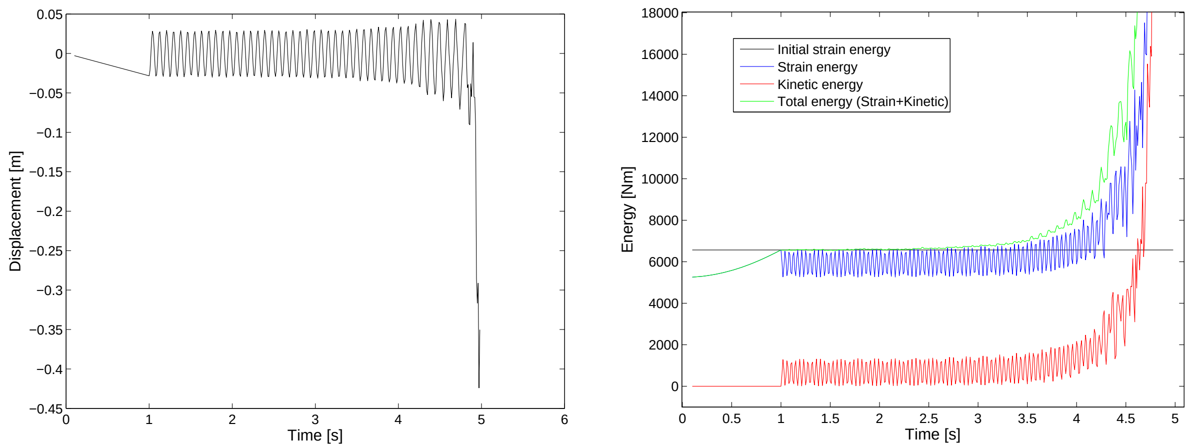


(a) (b)

**Figure 4-12 Example 2: Free vibration response starting from a deformed configuration with 24 slack cables computed using time step 0.01s (a) Displacement of the center node (b) Energy balance**

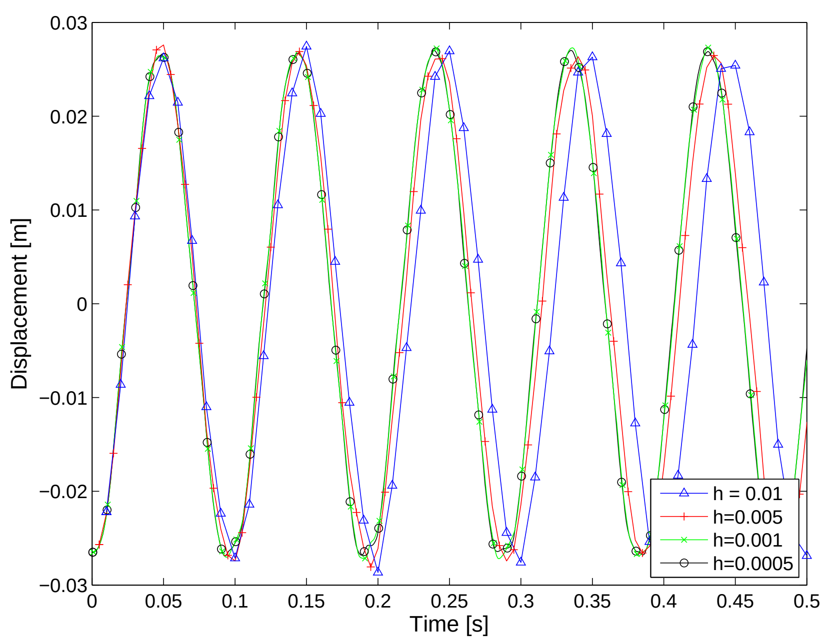


**Figure 4-13 Example 2: Convergence of displacement of the center node with decreasing time step size for free vibration starting from a deformed configuration with 12 slack cables**

*Case 1* ($\ddot{u}_{g0}$ = 0.01g): The computed response is shown in Figure 4-14. No cables slacken in the first 10s, and the displacement of the center node seen in Figure 4-14(a) shows the characteristic linear growth of resonance. We again explore the long-term energy balance. Unlike in the free vibration case, the input energy needs to be taken into account when considering energy balance. The input energy is computed as

$$\text{input energy}(t) = \int_0^t \sum R_s(\tau) v_s(\tau) \mathrm{d}\tau \tag{4-15}$$

where $R_s$ and $v_s$ are the reactions and velocities of the supports at the base.

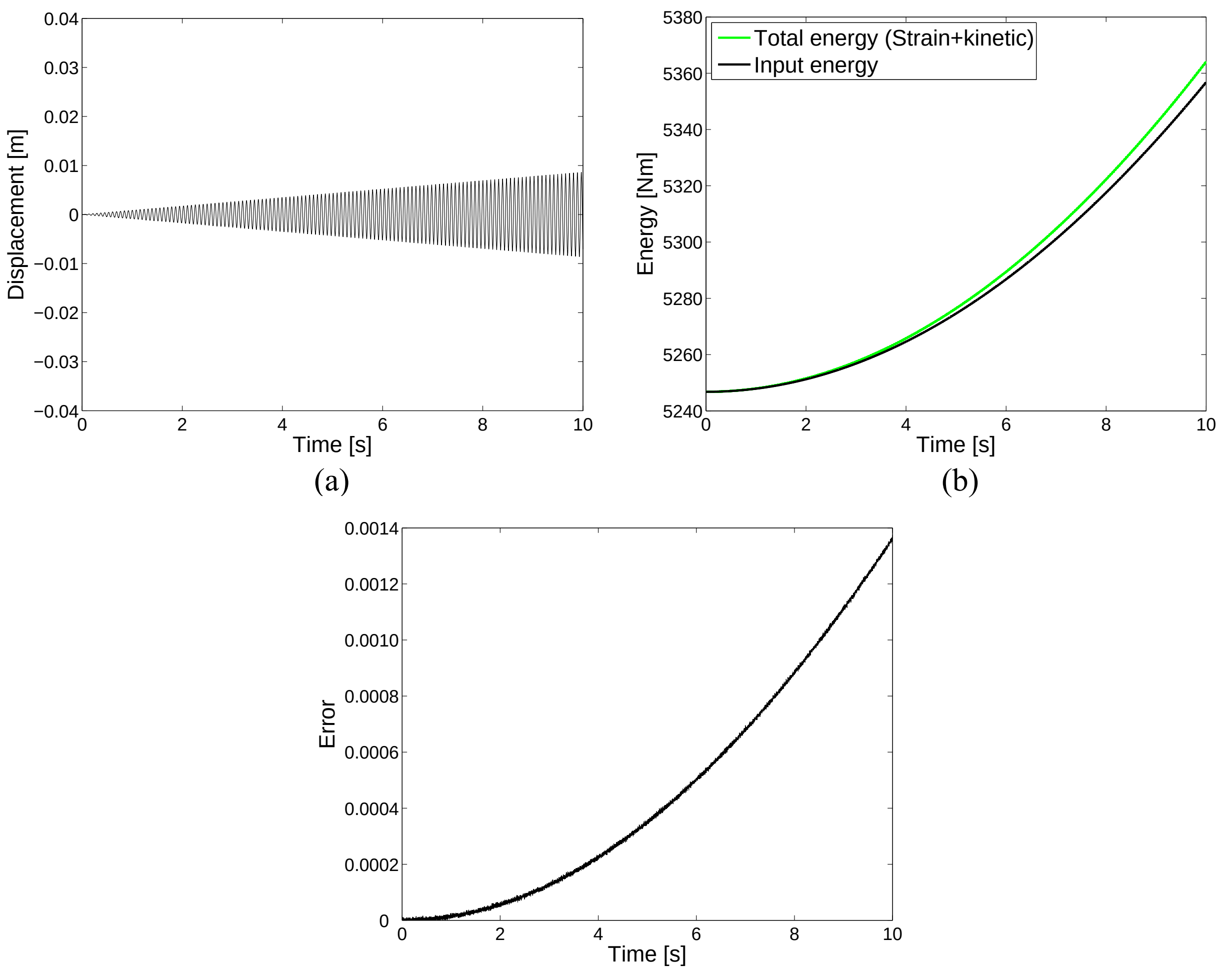


(a) (b)

(c)

**Figure 4-14 Example 2: Forced vibration with input acceleration amplitude 0.01g, computed using time step 0.001s (a) Displacement of center node (b) Energy balance (c) Energy error as defined in equation (4-16)**

The energy error in the forced vibration case is defined as

$$\text{energy error} = \frac{\text{total energy} - \text{input energy}}{\text{input energy}} \tag{4-16}$$

The total and input energies are shown in Figure 4-14(b), and the energy error in Figure 4-14(c).

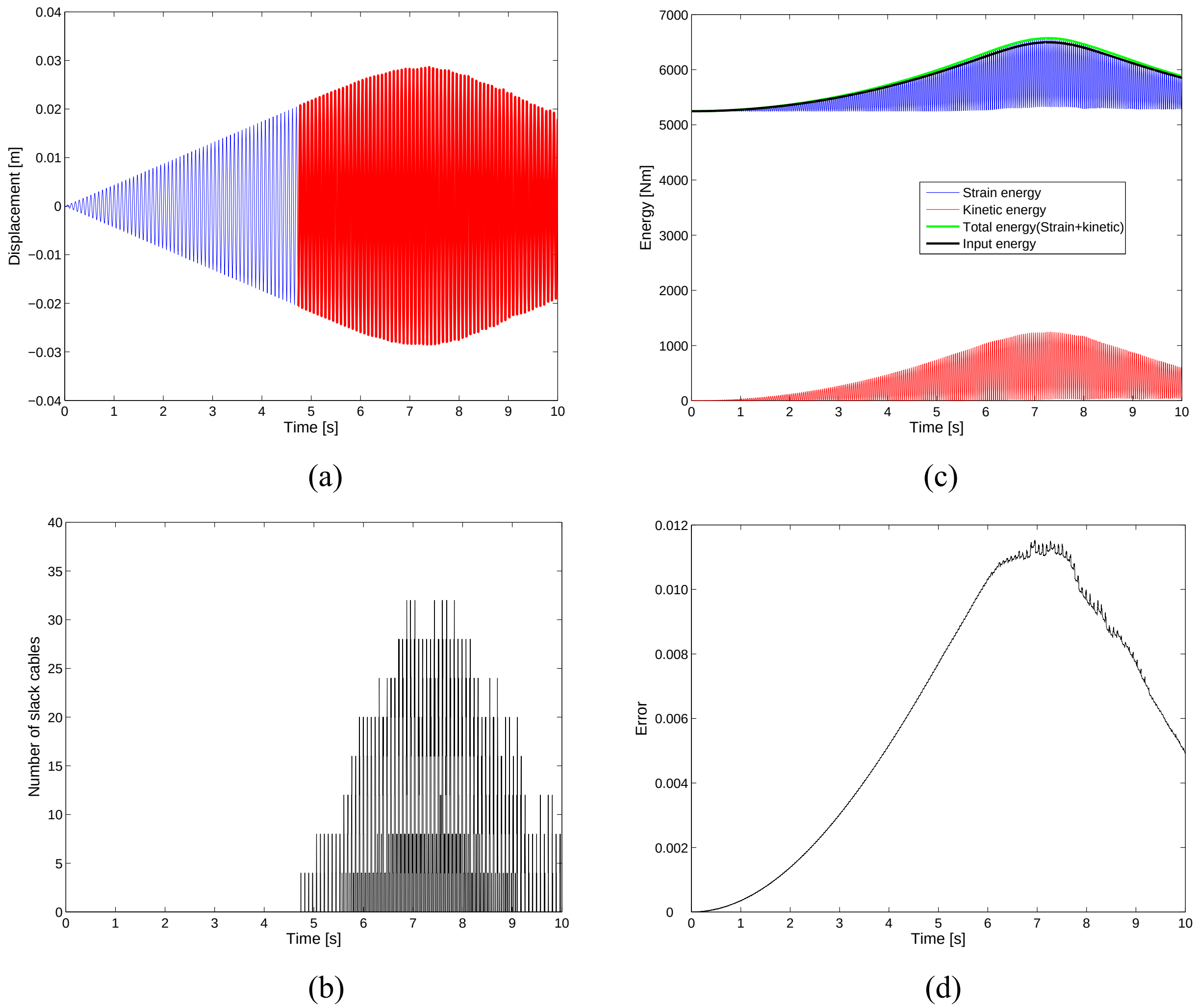


**Figure 4-15 Example 2: Forced vibration with input acceleration amplitude 0.05 g, computed using time step 0.001 s. (a) Displacement of the center node with the phase where some cables could be slack is shown in red. (b) Number of slack cables. (c) Energy balance. (d) Energy error as defined in Eq. (4-16)**

*Case 2* ($\ddot{u}_{g0} = 0.05\,$g): The displacement of the center node of the grid is shown in Figure 4-15(a). Just before 5 seconds, when the amplitude of the response is about 0.02 m, some cables become slack. The phase of motion where a number of cables in the structure go from being in tension to being slack and vice-versa is indicated in red in Figure 4-15(a). The number of slack cables at each instant of time is plotted in Figure 4-15(b). The energy balance and the error are shown in Figures 4-15(c) and 4-15(d) respectively. The largest error is seen to be smaller than 0.012.

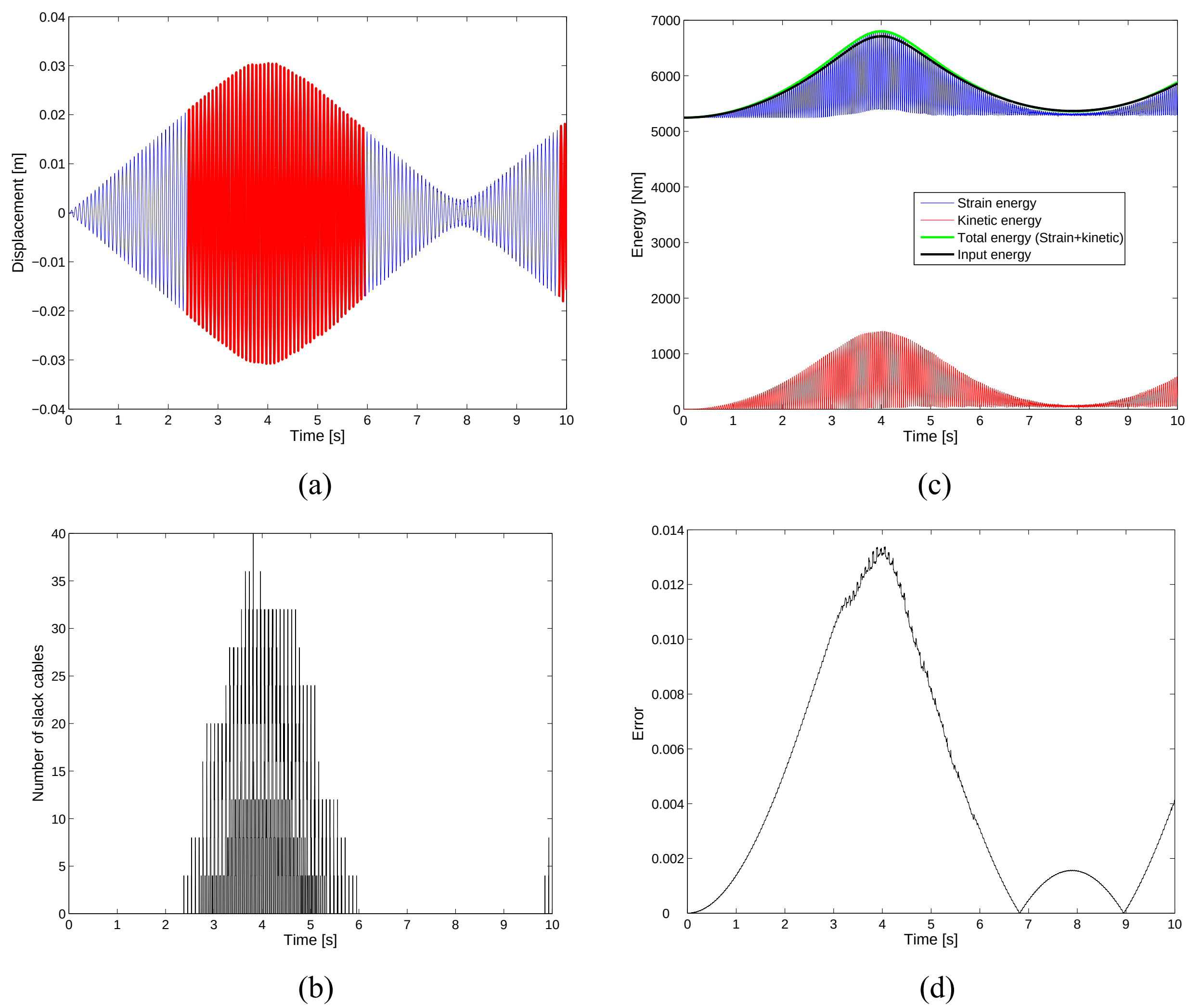


**Figure 4-16 Example 2: Forced vibration with input acceleration amplitude 0.1 g, computed using time step 0.001 s. (a) Displacement of the center node with the phase where some cables could be slack is shown in red. (b) Number of slack cables. (c) Energy balance. (d) Energy error as defined in Eq. (4-16)**

*Case 3* ($\ddot{u}_{g0} = 0.1$g): The displacement of the center node of the grid in shown in Figure 4-16(a). As in Case 2, cables start to become slack when the amplitude of this displacement is about 0.02

m, but this occurs at earlier time than in Case 2. The number of slack cables against time is shown in Figure 4.16b. The energy balance and energy are plotted in Figures 4.16c and 4.16d. The largest error in this case is smaller than 0.014. Thus excellent long-term energy balance is observed in forced vibration analysis as well.

## 4.6 Concluding remarks

An approach has been presented for the dynamic analysis of tensegrity structures. It is based on casting the computation in each time increment as a complementarity problem. Numerical examples illustrate the excellent long-term energy balance of the computed solutions. In addition, significant computational efficiency can be gained by linear algebra customizations in solving the complementarity problem. As discussed in subsection 4.2.1, due to the use of linear kinematics the above method is not applicable to tensegrity structures with internal mechanisms or where geometric stiffness is significant compared to material stiffness. A large displacement formulation based on complementarity is a topic of current work.

# SECTION 5
# CONCLUSION

## 5.1 Summary

In the first part of the report, the 3D finite deformation beam model developed by Simo has been re-examined and appropriately modified to derive a finite element formulation for the static and dynamic analysis of flexible cables. A linear viscoelastic constitutive equation and an additional mass proportional damping mechanism are introduced to account for energy dissipation. Numerical examples are presented, and energy balance calculations demonstrate the accuracy of the computed solutions. The beam model developed has been then used to describe the behavior of an electrical conductor tested at the Structural Engineering and Earthquake Simulation Laboratory (SEESL) at the University at Buffalo. Some preliminary results of the simulation of free and forced vibration tests have been presented. These reveal an amplitude dependence of both stiffness and damping, clearly pointing out the presence of material nonlinearity in the cable. This material nonlinearity, generally attributed to the fact that the bending stiffness of stranded cables varies with curvature, tension and deformation history, is not considered in the present beam model.

In the second part of the report, a novel approach has been presented for the dynamic analysis of tensegrity structures. The approach is based on casting the computations at each time increment as a complementarity problem. Numerical examples are presented to illustrate the approach. Despite the non-smooth nature of cables switching between taut and slack states, the computed solutions exhibit remarkable long-term energy balance. Furthermore, by exploiting some features of the tensegrity model, significant computational efficiency can be gained in the solution of the complementarity problem in each time increment.

## 5.2 Contributions

- The nonlinear equations of motion, and boundary conditions, of the 3D finite deformation beam model have been derived from the 3D theory of continuum mechanics, using the virtual power equation.
- Energy dissipation is included in the beam formulation in a physically consistent way. An extension of the Kelvin-Voigt damping model is introduced through the constitutive equations,

and additional mass proportional damping is modeled by appropriate modification of the equilibrium equations.

- A solution to issues concerning interpolation of total rotation vectors of magnitude greater than $\pi$ is proposed.
- Linearization of curvature is performed in a simpler fashion as compared to Simo (). An alternative approach for the update of curvatures is also proposed based on total rotation vectors, and taking advantage of special features of Lie groups and of the notion of right trivialized derivative.
- Energy plots are presented for all the numerical applications to illustrate the energy balance of the computed solutions.
- The developed 3D finite deformation beam model is used to simulate 3-dimensional dynamic tests on a real electrical conductor.
- An original approach is presented for the dynamic analysis of tensegrity structures based on casting the computations at each time increment as a Mixed Complementarity Problem (MCP).
- A Complementary Pivot Algorithm (CPA) is proposed, as an alternative to the general purpose solver PATH, for solving the MCP. Taking advantage of special properties of the tensegrity structure, it is shown that computational efficiency can be gained by using the CPA.

## 5.3 Future work

The 3D finite deformation beam model developed in the present work has proved to be totally satisfactory in accounting for the geometric nonlinearity of flexible cables. However, numerical simulations of dynamic tests performed at the University at Buffalo show that stranded cables can exhibit some kind of material nonlinearity related to their internal structure. Recent work in the literature reveals that material nonlineartity of stranded cables is not easy to handle. The objective of future work is to develop a physical model that can account for the amplitude dependence of bending stiffness and energy dissipation capacity, as well as for torsion-axial force interaction. Further analyses and experiments will be carried out to better understand what aspects of cable dynamics contribute to interaction between interconnected equipment.

With reference to the tensegrity structures, future work consists of extending the current MCP approach to the large displacement regime.

# SECTION 6
# REFERENCES


ABAQUS 6.13 [Computer software], (2013), Dassault Systèmes, Waltham, MA.

Acary, V., Brogliato, B., (2008), Numerical methods for nonsmooth dynamical systems: applications in mechanics and electronics, Springer, Berlin.

Aldrich, J. B., Skelton, R. E., Kreutz-Delgado, K., (2003), Control synthesis for a class of light and agile robotic tensegrity structures, Proceedings of the 2003 American Control Conference, IEEE, Piscataway, NJ, USA, 5245-5251.

Antman, S. S., (1974), Kirchhoff's problem for nonlinearly elastic rods, *Quarterly Journal of Applied Mathematics*, 32, 221-240.

Antman, S. S., (1996), Dynamical Problems for Geometrically Exact Theories of Nonlinearly Viscoelastic Rods, *Journal of Nonlinear Science*, 6,1-18.

Antman, S. S., (2003), Invariant Dissipative Mechanisms for the Spatial Motion of Rods Suggested by Artificial Viscosity, *Journal of Elasticity*, 70, 55-64.

Auricchio, F., Carotenuto, P., Reali, A., (2008), On the geometrically exact beam model: A consistent, effective and simple derivation from three-dimensional finite-elasticity, *International Journal of Solids and Structures*, 45, 4766-4781.

Boyer, F., De Nayer, G., Leroyer, A., Visonneau M., (2011), Geometrically Exact Kirchhoff Beam Theory: Application to Cable Dynamics, *Journal of Computational and Nonlinear Dynamics*, 6, 041004 (14 pages).

Calladine, C. R., (1978), Buckminster Fuller's `Tensegrity' structures and Clerk Maxwell's rules for the construction of stiff frames, *International Journal of Solids and Structures*, 14 (2), 161-172.

Chandran P., (2012), Experimental and numerical studies on the seismic response of flexible conductors with vertical drops, *Master of Science Project Report*: University at Buffalo, NY.

Chopra, A. K., (2007), Dynamics of structures: theory and applications to earthquake engineering, Prentice Hall, Upper Saddle River, N.J.

Costello, G. A., (1997), *Theory of Wire Rope*, Springer, New York.

Cottle, R., Pang, J. S., Stone, R. E., (1992), The linear complementarity problem, Academic Press, Boston.

Crisfield, M. A., Jelenic, G., (1999), Objectivity of strain measures in the geometrically exact three-dimensional beam theory and its finite-element implementation. *Proceedings of the Royal Society of London A*, 455, 1125-1147.

Dastous, J. B., Pierre, J. R., (1996), Experimental investigation on the dynamic behavior of flexible conductors, *IEEE Transactions on Power Delivery*, 11, 801-807.

Dastous, J. B., (2005), Nonlinear finite-element analysis of stranded conductors with variable bending stiffness using the tangent stiffness method, *IEEE Transactions on Power Delivery*, 20, 328-337.

Dastous, J. B., Der Kiureghian, A., (2010), PEER 2010/04 - Application Guide for the Design of Flexible and Rigid Bus Connections between Substation Equipment Subjected to Earthquakes.

Dirkse, S. P., Ferris, M. C., (1995), The PATH solver: A non-monotone stabilization scheme for mixed complementarity problems, Optimization Methods and Software, 5, 123-156.

EPRI, (1998), The 1986 North Palm Springs Earthquake: Effects on Power Facilities. EPRI report NP-5607.

Fetecau, R. C., Marsden, J. E., Ortiz, M., West, M., (2003), Nonsmooth lagrangian mechanics and variational collision integrators, SIAM Journal on Applied Dynamical Systems, 2, 381-416.

Filiatrault, A., Stearns, C., (2004), Seismic Response of Electrical Substation Equipment Interconnected by Flexible Conductors, *Journal of Structural Engineering*, 130, 769-778.

Filiatrault, A., Stearns, C., (2005), Flexural properties of flexural conductors interconnecting electrical substation equipment, *Journal of Structural Engineering*, 131, 151-159.

Ghalibafian, H., Ventura, C. E., Bhuyan, G. S., (2005), Seismic Interaction between Flexible Conductors and Electrical Substation Equipment, *Journal of Structural Engineering*, 131, 231-239.

Hong, K. J., DerKiureghian, A., Sackman, J. L., (2001), Seismic interaction in cable connected equipment items, *Journal of Engineering Mechanics*, 127,1096-1105.

Hong, K. J., DerKiureghian, A., Sackman, J. L., (2005), Bending behavior of helically wrapped cables, *Journal of Engineering Mechanics* (ASCE), 131, 500-511; Discussion and Closure, 132, 790-792.

Ibrahimbegovic, A., Frey, F., Kozar, I., (1995), Computationals aspects of vector-like parametrization of three-dimensional finite rotations, *International Journal for Numerical Methods in Engineering*, 38, 3653-3673.

Ibrahimbegovic, A., Mikdad, M. A., (1998), Finite rotations in dynamics of beams and implicit time-stepping schemes, *International Journal for Numerical Methods in Engineering*, 41, 781-814.

IEEE (2005), IEEE recommended practice for seismic design of substations, IEEE 693-2005.

IEEE (2006), Recommended practice for the design of flexible buswork located in seismically active areas, IEEE 1527-2006, Piscataway, NJ.

Ingber, D. E., (1998), The architecture of life, *Scientific American*, 278(1), 48-57.

Irvine, H., M., (1981), *Cable Structures*, MIT Press: Cambridge, Massachusetts.

Jelenic, G., Crisfield, M. A., (1998), Interpolation of rotation variables in nonlinear dynamics of 3D beams, *International Journal for Numerical Methods in Engineering*, 43(7), 1193-1222.

Jelenic, G., Crisfield, M. A., (1999), Geometrically exact 3D beam theory: implementation of a strain-invariant finite element for statics and dynamics. *Computer Methods in Applied Mechanics and Engineering*, 171, 141-171.

Juan, S. H., Tur, J. M. M., (2008), Tensegrity frameworks: Static analysis review, Mechanism and Machine Theory, 43(7), 859-881.

Juan, S. H., Skelton, R. E., Tur, J. M. M., (2009), Dynamically stable collision avoidance for tensegrity based robots, Proceedings of the 2009 ASME/IFToMM International Conference on Reconfigurable Mechanisms and Robots, ReMAR 2009, IEEE Computer Society, London, United Kingdom, 315-322.

K-Assist 1.7., (2003), Krypton Electronic Engineering n.v. Leuven, Belgium. Available from: http:// seesl.buffalo.edu/training/krypton/K-Assist_manual_EN.PDF (accessed June 2, 2014)

Lang, H., Linn,J., Arnold, M., (2011), Multi-body dynamics simulation of geometrically exact Cosserat rods, *Multibody System Dynamics*, 25(3), 285–312.

Linn, J., Lang, H., Tuganov, A., (2013), Geometrically exact Cosserat rods with Kelvin-Voigt type viscous damping, *Mechanical Sciences*, 4, 79 –96.

Love, A. E. H., (1944), *A Treatise on the Mathematical Theory of Elasticity*, Dover: New York.

Maier, G., (1970), A matrix structural theory of piecewise linear elastoplasticity with interacting yield planes, *Meccanica*, 5(1), 54-66.

Mata, P., Oller, S., Barbat, A. H., (2007), Static analysis of beam structures under nonlinear geometric and constitutive behavior, *Computer Methods in Applied Mechanics and Engineering*, 196, 4458-4478.

Munson, T. S., (2000), Algorithms and environments for complementarity, Ph.D. thesis, University of Wisconsin-Madison.

Nineb, S., Alart, P., Dureisseix, D., (2007), Domain decomposition approach for non-smooth discrete problems, example of a tensegrity structure, *Computers & Structures*, 85(9), 499-511.

Okada, T., Misaki, T., Hashimoto, Y., Momotari, T., Saito, K., Ito, N., Takahashi, Y., (1986), Seismic design of connecting leads in open-air type substations, Report 23-04, CIGRE.

Oliveto, N. D., Sivaselvan, M. V., (2011), Dynamic analysis of tensegrity structures using a complementarity framework, *Computers and Structures*, 89(23-24), 2471-2483.

Oliveto, N. D., Sivaselvan, M. V., (2014), Nonlinear finite element analysis of three-dimensional free and harmonically forced vibrations of stranded conductor cables, *Earthquake Engineering and Structural Dynamics*, 43, 2199-2216.

Oliveto, N. D., Sivaselvan, M. V., (2015), 3D finite-deformation beam model with viscous damping: computational aspects and applications, *Journal of Engineering Mechanics* (ASCE), 141(1), 04014103.

Ortolan, G., (2011), Topics on geometric integration, PhD thesis, Universita' Degli Studi di Padova, Italy.

Papailiou, K. O., (1995), Die seilbiegung mit einer durch die innereseibung, dir zugkraft und die seilkrümmung veränderlichen biegesteifigkeit, PhD Thesis No. 11057, Swiss Federal Institute of Technology (ETH), Zurich, Switzerland.

Papailiou, K. O., (1997), On the bending stiffness of transmission line conductors. *IEEE Transactions on Power Delivery*, 12, 1576-1588.

Pellegrino, S., Calladine, C. R., (1986), Matrix analysis of statically and kinematically indeterminate frameworks, *International Journal of Solids and Structures*, 22(4), 409-428.

Petrone C., Oliveto, N. D., Sivaselvan, M. V., (2015), Dynamic analysis of mooring cables with application to floating offshore wind turbines, *Journal of Engineering Mechanics* (ASCE), 142(3), 04015101.

Pierre, J. R., (1991) First experience concerning the seismic behavior of an electric power system in Eastern North America. Proceedings of the 3rd U.S. conference on Lifeline Earthquake Engineering; pp. 266-274.

Quirant, J., Kazi-Aoual, M. N., Motro, R., (2003), Designing tensegrity systems: the case of a double layer grid, *Engineering Structures*, 25(9), 1121-1130.

Reissner, E., (1972), On one-dimensional finite strain beam theory: The plane problem, *Journal of Applied Mathematics and Physics*, 23, 795-804.

Richter, H. L., (1988), Postquake lessons for power utilities, *IEEE Spectrum*, 25, 46-48.

Rieffel, J., Valero-Cuevas, F., Lipson, H., (2009), Automated discovery and optimization of large irregular tensegrity structures, *Computers & Structures*, 87(5-6), 368-379.

Shibata, M., Saijyo, F., Hirai, S., (2009), Crawling by body deformation of tensegrity structure robots, 2009 IEEE International Conference on Robotics and Automation (ICRA), IEEE, Piscataway, NJ, USA, 4375-4380.

Simo, J. C., (1985), A finite strain beam formulation. The three-dimensional dynamic problem. Part I, *Computer Methods in Applied Mechanics and Engineering*, 49, 55-70.

Simo, J. C., Vu-Quoc, L., (1986), A three-dimensional finite-strain rod model. Part II: computational aspects, *Computer Methods in Applied Mechanics and Engineering*, 58, 79-116.

Simo, J. C., Vu-Quoc, L., (1988), On the dynamics in space of rods undergoing large motions-a geometrically exact approach, *Computer Methods in Applied Mechanics and Engineering*, 66, 125-161.

Simo, J., C., Vu-Quoc, L., (1991), A geometrically-exact rod model incorporating shear and torsion-warping deformation, *International Journal of Solids and Structures*, 27, 371-393.

Sivaselvan, M. V., Reinhorn, A. M., (2006), Lagrangian approach to structural collapse simulation, *Journal of Engineering Mechanics-ASCE*, 132(8), 795-805.

Sivaselvan, M. V., Lavan, O., Dargush, G. F., Kurino, H., Hyodo, Y., Fukuda, R., Sato, K., Apostolakis, G., Reinhorn, A. M., (2009), Numerical collapse simulation of large-scale structural systems using an optimization based algorithm, *Earthquake Engineering & Structural Dynamics*, 38(5), 655-677.

Sivaselvan, M. V., (2010), Complementarity framework for nonlinear dynamic analysis of skeletal structures with softening plastic hinges, *International Journal for Numerical Methods in Engineering* 86(2), 182-223.

Skelton, R. E., de Oliveira, M. C., (2009), Tensegrity systems, Springer, Dordrecht, New York.

Spurrier, R. A., (1978), Comment on "Singularity-Free Extraction of a Quaternion from a Direction-Cosine Matrix", *Journal of Spacecraft and Rockets*, 15, 255.

Stamenovic, N., Wang, E., Ingber, D., Cellular tensegrity models and cell-substrate interactions, in: M. R. King (Ed.), *Principles of Cellular Engineering*, Academic Press, 81-104.

Sultan, C., Corless, M., Skelton, R. E., (1999), Peak to peak control of an adaptive tensegrity space telescope, Proceedings of the SPIE - The International Society for Optical Engineering, 3667, 190-201.

Sultan, C., Corless, M., Skelton, R. E., (2000), Tensegrity flight simulator, *Journal of Guidance, Control, and Dynamics*, 23(6), 1055-1064.

Sultan, C., (2009), Tensegrity: 60 years of art, science, and engineering, in: H. Aref, E. v. d. Giessen (Eds.), *Advances in Applied Mechanics*, 43, 69-145.

Taylor, R., L., (2001), FEAP Version 7.4 User Manual 2001. Berkeley, CA: Department of Civil and Environmental Engineering, University of California at Berkeley.

Tibert, A. G., Pellegrino, S., (2002), Deployable tensegrity reflectors for small satellites, *Journal of Spacecraft and Rockets*, 39(5), 701-709.

Tibert, A. G., Pellegrino, S., (2003), Review of form-finding methods for tensegrity structures, *International Journal of Space Structures*, 18(4), 209-223.

Tur, J. M. M., Juan, S. H., (2009), Tensegrity frameworks: Dynamic analysis review and open problems, *Mechanism and Machine Theory*, 44(1), 1-18.

Vernerey, F. J, Moran, B., (2010), Nonlinear, Large Deformation Finite-Element Beam/Column Formulation for the Study of the Human Spine: Investigation of the Role of Muscle on Spine Stability. *Journal of Engineering Mechanics* (ASCE), 136, 1319-1328.

Yaozhi, L., Xian, X., Lele, T., Kumar, S., Ingber, D. E., (2008), A multi-modular tensegrity model of an acting stress fiber, *Journal of Biomechanics*, 41(11), 2379-2387.

L. Zhang, B. Maurin, R. Motro, Form-finding of nonregular tensegrity systems, *Journal of Structural Engineering*, 132(9), 1435-1440.

# APPENDIX A

## A.1 External Power

*Boundary terms.* The first term on the left hand side of (2-11) may be decomposed as:

$$\iint_{\partial R_0} (\mathbf{P}\cdot\mathbf{N})\cdot\bar{\dot{\mathbf{x}}}\,dA = -\iint_{A_0}(\mathbf{P}\cdot\mathbf{E}_3)\cdot\bar{\dot{\mathbf{x}}}\,dA + \iint_{A_L}(\mathbf{P}\cdot\mathbf{E}_3)\cdot\bar{\dot{\mathbf{x}}}\,dA + \iint_{S_L}(\mathbf{P}\cdot\mathbf{N})\cdot\bar{\dot{\mathbf{x}}}\,dA = \\ -\iint_{A_0}\mathbf{P}_3\cdot\bar{\dot{\mathbf{x}}}\,dA + \iint_{A_L}\mathbf{P}_3\cdot\bar{\dot{\mathbf{x}}}\,dA + \iint_{S_L}(\mathbf{P}\cdot\mathbf{N})\cdot\bar{\dot{\mathbf{x}}}\,dA \tag{A-1}$$

where $A_0$ and $A_L$ are the areas of the cross section of the beam at $S$=0 and $S$=$L$, while $S_L$ is the lateral surface of the beam. The first term on the right hand side of (A-1) may be written as follows:

$$\iint_{A_0}\mathbf{P}_3\cdot\bar{\dot{\mathbf{x}}}\,dA = \iint_{A_0}\mathbf{P}_3\cdot\bar{\dot{\mathbf{x}}}_0\,dA + \iint_{A_0}\mathbf{P}_3\cdot\left(\bar{\dot{\mathbf{x}}}-\bar{\dot{\mathbf{x}}}_0\right)dA \tag{A-2}$$

Using (2-15) and (2-24), we can write:

$$\bar{\dot{\mathbf{x}}}-\bar{\dot{\mathbf{x}}}_0 = X_\alpha\frac{\partial\mathbf{t}_\alpha}{\partial t} = X_\alpha\bar{\mathbf{w}}\times\mathbf{t}_\alpha = \bar{\mathbf{w}}\times X_\alpha\mathbf{t}_\alpha = \bar{\mathbf{w}}\times(\mathbf{x}-\mathbf{x}_0) \tag{A-3}$$

Therefore, (A-2) may be written as:

$$\iint_{A_0}\mathbf{P}_3\cdot\bar{\dot{\mathbf{x}}}\,dA = \iint_{A_0}\mathbf{P}_3\cdot\bar{\dot{\mathbf{x}}}_0\,dA + \iint_{A_0}\mathbf{P}_3\cdot\bar{\mathbf{w}}\times(\mathbf{x}-\mathbf{x}_0)\,dA \tag{A-4}$$

Noting that $\bar{\dot{\mathbf{x}}}_0$ and $\bar{\mathbf{w}}$ do not depend on $X_\alpha$, and using the permutation rule of the mixed product of three vectors, (A-4) becomes:

$$\iint_{A_0}\mathbf{P}_3\cdot\bar{\dot{\mathbf{x}}}\,dA = \bar{\dot{\mathbf{x}}}_0(0,t)\cdot\iint_{A_0}\mathbf{P}_3\,dA + \bar{\mathbf{w}}(0,t)\cdot\iint_{A_0}(\mathbf{x}-\mathbf{x}_0)\times\mathbf{P}_3 dA = \\ \mathbf{n}(0,t)\cdot\bar{\dot{\mathbf{x}}}_0(0,t) + \mathbf{m}(0,t)\cdot\bar{\mathbf{w}}(0,t) \tag{A-5}$$

where $\mathbf{n}(0,t)$ and $\mathbf{m}(0,t)$ are the resultant force and moment acting on the cross section at $S$=0:

$$\mathbf{n}(0,t) = \iint_{A_0}\mathbf{P}_3\,dA \tag{A-6}$$

$$\mathbf{m}(0,t) = \iint_{A_0}(\mathbf{x}-\mathbf{x}_0)\times\mathbf{P}_3\,dA \tag{A-7}$$

In the same way, the second term on the right hand side of (A-1) may be written as:

$$\iint_{A_L}\mathbf{P}_3\cdot\bar{\dot{\mathbf{x}}}\,dA = \mathbf{n}(L,t)\cdot\bar{\dot{\mathbf{x}}}_0(L,t) + \mathbf{m}(L,t)\cdot\bar{\mathbf{w}}(L,t) \tag{A-8}$$

where $\mathbf{n}(L,t)$ and $\mathbf{m}(L,t)$ are the resultant force and moment acting on the cross section at $S$=$L$:

$$\mathbf{n}(L,t) = \iint_{A_L}\mathbf{P}_3\,dA \tag{A-9}$$

$$\mathbf{m}(L,t) = \iint_{A_L}(\mathbf{x}-\mathbf{x}_0)\times\mathbf{P}_3\,dA \tag{A-10}$$

The last term on the right hand side of (A-1) may be written as:

$$\iint_{S_L} (\mathbf{P}\cdot\mathbf{N})\cdot\dot{\bar{\mathbf{x}}}\,dA = \iint_{S_L} (\mathbf{P}\cdot\mathbf{N})\cdot\dot{\bar{\mathbf{x}}}_0\,dA + \iint_{S_L} (\mathbf{P}\cdot\mathbf{N})\cdot\left(\dot{\bar{\mathbf{x}}}-\dot{\bar{\mathbf{x}}}_0\right)dA \tag{A-11}$$

and the first term on the right hand side of (A-11) can be written as:

$$\iint_{S_L} (\mathbf{P}\cdot\mathbf{N})\cdot\dot{\bar{\mathbf{x}}}_0\,dA = \int_0^L \left(\oint_\Gamma (\mathbf{P}\cdot\mathbf{N})\,d\Gamma\right)\cdot\dot{\bar{\mathbf{x}}}_0\,dS \tag{A-12}$$

where $\Gamma$ is the boundary of the cross section in the reference configuration. Using (A-3), and the permutation rule of the mixed product of three vectors, the second term on the right hand side of (A-11) becomes:

$$\begin{aligned}&\iint_{S_L} (\mathbf{P}\cdot\mathbf{N})\cdot\left(\dot{\bar{\mathbf{x}}}-\dot{\bar{\mathbf{x}}}_0\right)dA = \iint_{S_L} (\mathbf{P}\cdot\mathbf{N})\cdot\bar{\mathbf{w}}\times(\mathbf{x}-\mathbf{x}_0)\,dA = \\ &\int_0^L \bar{\mathbf{w}}\cdot\left(\oint_\Gamma (\mathbf{x}-\mathbf{x}_0)\times(\mathbf{P}\cdot\mathbf{N})\,d\Gamma\right)dS = \int_0^L \left(\oint_\Gamma (\mathbf{x}-\mathbf{x}_0)\times(\mathbf{P}\cdot\mathbf{N})\,d\Gamma\right)\cdot\bar{\mathbf{w}}\,dS\end{aligned} \tag{A-13}$$

By means of these results, (A-1) may be finally written as:

$$\begin{aligned}&\iint_{\partial R_0} (\mathbf{P}\cdot\mathbf{N})\cdot\dot{\bar{\mathbf{x}}}\,dA = -\mathbf{n}(0,t)\cdot\dot{\bar{\mathbf{x}}}_0(0,t) - \mathbf{m}(0,t)\cdot\bar{\mathbf{w}}(0,t) + \mathbf{n}(L,t)\cdot\dot{\bar{\mathbf{x}}}_0(L,t) + \\ &\mathbf{m}(L,t)\cdot\bar{\mathbf{w}}(L,t) + \int_0^L \left(\oint_\Gamma (\mathbf{P}\cdot\mathbf{N})\,d\Gamma\right)\cdot\dot{\bar{\mathbf{x}}}_0\,dS + \int_0^L \left(\oint_\Gamma (\mathbf{x}-\mathbf{x}_0)\times(\mathbf{P}\cdot\mathbf{N})\,d\Gamma\right)\cdot\bar{\mathbf{w}}\,dS\end{aligned} \tag{A-14}$$

*Body forces.* We write the term of (2-11) related to the body forces as follows:

$$\iiint_{R_0} \rho_0\mathbf{B}\cdot\dot{\bar{\mathbf{x}}}\,dV = \iiint_{R_0} \rho_0\mathbf{B}\cdot\dot{\bar{\mathbf{x}}}_0\,dV + \iiint_{R_0} \rho_0\mathbf{B}\cdot\left(\dot{\bar{\mathbf{x}}}-\dot{\bar{\mathbf{x}}}_0\right)dV \tag{A-15}$$

The first term on the right hand side of (A-15) may be expressed as:

$$\iiint_{R_0} \rho_0\mathbf{B}\cdot\dot{\bar{\mathbf{x}}}_0\,dV = \int_0^L \left(\iint_A \rho_0\mathbf{B}\,dA\right)\cdot\dot{\bar{\mathbf{x}}}_0\,dS \tag{A-16}$$

Using (A-3), and the permutation rule of the mixed product of three vectors, the second term of (A-15) may be written as:

$$\begin{aligned}&\iiint_{R_0} \rho_0\mathbf{B}\cdot\left(\dot{\bar{\mathbf{x}}}-\dot{\bar{\mathbf{x}}}_0\right)dV = \iiint_{R_0} \rho_0\mathbf{B}\cdot\bar{\mathbf{w}}\times(\mathbf{x}-\mathbf{x}_0)\,dV = \\ &\int_0^L \left(\iint_A (\mathbf{x}-\mathbf{x}_0)\times\rho_0\mathbf{B}\,dA\right)\cdot\bar{\mathbf{w}}\,dS\end{aligned} \tag{A-17}$$

Finally, (A-15) becomes:

$$\iiint_{R_0} \rho_0\mathbf{B}\cdot\dot{\bar{\mathbf{x}}}\,dV = \int_0^L \left(\iint_A \rho_0\mathbf{B}\,dA\right)\cdot\dot{\bar{\mathbf{x}}}_0\,dS + \int_0^L \left(\iint_A (\mathbf{x}-\mathbf{x}_0)\times\rho_0\mathbf{B}\,dA\right)\cdot\bar{\mathbf{w}}\,dS \tag{A-18}$$

*Inertia forces.* To evaluate the term on the left hand side of (2-11) related to the inertia forces, we first carry out the product $\ddot{\mathbf{x}} \cdot \dot{\mathbf{x}}$. This can be written as:

$$\begin{aligned}
&\ddot{\mathbf{x}} \cdot \bar{\dot{\mathbf{x}}} = \left[\ddot{\mathbf{x}}_0 + \left(\ddot{\mathbf{x}} - \ddot{\mathbf{x}}_0\right)\right] \cdot \left[\bar{\dot{\mathbf{x}}}_0 + \left(\bar{\dot{\mathbf{x}}} - \bar{\dot{\mathbf{x}}}_0\right)\right] = \\
&\ddot{\mathbf{x}}_0 \cdot \bar{\dot{\mathbf{x}}}_0 + \ddot{\mathbf{x}}_0 \cdot \left(\bar{\dot{\mathbf{x}}} - \bar{\dot{\mathbf{x}}}_0\right) + \left(\ddot{\mathbf{x}} - \ddot{\mathbf{x}}_0\right) \cdot \bar{\dot{\mathbf{x}}}_0 + \left(\ddot{\mathbf{x}} - \ddot{\mathbf{x}}_0\right) \cdot \left(\bar{\dot{\mathbf{x}}} - \bar{\dot{\mathbf{x}}}_0\right)
\end{aligned} \tag{A-19}$$

Using (A-3), we can write (A-19) as:

$$\ddot{\mathbf{x}} \cdot \bar{\dot{\mathbf{x}}} = \ddot{\mathbf{x}}_0 \cdot \bar{\dot{\mathbf{x}}}_0 + \ddot{\mathbf{x}}_0 \cdot \bar{\mathbf{w}} \times \left(\mathbf{x} - \mathbf{x}_0\right) + \left(\ddot{\mathbf{x}} - \ddot{\mathbf{x}}_0\right) \cdot \bar{\dot{\mathbf{x}}}_0 + \left(\ddot{\mathbf{x}} - \ddot{\mathbf{x}}_0\right) \cdot \bar{\mathbf{w}} \times \left(\mathbf{x} - \mathbf{x}_0\right) \tag{A-20}$$

From (A-3), $\ddot{\mathbf{x}} - \ddot{\mathbf{x}}_0$ is easily evaluated as:

$$\ddot{\mathbf{x}} - \ddot{\mathbf{x}}_0 = \dot{\mathbf{w}} \times \left(\mathbf{x} - \mathbf{x}_0\right) + \mathbf{w} \times \left(\dot{\mathbf{x}} - \dot{\mathbf{x}}_0\right) = \dot{\mathbf{w}} \times \left(\mathbf{x} - \mathbf{x}_0\right) + \mathbf{w} \times \left[\mathbf{w} \times \left(\mathbf{x} - \mathbf{x}_0\right)\right] \tag{A-21}$$

Substituting (A-21) into (A-20), we get:

$$\begin{aligned}
&\ddot{\mathbf{x}} \cdot \dot{\mathbf{x}} = \ddot{\mathbf{x}}_0 \cdot \bar{\dot{\mathbf{x}}}_0 + \ddot{\mathbf{x}}_0 \cdot \bar{\mathbf{w}} \times \left(\mathbf{x} - \mathbf{x}_0\right) + \left\{\dot{\mathbf{w}} \times \left(\mathbf{x} - \mathbf{x}_0\right) + \mathbf{w} \times \left[\mathbf{w} \times \left(\mathbf{x} - \mathbf{x}_0\right)\right]\right\} \cdot \bar{\dot{\mathbf{x}}}_0 + \\
&\left\{\dot{\mathbf{w}} \times \left(\mathbf{x} - \mathbf{x}_0\right) + \mathbf{w} \times \left[\mathbf{w} \times \left(\mathbf{x} - \mathbf{x}_0\right)\right]\right\} \cdot \bar{\mathbf{w}} \times \left(\mathbf{x} - \mathbf{x}_0\right)
\end{aligned} \tag{A-22}$$

We can now write the term related to the inertia forces as follows:

$$\begin{aligned}
\iiint_{R_0} \rho_0 \ddot{\mathbf{x}} \cdot \bar{\dot{\mathbf{x}}}\, dV = &\iiint_{R_0} \rho_0 \ddot{\mathbf{x}}_0 \cdot \bar{\dot{\mathbf{x}}}_0\, dV + \iiint_{R_0} \rho_0 \ddot{\mathbf{x}}_0 \cdot \bar{\mathbf{w}} \times \left(\mathbf{x} - \mathbf{x}_0\right) dV + \\
&\iiint_{R_0} \rho_0 \left\{\dot{\mathbf{w}} \times \left(\mathbf{x} - \mathbf{x}_0\right) + \mathbf{w} \times \left[\mathbf{w} \times \left(\mathbf{x} - \mathbf{x}_0\right)\right]\right\} \cdot \bar{\dot{\mathbf{x}}}_0\, dV + \\
&\iiint_{R_0} \rho_0 \left\{\dot{\mathbf{w}} \times \left(\mathbf{x} - \mathbf{x}_0\right) + \mathbf{w} \times \left[\mathbf{w} \times \left(\mathbf{x} - \mathbf{x}_0\right)\right]\right\} \cdot \bar{\mathbf{w}} \times \left(\mathbf{x} - \mathbf{x}_0\right) dV
\end{aligned} \tag{A-23}$$

The first integral on the right hand side of (A-23) is evaluated as follows:

$$I_1 = \iiint_{R_0} \rho_0 \ddot{\mathbf{x}}_0 \cdot \bar{\dot{\mathbf{x}}}_0\, dV = \int_0^L \left(\iint_A \rho_0 dA\right) \ddot{\mathbf{x}}_0 \cdot \bar{\dot{\mathbf{x}}}_0\, dS = \int_0^L A_\rho \ddot{\mathbf{x}}_0 \cdot \bar{\dot{\mathbf{x}}}_0\, dS \tag{A-24}$$

where $A_\rho = \iint_A \rho_0 dA$ is the mass per unit length of the beam. Next we show that under certain conditions, the second and third integrals are both equal to zero. In fact, if the moving frame is placed in the centroid of the cross section of the beam, the first moment of area $\iint_{A_0} \left(\mathbf{x} - \mathbf{x}_0\right) \rho_0 dA$ is equal to zero, and therefore:

$$I_2 = \iiint_{R_0} \rho_0 \ddot{\mathbf{x}}_0 \cdot \bar{\mathbf{w}} \times \left(\mathbf{x} - \mathbf{x}_0\right) dV = \int_0^L \ddot{\mathbf{x}}_0 \cdot \bar{\mathbf{w}} \times \iint_{A_0} \left(\mathbf{x} - \mathbf{x}_0\right) \rho_0 dA = 0 \tag{A-25}$$

The third integral on the right hand side of (A-23) may be decomposed into the following two integrals:

$$I_3 = \iiint_{R_0} \rho_0 \left\{ \dot{\mathbf{w}} \times (\mathbf{x} - \mathbf{x}_0) + \mathbf{w} \times \left[ \mathbf{w} \times (\mathbf{x} - \mathbf{x}_0) \right] \right\} \cdot \bar{\dot{\mathbf{x}}}_0 \, dV = \iiint_{R_0} \rho_0 \left\{ \dot{\mathbf{w}} \times (\mathbf{x} - \mathbf{x}_0) \right\} \cdot \bar{\dot{\mathbf{x}}}_0 \, dV + \iiint_{R_0} \rho_0 \left\{ \mathbf{w} \times \left[ \mathbf{w} \times (\mathbf{x} - \mathbf{x}_0) \right] \right\} \cdot \bar{\dot{\mathbf{x}}}_0 \, dV = I_{31} + I_{32} \tag{A-26}$$

It is easy to see that both integrals in (A-26) are equal to zero:

$$I_{31} = \iiint_{R_0} \rho_0 \left\{ \dot{\mathbf{w}} \times (\mathbf{x} - \mathbf{x}_0) \right\} \cdot \bar{\dot{\mathbf{x}}}_0 \, dV = \int_0^L \dot{\mathbf{w}} \times \left( \iint_{A_0} (\mathbf{x} - \mathbf{x}_0) \rho_0 dA \right) \cdot \bar{\dot{\mathbf{x}}}_0 \, dS = 0 \tag{A-27}$$

$$I_{32} = \iiint_{R_0} \rho_0 \left\{ \mathbf{w} \times \left[ \mathbf{w} \times (\mathbf{x} - \mathbf{x}_0) \right] \right\} \cdot \bar{\dot{\mathbf{x}}}_0 \, dV = \int_0^L \mathbf{w} \times \mathbf{w} \times \left( \iint_{A_0} (\mathbf{x} - \mathbf{x}_0) \rho_0 dA \right) \cdot \bar{\dot{\mathbf{x}}}_0 \, dS = 0 \tag{A-28}$$

and therefore we have:

$$I_3 = I_{31} + I_{32} = 0 \tag{A-29}$$

The fourth integral on the right hand side of (A-23) can also be decomposed into two terms as follows:

$$\begin{aligned} I_4 &= \iiint_{R_0} \rho_0 \left\{ \dot{\mathbf{w}} \times (\mathbf{x} - \mathbf{x}_0) + \mathbf{w} \times \left[ \mathbf{w} \times (\mathbf{x} - \mathbf{x}_0) \right] \right\} \cdot \bar{\mathbf{w}} \times (\mathbf{x} - \mathbf{x}_0) dV = \\ & \iiint_{R_0} \rho_0 \left\{ \dot{\mathbf{w}} \times (\mathbf{x} - \mathbf{x}_0) \right\} \cdot \bar{\mathbf{w}} \times (\mathbf{x} - \mathbf{x}_0) dV + \\ & \iiint_{R_0} \rho_0 \left\{ \mathbf{w} \times \left[ \mathbf{w} \times (\mathbf{x} - \mathbf{x}_0) \right] \right\} \cdot \bar{\mathbf{w}} \times (\mathbf{x} - \mathbf{x}_0) dV = I_{41} + I_{42} \end{aligned} \tag{A-30}$$

We first evaluate the following term:

$$\begin{aligned} & \left\{ \dot{\mathbf{w}} \times (\mathbf{x} - \mathbf{x}_0) \right\} \cdot \bar{\mathbf{w}} \times (\mathbf{x} - \mathbf{x}_0) = e_{ijk} \dot{w}_j (x - x_0)_k \, \mathbf{e}_i \cdot e_{pqr} w_q (x - x_0)_r \, \mathbf{e}_p = \\ & = e_{ijk} \dot{w}_j (x - x_0)_k \, e_{pqr} w_q (x - x_0)_r \, \delta_{ip} = e_{ijk} \varepsilon_{iqr} \dot{w}_j (x - x_0)_k \, w_q (x - x_0)_r = \\ & \dot{w}_j (x - x_0)_k \, w_q (x - x_0)_r \, \delta_{jq} \delta_{kr} - \dot{w}_j (x - x_0)_k \, w_q (x - x_0)_r \, \delta_{jr} \delta_{kq} = \\ & = \dot{w}_j w_j (x - x_0)_k (x - x_0)_k - \dot{w}_j w_k (x - x_0)_k (x - x_0)_j = \\ & = (\dot{\mathbf{w}} \cdot \bar{\mathbf{w}}) \left[ (\mathbf{x} - \mathbf{x}_0) \cdot (\mathbf{x} - \mathbf{x}_0) \right] - \left[ \dot{\mathbf{w}} \cdot (\mathbf{x} - \mathbf{x}_0) \right] \left[ \bar{\mathbf{w}} \cdot (\mathbf{x} - \mathbf{x}_0) \right] = \\ & \dot{\mathbf{w}} \cdot \left[ (\mathbf{x} - \mathbf{x}_0) \cdot (\mathbf{x} - \mathbf{x}_0) \mathbf{I} - (\mathbf{x} - \mathbf{x}_0) \otimes (\mathbf{x} - \mathbf{x}_0) \right] \cdot \bar{\mathbf{w}} \end{aligned} \tag{A-31}$$

where $e_{ijk}$ is the permutation symbol and $\mathbf{I} = \mathbf{e}_i \otimes \mathbf{e}_i$ is the identity tensor. Therefore, we can write:

$$\begin{aligned} I_{41} &= \iiint_{R_0} \rho_0 \left\{ \dot{\mathbf{w}} \times (\mathbf{x} - \mathbf{x}_0) \right\} \cdot \bar{\mathbf{w}} \times (\mathbf{x} - \mathbf{x}_0) dV = \\ & \iiint_{R_0} \rho_0 \dot{\mathbf{w}} \cdot \left[ (\mathbf{x} - \mathbf{x}_0) \cdot (\mathbf{x} - \mathbf{x}_0) \mathbf{I} - (\mathbf{x} - \mathbf{x}_0) \otimes (\mathbf{x} - \mathbf{x}_0) \right] \cdot \bar{\mathbf{w}} \, dV = \\ & \int_0^L \dot{\mathbf{w}} \cdot \iint_{A_0} \rho_0 \left[ (\mathbf{x} - \mathbf{x}_0) \cdot (\mathbf{x} - \mathbf{x}_0) \mathbf{I} - (\mathbf{x} - \mathbf{x}_0) \otimes (\mathbf{x} - \mathbf{x}_0) \right] dA \cdot \bar{\mathbf{w}} dS = \\ & \int_0^L \dot{\mathbf{w}} \cdot \mathbf{I}_\rho \cdot \bar{\mathbf{w}} \, dS \end{aligned} \tag{A-32}$$

where $\mathbf{I}_\rho = \iint_{A_0} \rho_0 \left[ (\mathbf{x}-\mathbf{x}_0)\cdot(\mathbf{x}-\mathbf{x}_0)\mathbf{I} - (\mathbf{x}-\mathbf{x}_0)\otimes(\mathbf{x}-\mathbf{x}_0) \right] dA$ is the inertia tensor. Because of the symmetry of $\mathbf{I}_\rho$, (A-32) may be written as:

$$I_{41} = \int_0^L \left( \mathbf{I}_\rho \cdot \dot{\mathbf{w}} \right) \cdot \bar{\mathbf{w}}\, dS \tag{A-33}$$

Integral $I_{42}$ may be written as:

$$\begin{gathered} I_{42} = \iiint_{R_0} \rho_0 \left\{ \mathbf{w} \times \left[ \mathbf{w} \times (\mathbf{x}-\mathbf{x}_0) \right] \right\} \cdot \bar{\mathbf{w}} \times (\mathbf{x}-\mathbf{x}_0)\, dV = \\ \iiint_{R_0} \rho_0 \bar{\mathbf{w}} \times (\mathbf{x}-\mathbf{x}_0) \cdot \left\{ \mathbf{w} \times \left[ \mathbf{w} \times (\mathbf{x}-\mathbf{x}_0) \right] \right\} dV \end{gathered} \tag{A-34}$$

Using the permutation rule of the mixed product of three vectors, (A-34) may be written as:

$$I_{42} = \iiint_{R_0} \rho_0 (\mathbf{x}-\mathbf{x}_0) \times \left\{ \mathbf{w} \times \left[ \mathbf{w} \times (\mathbf{x}-\mathbf{x}_0) \right] \right\} \cdot \bar{\mathbf{w}}\, dV \tag{A-35}$$

We first write the term $(\mathbf{x}-\mathbf{x}_0) \times \left\{ \mathbf{w} \times \left[ \mathbf{w} \times (\mathbf{x}-\mathbf{x}_0) \right] \right\}$ as:

$$(\mathbf{x}-\mathbf{x}_0) \times \left\{ \mathbf{w} \times \left[ \mathbf{w} \times (\mathbf{x}-\mathbf{x}_0) \right] \right\} = -\left\{ (\mathbf{x}-\mathbf{x}_0) \times \left[ \mathbf{w} \times (\mathbf{x}-\mathbf{x}_0) \right] \right\} \times \mathbf{w} \tag{A-36}$$

We then carry out the double cross product $(\mathbf{x}-\mathbf{x}_0) \times \left[ \mathbf{w} \times (\mathbf{x}-\mathbf{x}_0) \right]$:

$$\begin{gathered} (\mathbf{x}-\mathbf{x}_0) \times \left[ \mathbf{w} \times (\mathbf{x}-\mathbf{x}_0) \right] = \left[ (\mathbf{x}-\mathbf{x}_0)\cdot(\mathbf{x}-\mathbf{x}_0) \right] \mathbf{w} - \left[ \mathbf{w} \cdot (\mathbf{x}-\mathbf{x}_0) \right] (\mathbf{x}-\mathbf{x}_0) = \\ \mathbf{w} \cdot \left[ (\mathbf{x}-\mathbf{x}_0)\cdot(\mathbf{x}-\mathbf{x}_0)\mathbf{I} - (\mathbf{x}-\mathbf{x}_0)\otimes(\mathbf{x}-\mathbf{x}_0) \right] \end{gathered} \tag{A-37}$$

Then, Eq. (A-36) may be written as:

$$\begin{gathered} (\mathbf{x}-\mathbf{x}_0) \times \left\{ \mathbf{w} \times \left[ \mathbf{w} \times (\mathbf{x}-\mathbf{x}_0) \right] \right\} = -\left\{ (\mathbf{x}-\mathbf{x}_0) \times \left[ \mathbf{w} \times (\mathbf{x}-\mathbf{x}_0) \right] \right\} \times \mathbf{w} = \\ -\left\{ \mathbf{w} \cdot \left[ (\mathbf{x}-\mathbf{x}_0)\cdot(\mathbf{x}-\mathbf{x}_0)\mathbf{I} - (\mathbf{x}-\mathbf{x}_0)\otimes(\mathbf{x}-\mathbf{x}_0) \right] \right\} \times \mathbf{w} \end{gathered} \tag{A-38}$$

Substituting (A-38) into (A-35) gives:

$$\begin{gathered} I_{42} = -\iiint_{R_0} \left\{ \mathbf{w} \cdot \rho_0 \left[ (\mathbf{x}-\mathbf{x}_0)\cdot(\mathbf{x}-\mathbf{x}_0)\mathbf{I} - (\mathbf{x}-\mathbf{x}_0)\otimes(\mathbf{x}-\mathbf{x}_0) \right] \times \mathbf{w} \right\} \cdot \bar{\mathbf{w}}\, dV = \\ -\int_0^L \left\{ \mathbf{w} \cdot \iint_{A_0} \rho_0 \left[ (\mathbf{x}-\mathbf{x}_0)\cdot(\mathbf{x}-\mathbf{x}_0)\mathbf{I} - (\mathbf{x}-\mathbf{x}_0)\otimes(\mathbf{x}-\mathbf{x}_0) \right] dA \times \mathbf{w} \right\} \cdot \bar{\mathbf{w}} dS = \\ -\int_0^L \left[ \left( \mathbf{w} \cdot \mathbf{I}_\rho \right) \times \mathbf{w} \right] \cdot \bar{\mathbf{w}}\, dS = \int_0^L \mathbf{w} \times \left( \mathbf{I}_\rho \cdot \mathbf{w} \right) \cdot \bar{\mathbf{w}}\, dS \end{gathered} \tag{A-39}$$

By means of the above results, we get the following expression for the inertia term:

$$\iiint_{R_0} \rho_0 \ddot{\mathbf{x}} \cdot \dot{\mathbf{x}} dV = \int_0^L A_\rho \ddot{\mathbf{x}}_0 \cdot \dot{\mathbf{x}}_0 dS + \int_0^L \left[ \mathbf{I}_\rho \cdot \dot{\mathbf{w}} + \mathbf{w} \times \left( \mathbf{I}_\rho \cdot \mathbf{w} \right) \right] \cdot \mathbf{w}\, dS \tag{A-40}$$

## A.2 Internal power

We now evaluate the right hand side of (2-11):

$$\iiint_{R_0} tr\left(\mathbf{P}^{\mathbf{T}} \cdot \dot{\mathbf{F}}\right) dV \tag{A-41}$$

We recall that the deformation gradient tensor $\mathbf{F}$ may be written as follows:

$$\mathbf{F} = \mathbf{t}_\alpha \otimes \mathbf{E}_\alpha + \left[\frac{\partial \mathbf{x}_0}{\partial S} + \boldsymbol{\omega} \times X_\alpha \mathbf{t}_\alpha\right] \otimes \mathbf{E}_3 = \mathbf{t}_\alpha \otimes \mathbf{E}_\alpha + \left[\frac{\partial \mathbf{x}_0}{\partial S} + \boldsymbol{\omega} \times \left(\mathbf{x} - \mathbf{x}_0\right)\right] \otimes \mathbf{E}_3 \tag{A-42}$$

Taking the time derivative of (A-42) gives:

$$\dot{\mathbf{F}} = \dot{\mathbf{t}}_\alpha \otimes \mathbf{E}_\alpha + \left[\frac{\partial^2 \mathbf{x}_0}{\partial S \partial t} + \dot{\boldsymbol{\omega}} \times \left(\mathbf{x} - \mathbf{x}_0\right)\right] \otimes \mathbf{E}_3 + \boldsymbol{\omega} \times \left(\dot{\mathbf{x}} - \dot{\mathbf{x}}_0\right) \otimes \mathbf{E}_3 \tag{A-43}$$

Using (2-24) and (A-3), for $\dot{\mathbf{t}}_\alpha$ and $\dot{\mathbf{x}} - \dot{\mathbf{x}}_0$, (A-43) becomes:

$$\dot{\mathbf{F}} = \left(\mathbf{w} \times \mathbf{t}_\alpha\right) \otimes \mathbf{E}_\alpha + \left[\frac{\partial^2 \mathbf{x}_0}{\partial S \partial t} + \dot{\boldsymbol{\omega}} \times \left(\mathbf{x} - \mathbf{x}_0\right)\right] \otimes \mathbf{E}_3 + \left[\boldsymbol{\omega} \times \mathbf{w} \times \left(\mathbf{x} - \mathbf{x}_0\right)\right] \otimes \mathbf{E}_3 \tag{A-44}$$

Recalling that the first Piola-Kirchhoff stress tensor can be expressed as $\mathbf{P} = \mathbf{P}_i \otimes \mathbf{E}_i$, with (A-44) in hand we can write:

$$\begin{gathered} tr\left(\mathbf{P}^{\mathbf{T}} \cdot \bar{\dot{\mathbf{F}}}\right) = tr\left[\left(\mathbf{E}_i \otimes \mathbf{P}_i\right) \cdot \bar{\dot{\mathbf{F}}}\right] = tr\left[\left(\mathbf{E}_i \otimes \mathbf{P}_i\right) \cdot \left(\bar{\mathbf{w}} \times \mathbf{t}_\alpha\right) \otimes \mathbf{E}_\alpha\right] + \\ tr\left\{\left(\mathbf{E}_i \otimes \mathbf{P}_i\right) \cdot \left[\frac{\partial \bar{\mathbf{x}}_0}{\partial S} + \bar{\dot{\boldsymbol{\omega}}} \times \left(\mathbf{x} - \mathbf{x}_0\right)\right] \otimes \mathbf{E}_3\right\} + \\ tr\left\{\left(\mathbf{E}_i \otimes \mathbf{P}_i\right) \cdot \left[\boldsymbol{\omega} \times \bar{\mathbf{w}} \times \left(\mathbf{x} - \mathbf{x}_0\right)\right] \otimes \mathbf{E}_3\right\} \end{gathered} \tag{A-45}$$

We will now consider each term of (A-45) separately. The first term may be written as follows:

$$\begin{gathered} tr\left[\left(\mathbf{E}_i \otimes \mathbf{P}_i\right) \cdot \left(\bar{\mathbf{w}} \times \mathbf{t}_\alpha\right) \otimes \mathbf{E}_\alpha\right] = tr\left[\left(\bar{\mathbf{w}} \times \mathbf{t}_\alpha\right) \otimes \mathbf{E}_\alpha \cdot \mathbf{E}_i \otimes \mathbf{P}_i\right] = tr\left[\left(\bar{\mathbf{w}} \times \mathbf{t}_\alpha\right) \otimes \mathbf{P}_\alpha\right] = \\ \left(\bar{\mathbf{w}} \times \mathbf{t}_\alpha\right) \cdot \mathbf{P}_\alpha = \mathbf{P}_\alpha \cdot \left(\bar{\mathbf{w}} \times \mathbf{t}_\alpha\right) = \bar{\mathbf{w}} \cdot \mathbf{t}_\alpha \times \mathbf{P}_\alpha \end{gathered} \tag{A-46}$$

The second term of (A-45) can be broken down as follows:

$$\begin{gathered} tr\left\{\left(\mathbf{E}_i \otimes \mathbf{P}_i\right) \cdot \left[\frac{\partial \bar{\dot{\mathbf{x}}}_0}{\partial S} + \bar{\dot{\boldsymbol{\omega}}} \times \left(\mathbf{x} - \mathbf{x}_0\right)\right] \otimes \mathbf{E}_3\right\} = tr\left[\left(\mathbf{E}_i \otimes \mathbf{P}_i\right) \cdot \frac{\partial \bar{\dot{\mathbf{x}}}_0}{\partial S} \otimes \mathbf{E}_3\right] + \\ tr\left[\left(\mathbf{E}_i \otimes \mathbf{P}_i\right) \cdot \bar{\dot{\boldsymbol{\omega}}} \times \left(\mathbf{x} - \mathbf{x}_0\right) \otimes \mathbf{E}_3\right] \end{gathered} \tag{A-47}$$

The first term on the right hand side of (A-47) can be written as:

$$tr\left[\left(\mathbf{E}_i \otimes \mathbf{P}_i\right)\cdot \frac{\partial \bar{\dot{\mathbf{x}}}_0}{\partial S} \otimes \mathbf{E}_3\right] = tr\left(\frac{\partial \bar{\dot{\mathbf{x}}}_0}{\partial S} \otimes \mathbf{E}_3 \cdot \mathbf{E}_i \otimes \mathbf{P}_i\right) = tr\left(\frac{\partial \bar{\dot{\mathbf{x}}}_0}{\partial S} \otimes \mathbf{P}_3\right) = \frac{\partial \bar{\dot{\mathbf{x}}}_0}{\partial S} \cdot \mathbf{P}_3 = \mathbf{P}_3 \cdot \frac{\partial \bar{\dot{\mathbf{x}}}_0}{\partial S} \tag{A-48}$$

The second term on the right hand side of (A-47) may be expressed as:

$$tr\left[\left(\mathbf{E}_i \otimes \mathbf{P}_i\right)\cdot \bar{\dot{\boldsymbol{\omega}}} \times \left(\mathbf{x}-\mathbf{x}_0\right) \otimes \mathbf{E}_3\right] = tr\left[\bar{\dot{\boldsymbol{\omega}}} \times \left(\mathbf{x}-\mathbf{x}_0\right) \otimes \mathbf{E}_3 \cdot \mathbf{E}_i \otimes \mathbf{P}_i\right] = tr\left[\bar{\dot{\boldsymbol{\omega}}} \times \left(\mathbf{x}-\mathbf{x}_0\right) \otimes \mathbf{P}_3\right] = \left[\bar{\dot{\boldsymbol{\omega}}} \times \left(\mathbf{x}-\mathbf{x}_0\right)\right] \cdot \mathbf{P}_3 = \mathbf{P}_3 \cdot \left[\bar{\dot{\boldsymbol{\omega}}} \times \left(\mathbf{x}-\mathbf{x}_0\right)\right] \tag{A-49}$$

With (A-48) and (A-49) in hand, (A-47) becomes:

$$tr\left\{\left(\mathbf{E}_i \otimes \mathbf{P}_i\right)\cdot \left[\frac{\partial \bar{\dot{\mathbf{x}}}_0}{\partial S} + \bar{\dot{\boldsymbol{\omega}}} \times \left(\mathbf{x}-\mathbf{x}_0\right)\right] \otimes \mathbf{E}_3\right\} = \mathbf{P}_3 \cdot \left[\frac{\partial \bar{\dot{\mathbf{x}}}_0}{\partial S} + \bar{\dot{\boldsymbol{\omega}}} \times \left(\mathbf{x}-\mathbf{x}_0\right)\right] \tag{A-50}$$

Finally, the third term on the right hand side of (A-45) may be written as:

$$tr\left\{\left(\mathbf{E}_i \otimes \mathbf{P}_i\right)\cdot \left[\boldsymbol{\omega} \times \bar{\mathbf{w}} \times \left(\mathbf{x}-\mathbf{x}_0\right)\right] \otimes \mathbf{E}_3\right\} = tr\left\{\left[\boldsymbol{\omega} \times \bar{\mathbf{w}} \times \left(\mathbf{x}-\mathbf{x}_0\right)\right] \otimes \mathbf{E}_3 \cdot \mathbf{E}_i \otimes \mathbf{P}_i\right\} = tr\left\{\left[\boldsymbol{\omega} \times \bar{\mathbf{w}} \times \left(\mathbf{x}-\mathbf{x}_0\right)\right] \otimes \mathbf{P}_3\right\} = \left[\boldsymbol{\omega} \times \bar{\mathbf{w}} \times \left(\mathbf{x}-\mathbf{x}_0\right)\right] \cdot \mathbf{P}_3 = \mathbf{P}_3 \cdot \left[\boldsymbol{\omega} \times \bar{\mathbf{w}} \times \left(\mathbf{x}-\mathbf{x}_0\right)\right] \tag{A-51}$$

Substituting (A-46), (A-50), and (A-51) into (A-45) we get:

$$tr\left(\mathbf{P}^{\mathbf{T}} \cdot \bar{\dot{\mathbf{F}}}\right) = \bar{\mathbf{w}} \cdot \mathbf{t}_\alpha \times \mathbf{P}_\alpha + \mathbf{P}_3 \cdot \left[\frac{\partial \bar{\dot{\mathbf{x}}}_0}{\partial S} + \bar{\dot{\boldsymbol{\omega}}} \times \left(\mathbf{x}-\mathbf{x}_0\right)\right] + \mathbf{P}_3 \cdot \left[\boldsymbol{\omega} \times \bar{\mathbf{w}} \times \left(\mathbf{x}-\mathbf{x}_0\right)\right] \tag{A-52}$$

A convenient expression for $\mathbf{t}_\alpha \times \mathbf{P}_\alpha$ may be obtained by means of the following equation, expressing conservation of the angular momentum for 3D continuum:

$$\mathbf{F} \cdot \mathbf{P}^{\mathbf{T}} = \mathbf{P} \cdot \mathbf{F}^{\mathbf{T}} \tag{A-53}$$

The left hand side of (A-53) may be written as:

$$\mathbf{F} \cdot \mathbf{P}^{\mathbf{T}} = \left\{\mathbf{t}_\alpha \otimes \mathbf{E}_\alpha + \left[\frac{\partial \mathbf{x}_0}{\partial S} + \boldsymbol{\omega} \times \left(\mathbf{x}-\mathbf{x}_0\right)\right] \otimes \mathbf{E}_3\right\} \cdot \mathbf{E}_i \otimes \mathbf{P}_i = \mathbf{t}_\alpha \otimes \mathbf{E}_\alpha \cdot \mathbf{E}_i \otimes \mathbf{P}_i + \frac{\partial \mathbf{x}_0}{\partial S} \otimes \mathbf{E}_3 \cdot \mathbf{E}_i \otimes \mathbf{P}_i + \boldsymbol{\omega} \times \left(\mathbf{x}-\mathbf{x}_0\right) \otimes \mathbf{E}_3 \cdot \mathbf{E}_i \otimes \mathbf{P}_i = \mathbf{t}_\alpha \otimes \mathbf{P}_\alpha + \frac{\partial \mathbf{x}_0}{\partial S} \otimes \mathbf{P}_3 + \boldsymbol{\omega} \times \left(\mathbf{x}-\mathbf{x}_0\right) \otimes \mathbf{P}_3 \tag{A-54}$$

Moreover, the right hand side of (A-54) may be written as:

$$\mathbf{P}\cdot\mathbf{F}^{\mathbf{T}}=\mathbf{P}_i\otimes\mathbf{E}_i\cdot\left\{\mathbf{E}_\alpha\otimes\mathbf{t}_\alpha+\mathbf{E}_3\otimes\left[\frac{\partial\mathbf{x}_0}{\partial S}+\boldsymbol{\omega}\times(\mathbf{x}-\mathbf{x}_0)\right]\right\}=\mathbf{P}_i\otimes\mathbf{E}_i\cdot\mathbf{E}_\alpha\otimes\mathbf{t}_\alpha+$$
$$\mathbf{P}_i\otimes\mathbf{E}_i\cdot\mathbf{E}_3\otimes\frac{\partial\mathbf{x}_0}{\partial S}+\mathbf{P}_i\otimes\mathbf{E}_i\cdot\mathbf{E}_3\otimes\left[\boldsymbol{\omega}\times(\mathbf{x}-\mathbf{x}_0)\right]= \tag{A-55}$$
$$\mathbf{P}_\alpha\otimes\mathbf{t}_\alpha+\mathbf{P}_3\otimes\frac{\partial\mathbf{x}_0}{\partial S}+\mathbf{P}_3\otimes\boldsymbol{\omega}\times(\mathbf{x}-\mathbf{x}_0)$$

Then, equating (A-54) to (A-55) gives:

$$\begin{aligned}&(\mathbf{t}_\alpha\otimes\mathbf{P}_\alpha-\mathbf{P}_\alpha\otimes\mathbf{t}_\alpha)+\left(\frac{\partial\mathbf{x}_0}{\partial S}\otimes\mathbf{P}_3-\mathbf{P}_3\otimes\frac{\partial\mathbf{x}_0}{\partial S}\right)+\\&\left[\boldsymbol{\omega}\times(\mathbf{x}-\mathbf{x}_0)\otimes\mathbf{P}_3-\mathbf{P}_3\otimes\boldsymbol{\omega}\times(\mathbf{x}-\mathbf{x}_0)\right]=\mathbf{0}\end{aligned} \tag{A-56}$$

It is easy to prove that, if (A-56) holds, then the following expression must also hold:

$$\mathbf{t}_\alpha\times\mathbf{P}_\alpha=-\left[\frac{\partial\mathbf{x}_0}{\partial S}+\boldsymbol{\omega}\times(\mathbf{x}-\mathbf{x}_0)\right]\times\mathbf{P}_3 \tag{A-57}$$

Substituting (A-57) into the first term on the right hand side of (A-52) gives:

$$\mathbf{w}\cdot\mathbf{t}_\alpha\times\mathbf{P}_\alpha=-\mathbf{w}\cdot\left[\frac{\partial\mathbf{x}_0}{\partial S}+\boldsymbol{\omega}\times(\mathbf{x}-\mathbf{x}_0)\right]\times\mathbf{P}_3=-\mathbf{P}_3\cdot\mathbf{w}\times\left[\frac{\partial\mathbf{x}_0}{\partial S}+\boldsymbol{\omega}\times(\mathbf{x}-\mathbf{x}_0)\right] \tag{A-58}$$

Therefore, Eq. (A-52) may be written as:

$$\begin{aligned}tr\left(\mathbf{P}^{\mathbf{T}}\cdot\dot{\bar{\mathbf{F}}}\right)=-\mathbf{P}_3\cdot\mathbf{w}\times\left[\frac{\partial\mathbf{x}_0}{\partial S}+\boldsymbol{\omega}\times(\mathbf{x}-\mathbf{x}_0)\right]+\mathbf{P}_3\cdot\left[\frac{\partial\dot{\bar{\mathbf{x}}}_0}{\partial S}+\dot{\bar{\boldsymbol{\omega}}}\times(\mathbf{x}-\mathbf{x}_0)\right]+\\\mathbf{P}_3\cdot\boldsymbol{\omega}\times\left[\bar{\mathbf{w}}\times(\mathbf{x}-\mathbf{x}_0)\right]\end{aligned} \tag{A-59}$$

or equivalently as

$$\begin{aligned}tr\left(\mathbf{P}^{\mathbf{T}}\cdot\dot{\bar{\mathbf{F}}}\right)=\mathbf{P}_3\cdot\left(\frac{\partial\dot{\bar{\mathbf{x}}}_0}{\partial S}-\bar{\mathbf{w}}\times\frac{\partial\mathbf{x}_0}{\partial S}\right)+\mathbf{P}_3\cdot\left\{\boldsymbol{\omega}\times\left[\bar{\mathbf{w}}\times(\mathbf{x}-\mathbf{x}_0)\right]-\bar{\mathbf{w}}\times\left[\boldsymbol{\omega}\times(\mathbf{x}-\mathbf{x}_0)\right]\right\}+\\\mathbf{P}_3\cdot\left[\dot{\bar{\boldsymbol{\omega}}}\times(\mathbf{x}-\mathbf{x}_0)\right]\end{aligned} \tag{A-60}$$

Observing that:

$$\begin{aligned}\boldsymbol{\omega}\times\left[\bar{\mathbf{w}}\times(\mathbf{x}-\mathbf{x}_0)\right]-\bar{\mathbf{w}}\times\left[\boldsymbol{\omega}\times(\mathbf{x}-\mathbf{x}_0)\right]=(\bar{\mathbf{w}}\otimes\boldsymbol{\omega}-\boldsymbol{\omega}\otimes\bar{\mathbf{w}})\cdot(\mathbf{x}-\mathbf{x}_0)=\\(\boldsymbol{\omega}\times\bar{\mathbf{w}})\times(\mathbf{x}-\mathbf{x}_0)\end{aligned} \tag{A-61}$$

then, Eq. (A-60) becomes:

$$tr\left(\mathbf{P}^{\mathbf{T}}\cdot\dot{\bar{\mathbf{F}}}\right)=\mathbf{P}_3\cdot\left(\frac{\partial\dot{\bar{\mathbf{x}}}_0}{\partial S}-\bar{\mathbf{w}}\times\frac{\partial\mathbf{x}_0}{\partial S}\right)+\mathbf{P}_3\cdot\left[\left(\dot{\bar{\boldsymbol{\omega}}}+\boldsymbol{\omega}\times\bar{\mathbf{w}}\right)\times(\mathbf{x}-\mathbf{x}_0)\right] \tag{A-62}$$

Eq. (A-62) can be written in the following equivalent form:

$$tr\left(\mathbf{P}^{\mathbf{T}}\cdot\dot{\bar{\mathbf{F}}}\right)=\mathbf{P}_3\cdot\left(\frac{\partial\dot{\bar{\mathbf{x}}}_0}{\partial S}-\bar{\mathbf{w}}\times\frac{\partial\mathbf{x}_0}{\partial S}\right)+\mathbf{P}_3\cdot\left[\left(\dot{\bar{\boldsymbol{\omega}}}-\bar{\mathbf{w}}\times\boldsymbol{\omega}\right)\times\left(\mathbf{x}-\mathbf{x}_0\right)\right] \tag{A-63}$$

Integrating (A-63) over the area of the cross section we obtain the internal power per unit length of the beam:

$$\begin{gathered}\iint_A tr\left(\mathbf{P}^{\mathbf{T}}\cdot\dot{\bar{\mathbf{F}}}\right)dA=\iint_A\mathbf{P}_3\,dA\cdot\left(\frac{\partial\dot{\bar{\mathbf{x}}}_0}{\partial S}-\bar{\mathbf{w}}\times\frac{\partial\mathbf{x}_0}{\partial S}\right)+\iint_A\left(\mathbf{x}-\mathbf{x}_0\right)\times\mathbf{P}_3\,dA\cdot\left(\dot{\bar{\boldsymbol{\omega}}}-\bar{\mathbf{w}}\times\boldsymbol{\omega}\right)=\\ \mathbf{n}\cdot\left(\frac{\partial\dot{\bar{\mathbf{x}}}_0}{\partial S}-\bar{\mathbf{w}}\times\frac{\partial\mathbf{x}_0}{\partial S}\right)+\mathbf{m}\cdot\left(\dot{\bar{\boldsymbol{\omega}}}-\bar{\mathbf{w}}\times\boldsymbol{\omega}\right)\end{gathered} \tag{A-64}$$

where **n** and **m** are the resultant force and moment acting on the generic cross section at *S*:

$$\mathbf{n}=\iint_A\mathbf{P}_3\,dA \tag{A-65}$$

$$\mathbf{m}=\iint_A\left(\mathbf{x}-\mathbf{x}_0\right)\times\mathbf{P}_3\,dA \tag{A-66}$$

Finally, the internal power may be written as:

$$\iiint_{R_0} tr\left(\mathbf{P}^{\mathbf{T}}\cdot\dot{\bar{\mathbf{F}}}\right)dV=\int_0^L\left[\mathbf{n}\cdot\left(\frac{\partial\dot{\bar{\mathbf{x}}}_0}{\partial S}-\bar{\mathbf{w}}\times\frac{\partial\mathbf{x}_0}{\partial S}\right)+\mathbf{m}\cdot\left(\dot{\bar{\boldsymbol{\omega}}}-\bar{\mathbf{w}}\times\boldsymbol{\omega}\right)\right]dS \tag{A-67}$$

# APPENDIX B

We want to prove that the following equality holds:

$$\dot{\boldsymbol{\omega}} - \mathbf{w} \times \boldsymbol{\omega} = \mathbf{w}' \tag{B-1}$$

To do so, we first write (B-1) in equivalent tensor form as follows:

$$\dot{\hat{\boldsymbol{\omega}}} - \left(\mathbf{w} \times \boldsymbol{\omega}\right)^{\wedge} = \hat{\mathbf{w}}' \tag{B-2}$$

where

$$\hat{\boldsymbol{\omega}} = \frac{\partial \mathbf{R}}{\partial S} \cdot \mathbf{R}^{\mathrm{T}} \qquad \hat{\mathbf{w}} = \frac{\partial \mathbf{R}}{\partial t} \cdot \mathbf{R}^{\mathrm{T}} \tag{B-3}$$

Differentiation of $\hat{\boldsymbol{\omega}}$ with respect to time gives:

$$\begin{aligned} \dot{\hat{\boldsymbol{\omega}}} &= \frac{\partial^2 \mathbf{R}}{\partial S \partial t} \cdot \mathbf{R}^{\mathrm{T}} + \frac{\partial \mathbf{R}}{\partial S} \cdot \frac{\partial \mathbf{R}^{\mathrm{T}}}{\partial t} = \frac{\partial^2 \mathbf{R}}{\partial S \partial t} \cdot \mathbf{R}^{\mathrm{T}} + \frac{\partial \mathbf{R}}{\partial S} \cdot \mathbf{R}^{\mathrm{T}} \cdot \mathbf{R} \cdot \frac{\partial \mathbf{R}^{\mathrm{T}}}{\partial t} = \\ &= \frac{\partial^2 \mathbf{R}}{\partial S \partial t} \cdot \mathbf{R}^{\mathrm{T}} + \left[\frac{\partial \mathbf{R}}{\partial S} \cdot \mathbf{R}^{\mathrm{T}}\right] \cdot \left[\frac{\partial \mathbf{R}}{\partial t} \cdot \mathbf{R}^{\mathrm{T}}\right]^{\mathrm{T}} = \frac{\partial^2 \mathbf{R}}{\partial S \partial t} \cdot \mathbf{R}^{\mathrm{T}} + \hat{\boldsymbol{\omega}} \cdot \hat{\mathbf{w}}^{\mathrm{T}} \end{aligned} \tag{B-4}$$

In the same fashion, differentiation of $\hat{\mathbf{w}}$ with respect to $S$ gives:

$$\begin{aligned} \hat{\mathbf{w}}' &= \frac{\partial^2 \mathbf{R}}{\partial S \partial t} \cdot \mathbf{R}^{\mathrm{T}} + \frac{\partial \mathbf{R}}{\partial t} \cdot \frac{\partial \mathbf{R}^{\mathrm{T}}}{\partial S} = \frac{\partial^2 \mathbf{R}}{\partial S \partial t} \cdot \mathbf{R}^{\mathrm{T}} + \frac{\partial \mathbf{R}}{\partial t} \cdot \mathbf{R}^{\mathrm{T}} \cdot \mathbf{R} \cdot \frac{\partial \mathbf{R}^{\mathrm{T}}}{\partial S} = \\ &= \frac{\partial^2 \mathbf{R}}{\partial S \partial t} \cdot \mathbf{R}^{\mathrm{T}} + \left[\frac{\partial \mathbf{R}}{\partial t} \cdot \mathbf{R}^{\mathrm{T}}\right] \cdot \left[\frac{\partial \mathbf{R}}{\partial S} \cdot \mathbf{R}^{\mathrm{T}}\right]^{\mathrm{T}} = \frac{\partial^2 \mathbf{R}}{\partial S \partial t} \cdot \mathbf{R}^{\mathrm{T}} + \hat{\mathbf{w}} \cdot \hat{\boldsymbol{\omega}}^{\mathrm{T}} \end{aligned} \tag{B-5}$$

We next make use of the following property involving skew-symmetric tensors and their associated axial vectors:

$$\left(\mathbf{w} \times \boldsymbol{\omega}\right)^{\wedge} = \hat{\mathbf{w}} \cdot \hat{\boldsymbol{\omega}} - \hat{\boldsymbol{\omega}} \cdot \hat{\mathbf{w}} \tag{B-6}$$

By substituting (B-4), (B-5) and (B-6) into (B-2), we then get:

$$\hat{\boldsymbol{\omega}} \cdot \hat{\mathbf{w}}^{\mathrm{T}} - \hat{\mathbf{w}} \cdot \hat{\boldsymbol{\omega}} + \hat{\boldsymbol{\omega}} \cdot \hat{\mathbf{w}} = \hat{\mathbf{w}} \cdot \hat{\boldsymbol{\omega}}^{\mathrm{T}} \tag{B-7}$$

It is now trivial to show that (B-7) holds. In fact, the left hand side may be written as the right hand side as follows:

$$\hat{\boldsymbol{\omega}} \cdot \hat{\mathbf{w}}^{\mathrm{T}} - \hat{\mathbf{w}} \cdot \hat{\boldsymbol{\omega}} + \hat{\boldsymbol{\omega}} \cdot \hat{\mathbf{w}} = -\hat{\boldsymbol{\omega}} \cdot \hat{\mathbf{w}} + \hat{\mathbf{w}} \cdot \hat{\boldsymbol{\omega}}^{\mathrm{T}} + \hat{\boldsymbol{\omega}} \cdot \hat{\mathbf{w}} = \hat{\mathbf{w}} \cdot \hat{\boldsymbol{\omega}}^{\mathrm{T}} \tag{B-8}$$

## MCEER Technical Reports

MCEER publishes technical reports on a variety of subjects written by authors funded through MCEER. These reports can be downloaded from the MCEER website at http://www.buffalo.edu/mceer. They can also be requested through NTIS, P.O. Box 1425, Springfield, Virginia 22151. NTIS accession numbers are shown in parenthesis, if available.

NCEER-87-0001 "First-Year Program in Research, Education and Technology Transfer," 3/5/87, (PB88-134275, A04, MF-A01).

NCEER-87-0002 "Experimental Evaluation of Instantaneous Optimal Algorithms for Structural Control," by R.C. Lin, T.T. Soong and A.M. Reinhorn, 4/20/87, (PB88-134341, A04, MF-A01).

NCEER-87-0003 "Experimentation Using the Earthquake Simulation Facilities at University at Buffalo," by A.M. Reinhorn and R.L. Ketter, not available.

NCEER-87-0004 "The System Characteristics and Performance of a Shaking Table," by J.S. Hwang, K.C. Chang and G.C. Lee, 6/1/87, (PB88-134259, A03, MF-A01). This report is available only through NTIS (see address given above).

NCEER-87-0005 "A Finite Element Formulation for Nonlinear Viscoplastic Material Using a Q Model," by O. Gyebi and G. Dasgupta, 11/2/87, (PB88-213764, A08, MF-A01).

NCEER-87-0006 "Symbolic Manipulation Program (SMP) - Algebraic Codes for Two and Three Dimensional Finite Element Formulations," by X. Lee and G. Dasgupta, 11/9/87, (PB88-218522, A05, MF-A01).

NCEER-87-0007 "Instantaneous Optimal Control Laws for Tall Buildings Under Seismic Excitations," by J.N. Yang, A. Akbarpour and P. Ghaemmaghami, 6/10/87, (PB88-134333, A06, MF-A01). This report is only available through NTIS (see address given above).

NCEER-87-0008 "IDARC: Inelastic Damage Analysis of Reinforced Concrete Frame - Shear-Wall Structures," by Y.J. Park, A.M. Reinhorn and S.K. Kunnath, 7/20/87, (PB88-134325, A09, MF-A01). This report is only available through NTIS (see address given above).

NCEER-87-0009 "Liquefaction Potential for New York State: A Preliminary Report on Sites in Manhattan and Buffalo," by M. Budhu, V. Vijayakumar, R.F. Giese and L. Baumgras, 8/31/87, (PB88-163704, A03, MF-A01). This report is available only through NTIS (see address given above).

NCEER-87-0010 "Vertical and Torsional Vibration of Foundations in Inhomogeneous Media," by A.S. Veletsos and K.W. Dotson, 6/1/87, (PB88-134291, A03, MF-A01). This report is only available through NTIS (see address given above).

NCEER-87-0011 "Seismic Probabilistic Risk Assessment and Seismic Margins Studies for Nuclear Power Plants," by Howard H.M. Hwang, 6/15/87, (PB88-134267, A03, MF-A01). This report is only available through NTIS (see address given above).

NCEER-87-0012 "Parametric Studies of Frequency Response of Secondary Systems Under Ground-Acceleration Excitations," by Y. Yong and Y.K. Lin, 6/10/87, (PB88-134309, A03, MF-A01). This report is only available through NTIS (see address given above).

NCEER-87-0013 "Frequency Response of Secondary Systems Under Seismic Excitation," by J.A. HoLung, J. Cai and Y.K. Lin, 7/31/87, (PB88-134317, A05, MF-A01). This report is only available through NTIS (see address given above).

NCEER-87-0014 "Modelling Earthquake Ground Motions in Seismically Active Regions Using Parametric Time Series Methods," by G.W. Ellis and A.S. Cakmak, 8/25/87, (PB88-134283, A08, MF-A01). This report is only available through NTIS (see address given above).

NCEER-87-0015 "Detection and Assessment of Seismic Structural Damage," by E. DiPasquale and A.S. Cakmak, 8/25/87, (PB88-163712, A05, MF-A01). This report is only available through NTIS (see address given above).

NCEER-87-0016 "Pipeline Experiment at Parkfield, California," by J. Isenberg and E. Richardson, 9/15/87, (PB88-163720, A03, MF-A01). This report is available only through NTIS (see address given above).

NCEER-87-0017 "Digital Simulation of Seismic Ground Motion," by M. Shinozuka, G. Deodatis and T. Harada, 8/31/87, (PB88-155197, A04, MF-A01). This report is available only through NTIS (see address given above).

NCEER-87-0018 "Practical Considerations for Structural Control: System Uncertainty, System Time Delay and Truncation of Small Control Forces," J.N. Yang and A. Akbarpour, 8/10/87, (PB88-163738, A08, MF-A01). This report is only available through NTIS (see address given above).

NCEER-87-0019 "Modal Analysis of Nonclassically Damped Structural Systems Using Canonical Transformation," by J.N. Yang, S. Sarkani and F.X. Long, 9/27/87, (PB88-187851, A04, MF-A01).

NCEER-87-0020 "A Nonstationary Solution in Random Vibration Theory," by J.R. Red-Horse and P.D. Spanos, 11/3/87, (PB88-163746, A03, MF-A01).

NCEER-87-0021 "Horizontal Impedances for Radially Inhomogeneous Viscoelastic Soil Layers," by A.S. Veletsos and K.W. Dotson, 10/15/87, (PB88-150859, A04, MF-A01).

NCEER-87-0022 "Seismic Damage Assessment of Reinforced Concrete Members," by Y.S. Chung, C. Meyer and M. Shinozuka, 10/9/87, (PB88-150867, A05, MF-A01). This report is available only through NTIS (see address given above).

NCEER-87-0023 "Active Structural Control in Civil Engineering," by T.T. Soong, 11/11/87, (PB88-187778, A03, MF-A01).

NCEER-87-0024 "Vertical and Torsional Impedances for Radially Inhomogeneous Viscoelastic Soil Layers," by K.W. Dotson and A.S. Veletsos, 12/87, (PB88-187786, A03, MF-A01).

NCEER-87-0025 "Proceedings from the Symposium on Seismic Hazards, Ground Motions, Soil-Liquefaction and Engineering Practice in Eastern North America," October 20-22, 1987, edited by K.H. Jacob, 12/87, (PB88-188115, A23, MF-A01). This report is available only through NTIS (see address given above).

NCEER-87-0026 "Report on the Whittier-Narrows, California, Earthquake of October 1, 1987," by J. Pantelic and A. Reinhorn, 11/87, (PB88-187752, A03, MF-A01). This report is available only through NTIS (see address given above).

NCEER-87-0027 "Design of a Modular Program for Transient Nonlinear Analysis of Large 3-D Building Structures," by S. Srivastav and J.F. Abel, 12/30/87, (PB88-187950, A05, MF-A01). This report is only available through NTIS (see address given above).

NCEER-87-0028 "Second-Year Program in Research, Education and Technology Transfer," 3/8/88, (PB88-219480, A04, MF-A01).

NCEER-88-0001 "Workshop on Seismic Computer Analysis and Design of Buildings With Interactive Graphics," by W. McGuire, J.F. Abel and C.H. Conley, 1/18/88, (PB88-187760, A03, MF-A01). This report is only available through NTIS (see address given above).

NCEER-88-0002 "Optimal Control of Nonlinear Flexible Structures," by J.N. Yang, F.X. Long and D. Wong, 1/22/88, (PB88-213772, A06, MF-A01).

NCEER-88-0003 "Substructuring Techniques in the Time Domain for Primary-Secondary Structural Systems," by G.D. Manolis and G. Juhn, 2/10/88, (PB88-213780, A04, MF-A01).

NCEER-88-0004 "Iterative Seismic Analysis of Primary-Secondary Systems," by A. Singhal, L.D. Lutes and P.D. Spanos, 2/23/88, (PB88-213798, A04, MF-A01).

NCEER-88-0005 "Stochastic Finite Element Expansion for Random Media," by P.D. Spanos and R. Ghanem, 3/14/88, (PB88-213806, A03, MF-A01).

NCEER-88-0006 "Combining Structural Optimization and Structural Control," by F.Y. Cheng and C.P. Pantelides, 1/10/88, (PB88-213814, A05, MF-A01).

NCEER-88-0007 "Seismic Performance Assessment of Code-Designed Structures," by H.H-M. Hwang, J-W. Jaw and H-J. Shau, 3/20/88, (PB88-219423, A04, MF-A01). This report is only available through NTIS (see address given above).

NCEER-88-0008 "Reliability Analysis of Code-Designed Structures Under Natural Hazards," by H.H-M. Hwang, H. Ushiba and M. Shinozuka, 2/29/88, (PB88-229471, A07, MF-A01). This report is only available through NTIS (see address given above).

NCEER-88-0009 "Seismic Fragility Analysis of Shear Wall Structures," by J-W Jaw and H.H-M. Hwang, 4/30/88, (PB89-102867, A04, MF-A01).

NCEER-88-0010 "Base Isolation of a Multi-Story Building Under a Harmonic Ground Motion - A Comparison of Performances of Various Systems," by F-G Fan, G. Ahmadi and I.G. Tadjbakhsh, 5/18/88, (PB89-122238, A06, MF-A01). This report is only available through NTIS (see address given above).

NCEER-88-0011 "Seismic Floor Response Spectra for a Combined System by Green's Functions," by F.M. Lavelle, L.A. Bergman and P.D. Spanos, 5/1/88, (PB89-102875, A03, MF-A01).

NCEER-88-0012 "A New Solution Technique for Randomly Excited Hysteretic Structures," by G.Q. Cai and Y.K. Lin, 5/16/88, (PB89-102883, A03, MF-A01).

NCEER-88-0013 "A Study of Radiation Damping and Soil-Structure Interaction Effects in the Centrifuge," by K. Weissman, supervised by J.H. Prevost, 5/24/88, (PB89-144703, A06, MF-A01).

NCEER-88-0014 "Parameter Identification and Implementation of a Kinematic Plasticity Model for Frictional Soils," by J.H. Prevost and D.V. Griffiths, not available.

NCEER-88-0015 "Two- and Three- Dimensional Dynamic Finite Element Analyses of the Long Valley Dam," by D.V. Griffiths and J.H. Prevost, 6/17/88, (PB89-144711, A04, MF-A01).

NCEER-88-0016 "Damage Assessment of Reinforced Concrete Structures in Eastern United States," by A.M. Reinhorn, M.J. Seidel, S.K. Kunnath and Y.J. Park, 6/15/88, (PB89-122220, A04, MF-A01). This report is only available through NTIS (see address given above).

NCEER-88-0017 "Dynamic Compliance of Vertically Loaded Strip Foundations in Multilayered Viscoelastic Soils," by S. Ahmad and A.S.M. Israil, 6/17/88, (PB89-102891, A04, MF-A01).

NCEER-88-0018 "An Experimental Study of Seismic Structural Response With Added Viscoelastic Dampers," by R.C. Lin, Z. Liang, T.T. Soong and R.H. Zhang, 6/30/88, (PB89-122212, A05, MF-A01). This report is available only through NTIS (see address given above).

NCEER-88-0019 "Experimental Investigation of Primary - Secondary System Interaction," by G.D. Manolis, G. Juhn and A.M. Reinhorn, 5/27/88, (PB89-122204, A04, MF-A01).

NCEER-88-0020 "A Response Spectrum Approach For Analysis of Nonclassically Damped Structures," by J.N. Yang, S. Sarkani and F.X. Long, 4/22/88, (PB89-102909, A04, MF-A01).

NCEER-88-0021 "Seismic Interaction of Structures and Soils: Stochastic Approach," by A.S. Veletsos and A.M. Prasad, 7/21/88, (PB89-122196, A04, MF-A01). This report is only available through NTIS (see address given above).

NCEER-88-0022 "Identification of the Serviceability Limit State and Detection of Seismic Structural Damage," by E. DiPasquale and A.S. Cakmak, 6/15/88, (PB89-122188, A05, MF-A01). This report is available only through NTIS (see address given above).

NCEER-88-0023 "Multi-Hazard Risk Analysis: Case of a Simple Offshore Structure," by B.K. Bhartia and E.H. Vanmarcke, 7/21/88, (PB89-145213, A05, MF-A01).

NCEER-88-0024 "Automated Seismic Design of Reinforced Concrete Buildings," by Y.S. Chung, C. Meyer and M. Shinozuka, 7/5/88, (PB89-122170, A06, MF-A01). This report is available only through NTIS (see address given above).

NCEER-88-0025 "Experimental Study of Active Control of MDOF Structures Under Seismic Excitations," by L.L. Chung, R.C. Lin, T.T. Soong and A.M. Reinhorn, 7/10/88, (PB89-122600, A04, MF-A01).

NCEER-88-0026 "Earthquake Simulation Tests of a Low-Rise Metal Structure," by J.S. Hwang, K.C. Chang, G.C. Lee and R.L. Ketter, 8/1/88, (PB89-102917, A04, MF-A01).

NCEER-88-0027 "Systems Study of Urban Response and Reconstruction Due to Catastrophic Earthquakes," by F. Kozin and H.K. Zhou, 9/22/88, (PB90-162348, A04, MF-A01).

NCEER-88-0028 "Seismic Fragility Analysis of Plane Frame Structures," by H.H-M. Hwang and Y.K. Low, 7/31/88, (PB89-131445, A06, MF-A01).

NCEER-88-0029 "Response Analysis of Stochastic Structures," by A. Kardara, C. Bucher and M. Shinozuka, 9/22/88, (PB89-174429, A04, MF-A01).

NCEER-88-0030 "Nonnormal Accelerations Due to Yielding in a Primary Structure," by D.C.K. Chen and L.D. Lutes, 9/19/88, (PB89-131437, A04, MF-A01).

NCEER-88-0031 "Design Approaches for Soil-Structure Interaction," by A.S. Veletsos, A.M. Prasad and Y. Tang, 12/30/88, (PB89-174437, A03, MF-A01). This report is available only through NTIS (see address given above).

NCEER-88-0032 "A Re-evaluation of Design Spectra for Seismic Damage Control," by C.J. Turkstra and A.G. Tallin, 11/7/88, (PB89-145221, A05, MF-A01).

NCEER-88-0033 "The Behavior and Design of Noncontact Lap Splices Subjected to Repeated Inelastic Tensile Loading," by V.E. Sagan, P. Gergely and R.N. White, 12/8/88, (PB89-163737, A08, MF-A01).

NCEER-88-0034 "Seismic Response of Pile Foundations," by S.M. Mamoon, P.K. Banerjee and S. Ahmad, 11/1/88, (PB89-145239, A04, MF-A01).

NCEER-88-0035 "Modeling of R/C Building Structures With Flexible Floor Diaphragms (IDARC2)," by A.M. Reinhorn, S.K. Kunnath and N. Panahshahi, 9/7/88, (PB89-207153, A07, MF-A01).

NCEER-88-0036 "Solution of the Dam-Reservoir Interaction Problem Using a Combination of FEM, BEM with Particular Integrals, Modal Analysis, and Substructuring," by C-S. Tsai, G.C. Lee and R.L. Ketter, 12/31/88, (PB89-207146, A04, MF-A01).

NCEER-88-0037 "Optimal Placement of Actuators for Structural Control," by F.Y. Cheng and C.P. Pantelides, 8/15/88, (PB89-162846, A05, MF-A01).

NCEER-88-0038 "Teflon Bearings in Aseismic Base Isolation: Experimental Studies and Mathematical Modeling," by A. Mokha, M.C. Constantinou and A.M. Reinhorn, 12/5/88, (PB89-218457, A10, MF-A01). This report is available only through NTIS (see address given above).

NCEER-88-0039 "Seismic Behavior of Flat Slab High-Rise Buildings in the New York City Area," by P. Weidlinger and M. Ettouney, 10/15/88, (PB90-145681, A04, MF-A01).

NCEER-88-0040 "Evaluation of the Earthquake Resistance of Existing Buildings in New York City," by P. Weidlinger and M. Ettouney, 10/15/88, not available.

NCEER-88-0041 "Small-Scale Modeling Techniques for Reinforced Concrete Structures Subjected to Seismic Loads," by W. Kim, A. El-Attar and R.N. White, 11/22/88, (PB89-189625, A05, MF-A01).

NCEER-88-0042 "Modeling Strong Ground Motion from Multiple Event Earthquakes," by G.W. Ellis and A.S. Cakmak, 10/15/88, (PB89-174445, A03, MF-A01).

NCEER-88-0043 "Nonstationary Models of Seismic Ground Acceleration," by M. Grigoriu, S.E. Ruiz and E. Rosenblueth, 7/15/88, (PB89-189617, A04, MF-A01).

NCEER-88-0044 "SARCF User's Guide: Seismic Analysis of Reinforced Concrete Frames," by Y.S. Chung, C. Meyer and M. Shinozuka, 11/9/88, (PB89-174452, A08, MF-A01).

NCEER-88-0045 "First Expert Panel Meeting on Disaster Research and Planning," edited by J. Pantelic and J. Stoyle, 9/15/88, (PB89-174460, A05, MF-A01).

NCEER-88-0046 "Preliminary Studies of the Effect of Degrading Infill Walls on the Nonlinear Seismic Response of Steel Frames," by C.Z. Chrysostomou, P. Gergely and J.F. Abel, 12/19/88, (PB89-208383, A05, MF-A01).

NCEER-88-0047 "Reinforced Concrete Frame Component Testing Facility - Design, Construction, Instrumentation and Operation," by S.P. Pessiki, C. Conley, T. Bond, P. Gergely and R.N. White, 12/16/88, (PB89-174478, A04, MF-A01).

NCEER-89-0001 "Effects of Protective Cushion and Soil Compliancy on the Response of Equipment Within a Seismically Excited Building," by J.A. HoLung, 2/16/89, (PB89-207179, A04, MF-A01).

NCEER-89-0002 "Statistical Evaluation of Response Modification Factors for Reinforced Concrete Structures," by H.H-M. Hwang and J-W. Jaw, 2/17/89, (PB89-207187, A05, MF-A01).

NCEER-89-0003 "Hysteretic Columns Under Random Excitation," by G-Q. Cai and Y.K. Lin, 1/9/89, (PB89-196513, A03, MF-A01).

NCEER-89-0004 "Experimental Study of `Elephant Foot Bulge' Instability of Thin-Walled Metal Tanks," by Z-H. Jia and R.L. Ketter, 2/22/89, (PB89-207195, A03, MF-A01).

NCEER-89-0005 "Experiment on Performance of Buried Pipelines Across San Andreas Fault," by J. Isenberg, E. Richardson and T.D. O'Rourke, 3/10/89, (PB89-218440, A04, MF-A01). This report is available only through NTIS (see address given above).

NCEER-89-0006 "A Knowledge-Based Approach to Structural Design of Earthquake-Resistant Buildings," by M. Subramani, P. Gergely, C.H. Conley, J.F. Abel and A.H. Zaghw, 1/15/89, (PB89-218465, A06, MF-A01).

NCEER-89-0007 "Liquefaction Hazards and Their Effects on Buried Pipelines," by T.D. O'Rourke and P.A. Lane, 2/1/89, (PB89-218481, A09, MF-A01).

NCEER-89-0008 "Fundamentals of System Identification in Structural Dynamics," by H. Imai, C-B. Yun, O. Maruyama and M. Shinozuka, 1/26/89, (PB89-207211, A04, MF-A01).

NCEER-89-0009 "Effects of the 1985 Michoacan Earthquake on Water Systems and Other Buried Lifelines in Mexico," by A.G. Ayala and M.J. O'Rourke, 3/8/89, (PB89-207229, A06, MF-A01).

NCEER-89-R010 "NCEER Bibliography of Earthquake Education Materials," by K.E.K. Ross, Second Revision, 9/1/89, (PB90-125352, A05, MF-A01). This report is replaced by NCEER-92-0018.

NCEER-89-0011 "Inelastic Three-Dimensional Response Analysis of Reinforced Concrete Building Structures (IDARC-3D), Part I - Modeling," by S.K. Kunnath and A.M. Reinhorn, 4/17/89, (PB90-114612, A07, MF-A01). This report is available only through NTIS (see address given above).

NCEER-89-0012 "Recommended Modifications to ATC-14," by C.D. Poland and J.O. Malley, 4/12/89, (PB90-108648, A15, MF-A01).

NCEER-89-0013 "Repair and Strengthening of Beam-to-Column Connections Subjected to Earthquake Loading," by M. Corazao and A.J. Durrani, 2/28/89, (PB90-109885, A06, MF-A01).

NCEER-89-0014 "Program EXKAL2 for Identification of Structural Dynamic Systems," by O. Maruyama, C-B. Yun, M. Hoshiya and M. Shinozuka, 5/19/89, (PB90-109877, A09, MF-A01).

NCEER-89-0015 "Response of Frames With Bolted Semi-Rigid Connections, Part I - Experimental Study and Analytical Predictions," by P.J. DiCorso, A.M. Reinhorn, J.R. Dickerson, J.B. Radziminski and W.L. Harper, 6/1/89, not available.

NCEER-89-0016 "ARMA Monte Carlo Simulation in Probabilistic Structural Analysis," by P.D. Spanos and M.P. Mignolet, 7/10/89, (PB90-109893, A03, MF-A01).

NCEER-89-P017 "Preliminary Proceedings from the Conference on Disaster Preparedness - The Place of Earthquake Education in Our Schools," Edited by K.E.K. Ross, 6/23/89, (PB90-108606, A03, MF-A01).

NCEER-89-0017 "Proceedings from the Conference on Disaster Preparedness - The Place of Earthquake Education in Our Schools," Edited by K.E.K. Ross, 12/31/89, (PB90-207895, A012, MF-A02). This report is available only through NTIS (see address given above).

NCEER-89-0018 "Multidimensional Models of Hysteretic Material Behavior for Vibration Analysis of Shape Memory Energy Absorbing Devices, by E.J. Graesser and F.A. Cozzarelli, 6/7/89, (PB90-164146, A04, MF-A01).

NCEER-89-0019 "Nonlinear Dynamic Analysis of Three-Dimensional Base Isolated Structures (3D-BASIS)," by S. Nagarajaiah, A.M. Reinhorn and M.C. Constantinou, 8/3/89, (PB90-161936, A06, MF-A01). This report has been replaced by NCEER-93-0011.

NCEER-89-0020 "Structural Control Considering Time-Rate of Control Forces and Control Rate Constraints," by F.Y. Cheng and C.P. Pantelides, 8/3/89, (PB90-120445, A04, MF-A01).

NCEER-89-0021 "Subsurface Conditions of Memphis and Shelby County," by K.W. Ng, T-S. Chang and H-H.M. Hwang, 7/26/89, (PB90-120437, A03, MF-A01).

NCEER-89-0022 "Seismic Wave Propagation Effects on Straight Jointed Buried Pipelines," by K. Elhmadi and M.J. O'Rourke, 8/24/89, (PB90-162322, A10, MF-A02).

NCEER-89-0023 "Workshop on Serviceability Analysis of Water Delivery Systems," edited by M. Grigoriu, 3/6/89, (PB90-127424, A03, MF-A01).

NCEER-89-0024 "Shaking Table Study of a 1/5 Scale Steel Frame Composed of Tapered Members," by K.C. Chang, J.S. Hwang and G.C. Lee, 9/18/89, (PB90-160169, A04, MF-A01).

NCEER-89-0025 "DYNA1D: A Computer Program for Nonlinear Seismic Site Response Analysis - Technical Documentation," by Jean H. Prevost, 9/14/89, (PB90-161944, A07, MF-A01). This report is available only through NTIS (see address given above).

NCEER-89-0026 "1:4 Scale Model Studies of Active Tendon Systems and Active Mass Dampers for Aseismic Protection," by A.M. Reinhorn, T.T. Soong, R.C. Lin, Y.P. Yang, Y. Fukao, H. Abe and M. Nakai, 9/15/89, (PB90-173246, A10, MF-A02). This report is available only through NTIS (see address given above).

NCEER-89-0027 "Scattering of Waves by Inclusions in a Nonhomogeneous Elastic Half Space Solved by Boundary Element Methods," by P.K. Hadley, A. Askar and A.S. Cakmak, 6/15/89, (PB90-145699, A07, MF-A01).

NCEER-89-0028 "Statistical Evaluation of Deflection Amplification Factors for Reinforced Concrete Structures," by H.H.M. Hwang, J-W. Jaw and A.L. Ch'ng, 8/31/89, (PB90-164633, A05, MF-A01).

NCEER-89-0029 "Bedrock Accelerations in Memphis Area Due to Large New Madrid Earthquakes," by H.H.M. Hwang, C.H.S. Chen and G. Yu, 11/7/89, (PB90-162330, A04, MF-A01).

NCEER-89-0030 "Seismic Behavior and Response Sensitivity of Secondary Structural Systems," by Y.Q. Chen and T.T. Soong, 10/23/89, (PB90-164658, A08, MF-A01).

NCEER-89-0031 "Random Vibration and Reliability Analysis of Primary-Secondary Structural Systems," by Y. Ibrahim, M. Grigoriu and T.T. Soong, 11/10/89, (PB90-161951, A04, MF-A01).

NCEER-89-0032 "Proceedings from the Second U.S. - Japan Workshop on Liquefaction, Large Ground Deformation and Their Effects on Lifelines, September 26-29, 1989," Edited by T.D. O'Rourke and M. Hamada, 12/1/89, (PB90-209388, A22, MF-A03).

NCEER-89-0033 "Deterministic Model for Seismic Damage Evaluation of Reinforced Concrete Structures," by J.M. Bracci, A.M. Reinhorn, J.B. Mander and S.K. Kunnath, 9/27/89, (PB91-108803, A06, MF-A01).

NCEER-89-0034 "On the Relation Between Local and Global Damage Indices," by E. DiPasquale and A.S. Cakmak, 8/15/89, (PB90-173865, A05, MF-A01).

NCEER-89-0035 "Cyclic Undrained Behavior of Nonplastic and Low Plasticity Silts," by A.J. Walker and H.E. Stewart, 7/26/89, (PB90-183518, A10, MF-A01).

NCEER-89-0036 "Liquefaction Potential of Surficial Deposits in the City of Buffalo, New York," by M. Budhu, R. Giese and L. Baumgrass, 1/17/89, (PB90-208455, A04, MF-A01).

NCEER-89-0037 "A Deterministic Assessment of Effects of Ground Motion Incoherence," by A.S. Veletsos and Y. Tang, 7/15/89, (PB90-164294, A03, MF-A01).

NCEER-89-0038 "Workshop on Ground Motion Parameters for Seismic Hazard Mapping," July 17-18, 1989, edited by R.V. Whitman, 12/1/89, (PB90-173923, A04, MF-A01).

NCEER-89-0039 "Seismic Effects on Elevated Transit Lines of the New York City Transit Authority," by C.J. Costantino, C.A. Miller and E. Heymsfield, 12/26/89, (PB90-207887, A06, MF-A01).

NCEER-89-0040 "Centrifugal Modeling of Dynamic Soil-Structure Interaction," by K. Weissman, Supervised by J.H. Prevost, 5/10/89, (PB90-207879, A07, MF-A01).

NCEER-89-0041 "Linearized Identification of Buildings With Cores for Seismic Vulnerability Assessment," by I-K. Ho and A.E. Aktan, 11/1/89, (PB90-251943, A07, MF-A01).

NCEER-90-0001 "Geotechnical and Lifeline Aspects of the October 17, 1989 Loma Prieta Earthquake in San Francisco," by T.D. O'Rourke, H.E. Stewart, F.T. Blackburn and T.S. Dickerman, 1/90, (PB90-208596, A05, MF-A01).

NCEER-90-0002 "Nonnormal Secondary Response Due to Yielding in a Primary Structure," by D.C.K. Chen and L.D. Lutes, 2/28/90, (PB90-251976, A07, MF-A01).

NCEER-90-0003 "Earthquake Education Materials for Grades K-12," by K.E.K. Ross, 4/16/90, (PB91-251984, A05, MF-A05). This report has been replaced by NCEER-92-0018.

NCEER-90-0004 "Catalog of Strong Motion Stations in Eastern North America," by R.W. Busby, 4/3/90, (PB90-251984, A05, MF-A01).

NCEER-90-0005 "NCEER Strong-Motion Data Base: A User Manual for the GeoBase Release (Version 1.0 for the Sun3)," by P. Friberg and K. Jacob, 3/31/90 (PB90-258062, A04, MF-A01).

NCEER-90-0006 "Seismic Hazard Along a Crude Oil Pipeline in the Event of an 1811-1812 Type New Madrid Earthquake," by H.H.M. Hwang and C-H.S. Chen, 4/16/90, (PB90-258054, A04, MF-A01).

NCEER-90-0007 "Site-Specific Response Spectra for Memphis Sheahan Pumping Station," by H.H.M. Hwang and C.S. Lee, 5/15/90, (PB91-108811, A05, MF-A01).

NCEER-90-0008 "Pilot Study on Seismic Vulnerability of Crude Oil Transmission Systems," by T. Ariman, R. Dobry, M. Grigoriu, F. Kozin, M. O'Rourke, T. O'Rourke and M. Shinozuka, 5/25/90, (PB91-108837, A06, MF-A01).

NCEER-90-0009 "A Program to Generate Site Dependent Time Histories: EQGEN," by G.W. Ellis, M. Srinivasan and A.S. Cakmak, 1/30/90, (PB91-108829, A04, MF-A01).

NCEER-90-0010 "Active Isolation for Seismic Protection of Operating Rooms," by M.E. Talbott, Supervised by M. Shinozuka, 6/8/9, (PB91-110205, A05, MF-A01).

NCEER-90-0011 "Program LINEARID for Identification of Linear Structural Dynamic Systems," by C-B. Yun and M. Shinozuka, 6/25/90, (PB91-110312, A08, MF-A01).

NCEER-90-0012 "Two-Dimensional Two-Phase Elasto-Plastic Seismic Response of Earth Dams," by A.N. Yiagos, Supervised by J.H. Prevost, 6/20/90, (PB91-110197, A13, MF-A02).

NCEER-90-0013 "Secondary Systems in Base-Isolated Structures: Experimental Investigation, Stochastic Response and Stochastic Sensitivity," by G.D. Manolis, G. Juhn, M.C. Constantinou and A.M. Reinhorn, 7/1/90, (PB91-110320, A08, MF-A01).

NCEER-90-0014 "Seismic Behavior of Lightly-Reinforced Concrete Column and Beam-Column Joint Details," by S.P. Pessiki, C.H. Conley, P. Gergely and R.N. White, 8/22/90, (PB91-108795, A11, MF-A02).

NCEER-90-0015 "Two Hybrid Control Systems for Building Structures Under Strong Earthquakes," by J.N. Yang and A. Danielians, 6/29/90, (PB91-125393, A04, MF-A01).

NCEER-90-0016 "Instantaneous Optimal Control with Acceleration and Velocity Feedback," by J.N. Yang and Z. Li, 6/29/90, (PB91-125401, A03, MF-A01).

NCEER-90-0017 "Reconnaissance Report on the Northern Iran Earthquake of June 21, 1990," by M. Mehrain, 10/4/90, (PB91-125377, A03, MF-A01).

NCEER-90-0018 "Evaluation of Liquefaction Potential in Memphis and Shelby County," by T.S. Chang, P.S. Tang, C.S. Lee and H. Hwang, 8/10/90, (PB91-125427, A09, MF-A01).

NCEER-90-0019 "Experimental and Analytical Study of a Combined Sliding Disc Bearing and Helical Steel Spring Isolation System," by M.C. Constantinou, A.S. Mokha and A.M. Reinhorn, 10/4/90, (PB91-125385, A06, MF-A01). This report is available only through NTIS (see address given above).

NCEER-90-0020 "Experimental Study and Analytical Prediction of Earthquake Response of a Sliding Isolation System with a Spherical Surface," by A.S. Mokha, M.C. Constantinou and A.M. Reinhorn, 10/11/90, (PB91-125419, A05, MF-A01).

NCEER-90-0021 "Dynamic Interaction Factors for Floating Pile Groups," by G. Gazetas, K. Fan, A. Kaynia and E. Kausel, 9/10/90, (PB91-170381, A05, MF-A01).

NCEER-90-0022 "Evaluation of Seismic Damage Indices for Reinforced Concrete Structures," by S. Rodriguez-Gomez and A.S. Cakmak, 9/30/90, PB91-171322, A06, MF-A01).

NCEER-90-0023 "Study of Site Response at a Selected Memphis Site," by H. Desai, S. Ahmad, E.S. Gazetas and M.R. Oh, 10/11/90, (PB91-196857, A03, MF-A01).

NCEER-90-0024 "A User's Guide to Strongmo: Version 1.0 of NCEER's Strong-Motion Data Access Tool for PCs and Terminals," by P.A. Friberg and C.A.T. Susch, 11/15/90, (PB91-171272, A03, MF-A01).

NCEER-90-0025 "A Three-Dimensional Analytical Study of Spatial Variability of Seismic Ground Motions," by L-L. Hong and A.H.-S. Ang, 10/30/90, (PB91-170399, A09, MF-A01).

NCEER-90-0026 "MUMOID User's Guide - A Program for the Identification of Modal Parameters," by S. Rodriguez-Gomez and E. DiPasquale, 9/30/90, (PB91-171298, A04, MF-A01).

NCEER-90-0027 "SARCF-II User's Guide - Seismic Analysis of Reinforced Concrete Frames," by S. Rodriguez-Gomez, Y.S. Chung and C. Meyer, 9/30/90, (PB91-171280, A05, MF-A01).

NCEER-90-0028 "Viscous Dampers: Testing, Modeling and Application in Vibration and Seismic Isolation," by N. Makris and M.C. Constantinou, 12/20/90 (PB91-190561, A06, MF-A01).

NCEER-90-0029 "Soil Effects on Earthquake Ground Motions in the Memphis Area," by H. Hwang, C.S. Lee, K.W. Ng and T.S. Chang, 8/2/90, (PB91-190751, A05, MF-A01).

NCEER-91-0001 "Proceedings from the Third Japan-U.S. Workshop on Earthquake Resistant Design of Lifeline Facilities and Countermeasures for Soil Liquefaction, December 17-19, 1990," edited by T.D. O'Rourke and M. Hamada, 2/1/91, (PB91-179259, A99, MF-A04).

NCEER-91-0002 "Physical Space Solutions of Non-Proportionally Damped Systems," by M. Tong, Z. Liang and G.C. Lee, 1/15/91, (PB91-179242, A04, MF-A01).

NCEER-91-0003 "Seismic Response of Single Piles and Pile Groups," by K. Fan and G. Gazetas, 1/10/91, (PB92-174994, A04, MF-A01).

NCEER-91-0004 "Damping of Structures: Part 1 - Theory of Complex Damping," by Z. Liang and G. Lee, 10/10/91, (PB92-197235, A12, MF-A03).

NCEER-91-0005 "3D-BASIS - Nonlinear Dynamic Analysis of Three Dimensional Base Isolated Structures: Part II," by S. Nagarajaiah, A.M. Reinhorn and M.C. Constantinou, 2/28/91, (PB91-190553, A07, MF-A01). This report has been replaced by NCEER-93-0011.

NCEER-91-0006 "A Multidimensional Hysteretic Model for Plasticity Deforming Metals in Energy Absorbing Devices," by E.J. Graesser and F.A. Cozzarelli, 4/9/91, (PB92-108364, A04, MF-A01).

NCEER-91-0007 "A Framework for Customizable Knowledge-Based Expert Systems with an Application to a KBES for Evaluating the Seismic Resistance of Existing Buildings," by E.G. Ibarra-Anaya and S.J. Fenves, 4/9/91, (PB91-210930, A08, MF-A01).

NCEER-91-0008 "Nonlinear Analysis of Steel Frames with Semi-Rigid Connections Using the Capacity Spectrum Method," by G.G. Deierlein, S-H. Hsieh, Y-J. Shen and J.F. Abel, 7/2/91, (PB92-113828, A05, MF-A01).

NCEER-91-0009 "Earthquake Education Materials for Grades K-12," by K.E.K. Ross, 4/30/91, (PB91-212142, A06, MF-A01). This report has been replaced by NCEER-92-0018.

NCEER-91-0010 "Phase Wave Velocities and Displacement Phase Differences in a Harmonically Oscillating Pile," by N. Makris and G. Gazetas, 7/8/91, (PB92-108356, A04, MF-A01).

NCEER-91-0011 "Dynamic Characteristics of a Full-Size Five-Story Steel Structure and a 2/5 Scale Model," by K.C. Chang, G.C. Yao, G.C. Lee, D.S. Hao and Y.C. Yeh," 7/2/91, (PB93-116648, A06, MF-A02).

NCEER-91-0012 "Seismic Response of a 2/5 Scale Steel Structure with Added Viscoelastic Dampers," by K.C. Chang, T.T. Soong, S-T. Oh and M.L. Lai, 5/17/91, (PB92-110816, A05, MF-A01).

NCEER-91-0013 "Earthquake Response of Retaining Walls; Full-Scale Testing and Computational Modeling," by S. Alampalli and A-W.M. Elgamal, 6/20/91, not available.

NCEER-91-0014 "3D-BASIS-M: Nonlinear Dynamic Analysis of Multiple Building Base Isolated Structures," by P.C. Tsopelas, S. Nagarajaiah, M.C. Constantinou and A.M. Reinhorn, 5/28/91, (PB92-113885, A09, MF-A02).

NCEER-91-0015 "Evaluation of SEAOC Design Requirements for Sliding Isolated Structures," by D. Theodossiou and M.C. Constantinou, 6/10/91, (PB92-114602, A11, MF-A03).

NCEER-91-0016 "Closed-Loop Modal Testing of a 27-Story Reinforced Concrete Flat Plate-Core Building," by H.R. Somaprasad, T. Toksoy, H. Yoshiyuki and A.E. Aktan, 7/15/91, (PB92-129980, A07, MF-A02).

NCEER-91-0017 "Shake Table Test of a 1/6 Scale Two-Story Lightly Reinforced Concrete Building," by A.G. El-Attar, R.N. White and P. Gergely, 2/28/91, (PB92-222447, A06, MF-A02).

NCEER-91-0018 "Shake Table Test of a 1/8 Scale Three-Story Lightly Reinforced Concrete Building," by A.G. El-Attar, R.N. White and P. Gergely, 2/28/91, (PB93-116630, A08, MF-A02).

NCEER-91-0019 "Transfer Functions for Rigid Rectangular Foundations," by A.S. Veletsos, A.M. Prasad and W.H. Wu, 7/31/91, not available.

NCEER-91-0020 "Hybrid Control of Seismic-Excited Nonlinear and Inelastic Structural Systems," by J.N. Yang, Z. Li and A. Danielians, 8/1/91, (PB92-143171, A06, MF-A02).

NCEER-91-0021 "The NCEER-91 Earthquake Catalog: Improved Intensity-Based Magnitudes and Recurrence Relations for U.S. Earthquakes East of New Madrid," by L. Seeber and J.G. Armbruster, 8/28/91, (PB92-176742, A06, MF-A02).

NCEER-91-0022 "Proceedings from the Implementation of Earthquake Planning and Education in Schools: The Need for Change - The Roles of the Changemakers," by K.E.K. Ross and F. Winslow, 7/23/91, (PB92-129998, A12, MF-A03).

NCEER-91-0023 "A Study of Reliability-Based Criteria for Seismic Design of Reinforced Concrete Frame Buildings," by H.H.M. Hwang and H-M. Hsu, 8/10/91, (PB92-140235, A09, MF-A02).

NCEER-91-0024 "Experimental Verification of a Number of Structural System Identification Algorithms," by R.G. Ghanem, H. Gavin and M. Shinozuka, 9/18/91, (PB92-176577, A18, MF-A04).

NCEER-91-0025 "Probabilistic Evaluation of Liquefaction Potential," by H.H.M. Hwang and C.S. Lee," 11/25/91, (PB92-143429, A05, MF-A01).

NCEER-91-0026 "Instantaneous Optimal Control for Linear, Nonlinear and Hysteretic Structures - Stable Controllers," by J.N. Yang and Z. Li, 11/15/91, (PB92-163807, A04, MF-A01).

NCEER-91-0027 "Experimental and Theoretical Study of a Sliding Isolation System for Bridges," by M.C. Constantinou, A. Kartoum, A.M. Reinhorn and P. Bradford, 11/15/91, (PB92-176973, A10, MF-A03).

NCEER-92-0001 "Case Studies of Liquefaction and Lifeline Performance During Past Earthquakes, Volume 1: Japanese Case Studies," Edited by M. Hamada and T. O'Rourke, 2/17/92, (PB92-197243, A18, MF-A04).

NCEER-92-0002 "Case Studies of Liquefaction and Lifeline Performance During Past Earthquakes, Volume 2: United States Case Studies," Edited by T. O'Rourke and M. Hamada, 2/17/92, (PB92-197250, A20, MF-A04).

NCEER-92-0003 "Issues in Earthquake Education," Edited by K. Ross, 2/3/92, (PB92-222389, A07, MF-A02).

NCEER-92-0004 "Proceedings from the First U.S. - Japan Workshop on Earthquake Protective Systems for Bridges," Edited by I.G. Buckle, 2/4/92, (PB94-142239, A99, MF-A06).

NCEER-92-0005 "Seismic Ground Motion from a Haskell-Type Source in a Multiple-Layered Half-Space," A.P. Theoharis, G. Deodatis and M. Shinozuka, 1/2/92, not available.

NCEER-92-0006 "Proceedings from the Site Effects Workshop," Edited by R. Whitman, 2/29/92, (PB92-197201, A04, MF-A01).

NCEER-92-0007 "Engineering Evaluation of Permanent Ground Deformations Due to Seismically-Induced Liquefaction," by M.H. Baziar, R. Dobry and A-W.M. Elgamal, 3/24/92, (PB92-222421, A13, MF-A03).

NCEER-92-0008 "A Procedure for the Seismic Evaluation of Buildings in the Central and Eastern United States," by C.D. Poland and J.O. Malley, 4/2/92, (PB92-222439, A20, MF-A04).

NCEER-92-0009 "Experimental and Analytical Study of a Hybrid Isolation System Using Friction Controllable Sliding Bearings," by M.Q. Feng, S. Fujii and M. Shinozuka, 5/15/92, (PB93-150282, A06, MF-A02).

NCEER-92-0010 "Seismic Resistance of Slab-Column Connections in Existing Non-Ductile Flat-Plate Buildings," by A.J. Durrani and Y. Du, 5/18/92, (PB93-116812, A06, MF-A02).

NCEER-92-0011 "The Hysteretic and Dynamic Behavior of Brick Masonry Walls Upgraded by Ferrocement Coatings Under Cyclic Loading and Strong Simulated Ground Motion," by H. Lee and S.P. Prawel, 5/11/92, not available.

NCEER-92-0012 "Study of Wire Rope Systems for Seismic Protection of Equipment in Buildings," by G.F. Demetriades, M.C. Constantinou and A.M. Reinhorn, 5/20/92, (PB93-116655, A08, MF-A02).

NCEER-92-0013 "Shape Memory Structural Dampers: Material Properties, Design and Seismic Testing," by P.R. Witting and F.A. Cozzarelli, 5/26/92, (PB93-116663, A05, MF-A01).

NCEER-92-0014 "Longitudinal Permanent Ground Deformation Effects on Buried Continuous Pipelines," by M.J. O'Rourke, and C. Nordberg, 6/15/92, (PB93-116671, A08, MF-A02).

NCEER-92-0015 "A Simulation Method for Stationary Gaussian Random Functions Based on the Sampling Theorem," by M. Grigoriu and S. Balopoulou, 6/11/92, (PB93-127496, A05, MF-A01).

NCEER-92-0016 "Gravity-Load-Designed Reinforced Concrete Buildings: Seismic Evaluation of Existing Construction and Detailing Strategies for Improved Seismic Resistance," by G.W. Hoffmann, S.K. Kunnath, A.M. Reinhorn and J.B. Mander, 7/15/92, (PB94-142007, A08, MF-A02).

NCEER-92-0017 "Observations on Water System and Pipeline Performance in the Limón Area of Costa Rica Due to the April 22, 1991 Earthquake," by M. O'Rourke and D. Ballantyne, 6/30/92, (PB93-126811, A06, MF-A02).

NCEER-92-0018 "Fourth Edition of Earthquake Education Materials for Grades K-12," Edited by K.E.K. Ross, 8/10/92, (PB93-114023, A07, MF-A02).

NCEER-92-0019 "Proceedings from the Fourth Japan-U.S. Workshop on Earthquake Resistant Design of Lifeline Facilities and Countermeasures for Soil Liquefaction," Edited by M. Hamada and T.D. O'Rourke, 8/12/92, (PB93-163939, A99, MF-E11).

NCEER-92-0020 "Active Bracing System: A Full Scale Implementation of Active Control," by A.M. Reinhorn, T.T. Soong, R.C. Lin, M.A. Riley, Y.P. Wang, S. Aizawa and M. Higashino, 8/14/92, (PB93-127512, A06, MF-A02).

NCEER-92-0021 "Empirical Analysis of Horizontal Ground Displacement Generated by Liquefaction-Induced Lateral Spreads," by S.F. Bartlett and T.L. Youd, 8/17/92, (PB93-188241, A06, MF-A02).

NCEER-92-0022 "IDARC Version 3.0: Inelastic Damage Analysis of Reinforced Concrete Structures," by S.K. Kunnath, A.M. Reinhorn and R.F. Lobo, 8/31/92, (PB93-227502, A07, MF-A02).

NCEER-92-0023 "A Semi-Empirical Analysis of Strong-Motion Peaks in Terms of Seismic Source, Propagation Path and Local Site Conditions, by M. Kamiyama, M.J. O'Rourke and R. Flores-Berrones, 9/9/92, (PB93-150266, A08, MF-A02).

NCEER-92-0024 "Seismic Behavior of Reinforced Concrete Frame Structures with Nonductile Details, Part I: Summary of Experimental Findings of Full Scale Beam-Column Joint Tests," by A. Beres, R.N. White and P. Gergely, 9/30/92, (PB93-227783, A05, MF-A01).

NCEER-92-0025 "Experimental Results of Repaired and Retrofitted Beam-Column Joint Tests in Lightly Reinforced Concrete Frame Buildings," by A. Beres, S. El-Borgi, R.N. White and P. Gergely, 10/29/92, (PB93-227791, A05, MF-A01).

NCEER-92-0026 "A Generalization of Optimal Control Theory: Linear and Nonlinear Structures," by J.N. Yang, Z. Li and S. Vongchavalitkul, 11/2/92, (PB93-188621, A05, MF-A01).

NCEER-92-0027 "Seismic Resistance of Reinforced Concrete Frame Structures Designed Only for Gravity Loads: Part I - Design and Properties of a One-Third Scale Model Structure," by J.M. Bracci, A.M. Reinhorn and J.B. Mander, 12/1/92, (PB94-104502, A08, MF-A02).

NCEER-92-0028 "Seismic Resistance of Reinforced Concrete Frame Structures Designed Only for Gravity Loads: Part II - Experimental Performance of Subassemblages," by L.E. Aycardi, J.B. Mander and A.M. Reinhorn, 12/1/92, (PB94-104510, A08, MF-A02).

NCEER-92-0029 "Seismic Resistance of Reinforced Concrete Frame Structures Designed Only for Gravity Loads: Part III - Experimental Performance and Analytical Study of a Structural Model," by J.M. Bracci, A.M. Reinhorn and J.B. Mander, 12/1/92, (PB93-227528, A09, MF-A01).

NCEER-92-0030 "Evaluation of Seismic Retrofit of Reinforced Concrete Frame Structures: Part I - Experimental Performance of Retrofitted Subassemblages," by D. Choudhuri, J.B. Mander and A.M. Reinhorn, 12/8/92, (PB93-198307, A07, MF-A02).

NCEER-92-0031 "Evaluation of Seismic Retrofit of Reinforced Concrete Frame Structures: Part II - Experimental Performance and Analytical Study of a Retrofitted Structural Model," by J.M. Bracci, A.M. Reinhorn and J.B. Mander, 12/8/92, (PB93-198315, A09, MF-A03).

NCEER-92-0032 "Experimental and Analytical Investigation of Seismic Response of Structures with Supplemental Fluid Viscous Dampers," by M.C. Constantinou and M.D. Symans, 12/21/92, (PB93-191435, A10, MF-A03). This report is available only through NTIS (see address given above).

NCEER-92-0033 "Reconnaissance Report on the Cairo, Egypt Earthquake of October 12, 1992," by M. Khater, 12/23/92, (PB93-188621, A03, MF-A01).

NCEER-92-0034 "Low-Level Dynamic Characteristics of Four Tall Flat-Plate Buildings in New York City," by H. Gavin, S. Yuan, J. Grossman, E. Pekelis and K. Jacob, 12/28/92, (PB93-188217, A07, MF-A02).

NCEER-93-0001 "An Experimental Study on the Seismic Performance of Brick-Infilled Steel Frames With and Without Retrofit," by J.B. Mander, B. Nair, K. Wojtkowski and J. Ma, 1/29/93, (PB93-227510, A07, MF-A02).

NCEER-93-0002 "Social Accounting for Disaster Preparedness and Recovery Planning," by S. Cole, E. Pantoja and V. Razak, 2/22/93, (PB94-142114, A12, MF-A03).

NCEER-93-0003 "Assessment of 1991 NEHRP Provisions for Nonstructural Components and Recommended Revisions," by T.T. Soong, G. Chen, Z. Wu, R-H. Zhang and M. Grigoriu, 3/1/93, (PB93-188639, A06, MF-A02).

NCEER-93-0004 "Evaluation of Static and Response Spectrum Analysis Procedures of SEAOC/UBC for Seismic Isolated Structures," by C.W. Winters and M.C. Constantinou, 3/23/93, (PB93-198299, A10, MF-A03).

NCEER-93-0005 "Earthquakes in the Northeast - Are We Ignoring the Hazard? A Workshop on Earthquake Science and Safety for Educators," edited by K.E.K. Ross, 4/2/93, (PB94-103066, A09, MF-A02).

NCEER-93-0006 "Inelastic Response of Reinforced Concrete Structures with Viscoelastic Braces," by R.F. Lobo, J.M. Bracci, K.L. Shen, A.M. Reinhorn and T.T. Soong, 4/5/93, (PB93-227486, A05, MF-A02).

NCEER-93-0007 "Seismic Testing of Installation Methods for Computers and Data Processing Equipment," by K. Kosar, T.T. Soong, K.L. Shen, J.A. HoLung and Y.K. Lin, 4/12/93, (PB93-198299, A07, MF-A02).

NCEER-93-0008 "Retrofit of Reinforced Concrete Frames Using Added Dampers," by A. Reinhorn, M. Constantinou and C. Li, not available.

NCEER-93-0009 "Seismic Behavior and Design Guidelines for Steel Frame Structures with Added Viscoelastic Dampers," by K.C. Chang, M.L. Lai, T.T. Soong, D.S. Hao and Y.C. Yeh, 5/1/93, (PB94-141959, A07, MF-A02).

NCEER-93-0010 "Seismic Performance of Shear-Critical Reinforced Concrete Bridge Piers," by J.B. Mander, S.M. Waheed, M.T.A. Chaudhary and S.S. Chen, 5/12/93, (PB93-227494, A08, MF-A02).

NCEER-93-0011 "3D-BASIS-TABS: Computer Program for Nonlinear Dynamic Analysis of Three Dimensional Base Isolated Structures," by S. Nagarajaiah, C. Li, A.M. Reinhorn and M.C. Constantinou, 8/2/93, (PB94-141819, A09, MF-A02).

NCEER-93-0012 "Effects of Hydrocarbon Spills from an Oil Pipeline Break on Ground Water," by O.J. Helweg and H.H.M. Hwang, 8/3/93, (PB94-141942, A06, MF-A02).

NCEER-93-0013 "Simplified Procedures for Seismic Design of Nonstructural Components and Assessment of Current Code Provisions," by M.P. Singh, L.E. Suarez, E.E. Matheu and G.O. Maldonado, 8/4/93, (PB94-141827, A09, MF-A02).

NCEER-93-0014 "An Energy Approach to Seismic Analysis and Design of Secondary Systems," by G. Chen and T.T. Soong, 8/6/93, (PB94-142767, A11, MF-A03).

NCEER-93-0015 "Proceedings from School Sites: Becoming Prepared for Earthquakes - Commemorating the Third Anniversary of the Loma Prieta Earthquake," Edited by F.E. Winslow and K.E.K. Ross, 8/16/93, (PB94-154275, A16, MF-A02).

NCEER-93-0016 "Reconnaissance Report of Damage to Historic Monuments in Cairo, Egypt Following the October 12, 1992 Dahshur Earthquake," by D. Sykora, D. Look, G. Croci, E. Karaesmen and E. Karaesmen, 8/19/93, (PB94-142221, A08, MF-A02).

NCEER-93-0017 "The Island of Guam Earthquake of August 8, 1993," by S.W. Swan and S.K. Harris, 9/30/93, (PB94-141843, A04, MF-A01).

NCEER-93-0018 "Engineering Aspects of the October 12, 1992 Egyptian Earthquake," by A.W. Elgamal, M. Amer, K. Adalier and A. Abul-Fadl, 10/7/93, (PB94-141983, A05, MF-A01).

NCEER-93-0019 "Development of an Earthquake Motion Simulator and its Application in Dynamic Centrifuge Testing," by I. Krstelj, Supervised by J.H. Prevost, 10/23/93, (PB94-181773, A-10, MF-A03).

NCEER-93-0020 "NCEER-Taisei Corporation Research Program on Sliding Seismic Isolation Systems for Bridges: Experimental and Analytical Study of a Friction Pendulum System (FPS)," by M.C. Constantinou, P. Tsopelas, Y-S. Kim and S. Okamoto, 11/1/93, (PB94-142775, A08, MF-A02).

NCEER-93-0021 "Finite Element Modeling of Elastomeric Seismic Isolation Bearings," by L.J. Billings, Supervised by R. Shepherd, 11/8/93, not available.

NCEER-93-0022 "Seismic Vulnerability of Equipment in Critical Facilities: Life-Safety and Operational Consequences," by K. Porter, G.S. Johnson, M.M. Zadeh, C. Scawthorn and S. Eder, 11/24/93, (PB94-181765, A16, MF-A03).

NCEER-93-0023 "Hokkaido Nansei-oki, Japan Earthquake of July 12, 1993, by P.I. Yanev and C.R. Scawthorn, 12/23/93, (PB94-181500, A07, MF-A01).

NCEER-94-0001 "An Evaluation of Seismic Serviceability of Water Supply Networks with Application to the San Francisco Auxiliary Water Supply System," by I. Markov, Supervised by M. Grigoriu and T. O'Rourke, 1/21/94, (PB94-204013, A07, MF-A02).

NCEER-94-0002 "NCEER-Taisei Corporation Research Program on Sliding Seismic Isolation Systems for Bridges: Experimental and Analytical Study of Systems Consisting of Sliding Bearings, Rubber Restoring Force Devices and Fluid Dampers," Volumes I and II, by P. Tsopelas, S. Okamoto, M.C. Constantinou, D. Ozaki and S. Fujii, 2/4/94, (PB94-181740, A09, MF-A02 and PB94-181757, A12, MF-A03).

NCEER-94-0003 "A Markov Model for Local and Global Damage Indices in Seismic Analysis," by S. Rahman and M. Grigoriu, 2/18/94, (PB94-206000, A12, MF-A03).

NCEER-94-0004 "Proceedings from the NCEER Workshop on Seismic Response of Masonry Infills," edited by D.P. Abrams, 3/1/94, (PB94-180783, A07, MF-A02).

NCEER-94-0005 "The Northridge, California Earthquake of January 17, 1994: General Reconnaissance Report," edited by J.D. Goltz, 3/11/94, (PB94-193943, A10, MF-A03).

NCEER-94-0006 "Seismic Energy Based Fatigue Damage Analysis of Bridge Columns: Part I - Evaluation of Seismic Capacity," by G.A. Chang and J.B. Mander, 3/14/94, (PB94-219185, A11, MF-A03).

NCEER-94-0007 "Seismic Isolation of Multi-Story Frame Structures Using Spherical Sliding Isolation Systems," by T.M. Al-Hussaini, V.A. Zayas and M.C. Constantinou, 3/17/94, (PB94-193745, A09, MF-A02).

NCEER-94-0008 "The Northridge, California Earthquake of January 17, 1994: Performance of Highway Bridges," edited by I.G. Buckle, 3/24/94, (PB94-193851, A06, MF-A02).

NCEER-94-0009 "Proceedings of the Third U.S.-Japan Workshop on Earthquake Protective Systems for Bridges," edited by I.G. Buckle and I. Friedland, 3/31/94, (PB94-195815, A99, MF-A06).

NCEER-94-0010 "3D-BASIS-ME: Computer Program for Nonlinear Dynamic Analysis of Seismically Isolated Single and Multiple Structures and Liquid Storage Tanks," by P.C. Tsopelas, M.C. Constantinou and A.M. Reinhorn, 4/12/94, (PB94-204922, A09, MF-A02).

NCEER-94-0011 "The Northridge, California Earthquake of January 17, 1994: Performance of Gas Transmission Pipelines," by T.D. O'Rourke and M.C. Palmer, 5/16/94, (PB94-204989, A05, MF-A01).

NCEER-94-0012 "Feasibility Study of Replacement Procedures and Earthquake Performance Related to Gas Transmission Pipelines," by T.D. O'Rourke and M.C. Palmer, 5/25/94, (PB94-206638, A09, MF-A02).

NCEER-94-0013 "Seismic Energy Based Fatigue Damage Analysis of Bridge Columns: Part II - Evaluation of Seismic Demand," by G.A. Chang and J.B. Mander, 6/1/94, (PB95-18106, A08, MF-A02).

NCEER-94-0014 "NCEER-Taisei Corporation Research Program on Sliding Seismic Isolation Systems for Bridges: Experimental and Analytical Study of a System Consisting of Sliding Bearings and Fluid Restoring Force/Damping Devices," by P. Tsopelas and M.C. Constantinou, 6/13/94, (PB94-219144, A10, MF-A03).

NCEER-94-0015 "Generation of Hazard-Consistent Fragility Curves for Seismic Loss Estimation Studies," by H. Hwang and J-R. Huo, 6/14/94, (PB95-181996, A09, MF-A02).

NCEER-94-0016 "Seismic Study of Building Frames with Added Energy-Absorbing Devices," by W.S. Pong, C.S. Tsai and G.C. Lee, 6/20/94, (PB94-219136, A10, A03).

NCEER-94-0017 "Sliding Mode Control for Seismic-Excited Linear and Nonlinear Civil Engineering Structures," by J. Yang, J. Wu, A. Agrawal and Z. Li, 6/21/94, (PB95-138483, A06, MF-A02).

NCEER-94-0018 "3D-BASIS-TABS Version 2.0: Computer Program for Nonlinear Dynamic Analysis of Three Dimensional Base Isolated Structures," by A.M. Reinhorn, S. Nagarajaiah, M.C. Constantinou, P. Tsopelas and R. Li, 6/22/94, (PB95-182176, A08, MF-A02).

NCEER-94-0019 "Proceedings of the International Workshop on Civil Infrastructure Systems: Application of Intelligent Systems and Advanced Materials on Bridge Systems," Edited by G.C. Lee and K.C. Chang, 7/18/94, (PB95-252474, A20, MF-A04).

NCEER-94-0020 "Study of Seismic Isolation Systems for Computer Floors," by V. Lambrou and M.C. Constantinou, 7/19/94, (PB95-138533, A10, MF-A03).

NCEER-94-0021 "Proceedings of the U.S.-Italian Workshop on Guidelines for Seismic Evaluation and Rehabilitation of Unreinforced Masonry Buildings," Edited by D.P. Abrams and G.M. Calvi, 7/20/94, (PB95-138749, A13, MF-A03).

NCEER-94-0022 "NCEER-Taisei Corporation Research Program on Sliding Seismic Isolation Systems for Bridges: Experimental and Analytical Study of a System Consisting of Lubricated PTFE Sliding Bearings and Mild Steel Dampers," by P. Tsopelas and M.C. Constantinou, 7/22/94, (PB95-182184, A08, MF-A02).

NCEER-94-0023 “Development of Reliability-Based Design Criteria for Buildings Under Seismic Load,” by Y.K. Wen, H. Hwang and M. Shinozuka, 8/1/94, (PB95-211934, A08, MF-A02).

NCEER-94-0024 “Experimental Verification of Acceleration Feedback Control Strategies for an Active Tendon System,” by S.J. Dyke, B.F. Spencer, Jr., P. Quast, M.K. Sain, D.C. Kaspari, Jr. and T.T. Soong, 8/29/94, (PB95-212320, A05, MF-A01).

NCEER-94-0025 “Seismic Retrofitting Manual for Highway Bridges,” Edited by I.G. Buckle and I.F. Friedland, published by the Federal Highway Administration (PB95-212676, A15, MF-A03).

NCEER-94-0026 “Proceedings from the Fifth U.S.-Japan Workshop on Earthquake Resistant Design of Lifeline Facilities and Countermeasures Against Soil Liquefaction,” Edited by T.D. O’Rourke and M. Hamada, 11/7/94, (PB95-220802, A99, MF-E08).

NCEER-95-0001 "Experimental and Analytical Investigation of Seismic Retrofit of Structures with Supplemental Damping: Part 1 - Fluid Viscous Damping Devices," by A.M. Reinhorn, C. Li and M.C. Constantinou, 1/3/95, (PB95-266599, A09, MF-A02).

NCEER-95-0002 "Experimental and Analytical Study of Low-Cycle Fatigue Behavior of Semi-Rigid Top-And-Seat Angle Connections," by G. Pekcan, J.B. Mander and S.S. Chen, 1/5/95, (PB95-220042, A07, MF-A02).

NCEER-95-0003 "NCEER-ATC Joint Study on Fragility of Buildings," by T. Anagnos, C. Rojahn and A.S. Kiremidjian, 1/20/95, (PB95-220026, A06, MF-A02).

NCEER-95-0004 "Nonlinear Control Algorithms for Peak Response Reduction," by Z. Wu, T.T. Soong, V. Gattulli and R.C. Lin, 2/16/95, (PB95-220349, A05, MF-A01).

NCEER-95-0005 "Pipeline Replacement Feasibility Study: A Methodology for Minimizing Seismic and Corrosion Risks to Underground Natural Gas Pipelines," by R.T. Eguchi, H.A. Seligson and D.G. Honegger, 3/2/95, (PB95-252326, A06, MF-A02).

NCEER-95-0006 "Evaluation of Seismic Performance of an 11-Story Frame Building During the 1994 Northridge Earthquake," by F. Naeim, R. DiSulio, K. Benuska, A. Reinhorn and C. Li, not available.

NCEER-95-0007 "Prioritization of Bridges for Seismic Retrofitting," by N. Basöz and A.S. Kiremidjian, 4/24/95, (PB95-252300, A08, MF-A02).

NCEER-95-0008 "Method for Developing Motion Damage Relationships for Reinforced Concrete Frames," by A. Singhal and A.S. Kiremidjian, 5/11/95, (PB95-266607, A06, MF-A02).

NCEER-95-0009 "Experimental and Analytical Investigation of Seismic Retrofit of Structures with Supplemental Damping: Part II - Friction Devices," by C. Li and A.M. Reinhorn, 7/6/95, (PB96-128087, A11, MF-A03).

NCEER-95-0010 "Experimental Performance and Analytical Study of a Non-Ductile Reinforced Concrete Frame Structure Retrofitted with Elastomeric Spring Dampers," by G. Pekcan, J.B. Mander and S.S. Chen, 7/14/95, (PB96-137161, A08, MF-A02).

NCEER-95-0011 "Development and Experimental Study of Semi-Active Fluid Damping Devices for Seismic Protection of Structures," by M.D. Symans and M.C. Constantinou, 8/3/95, (PB96-136940, A23, MF-A04).

NCEER-95-0012 "Real-Time Structural Parameter Modification (RSPM): Development of Innervated Structures," by Z. Liang, M. Tong and G.C. Lee, 4/11/95, (PB96-137153, A06, MF-A01).

NCEER-95-0013 "Experimental and Analytical Investigation of Seismic Retrofit of Structures with Supplemental Damping: Part III - Viscous Damping Walls," by A.M. Reinhorn and C. Li, 10/1/95, (PB96-176409, A11, MF-A03).

NCEER-95-0014 "Seismic Fragility Analysis of Equipment and Structures in a Memphis Electric Substation," by J-R. Huo and H.H.M. Hwang, 8/10/95, (PB96-128087, A09, MF-A02).

NCEER-95-0015 "The Hanshin-Awaji Earthquake of January 17, 1995: Performance of Lifelines," Edited by M. Shinozuka, 11/3/95, (PB96-176383, A15, MF-A03).

NCEER-95-0016 "Highway Culvert Performance During Earthquakes," by T.L. Youd and C.J. Beckman, available as NCEER-96-0015.

NCEER-95-0017 "The Hanshin-Awaji Earthquake of January 17, 1995: Performance of Highway Bridges," Edited by I.G. Buckle, 12/1/95, not available.

NCEER-95-0018 "Modeling of Masonry Infill Panels for Structural Analysis," by A.M. Reinhorn, A. Madan, R.E. Valles, Y. Reichmann and J.B. Mander, 12/8/95, (PB97-110886, MF-A01, A06).

NCEER-95-0019 "Optimal Polynomial Control for Linear and Nonlinear Structures," by A.K. Agrawal and J.N. Yang, 12/11/95, (PB96-168737, A07, MF-A02).

NCEER-95-0020 "Retrofit of Non-Ductile Reinforced Concrete Frames Using Friction Dampers," by R.S. Rao, P. Gergely and R.N. White, 12/22/95, (PB97-133508, A10, MF-A02).

NCEER-95-0021 "Parametric Results for Seismic Response of Pile-Supported Bridge Bents," by G. Mylonakis, A. Nikolaou and G. Gazetas, 12/22/95, (PB97-100242, A12, MF-A03).

NCEER-95-0022 "Kinematic Bending Moments in Seismically Stressed Piles," by A. Nikolaou, G. Mylonakis and G. Gazetas, 12/23/95, (PB97-113914, MF-A03, A13).

NCEER-96-0001 "Dynamic Response of Unreinforced Masonry Buildings with Flexible Diaphragms," by A.C. Costley and D.P. Abrams," 10/10/96, (PB97-133573, MF-A03, A15).

NCEER-96-0002 "State of the Art Review: Foundations and Retaining Structures," by I. Po Lam, not available.

NCEER-96-0003 "Ductility of Rectangular Reinforced Concrete Bridge Columns with Moderate Confinement," by N. Wehbe, M. Saiidi, D. Sanders and B. Douglas, 11/7/96, (PB97-133557, A06, MF-A02).

NCEER-96-0004 "Proceedings of the Long-Span Bridge Seismic Research Workshop," edited by I.G. Buckle and I.M. Friedland, not available.

NCEER-96-0005 "Establish Representative Pier Types for Comprehensive Study: Eastern United States," by J. Kulicki and Z. Prucz, 5/28/96, (PB98-119217, A07, MF-A02).

NCEER-96-0006 "Establish Representative Pier Types for Comprehensive Study: Western United States," by R. Imbsen, R.A. Schamber and T.A. Osterkamp, 5/28/96, (PB98-118607, A07, MF-A02).

NCEER-96-0007 "Nonlinear Control Techniques for Dynamical Systems with Uncertain Parameters," by R.G. Ghanem and M.I. Bujakov, 5/27/96, (PB97-100259, A17, MF-A03).

NCEER-96-0008 "Seismic Evaluation of a 30-Year Old Non-Ductile Highway Bridge Pier and Its Retrofit," by J.B. Mander, B. Mahmoodzadegan, S. Bhadra and S.S. Chen, 5/31/96, (PB97-110902, MF-A03, A10).

NCEER-96-0009 "Seismic Performance of a Model Reinforced Concrete Bridge Pier Before and After Retrofit," by J.B. Mander, J.H. Kim and C.A. Ligozio, 5/31/96, (PB97-110910, MF-A02, A10).

NCEER-96-0010 "IDARC2D Version 4.0: A Computer Program for the Inelastic Damage Analysis of Buildings," by R.E. Valles, A.M. Reinhorn, S.K. Kunnath, C. Li and A. Madan, 6/3/96, (PB97-100234, A17, MF-A03).

NCEER-96-0011 "Estimation of the Economic Impact of Multiple Lifeline Disruption: Memphis Light, Gas and Water Division Case Study," by S.E. Chang, H.A. Seligson and R.T. Eguchi, 8/16/96, (PB97-133490, A11, MF-A03).

NCEER-96-0012 "Proceedings from the Sixth Japan-U.S. Workshop on Earthquake Resistant Design of Lifeline Facilities and Countermeasures Against Soil Liquefaction, Edited by M. Hamada and T. O'Rourke, 9/11/96, (PB97-133581, A99, MF-A06).

NCEER-96-0013 "Chemical Hazards, Mitigation and Preparedness in Areas of High Seismic Risk: A Methodology for Estimating the Risk of Post-Earthquake Hazardous Materials Release," by H.A. Seligson, R.T. Eguchi, K.J. Tierney and K. Richmond, 11/7/96, (PB97-133565, MF-A02, A08).

NCEER-96-0014 "Response of Steel Bridge Bearings to Reversed Cyclic Loading," by J.B. Mander, D-K. Kim, S.S. Chen and G.J. Premus, 11/13/96, (PB97-140735, A12, MF-A03).

NCEER-96-0015 "Highway Culvert Performance During Past Earthquakes," by T.L. Youd and C.J. Beckman, 11/25/96, (PB97-133532, A06, MF-A01).

NCEER-97-0001 "Evaluation, Prevention and Mitigation of Pounding Effects in Building Structures," by R.E. Valles and A.M. Reinhorn, 2/20/97, (PB97-159552, A14, MF-A03).

NCEER-97-0002 "Seismic Design Criteria for Bridges and Other Highway Structures," by C. Rojahn, R. Mayes, D.G. Anderson, J. Clark, J.H. Hom, R.V. Nutt and M.J. O'Rourke, 4/30/97, (PB97-194658, A06, MF-A03).

NCEER-97-0003 “Proceedings of the U.S.-Italian Workshop on Seismic Evaluation and Retrofit,” Edited by D.P. Abrams and G.M. Calvi, 3/19/97, (PB97-194666, A13, MF-A03).

NCEER-97-0004 "Investigation of Seismic Response of Buildings with Linear and Nonlinear Fluid Viscous Dampers," by A.A. Seleemah and M.C. Constantinou, 5/21/97, (PB98-109002, A15, MF-A03).

NCEER-97-0005 "Proceedings of the Workshop on Earthquake Engineering Frontiers in Transportation Facilities," edited by G.C. Lee and I.M. Friedland, 8/29/97, (PB98-128911, A25, MR-A04).

NCEER-97-0006 "Cumulative Seismic Damage of Reinforced Concrete Bridge Piers," by S.K. Kunnath, A. El-Bahy, A. Taylor and W. Stone, 9/2/97, (PB98-108814, A11, MF-A03).

NCEER-97-0007 "Structural Details to Accommodate Seismic Movements of Highway Bridges and Retaining Walls," by R.A. Imbsen, R.A. Schamber, E. Thorkildsen, A. Kartoum, B.T. Martin, T.N. Rosser and J.M. Kulicki, 9/3/97, (PB98-108996, A09, MF-A02).

NCEER-97-0008 "A Method for Earthquake Motion-Damage Relationships with Application to Reinforced Concrete Frames," by A. Singhal and A.S. Kiremidjian, 9/10/97, (PB98-108988, A13, MF-A03).

NCEER-97-0009 "Seismic Analysis and Design of Bridge Abutments Considering Sliding and Rotation," by K. Fishman and R. Richards, Jr., 9/15/97, (PB98-108897, A06, MF-A02).

NCEER-97-0010 "Proceedings of the FHWA/NCEER Workshop on the National Representation of Seismic Ground Motion for New and Existing Highway Facilities," edited by I.M. Friedland, M.S. Power and R.L. Mayes, 9/22/97, (PB98-128903, A21, MF-A04).

NCEER-97-0011 "Seismic Analysis for Design or Retrofit of Gravity Bridge Abutments," by K.L. Fishman, R. Richards, Jr. and R.C. Divito, 10/2/97, (PB98-128937, A08, MF-A02).

NCEER-97-0012 "Evaluation of Simplified Methods of Analysis for Yielding Structures," by P. Tsopelas, M.C. Constantinou, C.A. Kircher and A.S. Whittaker, 10/31/97, (PB98-128929, A10, MF-A03).

NCEER-97-0013 "Seismic Design of Bridge Columns Based on Control and Repairability of Damage," by C-T. Cheng and J.B. Mander, 12/8/97, (PB98-144249, A11, MF-A03).

NCEER-97-0014 "Seismic Resistance of Bridge Piers Based on Damage Avoidance Design," by J.B. Mander and C-T. Cheng, 12/10/97, (PB98-144223, A09, MF-A02).

NCEER-97-0015 “Seismic Response of Nominally Symmetric Systems with Strength Uncertainty,” by S. Balopoulou and M. Grigoriu, 12/23/97, (PB98-153422, A11, MF-A03).

NCEER-97-0016 “Evaluation of Seismic Retrofit Methods for Reinforced Concrete Bridge Columns,” by T.J. Wipf, F.W. Klaiber and F.M. Russo, 12/28/97, (PB98-144215, A12, MF-A03).

NCEER-97-0017 “Seismic Fragility of Existing Conventional Reinforced Concrete Highway Bridges,” by C.L. Mullen and A.S. Cakmak, 12/30/97, (PB98-153406, A08, MF-A02).

NCEER-97-0018 “Loss Asssessment of Memphis Buildings,” edited by D.P. Abrams and M. Shinozuka, 12/31/97, (PB98-144231, A13, MF-A03).

NCEER-97-0019 “Seismic Evaluation of Frames with Infill Walls Using Quasi-static Experiments,” by K.M. Mosalam, R.N. White and P. Gergely, 12/31/97, (PB98-153455, A07, MF-A02).

NCEER-97-0020 “Seismic Evaluation of Frames with Infill Walls Using Pseudo-dynamic Experiments,” by K.M. Mosalam, R.N. White and P. Gergely, 12/31/97, (PB98-153430, A07, MF-A02).

NCEER-97-0021 “Computational Strategies for Frames with Infill Walls: Discrete and Smeared Crack Analyses and Seismic Fragility,” by K.M. Mosalam, R.N. White and P. Gergely, 12/31/97, (PB98-153414, A10, MF-A02).

NCEER-97-0022 "Proceedings of the NCEER Workshop on Evaluation of Liquefaction Resistance of Soils," edited by T.L. Youd and I.M. Idriss, 12/31/97, (PB98-155617, A15, MF-A03).

MCEER-98-0001 "Extraction of Nonlinear Hysteretic Properties of Seismically Isolated Bridges from Quick-Release Field Tests," by Q. Chen, B.M. Douglas, E.M. Maragakis and I.G. Buckle, 5/26/98, (PB99-118838, A06, MF-A01).

MCEER-98-0002 "Methodologies for Evaluating the Importance of Highway Bridges," by A. Thomas, S. Eshenaur and J. Kulicki, 5/29/98, (PB99-118846, A10, MF-A02).

MCEER-98-0003 "Capacity Design of Bridge Piers and the Analysis of Overstrength," by J.B. Mander, A. Dutta and P. Goel, 6/1/98, (PB99-118853, A09, MF-A02).

MCEER-98-0004 "Evaluation of Bridge Damage Data from the Loma Prieta and Northridge, California Earthquakes," by N. Basoz and A. Kiremidjian, 6/2/98, (PB99-118861, A15, MF-A03).

MCEER-98-0005 "Screening Guide for Rapid Assessment of Liquefaction Hazard at Highway Bridge Sites," by T. L. Youd, 6/16/98, (PB99-118879, A06, not available on microfiche).

MCEER-98-0006 "Structural Steel and Steel/Concrete Interface Details for Bridges," by P. Ritchie, N. Kauhl and J. Kulicki, 7/13/98, (PB99-118945, A06, MF-A01).

MCEER-98-0007 "Capacity Design and Fatigue Analysis of Confined Concrete Columns," by A. Dutta and J.B. Mander, 7/14/98, (PB99-118960, A14, MF-A03).

MCEER-98-0008 "Proceedings of the Workshop on Performance Criteria for Telecommunication Services Under Earthquake Conditions," edited by A.J. Schiff, 7/15/98, (PB99-118952, A08, MF-A02).

MCEER-98-0009 "Fatigue Analysis of Unconfined Concrete Columns," by J.B. Mander, A. Dutta and J.H. Kim, 9/12/98, (PB99-123655, A10, MF-A02).

MCEER-98-0010 "Centrifuge Modeling of Cyclic Lateral Response of Pile-Cap Systems and Seat-Type Abutments in Dry Sands," by A.D. Gadre and R. Dobry, 10/2/98, (PB99-123606, A13, MF-A03).

MCEER-98-0011 "IDARC-BRIDGE: A Computational Platform for Seismic Damage Assessment of Bridge Structures," by A.M. Reinhorn, V. Simeonov, G. Mylonakis and Y. Reichman, 10/2/98, (PB99-162919, A15, MF-A03).

MCEER-98-0012 "Experimental Investigation of the Dynamic Response of Two Bridges Before and After Retrofitting with Elastomeric Bearings," by D.A. Wendichansky, S.S. Chen and J.B. Mander, 10/2/98, (PB99-162927, A15, MF-A03).

MCEER-98-0013 "Design Procedures for Hinge Restrainers and Hinge Sear Width for Multiple-Frame Bridges," by R. Des Roches and G.L. Fenves, 11/3/98, (PB99-140477, A13, MF-A03).

MCEER-98-0014 "Response Modification Factors for Seismically Isolated Bridges," by M.C. Constantinou and J.K. Quarshie, 11/3/98, (PB99-140485, A14, MF-A03).

MCEER-98-0015 "Proceedings of the U.S.-Italy Workshop on Seismic Protective Systems for Bridges," edited by I.M. Friedland and M.C. Constantinou, 11/3/98, (PB2000-101711, A22, MF-A04).

MCEER-98-0016 "Appropriate Seismic Reliability for Critical Equipment Systems: Recommendations Based on Regional Analysis of Financial and Life Loss," by K. Porter, C. Scawthorn, C. Taylor and N. Blais, 11/10/98, (PB99-157265, A08, MF-A02).

MCEER-98-0017 "Proceedings of the U.S. Japan Joint Seminar on Civil Infrastructure Systems Research," edited by M. Shinozuka and A. Rose, 11/12/98, (PB99-156713, A16, MF-A03).

MCEER-98-0018 "Modeling of Pile Footings and Drilled Shafts for Seismic Design," by I. PoLam, M. Kapuskar and D. Chaudhuri, 12/21/98, (PB99-157257, A09, MF-A02).

MCEER-99-0001 "Seismic Evaluation of a Masonry Infilled Reinforced Concrete Frame by Pseudodynamic Testing," by S.G. Buonopane and R.N. White, 2/16/99, (PB99-162851, A09, MF-A02).

MCEER-99-0002 "Response History Analysis of Structures with Seismic Isolation and Energy Dissipation Systems: Verification Examples for Program SAP2000," by J. Scheller and M.C. Constantinou, 2/22/99, (PB99-162869, A08, MF-A02).

MCEER-99-0003 "Experimental Study on the Seismic Design and Retrofit of Bridge Columns Including Axial Load Effects," by A. Dutta, T. Kokorina and J.B. Mander, 2/22/99, (PB99-162877, A09, MF-A02).

MCEER-99-0004 "Experimental Study of Bridge Elastomeric and Other Isolation and Energy Dissipation Systems with Emphasis on Uplift Prevention and High Velocity Near-source Seismic Excitation," by A. Kasalanati and M. C. Constantinou, 2/26/99, (PB99-162885, A12, MF-A03).

MCEER-99-0005 "Truss Modeling of Reinforced Concrete Shear-flexure Behavior," by J.H. Kim and J.B. Mander, 3/8/99, (PB99-163693, A12, MF-A03).

MCEER-99-0006 "Experimental Investigation and Computational Modeling of Seismic Response of a 1:4 Scale Model Steel Structure with a Load Balancing Supplemental Damping System," by G. Pekcan, J.B. Mander and S.S. Chen, 4/2/99, (PB99-162893, A11, MF-A03).

MCEER-99-0007 "Effect of Vertical Ground Motions on the Structural Response of Highway Bridges," by M.R. Button, C.J. Cronin and R.L. Mayes, 4/10/99, (PB2000-101411, A10, MF-A03).

MCEER-99-0008 "Seismic Reliability Assessment of Critical Facilities: A Handbook, Supporting Documentation, and Model Code Provisions," by G.S. Johnson, R.E. Sheppard, M.D. Quilici, S.J. Eder and C.R. Scawthorn, 4/12/99, (PB2000-101701, A18, MF-A04).

MCEER-99-0009 "Impact Assessment of Selected MCEER Highway Project Research on the Seismic Design of Highway Structures," by C. Rojahn, R. Mayes, D.G. Anderson, J.H. Clark, D'Appolonia Engineering, S. Gloyd and R.V. Nutt, 4/14/99, (PB99-162901, A10, MF-A02).

MCEER-99-0010 "Site Factors and Site Categories in Seismic Codes," by R. Dobry, R. Ramos and M.S. Power, 7/19/99, (PB2000-101705, A08, MF-A02).

MCEER-99-0011 "Restrainer Design Procedures for Multi-Span Simply-Supported Bridges," by M.J. Randall, M. Saiidi, E. Maragakis and T. Isakovic, 7/20/99, (PB2000-101702, A10, MF-A02).

MCEER-99-0012 "Property Modification Factors for Seismic Isolation Bearings," by M.C. Constantinou, P. Tsopelas, A. Kasalanati and E. Wolff, 7/20/99, (PB2000-103387, A11, MF-A03).

MCEER-99-0013 "Critical Seismic Issues for Existing Steel Bridges," by P. Ritchie, N. Kauhl and J. Kulicki, 7/20/99, (PB2000-101697, A09, MF-A02).

MCEER-99-0014 "Nonstructural Damage Database," by A. Kao, T.T. Soong and A. Vender, 7/24/99, (PB2000-101407, A06, MF-A01).

MCEER-99-0015 "Guide to Remedial Measures for Liquefaction Mitigation at Existing Highway Bridge Sites," by H.G. Cooke and J. K. Mitchell, 7/26/99, (PB2000-101703, A11, MF-A03).

MCEER-99-0016 "Proceedings of the MCEER Workshop on Ground Motion Methodologies for the Eastern United States," edited by N. Abrahamson and A. Becker, 8/11/99, (PB2000-103385, A07, MF-A02).

MCEER-99-0017 "Quindío, Colombia Earthquake of January 25, 1999: Reconnaissance Report," by A.P. Asfura and P.J. Flores, 10/4/99, (PB2000-106893, A06, MF-A01).

MCEER-99-0018 "Hysteretic Models for Cyclic Behavior of Deteriorating Inelastic Structures," by M.V. Sivaselvan and A.M. Reinhorn, 11/5/99, (PB2000-103386, A08, MF-A02).

MCEER-99-0019 "Proceedings of the 7th U.S.- Japan Workshop on Earthquake Resistant Design of Lifeline Facilities and Countermeasures Against Soil Liquefaction," edited by T.D. O'Rourke, J.P. Bardet and M. Hamada, 11/19/99, (PB2000-103354, A99, MF-A06).

MCEER-99-0020 "Development of Measurement Capability for Micro-Vibration Evaluations with Application to Chip Fabrication Facilities," by G.C. Lee, Z. Liang, J.W. Song, J.D. Shen and W.C. Liu, 12/1/99, (PB2000-105993, A08, MF-A02).

MCEER-99-0021 "Design and Retrofit Methodology for Building Structures with Supplemental Energy Dissipating Systems," by G. Pekcan, J.B. Mander and S.S. Chen, 12/31/99, (PB2000-105994, A11, MF-A03).

MCEER-00-0001 "The Marmara, Turkey Earthquake of August 17, 1999: Reconnaissance Report," edited by C. Scawthorn; with major contributions by M. Bruneau, R. Eguchi, T. Holzer, G. Johnson, J. Mander, J. Mitchell, W. Mitchell, A. Papageorgiou, C. Scaethorn, and G. Webb, 3/23/00, (PB2000-106200, A11, MF-A03).

MCEER-00-0002 "Proceedings of the MCEER Workshop for Seismic Hazard Mitigation of Health Care Facilities," edited by G.C. Lee, M. Ettouney, M. Grigoriu, J. Hauer and J. Nigg, 3/29/00, (PB2000-106892, A08, MF-A02).

MCEER-00-0003 "The Chi-Chi, Taiwan Earthquake of September 21, 1999: Reconnaissance Report," edited by G.C. Lee and C.H. Loh, with major contributions by G.C. Lee, M. Bruneau, I.G. Buckle, S.E. Chang, P.J. Flores, T.D. O'Rourke, M. Shinozuka, T.T. Soong, C-H. Loh, K-C. Chang, Z-J. Chen, J-S. Hwang, M-L. Lin, G-Y. Liu, K-C. Tsai, G.C. Yao and C-L. Yen, 4/30/00, (PB2001-100980, A10, MF-A02).

MCEER-00-0004 "Seismic Retrofit of End-Sway Frames of Steel Deck-Truss Bridges with a Supplemental Tendon System: Experimental and Analytical Investigation," by G. Pekcan, J.B. Mander and S.S. Chen, 7/1/00, (PB2001-100982, A10, MF-A02).

MCEER-00-0005 "Sliding Fragility of Unrestrained Equipment in Critical Facilities," by W.H. Chong and T.T. Soong, 7/5/00, (PB2001-100983, A08, MF-A02).

MCEER-00-0006 "Seismic Response of Reinforced Concrete Bridge Pier Walls in the Weak Direction," by N. Abo-Shadi, M. Saiidi and D. Sanders, 7/17/00, (PB2001-100981, A17, MF-A03).

MCEER-00-0007 "Low-Cycle Fatigue Behavior of Longitudinal Reinforcement in Reinforced Concrete Bridge Columns," by J. Brown and S.K. Kunnath, 7/23/00, (PB2001-104392, A08, MF-A02).

MCEER-00-0008 "Soil Structure Interaction of Bridges for Seismic Analysis," I. PoLam and H. Law, 9/25/00, (PB2001-105397, A08, MF-A02).

MCEER-00-0009 "Proceedings of the First MCEER Workshop on Mitigation of Earthquake Disaster by Advanced Technologies (MEDAT-1), edited by M. Shinozuka, D.J. Inman and T.D. O'Rourke, 11/10/00, (PB2001-105399, A14, MF-A03).

MCEER-00-0010 "Development and Evaluation of Simplified Procedures for Analysis and Design of Buildings with Passive Energy Dissipation Systems, Revision 01," by O.M. Ramirez, M.C. Constantinou, C.A. Kircher, A.S. Whittaker, M.W. Johnson, J.D. Gomez and C. Chrysostomou, 11/16/01, (PB2001-105523, A23, MF-A04).

MCEER-00-0011 "Dynamic Soil-Foundation-Structure Interaction Analyses of Large Caissons," by C-Y. Chang, C-M. Mok, Z-L. Wang, R. Settgast, F. Waggoner, M.A. Ketchum, H.M. Gonnermann and C-C. Chin, 12/30/00, (PB2001-104373, A07, MF-A02).

MCEER-00-0012 "Experimental Evaluation of Seismic Performance of Bridge Restrainers," by A.G. Vlassis, E.M. Maragakis and M. Saiid Saiidi, 12/30/00, (PB2001-104354, A09, MF-A02).

MCEER-00-0013 "Effect of Spatial Variation of Ground Motion on Highway Structures," by M. Shinozuka, V. Saxena and G. Deodatis, 12/31/00, (PB2001-108755, A13, MF-A03).

MCEER-00-0014 "A Risk-Based Methodology for Assessing the Seismic Performance of Highway Systems," by S.D. Werner, C.E. Taylor, J.E. Moore, II, J.S. Walton and S. Cho, 12/31/00, (PB2001-108756, A14, MF-A03).

MCEER-01-0001 "Experimental Investigation of P-Delta Effects to Collapse During Earthquakes," by D. Vian and M. Bruneau, 6/25/01, (PB2002-100534, A17, MF-A03).

MCEER-01-0002 "Proceedings of the Second MCEER Workshop on Mitigation of Earthquake Disaster by Advanced Technologies (MEDAT-2)," edited by M. Bruneau and D.J. Inman, 7/23/01, (PB2002-100434, A16, MF-A03).

MCEER-01-0003 "Sensitivity Analysis of Dynamic Systems Subjected to Seismic Loads," by C. Roth and M. Grigoriu, 9/18/01, (PB2003-100884, A12, MF-A03).

MCEER-01-0004 "Overcoming Obstacles to Implementing Earthquake Hazard Mitigation Policies: Stage 1 Report," by D.J. Alesch and W.J. Petak, 12/17/01, (PB2002-107949, A07, MF-A02).

MCEER-01-0005 "Updating Real-Time Earthquake Loss Estimates: Methods, Problems and Insights," by C.E. Taylor, S.E. Chang and R.T. Eguchi, 12/17/01, (PB2002-107948, A05, MF-A01).

MCEER-01-0006 "Experimental Investigation and Retrofit of Steel Pile Foundations and Pile Bents Under Cyclic Lateral Loadings," by A. Shama, J. Mander, B. Blabac and S. Chen, 12/31/01, (PB2002-107950, A13, MF-A03).

MCEER-02-0001 "Assessment of Performance of Bolu Viaduct in the 1999 Duzce Earthquake in Turkey" by P.C. Roussis, M.C. Constantinou, M. Erdik, E. Durukal and M. Dicleli, 5/8/02, (PB2003-100883, A08, MF-A02).

MCEER-02-0002 "Seismic Behavior of Rail Counterweight Systems of Elevators in Buildings," by M.P. Singh, Rildova and L.E. Suarez, 5/27/02. (PB2003-100882, A11, MF-A03).

MCEER-02-0003 "Development of Analysis and Design Procedures for Spread Footings," by G. Mylonakis, G. Gazetas, S. Nikolaou and A. Chauncey, 10/02/02, (PB2004-101636, A13, MF-A03, CD-A13).

MCEER-02-0004 "Bare-Earth Algorithms for Use with SAR and LIDAR Digital Elevation Models," by C.K. Huyck, R.T. Eguchi and B. Houshmand, 10/16/02, (PB2004-101637, A07, CD-A07).

MCEER-02-0005 "Review of Energy Dissipation of Compression Members in Concentrically Braced Frames," by K.Lee and M. Bruneau, 10/18/02, (PB2004-101638, A10, CD-A10).

MCEER-03-0001 "Experimental Investigation of Light-Gauge Steel Plate Shear Walls for the Seismic Retrofit of Buildings" by J. Berman and M. Bruneau, 5/2/03, (PB2004-101622, A10, MF-A03, CD-A10).

MCEER-03-0002 "Statistical Analysis of Fragility Curves," by M. Shinozuka, M.Q. Feng, H. Kim, T. Uzawa and T. Ueda, 6/16/03, (PB2004-101849, A09, CD-A09).

MCEER-03-0003 "Proceedings of the Eighth U.S.-Japan Workshop on Earthquake Resistant Design f Lifeline Facilities and Countermeasures Against Liquefaction," edited by M. Hamada, J.P. Bardet and T.D. O'Rourke, 6/30/03, (PB2004-104386, A99, CD-A99).

MCEER-03-0004 "Proceedings of the PRC-US Workshop on Seismic Analysis and Design of Special Bridges," edited by L.C. Fan and G.C. Lee, 7/15/03, (PB2004-104387, A14, CD-A14).

MCEER-03-0005 "Urban Disaster Recovery: A Framework and Simulation Model," by S.B. Miles and S.E. Chang, 7/25/03, (PB2004-104388, A07, CD-A07).

MCEER-03-0006 "Behavior of Underground Piping Joints Due to Static and Dynamic Loading," by R.D. Meis, M. Maragakis and R. Siddharthan, 11/17/03, (PB2005-102194, A13, MF-A03, CD-A00).

MCEER-04-0001 "Experimental Study of Seismic Isolation Systems with Emphasis on Secondary System Response and Verification of Accuracy of Dynamic Response History Analysis Methods," by E. Wolff and M. Constantinou, 1/16/04 (PB2005-102195, A99, MF-E08, CD-A00).

MCEER-04-0002 "Tension, Compression and Cyclic Testing of Engineered Cementitious Composite Materials," by K. Kesner and S.L. Billington, 3/1/04, (PB2005-102196, A08, CD-A08).

MCEER-04-0003 "Cyclic Testing of Braces Laterally Restrained by Steel Studs to Enhance Performance During Earthquakes," by O.C. Celik, J.W. Berman and M. Bruneau, 3/16/04, (PB2005-102197, A13, MF-A03, CD-A00).

MCEER-04-0004 "Methodologies for Post Earthquake Building Damage Detection Using SAR and Optical Remote Sensing: Application to the August 17, 1999 Marmara, Turkey Earthquake," by C.K. Huyck, B.J. Adams, S. Cho, R.T. Eguchi, B. Mansouri and B. Houshmand, 6/15/04, (PB2005-104888, A10, CD-A00).

MCEER-04-0005 "Nonlinear Structural Analysis Towards Collapse Simulation: A Dynamical Systems Approach," by M.V. Sivaselvan and A.M. Reinhorn, 6/16/04, (PB2005-104889, A11, MF-A03, CD-A00).

MCEER-04-0006 "Proceedings of the Second PRC-US Workshop on Seismic Analysis and Design of Special Bridges," edited by G.C. Lee and L.C. Fan, 6/25/04, (PB2005-104890, A16, CD-A00).

MCEER-04-0007 "Seismic Vulnerability Evaluation of Axially Loaded Steel Built-up Laced Members," by K. Lee and M. Bruneau, 6/30/04, (PB2005-104891, A16, CD-A00).

MCEER-04-0008 "Evaluation of Accuracy of Simplified Methods of Analysis and Design of Buildings with Damping Systems for Near-Fault and for Soft-Soil Seismic Motions," by E.A. Pavlou and M.C. Constantinou, 8/16/04, (PB2005-104892, A08, MF-A02, CD-A00).

MCEER-04-0009 "Assessment of Geotechnical Issues in Acute Care Facilities in California," by M. Lew, T.D. O'Rourke, R. Dobry and M. Koch, 9/15/04, (PB2005-104893, A08, CD-A00).

MCEER-04-0010 "Scissor-Jack-Damper Energy Dissipation System," by A.N. Sigaher-Boyle and M.C. Constantinou, 12/1/04 (PB2005-108221).

MCEER-04-0011 "Seismic Retrofit of Bridge Steel Truss Piers Using a Controlled Rocking Approach," by M. Pollino and M. Bruneau, 12/20/04 (PB2006-105795).

MCEER-05-0001 "Experimental and Analytical Studies of Structures Seismically Isolated with an Uplift-Restraint Isolation System," by P.C. Roussis and M.C. Constantinou, 1/10/05 (PB2005-108222).

MCEER-05-0002 "A Versatile Experimentation Model for Study of Structures Near Collapse Applied to Seismic Evaluation of Irregular Structures," by D. Kusumastuti, A.M. Reinhorn and A. Rutenberg, 3/31/05 (PB2006-101523).

MCEER-05-0003 "Proceedings of the Third PRC-US Workshop on Seismic Analysis and Design of Special Bridges," edited by L.C. Fan and G.C. Lee, 4/20/05, (PB2006-105796).

MCEER-05-0004 "Approaches for the Seismic Retrofit of Braced Steel Bridge Piers and Proof-of-Concept Testing of an Eccentrically Braced Frame with Tubular Link," by J.W. Berman and M. Bruneau, 4/21/05 (PB2006-101524).

MCEER-05-0005 "Simulation of Strong Ground Motions for Seismic Fragility Evaluation of Nonstructural Components in Hospitals," by A. Wanitkorkul and A. Filiatrault, 5/26/05 (PB2006-500027).

MCEER-05-0006 "Seismic Safety in California Hospitals: Assessing an Attempt to Accelerate the Replacement or Seismic Retrofit of Older Hospital Facilities," by D.J. Alesch, L.A. Arendt and W.J. Petak, 6/6/05 (PB2006-105794).

MCEER-05-0007 "Development of Seismic Strengthening and Retrofit Strategies for Critical Facilities Using Engineered Cementitious Composite Materials," by K. Kesner and S.L. Billington, 8/29/05 (PB2006-111701).

MCEER-05-0008 "Experimental and Analytical Studies of Base Isolation Systems for Seismic Protection of Power Transformers," by N. Murota, M.Q. Feng and G-Y. Liu, 9/30/05 (PB2006-111702).

MCEER-05-0009 "3D-BASIS-ME-MB: Computer Program for Nonlinear Dynamic Analysis of Seismically Isolated Structures," by P.C. Tsopelas, P.C. Roussis, M.C. Constantinou, R. Buchanan and A.M. Reinhorn, 10/3/05 (PB2006-111703).

MCEER-05-0010 "Steel Plate Shear Walls for Seismic Design and Retrofit of Building Structures," by D. Vian and M. Bruneau, 12/15/05 (PB2006-111704).

MCEER-05-0011 "The Performance-Based Design Paradigm," by M.J. Astrella and A. Whittaker, 12/15/05 (PB2006-111705).

MCEER-06-0001 "Seismic Fragility of Suspended Ceiling Systems," H. Badillo-Almaraz, A.S. Whittaker, A.M. Reinhorn and G.P. Cimellaro, 2/4/06 (PB2006-111706).

MCEER-06-0002 "Multi-Dimensional Fragility of Structures," by G.P. Cimellaro, A.M. Reinhorn and M. Bruneau, 3/1/06 (PB2007-106974, A09, MF-A02, CD A00).

MCEER-06-0003 "Built-Up Shear Links as Energy Dissipators for Seismic Protection of Bridges," by P. Dusicka, A.M. Itani and I.G. Buckle, 3/15/06 (PB2006-111708).

MCEER-06-0004 "Analytical Investigation of the Structural Fuse Concept," by R.E. Vargas and M. Bruneau, 3/16/06 (PB2006-111709).

MCEER-06-0005 "Experimental Investigation of the Structural Fuse Concept," by R.E. Vargas and M. Bruneau, 3/17/06 (PB2006-111710).

MCEER-06-0006 "Further Development of Tubular Eccentrically Braced Frame Links for the Seismic Retrofit of Braced Steel Truss Bridge Piers," by J.W. Berman and M. Bruneau, 3/27/06 (PB2007-105147).

MCEER-06-0007 "REDARS Validation Report," by S. Cho, C.K. Huyck, S. Ghosh and R.T. Eguchi, 8/8/06 (PB2007-106983).

MCEER-06-0008 "Review of Current NDE Technologies for Post-Earthquake Assessment of Retrofitted Bridge Columns," by J.W. Song, Z. Liang and G.C. Lee, 8/21/06 (PB2007-106984).

MCEER-06-0009 "Liquefaction Remediation in Silty Soils Using Dynamic Compaction and Stone Columns," by S. Thevanayagam, G.R. Martin, R. Nashed, T. Shenthan, T. Kanagalingam and N. Ecemis, 8/28/06 (PB2007-106985).

MCEER-06-0010 "Conceptual Design and Experimental Investigation of Polymer Matrix Composite Infill Panels for Seismic Retrofitting," by W. Jung, M. Chiewanichakorn and A.J. Aref, 9/21/06 (PB2007-106986).

MCEER-06-0011 "A Study of the Coupled Horizontal-Vertical Behavior of Elastomeric and Lead-Rubber Seismic Isolation Bearings," by G.P. Warn and A.S. Whittaker, 9/22/06 (PB2007-108679).

MCEER-06-0012 "Proceedings of the Fourth PRC-US Workshop on Seismic Analysis and Design of Special Bridges: Advancing Bridge Technologies in Research, Design, Construction and Preservation," Edited by L.C. Fan, G.C. Lee and L. Ziang, 10/12/06 (PB2007-109042).

MCEER-06-0013 "Cyclic Response and Low Cycle Fatigue Characteristics of Plate Steels," by P. Dusicka, A.M. Itani and I.G. Buckle, 11/1/06 06 (PB2007-106987).

MCEER-06-0014 "Proceedings of the Second US-Taiwan Bridge Engineering Workshop," edited by W.P. Yen, J. Shen, J-Y. Chen and M. Wang, 11/15/06 (PB2008-500041).

MCEER-06-0015 "User Manual and Technical Documentation for the REDARS$^{TM}$ Import Wizard," by S. Cho, S. Ghosh, C.K. Huyck and S.D. Werner, 11/30/06 (PB2007-114766).

MCEER-06-0016 "Hazard Mitigation Strategy and Monitoring Technologies for Urban and Infrastructure Public Buildings: Proceedings of the China-US Workshops," edited by X.Y. Zhou, A.L. Zhang, G.C. Lee and M. Tong, 12/12/06 (PB2008-500018).

MCEER-07-0001 "Static and Kinetic Coefficients of Friction for Rigid Blocks," by C. Kafali, S. Fathali, M. Grigoriu and A.S. Whittaker, 3/20/07 (PB2007-114767).

MCEER-07-0002 "Hazard Mitigation Investment Decision Making: Organizational Response to Legislative Mandate," by L.A. Arendt, D.J. Alesch and W.J. Petak, 4/9/07 (PB2007-114768).

MCEER-07-0003 "Seismic Behavior of Bidirectional-Resistant Ductile End Diaphragms with Unbonded Braces in Straight or Skewed Steel Bridges," by O. Celik and M. Bruneau, 4/11/07 (PB2008-105141).

MCEER-07-0004 "Modeling Pile Behavior in Large Pile Groups Under Lateral Loading," by A.M. Dodds and G.R. Martin, 4/16/07(PB2008-105142).

MCEER-07-0005 "Experimental Investigation of Blast Performance of Seismically Resistant Concrete-Filled Steel Tube Bridge Piers," by S. Fujikura, M. Bruneau and D. Lopez-Garcia, 4/20/07 (PB2008-105143).

MCEER-07-0006 "Seismic Analysis of Conventional and Isolated Liquefied Natural Gas Tanks Using Mechanical Analogs," by I.P. Christovasilis and A.S. Whittaker, 5/1/07, not available.

MCEER-07-0007 "Experimental Seismic Performance Evaluation of Isolation/Restraint Systems for Mechanical Equipment – Part 1: Heavy Equipment Study," by S. Fathali and A. Filiatrault, 6/6/07 (PB2008-105144).

MCEER-07-0008 "Seismic Vulnerability of Timber Bridges and Timber Substructures," by A.A. Sharma, J.B. Mander, I.M. Friedland and D.R. Allicock, 6/7/07 (PB2008-105145).

MCEER-07-0009 "Experimental and Analytical Study of the XY-Friction Pendulum (XY-FP) Bearing for Bridge Applications," by C.C. Marin-Artieda, A.S. Whittaker and M.C. Constantinou, 6/7/07 (PB2008-105191).

MCEER-07-0010 "Proceedings of the PRC-US Earthquake Engineering Forum for Young Researchers," Edited by G.C. Lee and X.Z. Qi, 6/8/07 (PB2008-500058).

MCEER-07-0011 "Design Recommendations for Perforated Steel Plate Shear Walls," by R. Purba and M. Bruneau, 6/18/07, (PB2008-105192).

MCEER-07-0012 "Performance of Seismic Isolation Hardware Under Service and Seismic Loading," by M.C. Constantinou, A.S. Whittaker, Y. Kalpakidis, D.M. Fenz and G.P. Warn, 8/27/07, (PB2008-105193).

MCEER-07-0013 "Experimental Evaluation of the Seismic Performance of Hospital Piping Subassemblies," by E.R. Goodwin, E. Maragakis and A.M. Itani, 9/4/07, (PB2008-105194).

MCEER-07-0014 "A Simulation Model of Urban Disaster Recovery and Resilience: Implementation for the 1994 Northridge Earthquake," by S. Miles and S.E. Chang, 9/7/07, (PB2008-106426).

MCEER-07-0015 "Statistical and Mechanistic Fragility Analysis of Concrete Bridges," by M. Shinozuka, S. Banerjee and S-H. Kim, 9/10/07, (PB2008-106427).

MCEER-07-0016 "Three-Dimensional Modeling of Inelastic Buckling in Frame Structures," by M. Schachter and AM. Reinhorn, 9/13/07, (PB2008-108125).

MCEER-07-0017 "Modeling of Seismic Wave Scattering on Pile Groups and Caissons," by I. Po Lam, H. Law and C.T. Yang, 9/17/07 (PB2008-108150).

MCEER-07-0018 "Bridge Foundations: Modeling Large Pile Groups and Caissons for Seismic Design," by I. Po Lam, H. Law and G.R. Martin (Coordinating Author), 12/1/07 (PB2008-111190).

MCEER-07-0019 "Principles and Performance of Roller Seismic Isolation Bearings for Highway Bridges," by G.C. Lee, Y.C. Ou, Z. Liang, T.C. Niu and J. Song, 12/10/07 (PB2009-110466).

MCEER-07-0020 "Centrifuge Modeling of Permeability and Pinning Reinforcement Effects on Pile Response to Lateral Spreading," by L.L Gonzalez-Lagos, T. Abdoun and R. Dobry, 12/10/07 (PB2008-111191).

MCEER-07-0021 "Damage to the Highway System from the Pisco, Perú Earthquake of August 15, 2007," by J.S. O'Connor, L. Mesa and M. Nykamp, 12/10/07, (PB2008-108126).

MCEER-07-0022 "Experimental Seismic Performance Evaluation of Isolation/Restraint Systems for Mechanical Equipment – Part 2: Light Equipment Study," by S. Fathali and A. Filiatrault, 12/13/07 (PB2008-111192).

MCEER-07-0023 "Fragility Considerations in Highway Bridge Design," by M. Shinozuka, S. Banerjee and S.H. Kim, 12/14/07 (PB2008-111193).

MCEER-07-0024 "Performance Estimates for Seismically Isolated Bridges," by G.P. Warn and A.S. Whittaker, 12/30/07 (PB2008-112230).

MCEER-08-0001 "Seismic Performance of Steel Girder Bridge Superstructures with Conventional Cross Frames," by L.P. Carden, A.M. Itani and I.G. Buckle, 1/7/08, (PB2008-112231).

MCEER-08-0002 "Seismic Performance of Steel Girder Bridge Superstructures with Ductile End Cross Frames with Seismic Isolators," by L.P. Carden, A.M. Itani and I.G. Buckle, 1/7/08 (PB2008-112232).

MCEER-08-0003 "Analytical and Experimental Investigation of a Controlled Rocking Approach for Seismic Protection of Bridge Steel Truss Piers," by M. Pollino and M. Bruneau, 1/21/08 (PB2008-112233).

MCEER-08-0004 "Linking Lifeline Infrastructure Performance and Community Disaster Resilience: Models and Multi-Stakeholder Processes," by S.E. Chang, C. Pasion, K. Tatebe and R. Ahmad, 3/3/08 (PB2008-112234).

MCEER-08-0005 "Modal Analysis of Generally Damped Linear Structures Subjected to Seismic Excitations," by J. Song, Y-L. Chu, Z. Liang and G.C. Lee, 3/4/08 (PB2009-102311).

MCEER-08-0006 "System Performance Under Multi-Hazard Environments," by C. Kafali and M. Grigoriu, 3/4/08 (PB2008-112235).

MCEER-08-0007 "Mechanical Behavior of Multi-Spherical Sliding Bearings," by D.M. Fenz and M.C. Constantinou, 3/6/08 (PB2008-112236).

MCEER-08-0008 "Post-Earthquake Restoration of the Los Angeles Water Supply System," by T.H.P. Tabucchi and R.A. Davidson, 3/7/08 (PB2008-112237).

MCEER-08-0009 "Fragility Analysis of Water Supply Systems," by A. Jacobson and M. Grigoriu, 3/10/08 (PB2009-105545).

MCEER-08-0010 "Experimental Investigation of Full-Scale Two-Story Steel Plate Shear Walls with Reduced Beam Section Connections," by B. Qu, M. Bruneau, C-H. Lin and K-C. Tsai, 3/17/08 (PB2009-106368).

MCEER-08-0011 "Seismic Evaluation and Rehabilitation of Critical Components of Electrical Power Systems," S. Ersoy, B. Feizi, A. Ashrafi and M. Ala Saadeghvaziri, 3/17/08 (PB2009-105546).

MCEER-08-0012 "Seismic Behavior and Design of Boundary Frame Members of Steel Plate Shear Walls," by B. Qu and M. Bruneau, 4/26/08 . (PB2009-106744).

MCEER-08-0013 "Development and Appraisal of a Numerical Cyclic Loading Protocol for Quantifying Building System Performance," by A. Filiatrault, A. Wanitkorkul and M. Constantinou, 4/27/08 (PB2009-107906).

MCEER-08-0014 "Structural and Nonstructural Earthquake Design: The Challenge of Integrating Specialty Areas in Designing Complex, Critical Facilities," by W.J. Petak and D.J. Alesch, 4/30/08 (PB2009-107907).

MCEER-08-0015 "Seismic Performance Evaluation of Water Systems," by Y. Wang and T.D. O'Rourke, 5/5/08 (PB2009-107908).

MCEER-08-0016 "Seismic Response Modeling of Water Supply Systems," by P. Shi and T.D. O'Rourke, 5/5/08 (PB2009-107910).

MCEER-08-0017 "Numerical and Experimental Studies of Self-Centering Post-Tensioned Steel Frames," by D. Wang and A. Filiatrault, 5/12/08 (PB2009-110479).

MCEER-08-0018 "Development, Implementation and Verification of Dynamic Analysis Models for Multi-Spherical Sliding Bearings," by D.M. Fenz and M.C. Constantinou, 8/15/08 (PB2009-107911).

MCEER-08-0019 "Performance Assessment of Conventional and Base Isolated Nuclear Power Plants for Earthquake Blast Loadings," by Y.N. Huang, A.S. Whittaker and N. Luco, 10/28/08 (PB2009-107912).

MCEER-08-0020 "Remote Sensing for Resilient Multi-Hazard Disaster Response – Volume I: Introduction to Damage Assessment Methodologies," by B.J. Adams and R.T. Eguchi, 11/17/08 (PB2010-102695).

MCEER-08-0021 "Remote Sensing for Resilient Multi-Hazard Disaster Response – Volume II: Counting the Number of Collapsed Buildings Using an Object-Oriented Analysis: Case Study of the 2003 Bam Earthquake," by L. Gusella, C.K. Huyck and B.J. Adams, 11/17/08 (PB2010-100925).

MCEER-08-0022 "Remote Sensing for Resilient Multi-Hazard Disaster Response – Volume III: Multi-Sensor Image Fusion Techniques for Robust Neighborhood-Scale Urban Damage Assessment," by B.J. Adams and A. McMillan, 11/17/08 (PB2010-100926).

MCEER-08-0023 "Remote Sensing for Resilient Multi-Hazard Disaster Response – Volume IV: A Study of Multi-Temporal and Multi-Resolution SAR Imagery for Post-Katrina Flood Monitoring in New Orleans," by A. McMillan, J.G. Morley, B.J. Adams and S. Chesworth, 11/17/08 (PB2010-100927).

MCEER-08-0024 "Remote Sensing for Resilient Multi-Hazard Disaster Response – Volume V: Integration of Remote Sensing Imagery and VIEWS$^{TM}$ Field Data for Post-Hurricane Charley Building Damage Assessment," by J.A. Womble, K. Mehta and B.J. Adams, 11/17/08 (PB2009-115532).

MCEER-08-0025 "Building Inventory Compilation for Disaster Management: Application of Remote Sensing and Statistical Modeling," by P. Sarabandi, A.S. Kiremidjian, R.T. Eguchi and B. J. Adams, 11/20/08 (PB2009-110484).

MCEER-08-0026 "New Experimental Capabilities and Loading Protocols for Seismic Qualification and Fragility Assessment of Nonstructural Systems," by R. Retamales, G. Mosqueda, A. Filiatrault and A. Reinhorn, 11/24/08 (PB2009-110485).

MCEER-08-0027 "Effects of Heating and Load History on the Behavior of Lead-Rubber Bearings," by I.V. Kalpakidis and M.C. Constantinou, 12/1/08 (PB2009-115533).

MCEER-08-0028 "Experimental and Analytical Investigation of Blast Performance of Seismically Resistant Bridge Piers," by S.Fujikura and M. Bruneau, 12/8/08 (PB2009-115534).

MCEER-08-0029 "Evolutionary Methodology for Aseismic Decision Support," by Y. Hu and G. Dargush, 12/15/08.

MCEER-08-0030 "Development of a Steel Plate Shear Wall Bridge Pier System Conceived from a Multi-Hazard Perspective," by D. Keller and M. Bruneau, 12/19/08 (PB2010-102696).

MCEER-09-0001 "Modal Analysis of Arbitrarily Damped Three-Dimensional Linear Structures Subjected to Seismic Excitations," by Y.L. Chu, J. Song and G.C. Lee, 1/31/09 (PB2010-100922).

MCEER-09-0002 "Air-Blast Effects on Structural Shapes," by G. Ballantyne, A.S. Whittaker, A.J. Aref and G.F. Dargush, 2/2/09 (PB2010-102697).

MCEER-09-0003 "Water Supply Performance During Earthquakes and Extreme Events," by A.L. Bonneau and T.D. O'Rourke, 2/16/09 (PB2010-100923).

MCEER-09-0004 "Generalized Linear (Mixed) Models of Post-Earthquake Ignitions," by R.A. Davidson, 7/20/09 (PB2010-102698).

MCEER-09-0005 "Seismic Testing of a Full-Scale Two-Story Light-Frame Wood Building: NEESWood Benchmark Test," by I.P. Christovasilis, A. Filiatrault and A. Wanitkorkul, 7/22/09 (PB2012-102401).

MCEER-09-0006 "IDARC2D Version 7.0: A Program for the Inelastic Damage Analysis of Structures," by A.M. Reinhorn, H. Roh, M. Sivaselvan, S.K. Kunnath, R.E. Valles, A. Madan, C. Li, R. Lobo and Y.J. Park, 7/28/09 (PB2010-103199).

MCEER-09-0007 "Enhancements to Hospital Resiliency: Improving Emergency Planning for and Response to Hurricanes," by D.B. Hess and L.A. Arendt, 7/30/09 (PB2010-100924).

MCEER-09-0008 "Assessment of Base-Isolated Nuclear Structures for Design and Beyond-Design Basis Earthquake Shaking," by Y.N. Huang, A.S. Whittaker, R.P. Kennedy and R.L. Mayes, 8/20/09 (PB2010-102699).

MCEER-09-0009 "Quantification of Disaster Resilience of Health Care Facilities," by G.P. Cimellaro, C. Fumo, A.M Reinhorn and M. Bruneau, 9/14/09 (PB2010-105384).

MCEER-09-0010 "Performance-Based Assessment and Design of Squat Reinforced Concrete Shear Walls," by C.K. Gulec and A.S. Whittaker, 9/15/09 (PB2010-102700).

MCEER-09-0011 "Proceedings of the Fourth US-Taiwan Bridge Engineering Workshop," edited by W.P. Yen, J.J. Shen, T.M. Lee and R.B. Zheng, 10/27/09 (PB2010-500009).

MCEER-09-0012 "Proceedings of the Special International Workshop on Seismic Connection Details for Segmental Bridge Construction," edited by W. Phillip Yen and George C. Lee, 12/21/09 (PB2012-102402).

MCEER-10-0001 "Direct Displacement Procedure for Performance-Based Seismic Design of Multistory Woodframe Structures," by W. Pang and D. Rosowsky, 4/26/10 (PB2012-102403).

MCEER-10-0002 "Simplified Direct Displacement Design of Six-Story NEESWood Capstone Building and Pre-Test Seismic Performance Assessment," by W. Pang, D. Rosowsky, J. van de Lindt and S. Pei, 5/28/10 (PB2012-102404).

MCEER-10-0003 "Integration of Seismic Protection Systems in Performance-Based Seismic Design of Woodframed Structures," by J.K. Shinde and M.D. Symans, 6/18/10 (PB2012-102405).

MCEER-10-0004 "Modeling and Seismic Evaluation of Nonstructural Components: Testing Frame for Experimental Evaluation of Suspended Ceiling Systems," by A.M. Reinhorn, K.P. Ryu and G. Maddaloni, 6/30/10 (PB2012-102406).

MCEER-10-0005 "Analytical Development and Experimental Validation of a Structural-Fuse Bridge Pier Concept," by S. El-Bahey and M. Bruneau, 10/1/10 (PB2012-102407).

MCEER-10-0006 "A Framework for Defining and Measuring Resilience at the Community Scale: The PEOPLES Resilience Framework," by C.S. Renschler, A.E. Frazier, L.A. Arendt, G.P. Cimellaro, A.M. Reinhorn and M. Bruneau, 10/8/10 (PB2012-102408).

MCEER-10-0007 "Impact of Horizontal Boundary Elements Design on Seismic Behavior of Steel Plate Shear Walls," by R. Purba and M. Bruneau, 11/14/10 (PB2012-102409).

MCEER-10-0008 "Seismic Testing of a Full-Scale Mid-Rise Building: The NEESWood Capstone Test," by S. Pei, J.W. van de Lindt, S.E. Pryor, H. Shimizu, H. Isoda and D.R. Rammer, 12/1/10 (PB2012-102410).

MCEER-10-0009 "Modeling the Effects of Detonations of High Explosives to Inform Blast-Resistant Design," by P. Sherkar, A.S. Whittaker and A.J. Aref, 12/1/10 (PB2012-102411).

MCEER-10-0010 "L'Aquila Earthquake of April 6, 2009 in Italy: Rebuilding a Resilient City to Withstand Multiple Hazards," by G.P. Cimellaro, I.P. Christovasilis, A.M. Reinhorn, A. De Stefano and T. Kirova, 12/29/10.

MCEER-11-0001 "Numerical and Experimental Investigation of the Seismic Response of Light-Frame Wood Structures," by I.P. Christovasilis and A. Filiatrault, 8/8/11 (PB2012-102412).

MCEER-11-0002 "Seismic Design and Analysis of a Precast Segmental Concrete Bridge Model," by M. Anagnostopoulou, A. Filiatrault and A. Aref, 9/15/11.

MCEER-11-0003 'Proceedings of the Workshop on Improving Earthquake Response of Substation Equipment," Edited by A.M. Reinhorn, 9/19/11 (PB2012-102413).

MCEER-11-0004 "LRFD-Based Analysis and Design Procedures for Bridge Bearings and Seismic Isolators," by M.C. Constantinou, I. Kalpakidis, A. Filiatrault and R.A. Ecker Lay, 9/26/11.

MCEER-11-0005 "Experimental Seismic Evaluation, Model Parameterization, and Effects of Cold-Formed Steel-Framed Gypsum Partition Walls on the Seismic Performance of an Essential Facility," by R. Davies, R. Retamales, G. Mosqueda and A. Filiatrault, 10/12/11.

MCEER-11-0006 "Modeling and Seismic Performance Evaluation of High Voltage Transformers and Bushings," by A.M. Reinhorn, K. Oikonomou, H. Roh, A. Schiff and L. Kempner, Jr., 10/3/11.

MCEER-11-0007 "Extreme Load Combinations: A Survey of State Bridge Engineers," by G.C. Lee, Z. Liang, J.J. Shen and J.S. O'Connor, 10/14/11.

MCEER-12-0001 "Simplified Analysis Procedures in Support of Performance Based Seismic Design," by Y.N. Huang and A.S. Whittaker.

MCEER-12-0002 "Seismic Protection of Electrical Transformer Bushing Systems by Stiffening Techniques," by M. Koliou, A. Filiatrault, A.M. Reinhorn and N. Oliveto, 6/1/12.

MCEER-12-0003 "Post-Earthquake Bridge Inspection Guidelines," by J.S. O'Connor and S. Alampalli, 6/8/12.

MCEER-12-0004 "Integrated Design Methodology for Isolated Floor Systems in Single-Degree-of-Freedom Structural Fuse Systems," by S. Cui, M. Bruneau and M.C. Constantinou, 6/13/12.

MCEER-12-0005 "Characterizing the Rotational Components of Earthquake Ground Motion," by D. Basu, A.S. Whittaker and M.C. Constantinou, 6/15/12.

MCEER-12-0006 "Bayesian Fragility for Nonstructural Systems," by C.H. Lee and M.D. Grigoriu, 9/12/12.

MCEER-12-0007 "A Numerical Model for Capturing the In-Plane Seismic Response of Interior Metal Stud Partition Walls," by R.L. Wood and T.C. Hutchinson, 9/12/12.

MCEER-12-0008 "Assessment of Floor Accelerations in Yielding Buildings," by J.D. Wieser, G. Pekcan, A.E. Zaghi, A.M. Itani and E. Maragakis, 10/5/12.

MCEER-13-0001 "Experimental Seismic Study of Pressurized Fire Sprinkler Piping Systems," by Y. Tian, A. Filiatrault and G. Mosqueda, 4/8/13.

MCEER-13-0002 "Enhancing Resource Coordination for Multi-Modal Evacuation Planning," by D.B. Hess, B.W. Conley and C.M. Farrell, 2/8/13.

MCEER-13-0003 "Seismic Response of Base Isolated Buildings Considering Pounding to Moat Walls," by A. Masroor and G. Mosqueda, 2/26/13.

MCEER-13-0004 "Seismic Response Control of Structures Using a Novel Adaptive Passive Negative Stiffness Device," by D.T.R. Pasala, A.A. Sarlis, S. Nagarajaiah, A.M. Reinhorn, M.C. Constantinou and D.P. Taylor, 6/10/13.

MCEER-13-0005 "Negative Stiffness Device for Seismic Protection of Structures," by A.A. Sarlis, D.T.R. Pasala, M.C. Constantinou, A.M. Reinhorn, S. Nagarajaiah and D.P. Taylor, 6/12/13.

MCEER-13-0006 "Emilia Earthquake of May 20, 2012 in Northern Italy: Rebuilding a Resilient Community to Withstand Multiple Hazards," by G.P. Cimellaro, M. Chiriatti, A.M. Reinhorn and L. Tirca, June 30, 2013.

MCEER-13-0007 "Precast Concrete Segmental Components and Systems for Accelerated Bridge Construction in Seismic Regions," by A.J. Aref, G.C. Lee, Y.C. Ou and P. Sideris, with contributions from K.C. Chang, S. Chen, A. Filiatrault and Y. Zhou, June 13, 2013.

MCEER-13-0008 "A Study of U.S. Bridge Failures (1980-2012)," by G.C. Lee, S.B. Mohan, C. Huang and B.N. Fard, June 15, 2013.

MCEER-13-0009 "Development of a Database Framework for Modeling Damaged Bridges," by G.C. Lee, J.C. Qi and C. Huang, June 16, 2013.

MCEER-13-0010 "Model of Triple Friction Pendulum Bearing for General Geometric and Frictional Parameters and for Uplift Conditions," by A.A. Sarlis and M.C. Constantinou, July 1, 2013.

MCEER-13-0011 "Shake Table Testing of Triple Friction Pendulum Isolators under Extreme Conditions," by A.A. Sarlis, M.C. Constantinou and A.M. Reinhorn, July 2, 2013.

MCEER-13-0012 "Theoretical Framework for the Development of MH-LRFD," by G.C. Lee (coordinating author), H.A Capers, Jr., C. Huang, J.M. Kulicki, Z. Liang, T. Murphy, J.J.D. Shen, M. Shinozuka and P.W.H. Yen, July 31, 2013.

MCEER-13-0013 "Seismic Protection of Highway Bridges with Negative Stiffness Devices," by N.K.A. Attary, M.D. Symans, S. Nagarajaiah, A.M. Reinhorn, M.C. Constantinou, A.A. Sarlis, D.T.R. Pasala, and D.P. Taylor, September 3, 2014.

MCEER-14-0001 "Simplified Seismic Collapse Capacity-Based Evaluation and Design of Frame Buildings with and without Supplemental Damping Systems," by M. Hamidia, A. Filiatrault, and A. Aref, May 19, 2014.

MCEER-14-0002 "Comprehensive Analytical Seismic Fragility of Fire Sprinkler Piping Systems," by Siavash Soroushian, Emmanuel "Manos" Maragakis, Arash E. Zaghi, Alicia Echevarria, Yuan Tian and Andre Filiatrault, August 26, 2014.

MCEER-14-0003 "Hybrid Simulation of the Seismic Response of a Steel Moment Frame Building Structure through Collapse," by M. Del Carpio Ramos, G. Mosqueda and D.G. Lignos, October 30, 2014.

MCEER-14-0004 "Blast and Seismic Resistant Concrete-Filled Double Skin Tubes and Modified Steel Jacketed Bridge Columns," by P.P. Fouche and M. Bruneau, June 30, 2015.

MCEER-14-0005 "Seismic Performance of Steel Plate Shear Walls Considering Various Design Approaches," by R. Purba and M. Bruneau, October 31, 2014.

MCEER-14-0006 "Air-Blast Effects on Civil Structures," by Jinwon Shin, Andrew S. Whittaker, Amjad J. Aref and David Cormie, October 30, 2014.

MCEER-14-0007 "Seismic Performance Evaluation of Precast Girders with Field-Cast Ultra High Performance Concrete (UHPC) Connections," by G.C. Lee, C. Huang, J. Song, and J. S. O'Connor, July 31, 2014.

MCEER-14-0008 "Post-Earthquake Fire Resistance of Ductile Concrete-Filled Double-Skin Tube Columns," by Reza Imani, Gilberto Mosqueda and Michel Bruneau, December 1, 2014.

MCEER-14-0009 "Cyclic Inelastic Behavior of Concrete Filled Sandwich Panel Walls Subjected to In-Plane Flexure," by Y. Alzeni and M. Bruneau, December 19, 2014.

MCEER-14-0010 "Analytical and Experimental Investigation of Self-Centering Steel Plate Shear Walls," by D.M. Dowden and M. Bruneau, December 19, 2014.

MCEER-15-0001 "Seismic Analysis of Multi-story Unreinforced Masonry Buildings with Flexible Diaphragms," by J. Aleman, G. Mosqueda and A.S. Whittaker, June 12, 2015.

MCEER-15-0002 "Site Response, Soil-Structure Interaction and Structure-Soil-Structure Interaction for Performance Assessment of Buildings and Nuclear Structures," by C. Bolisetti and A.S. Whittaker, June 15, 2015.

MCEER-15-0003 "Stress Wave Attenuation in Solids for Mitigating Impulsive Loadings," by R. Rafiee-Dehkharghani, A.J. Aref and G. Dargush, August 15, 2015.

MCEER-15-0004 "Computational, Analytical, and Experimental Modeling of Masonry Structures," by K.M. Dolatshahi and A.J. Aref, November 16, 2015.

MCEER-15-0005 "Property Modification Factors for Seismic Isolators: Design Guidance for Buildings," by W.J. McVitty and M.C. Constantinou, June 30, 2015.

MCEER-15-0006 “Seismic Isolation of Nuclear Power Plants using Sliding Bearings,” by Manish Kumar, Andrew S. Whittaker and Michael C. Constantinou, December 27, 2015.

MCEER-15-0007 “Quintuple Friction Pendulum Isolator Behavior, Modeling and Validation,” by Donghun Lee and Michael C. Constantinou, December 28, 2015.

MCEER-15-0008 “Seismic Isolation of Nuclear Power Plants using Elastomeric Bearings,” by Manish Kumar, Andrew S. Whittaker and Michael C. Constantinou, December 29, 2015.

MCEER-16-0001 “Experimental, Numerical and Analytical Studies on the Seismic Response of Steel-Plate Concrete (SC) Composite Shear Walls,” by Siamak Epackachi and Andrew S. Whittaker, June 15, 2016.

MCEER-16-0002 “Seismic Demand in Columns of Steel Frames,” by Lisa Shrestha and Michel Bruneau, June 17, 2016.

MCEER-16-0003 “Development and Evaluation of Procedures for Analysis and Design of Buildings with Fluidic Self-Centering Systems” by Shoma Kitayama and Michael C. Constantinou, July 21, 2016.

MCEER-16-0004 “Real Time Control of Shake Tables for Nonlinear Hysteretic Systems,” by Ki Pung Ryu and Andrei M. Reinhorn, October 22, 2016.

MCEER-16-0006 “Seismic Isolation of High Voltage Electrical Power Transformers,” by Kostis Oikonomou, Michael C. Constantinou, Andrei M. Reinhorn and Leon Kemper, Jr., November 2, 2016.

MCEER-16-0007 “Open Space Damping System Theory and Experimental Validation,” by Erkan Polat and Michael C. Constantinou, December 13, 2016.

MCEER-16-0008 “Seismic Response of Low Aspect Ratio Reinforced Concrete Walls for Buildings and Safety-Related Nuclear Applications,” by Bismarck N. Luna and Andrew S. Whittaker.

MCEER-16-0009 “Buckling Restrained Braces Applications for Superstructure and Substructure Protection in Bridges,” by Xiaone Wei and Michel Bruneau, December 28, 2016.

MCEER-16-0010 “Procedures and Results of Assessment of Seismic Performance of Seismically Isolated Electrical Transformers with Due Consideration for Vertical Isolation and Vertical Ground Motion Effects,” by Shoma Kitayama, Michael C. Constantinou and Donghun Lee, December 31, 2016.

MCEER-17-0001 “Diagonal Tension Field Inclination Angle in Steel Plate Shear Walls,” by Yushan Fu, Fangbo Wang and Michel Bruneau, February 10, 2017.

MCEER-17-0002 “Behavior of Steel Plate Shear Walls Subjected to Long Duration Earthquakes,” by Ramla Qureshi and Michel Bruneau, September 1, 2017.

MCEER-17-0003 “Response of Steel-plate Concrete (SC) Wall Piers to Combined In-plane and Out-of-plane Seismic Loadings,” by Brian Terranova, Andrew S. Whittaker, Siamak Epackachi and Nebojsa Orbovic, July 17, 2017.

MCEER-17-0004 “Design of Reinforced Concrete Panels for Wind-borne Missile Impact,” by Brian Terranova, Andrew S. Whittaker and Len Schwer, July 18, 2017.

MCEER-17-0005 “A Simple Strategy for Dynamic Substructuring and its Application to Soil-Foundation-Structure Interaction,” by Aikaterini Stefanaki and Metttupalayam V. Sivaselvan, December 15, 2017.

MCEER-17-0006 “Dynamics of Cable Structures: Modeling and Applications,” by Nicholas D. Oliveto and Mettupalayam V. Sivaselvan, December 1, 2017.

MCEER
EARTHQUAKE ENGINEERING TO EXTREME EVENTS
University at Buffalo, The State University of New York
133A Ketter Hall ▪ Buffalo, New York 14260-4300
Phone: (716) 645-3391 ▪ Fax: (716) 645-3399
Email: *mceer@buffalo.edu* ▪ Web: *http://mceer.buffalo.edu*
University at Buffalo *The State University of New York*

ISSN 1520-295X